Nonlinear Control of Switching Power Converters

by

Seth R. Sanders

S.B. Electrical Engineering and Computer Science, S.B. Physics
Massachusetts Institute of Technology, 1981.

S.M. Electrical Engineering and Computer Science
Massachusetts Institute of Technology, 1985.

Submitted to the Department of
Electrical Engineering and Computer Science
In Partial Fulfillment of the Requirements
for the Degree of

Doctor of Philosophy
in Electrical Engineering

at the
Massachusetts Institute of Technology
January, 1989.

Signature of Author _____
Department of Electrical Engineering and Computer Science
January 11, 1989

Certified by _____
George C. Verghese
Associate Professor of Electrical Engineering and Computer Science
Thesis Supervisor

Accepted by _____
Arthur C. Smith
Chairman, Department Committee on Graduate Students

Nonlinear Control of Switching Power Converters

by

Seth R. Sanders

Submitted to the Department of Electrical Engineering and Computer Science on January 18, 1989 in partial fulfillment of the requirements for the Degree of Doctor of Philosophy in Electrical Engineering

Abstract

This thesis addresses the modeling and control of large signal behavior in switching power converters. Most present day control schemes for switching converters are based on small signal, linearized models, and hence do not easily handle large transients. The aim here is to obtain readily implementable control laws that result in globally stable dynamics and satisfactory behavior in the case of both large and small signal operation.

State-space averaged models are first introduced for switched nonlinear circuits that may contain multiple switches. An approach to synthesizing a natural averaged circuit model is then obtained. Such an averaged circuit synthesis provides intuition on the converter operation and permits the use of circuit based analysis methods.

The nominal open-loop operation of a broad class of switching converters is next shown to be stable in the large via a Lyapunov argument. Globally stabilizing control schemes, based on Lyapunov functions, are derived. These include adaptive controllers that handle uncertainties in parameter values. A dual approach to estimating the converter state from incomplete or noisy measurement data, using observers, is also developed. It is demonstrated that the Lyapunov-based schemes can provide satisfactory control performance in terms of robustness, reduced sensitivity, and improved transient response. Simulations of several examples of controlled converters amplify these conclusions.

An alternative approach for large signal control design based on state-space transformations is also considered. A coordinate transformation that arises in feedback linearization is used to facilitate a sliding mode control design. Numerical simulations and experimental results indicate the feasibility of such a design.

Thesis Supervisor: George C. Verghese, Associate Professor of Electrical Engineering and Computer Science

Dedication

This thesis is dedicated to my family: my parents Harold and Deloris and my sisters Karen and Lisa, who have been a constant source of love and support.

Acknowledgements

As I approach the completion of this thesis, it is a pleasure to look back on the past years, and to express my gratitude to the many people who have been essential to my reaching this stage. First and foremost, I thank my advisor Professor George Verghese for years of patient guidance. Besides sharing his technical expertise, George has served as a leader and role model. Among the many ideas professed by George, is the concept of a question. George has taught me that the key to carrying out interesting research is in asking the right questions, and often, the questions are of more importance than the answers.

I am very grateful to Professors Marija Ilic, Marty Schlecht, Dick Thornton, and John Wyatt, who served on my thesis committee, for their contributions, support, and constructive criticism. In particular, I am indebted to Professor Wyatt for introducing me to many network theoretic ideas, which proved essential for the best results in this thesis. Professors Schlecht and Thornton helped me keep my feet on the ground, in guiding the research in this thesis toward practical and important issues. I thank Professor Ilic for her keen interest, and for raising tough theoretical questions.

Two faculty members who were not on my thesis committee, but who have provided guidance throughout my career as a graduate student are Professors John Kassakian and Jeff Lang. I am grateful to John for introducing me to the field of power electronics when I was an undergraduate, and for encouraging me to continue my studies as a graduate student. Jeff has been very helpful at various stages in my graduate career with both technical and general advice.

I would like to thank all the members of the Laboratory for Electromagnetic and Electronic Systems for their comraderie in terms of uncountable technical and philosophical discussions (including those of the sports pages). Over the years many individuals in this lab have influenced my life, but at this point two that emerge are my present and previous office mates, Leo Casey and Clem Karl. Leo was a willing consultant on any practical issue concerning power electronics (and many other areas as well) while Clem served as a listener and sounding board for new ideas. I also thank Miguel Velez, Larry Jones, Derrick Cameron, Ray Sepe, Xiaojun Liu, Kris Mahabir, Steve Leeb, Alex Stankovic, Barry Culpepper, Andy Goldberg, Sharlene Liu, Loveday Mweene, Carlos Bruzos, and Karen Walrath for their help at various points in the execution of this thesis.

An essential ingredient for the completion of this thesis has been financial support. The work (of both author and supervisor) in this thesis has

been supported by many sources. These included the MIT Power Electronics Collegium, International Business Machines Corporation (IBM), Digital Equipment Corporation (DEC), the MIT Department of Electrical Engineering and Computer Science, the Air Force Office of Scientific Research, and the Soderberg Chair in Power Engineering.

Contents

List of Figures

Chapter 1

Introduction

Switching power converters are finding wide applications in the area of electrical energy conditioning, and are therefore of increasing importance. A switching power converter is composed essentially of switches and energy storage elements, since it is designed to achieve high efficiency energy conversion. The nominal steady state operation of a DC-DC converter involves a cyclic operation of the switches to produce a commanded average output voltage or current from a specified DC input source. By modulating the nominal cyclic switching operation, DC-AC operation (inversion) can be obtained. In the case of an AC input source, AC-DC conversion (rectification) and AC-AC conversion (cyclo-conversion) can also be obtained by appropriately modulating the switching operation. Because of the nearly lossless design and construction, the open-loop dynamical behavior of a converter is often poorly damped.

The control of switching power converters is an interesting and challenging research topic for many reasons. Most importantly, the control schemes in present use are based on small signal models obtained by linearizing about a given steady state operating point or trajectory. Large signal transients such as those that occur at power-up or on overload recovery are handled in an ad hoc manner. Designers analyze each circuit individually to prescribe a scheme to accommodate a designated set of large signal transients. The challenge here is to explore how one might do better.

Contents and Contributions of This Thesis

This thesis studies switching converter control schemes that are nonlinear and not limited to small signal behavior. In particular, the thesis develops design methodologies for prescribing easily implemented control algorithms that provide satisfactory global behavior, including robustness with respect to uncertain circuit parameters. Further, these control schemes permit variable or user-programmable output waveforms.

Chapter 2 gives some background information on the operation of switching converters and on control via linear state feedback based on small signal models. Some of the main results of this thesis are also previewed in Chapter 2 with simple examples. A discussion of the relevant literature is given in Chapter 3, but note that details on the literature are included throughout the thesis as appropriate.

An important approach to analysis of switching power converters using averaged circuit models is studied in Chapter 4. In particular, earlier and incomplete results on averaged circuit models for these converters are extended significantly, and now also cover converters whose non-switch components include *nonlinear* circuit elements. The other main area of this thesis is the development of large signal and adaptive control laws for switching converters, using ideas from dissipative systems theory and feedback linearization.

One of our main approaches for large signal control design is based on a Lyapunov function for the switching converter. In order to carry out such a design, it is required to establish that the open-loop behavior of the converter is stable, and to determine the explicit form of a suitable Lyapunov function. For this purpose, Chapter 4 develops certain fundamental results on open-loop stability by demonstrating the existence of an internal energy-like function, termed the *energy in the increment*, which constitutes a natural Lyapunov function.

The basic idea underlying control design using Lyapunov functions is presented in Chapter 5. This chapter also demonstrates some particular advantages of using the natural Lyapunov function. The chapter shows how to apply this

type of control to converters that have nonlinear circuit elements, that handle time-varying source and/or load waveforms, and that operate in the discontinuous conduction mode. A dual approach for designing observers that estimate the converter state from incomplete or noisy measurement data is also developed in Chapter 5, again based on the energy in the increment.

One of the main contributions of this thesis is the unification of certain network theoretic properties with a framework for control design. An important aspect of this unification is the formulation of control designs based on the energy in the increment, as captured in Chapter 5. Another aspect, contained in Chapter 6, involves the interpretation of a Lyapunov based control scheme as a network interconnection. Such a point of view suggests the use of dynamical compensators (whereas static ones were used in Chapter 5) to improve control performance. In particular, Chapter 6 shows how to deal with uncertain circuit parameters (such as unknown nominal state values) with a globally stable self-tuning adaptation scheme. It is also demonstrated that this type of scheme can result in satisfactory performance in terms of reduced system sensitivity and transient response. A novel but heuristic approach, motivated by circuit based principles, is developed for obtaining fast transient behavior in a system modeled as a network interconnection. The background on nonlinear network theory necessary to support the discussions in Chapters 4, 5, and 6 is included in Appendix A.

Chapter 7 explores an entirely different approach to control with coordinate transformations that are used to simplify control design. Such coordinate transformations arise in the so-called *feedback linearization* approach to control design for nonlinear systems. Most of this chapter focuses on an example up-down converter (introduced in Chapter 2). Rather than obtaining an explicit feedback linearization for the up-down converter, the transformation required in such a linearization is used to facilitate a sliding mode control design for this converter. Results of a hybrid experiment/simulation for this control, using an experimental controller in conjunction with the MIT Parity Simulator, are

reported.

A summary and suggestions for future research are given in Chapter 8.

Chapter 2

Background and Preview of Main Results

This chapter presents some background on the operation, modeling, and control of switching power converters. After giving the necessary introductory information, the main results of the thesis are previewed with some simple examples.

2.1 State-Space Models for Power Electronic Circuits

This section develops a state-space model for an up-down converter to illustrate the nature of state-space models for power electronic circuits. The model is used extensively as an example in the remainder of the thesis. For more details on modeling of power electronic circuits, see [1,2,3,48].

Consider the up-down converter shown in Figure 2.1a). The nominal steady state operation of such a converter involves a cyclic process. The transistor is turned on in the first part of the cycle, so that the inductor current ramps up. During this time, the diode is reverse biased (a non-conducting state) so that the capacitor voltage decays into the load. Then, in the second part of the cycle, the transistor is turned off and the diode becomes forward biased (a conducting state), so that the inductor current flows through the diode into the capacitor and the load. Typical waveforms are displayed in Figure 2.1b). With this type of cyclic operation, the average value of the capacitor voltage v in the steady

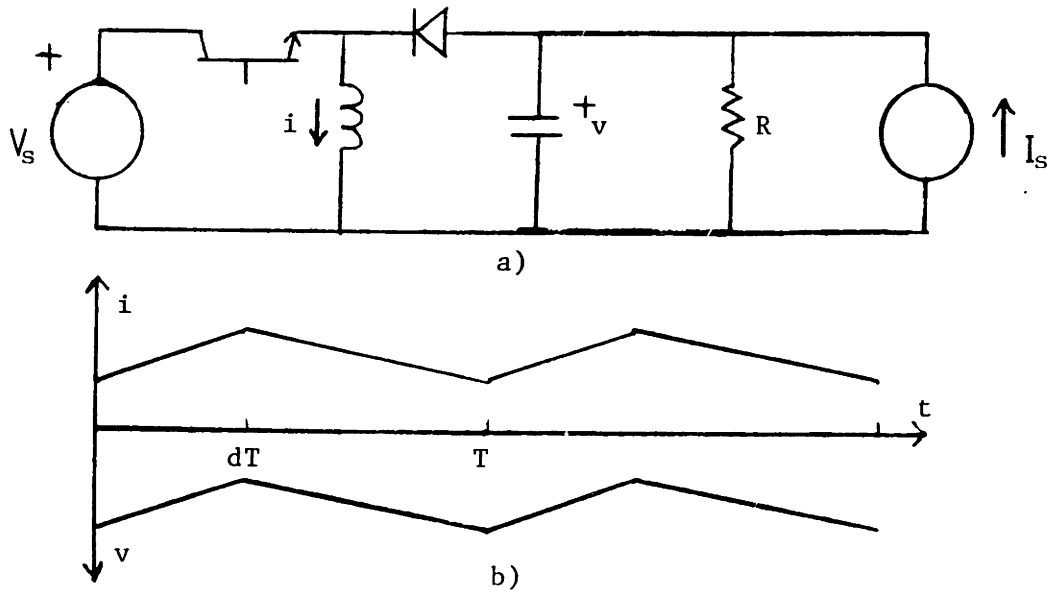

Figure 2.1: a) Up-Down Converter and b) Typical Waveforms

state can be made either larger or smaller in magnitude than the source voltage V_s. (This is why the circuit is termed an *up-down converter.*) One can determine the steady state transfer ratio from source voltage to average capacitor voltage by noting that the average voltage across the inductor is zero in steady state, and hence

$$(d)V_s + (1-d)v_n = 0 \tag{2.1}$$

where v_n is the nominal steady state value of the capacitor voltage and d is the *duty ratio*, that is, the fraction of each cycle that the transistor is on. From (2.1), we readily obtain

$$v_n = -\frac{d}{1-d}V_s. \tag{2.2}$$

Under the restriction that the inductor current i is always positive (so-called continuous conduction), we can model the transistor-diode pair as a single pole, double throw (SPDT) switch. Note that the position of the switch can always be dictated by turning the transistor on ($u = 1$) or off ($u = 0$). When either switch position is specified, the circuit can be characterized by a linear, time-invariant (LTI) model. Suppose that under $u = 1$, the model is given by

$$x' = A_1 x + B_1 w \tag{2.3}$$

and under $u = 0$, is given by

$$x' = A_0 x + B_0 w \tag{2.4}$$

where x is the state vector of the capacitor voltage and the inductor current, x' is its time derivative, and w is the vector of voltage and current source values. Note that we have not explicitly noted the time dependence in the state x and its derivative x', and we shall continue this omission throughout the thesis when such dependence is clear from the context. An ensemble model can be obtained by combining (2.3) and (2.4) as

$$x' = [A_0 + u(A_1 - A_0)]x + [B_0 + u(B_1 - B_0)]w. \tag{2.5}$$

This is termed a bilinear state-space model because the control u enters multiplicatively with the state, as well as linearly. For the up-down converter of Figure 2.1, the state-space representation takes the form:

$$\begin{bmatrix} i' \\ v' \end{bmatrix} = \left\{ \begin{bmatrix} 0 & 1/L \\ -1/C & -1/RC \end{bmatrix} - u \begin{bmatrix} 0 & -1/L \\ 1/C & 0 \end{bmatrix} \right\} \begin{bmatrix} i \\ v \end{bmatrix} + u \begin{bmatrix} V_s/L \\ 0 \end{bmatrix} + \begin{bmatrix} 0 \\ I_o/C \end{bmatrix} \tag{2.6}$$

Note that the control variable u takes on only the values 0 and 1.

In the more general case where nonlinear circuit elements are present in a switching converter, the ensemble model (2.5) would take the more general form

$$x' = f_0(x) + u(f_1(x) - f_0(x)). \tag{2.7}$$

Note that terms corresponding to independent sources may be absorbed into $f_0(\bullet)$ and $f_1(\bullet)$ in (2.7). In some applications involving time-varying source and/or load waveforms, the vector-valued functions $f_0(\bullet)$ and $f_1(\bullet)$ may be time dependent. For all cases of interest in this thesis, $f_0(\bullet)$ and $f_1(\bullet)$ will be continuous functions of their arguments. We shall be interested in a still more general case where the switched circuit admits an arbitrary, finite number of distinct switch configurations. In the case where the circuit has $m + 1$ distinct switch configurations, the state-space model takes the form

$$x' = (1 - u_1 - \ldots - u_m)f_0(x) + u_1 f_1(x) + \ldots + u_m f_m(x). \tag{2.8}$$

Each of the inputs u_k can take on only the discrete values 0 and 1, with at most one input equal to 1 at a given time instant. Note that the $m+1$ instances of the right-hand side of (2.8) correspond to the $m+1$ switch configurations and to the inputs u_k in the following way:

$$\begin{aligned} f_0(x) &\leftrightarrow u_1 = \ldots = u_m = 0 \\ f_1(x) &\leftrightarrow u_1 = 1 \\ &\vdots \\ f_m(x) &\leftrightarrow u_m = 1. \end{aligned} \tag{2.9}$$

State-Space Averaged Models

To facilitate the use of well established control design methods based on state-space models that have a continuously variable input, *state-space averaged* models for switching converters have been developed [17,23,48]. A state-space averaged model is an approximation to a model such as (2.6), that contains discrete control inputs, and can be obtained by replacing the instantaneous values of all state and control variables by their one-cycle averages, i.e.

$$\overline{x}(t) = \frac{1}{T}\int_{t-T}^{t} x(s)\,ds, \tag{2.10}$$

$$d(t) = \overline{u}(t) = \frac{1}{T}\int_{t-T}^{t} u(s)ds, \tag{2.11}$$

in the case where the converter is operated cyclically with period T. The symbol d is used to represent the duty ratio, that is the one-cycle averaged value of u. See [46,48] for discussions on the use of one-cycle averaging for developing state-space averaged models.

To develop some intuition on the approximations involved, consider applying the one-cycle average to the model (2.7). We obtain

$$\overline{x'} = \overline{f_0(x)} + \overline{u(f_1(x) - f_0(x))}. \tag{2.12}$$

Note that the one-cycle averaging operation commutes with differentiation, and hence the left-hand side of (2.12) is equal to $\overline{x}'$. Under the conditions that the

states do not vary much over the period of length T (small ripple assumption), and that the functions $f_0(\bullet), f_1(\bullet)$ are continuous, the right-hand side of (2.12) can be approximated as

$$f_0(\overline{x}) + d(f_1(\overline{x}) - f_0(\overline{x})). \tag{2.13}$$

This approximation can be justified by first noting that the small ripple and continuity conditions assure that the relative variation in the functions $f_0(\bullet), f_1(\bullet)$ is small over the period T, and hence

$$\overline{u(f_1(x) - f_0(x))} \approx \overline{u}\,\overline{(f_1(x) - f_0(x)} = d\,\overline{(f_1(x) - f_0(x)}. \tag{2.14}$$

The small ripple and continuity conditions also permit the approximations

$$\begin{aligned} \overline{f_0(x)} &\approx f_0(\overline{x}) \\ \overline{f_1(x)} &\approx f_1(\overline{x}). \end{aligned} \tag{2.15}$$

which lead to our result. (Note that in the case where the functions $f_0(\bullet), f_1(\bullet)$ are linear or affine, (2.15) involves no approximation.) In summary, the state-space averaged model for (2.7) takes the form

$$\overline{x}' = f_0(\overline{x}) + d(f_1(\overline{x}) - f_0(\overline{x})). \tag{2.16}$$

In the remainder of the thesis, we shall omit (except where otherwise indicated) the overbar notation when considering state-space averaged models, to simplify the presentation. The nature of the model of interest should be clear from the context.

For sufficiently small T, the trajectories of the averaged model can be shown to approximate those of the underlying switched system model on a finite interval with arbitrarily small error, in the case where the functions $f_0(\bullet)$ and $f_1(\bullet)$ possess bounded and continuous first partial derivatives with respect to x, as demonstrated in [84]. Further, [84] proves that the underlying switched system is exponentially stable if the state-space averaged system is exponentially stable (provided T is sufficiently small). A direct application of the results of [84]

would require that the switched system be operated in an open-loop manner. (The results in [84] are actually stronger than what is needed here for the case where the system is operated periodically.) However, technical difficulties can arise if one considers a closed-loop control system with the control defined in the form

$$u = \begin{cases} 1, & h(x) < r(t) \\ 0, & h(x) \geq r(t) \end{cases} \tag{2.17}$$

where $r(t)$ is the ramp function shown in Figure 2.2. This is a typical approach to implementing a control law of the form $d = -h(x)$ that is based on the state-space averaged model. The problem here is that u is no longer even a continuous function of the state x at any instant of time, and hence the resulting closed-loop system will violate the assumptions required in [84]. There is some relevant literature on sliding mode control (i.e. [4,91]) that treats averaging for state-space models with discontinuities on their right-hand sides. For the present case, it is possible to circumvent this technicality by noting that any well designed control system of this form will execute at most two switch transitions per cycle (once "on" and once "off"). Therefore, the required smoothness conditions can be satisfied at every time instant, except exactly when the switch transitions occur. Consequently, the results of [84] could be carried over to this case by replacing the control law (2.17) with a smoothed version such as

$$u = 0.5 - \frac{1}{\pi} tan^{-1}\{\frac{h(x) - r(t)}{\epsilon}\}. \tag{2.18}$$

Of course, this control scheme cannot actually be implemented. But for sufficiently small ϵ, it converges (pointwise) to the control law (2.17) for all values of $h(x) - r(t)$ except $h(x) - r(t) = 0$. Therefore, this control law can result in identical behavior to that obtained with (2.17) if $h(x) - r(t)$ is almost never zero. This will be the case if only a finite number of switch transitions occur during each period.

For the up-down converter, the state-space averaged model has an identical form to that of (2.6), except that we replace the discrete input u with the continuous duty ratio d, which can take on any value satisfying $0 \leq d \leq 1$.

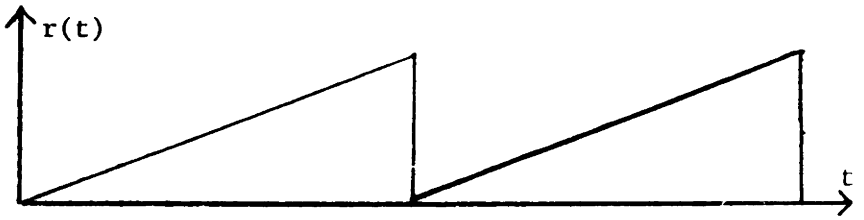

Figure 2.2: Ramp Waveform Used to Implement Control Based on State-Space Averaged Model

The state-space averaged model for a switching converter with $m + 1$ switch configurations takes a form identical to that of (2.8), except that each of the inputs u_k is replaced by its duty ratio d_k. The $m + 1$ duty ratios satisfy the constraints

$$\begin{aligned} 0 \leq d_1 \leq 1 \\ \vdots \\ 0 \leq d_m \leq 1 \\ 0 \leq d_1 + \ldots + d_m \leq 1. \end{aligned} \tag{2.19}$$

Note that the right-hand side of the state-space averaged model for (2.8) is a convex combination of the $m + 1$ instances of the right-hand side of (2.8), determined by the duty ratios d_k. This fact will be of some importance in Chapter 4, where averaged circuit models are discussed.

As mentioned in the Introduction, present day control designs for switching converters are usually based upon linear state feedback for small signal models obtained by linearizing large signal state-space averaged models. In this thesis, we shall be mainly concerned with control designs based upon the large signal model (e.g. (2.5), (2.7),(2.8)) where the control is constrained to discrete values, or the large signal state-space averaged model where the control satisfies a constraint such as $0 \leq d \leq 1$ or (2.19).

2.2 Preview: Averaged Circuits

One of the questions this thesis will answer is the following:

> *Does there exist a non-switched, averaged circuit that corresponds to the state-space averaged model of a switching converter in a natural way?*

By a natural correspondence, we mean that the state-space averaged model should exactly describe the dynamical behavior of the averaged circuit. Further, the averaged circuit should topologically resemble the underlying switched circuit as closely as possible. In Chapter 4, we shall describe procedures for synthesizing averaged circuits that are closely related to the underlying circuit, with the main differences arising from the switch elements.

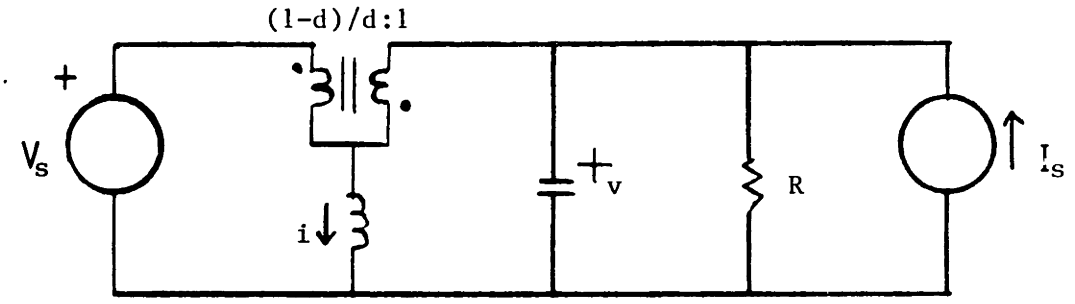

Figure 2.3: Averaged Circuit Model for Up-Down Converter

An averaged circuit synthesis is useful for purposes of analysis (e.g. circuit-based simulation) and obtaining insight into the operation of the switching converter. An averaged circuit model for the up-down converter of Figure 2.1 is shown in Figure 2.3. Many calculations can be performed by inspection with the averaged circuit. For instance, for the up-down converter operated with constant duty ratio, one can readily determine the characteristic polynomial that determines the natural frequencies of the state-space averaged model. To obtain the characteristic polynomial, one would first replace the voltage source with a short circuit and replace the current source with an open circuit, and then

analyze the resulting $L - R - C$ circuit. This polynomial is given by

$$p(s) = s^2 + \frac{1}{RC}s + \frac{(1-d)^2}{LC}. \tag{2.20}$$

It is therefore evident that in the case where R is large, or infinite because the load is a pure current source, that the open-loop dynamics is poorly damped. For the case where $R = \infty$, the purely imaginary eigenvalues (roots of $p(s)$ in (2.20)) are given by

$$\lambda = \pm j\frac{1-d}{\sqrt{LC}}. \tag{2.21}$$

Many previous researchers have dealt with the question of existence and synthesis of averaged circuits. Wester and Middlebrook [46] used an approach that could be termed *in-place averaging* to develop averaged circuit models for switching converters. Our development in Chapter 4 will pick up on the approach of [46]. In this approach, an averaged circuit is realized that has branch variables that are consistent with the one-cycle averaged values of those of the underlying circuit. The results in [46] were not quite correct since the averaged element(s) required to replace the switch branches were not adequately realized. More recent researchers [45] have taken a similar approach to that of [46], and unfortunately made the same error. A somewhat different approach was taken in the work of Middlebrook and Cuk [23,44]. References [23,44] derived averaged circuit models for a fundamental set of switching converters by studying the averaged state-space equations and synthesizing the circuit models by inspection. The circuit models obtained in [23,44] are equivalent to those obtained by the methods of this thesis. However, this thesis will give a methodical approach to synthesis which can be applied to any converter, including those containing nonlinear circuit elements.

We reserve for Chapter 4 a more detailed exposition on averaged circuit models. In the next subsection, we briefly investigate two relatively simple approaches (constant duty ratio and small signal linear state feedback) to the control of switching converters, for comparison with the large signal control schemes to be developed in Chapters 5, 6, and 7.

2.3 Linear State Feedback Control

Why consider feedback control at all? We shall demonstrate in Chapter 4 that all switching converters of a large and important class are stable when a constant nominal duty ratio is applied as input. However, the resulting dynamical behavior is not satisfactory in nearly all cases, and can be shown to exhibit a pronounced ringing transient response in the case of the example up-down converter. Under the constant nominal duty ratio d_n, the transient response corresponding to the state-space averaged model of a converter modeled by (2.5) is governed by the eigenvalues of the matrix

$$A_0 + d_n(A_1 - A_0). \tag{2.22}$$

In the case of the up-down converter of Figure 2.1 and (2.6), these are given by $\lambda = \pm j20$rad/sec, where numerical values for the circuit parameters are as follows:

$$\begin{aligned} C &= 5400\mu\text{F} \\ L &= 180\text{mH} \\ R &= \infty \\ d &= 3/8 \end{aligned}$$

A simulation on the MIT Parity Simulator [24] shown in Figure 2.4 exhibits transients in the state variables, namely inductor current and capacitor voltage, due to a perturbation in the load current I_o. Note that these transients die very slowly under constant duty ratio control, and the rate of decay is controlled by parasitic open-loop resistance in the circuit. This is typical of a switching converter, since these converters are designed to have as little internal loss as possible.

The discussion above indicates the necessity of closed-loop control to damp the transient behavior of a switching converter. Another equally important function of closed-loop control is the reduction of the sensitivity to disturbances

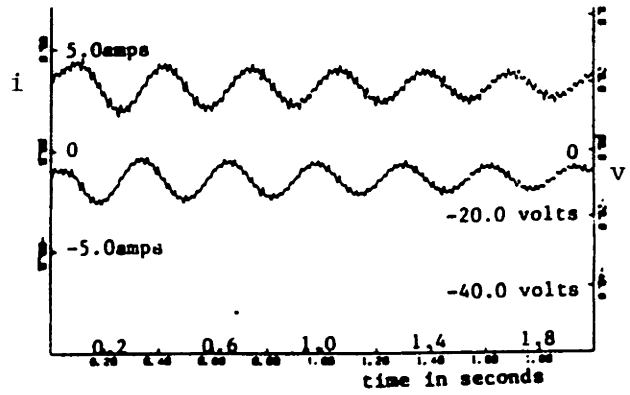

Figure 2.4: Transient under Constant Duty Ratio

and/or uncertainties. The disturbances that typically need to be dealt with are variations in the load and source. Feedback controls can be designed to reject or reduce sensitivity to these disturbances. However, since a control design is inherently model based, the resulting closed-loop system may be sensitive to parameter uncertainties and/or variations. A first cut at dealing with the sensitivity problem can be made with a linear feedback control design, since the small signal model will adequately model the effects of small disturbances. We discuss some of the problems encountered with linear feedback controls based on small signal models, below.

2.3.1 Linear State Feedback Control Based On Small Signal Model

In the following discussion, we consider linear state feedback control laws for the state-space averaged model

$$x' = (A + dB)x + bd + f \tag{2.23}$$

where the input d is the duty ratio that satisfies the constraint $0 \leq d \leq 1$, and the model parameters are defined in terms of those of (2.5) by

$$\begin{aligned} A &= A_0 \\ B &= A_1 - A_0 \\ f &= B_0 w \end{aligned}$$

$$b = (B_1 - B_0)w.$$

Typically, to each constant value of $d = d_n$ (apart from the limits 0 and 1), there corresponds an equilibrium point x_n, given by

$$x_n = -(A + d_n B)^{-1}(bd_n + f) \tag{2.24}$$

By defining variables that reflect variations centered about (x_n,d_n), an equivalent model is obtained as follows:

$$\tilde{x}' = (A + d_n B)\tilde{x} + \tilde{d}B\tilde{x} + (Bx_n + b)\tilde{d} \tag{2.25}$$

where $\tilde{x} = x - x_n$, $\tilde{d} = d - d_n$, and $\tilde{d}$ satisfies the constraint

$$-d_n \leq \tilde{d} \leq 1 - d_n. \tag{2.26}$$

A linear state feedback control for (2.25) takes the form $\tilde{d} = k\tilde{x}$ (for a vector k), and results in the closed loop system

$$\tilde{x}' = \begin{cases} [A + d_n B + (Bx_n + b)k]\tilde{x} + B\tilde{x}(k\tilde{x}) & -d_n \leq k\tilde{x} \leq 1 - d_n \\ A\tilde{x} + (Bx_n + b)(-d_n) & -d_n > k\tilde{x} \\ (A + B)\tilde{x} + (Bx_n + b)(1 - d_n) & 1 - d_n < k\tilde{x} \end{cases} \tag{2.27}$$

In the case where the pair $\{(A+d_nB),(Bx_n+b)\}$ is controllable, the eigenvalues of the small-signal linearization of (2.27) about $\tilde{x} = 0$ can be assigned arbitrarily (in conjugate pairs) by choice of k. However, the behavior of (2.27) in the case of large perturbations from the origin cannot be predicted by the small-signal linearization.

One must consider the effects of the nonlinear (quadratic) term in (2.27) and of control saturation in the case of a large perturbation. The paper [16] of Erickson, Cuk, and Middlebrook provides an example of a linear state feedback controller for a boost (up) converter that locally stabilizes the circuit, but exhibits instability in the case of large perturbations. As noted in [16], quadratic systems such as (2.27) can exhibit multiple equilibria, and the presence of multiple equilibria would preclude the possibility of global asymptotic stability. In the analysis of a feedback control law, the duty ratio constraints need to be

considered, and may potentially be used to some advantage, as [16] indicates. It may be possible to place any "virtual" equilibrium point (i.e. an equilibrium of the unsaturated system) in a region of the state-space where the control is saturated, and hence avoid any undesired equilibria.

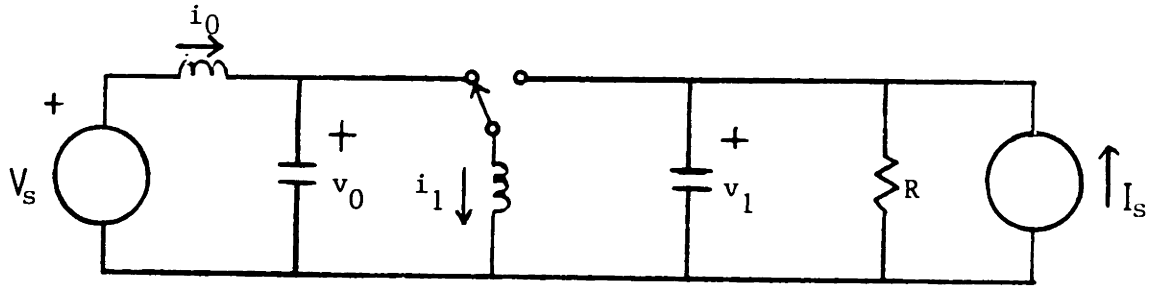

Figure 2.5: Up-Down Converter with Input Filter

Another difficulty with a linear state feedback control is that such a controller must stabilize the converter for all possible nominal operating conditions, i.e. all possible load levels and all possible nominal duty ratios. One might make separate distinct feedback designs for various output levels (e.g. output voltages) that may be commanded, but it is usually required that the control scheme stabilize the converter for all possible loads. One crucial step in implementing the feedback control is in supplying the appropriate nominal state values to the controller. A standard way to treat this problem for a LTI system is through the use of integral control, where all the uncertain nominal values are lumped into a single unknown constant that is reconstructed by the controller. (Such a control design can also result in excellent low frequency sensitivity properties.) This approach can be taken for the switching converter model (2.23), but the resulting small signal dynamics will depend upon the operating point. This dependence can lead to instability for certain operating points.

As an example of this, we have designed a linear feedback controller that incorporates integral control for the fourth order up-down converter of Figure 2.5. The additional filter section in the converter of Figure 2.5 reduces current ripple in the line, generated by the switching action of the converter. The control design was made via a pole-placement scheme for a nominal load current level

of 2amps where the load was entirely stiff ($R = \infty$). The closed loop poles were placed at -20Krad/sec, $-20 \pm j5$Krad/sec, and $-20 \pm j10$Krad/sec. However, in the case where the load current is doubled to 4amps, the small signal behavior becomes unstable. Figure 2.6 illustrates this with a numerical simulation of a transient that occurs when the load increases from 2amps to 4amps.

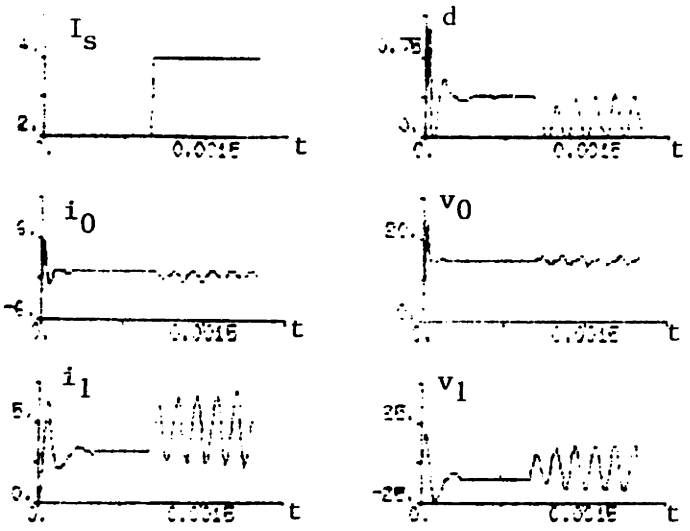

Figure 2.6: Instability due to Change in Operating Condition with Linear Feedback Control

The control techniques to be investigated in the remainder of this thesis are based on the large signal nonlinear models that have control inputs that are either constrained to a continuous interval or are constrained to take on discrete values. Further, we shall develop methods (e.g. self-tuning schemes) that permit stable operation at a wide range of operating conditions. In the following two sections, we preview two of the main approaches to large signal control to be taken in Chapters 5, 6, and 7.

2.4 Preview: Control Design via Lyapunov Functions

Consider the up-down converter shown in Figure 2.5. The state-space averaged model for this converter takes the form (2.23) where the state vector $x = [i_0\ v_0\ i_1\ v_1]^*$. (Note that the superscript $*$ indicates the transpose of the associated vector or matrix throughout this thesis.) It can be readily verified that a Lyapunov function for operation at the nominal steady state (x_n, d_n) is given by

$$\mathbf{V} = \frac{1}{2}(x - x_n)^* Q(x - x_n), \tag{2.28}$$

where

$$Q = diag\{L_0\ C_0\ L_1\ C_1\}.$$

In Chapter 4 it will be demonstrated that a broad class of switching converters has a Lyapunov function of this form for open-loop operation. Note that this function has the form of energy with respect to the nominal operating condition x_n. In the remainder of the thesis, we shall refer to this as the **energy in the increment**. A control scheme can be obtained by differentiating the energy in the increment along an arbitrary state-control trajectory:

$$\frac{d}{dt}\mathbf{V} = \tilde{x}^* Q(A + d_n B)\tilde{x} + \tilde{x}^* Q(B\tilde{x} + Bx_n + b)\tilde{d} \tag{2.29}$$

where $\tilde{x} = x - x_n$ and $\tilde{d} = d - d_n$. It turns out that the first term on the right-hand side of (2.29) is always non-positive (since $\mathbf{V}$ is a Lyapunov function for open-loop operation ($\tilde{d} = 0$)). It is then possible to make the second term on the right-hand side non-positive by choice of $\tilde{d}$. One particular choice that gives this result is

$$\tilde{d} = \begin{cases} -\alpha y, & -d_n < -\alpha y < 1 - d_n \\ -d_n, & -\alpha y \leq -d_n \\ 1 - d_n, & -\alpha y \geq 1 - d_n \end{cases} \tag{2.30}$$

where y takes the form

$$y = \tilde{x}^* Q(B\tilde{x} + Bx_n + b), \tag{2.31}$$

which in this example is given by

$$y = (v_1 - v_{1n})i_1 + (i_1 - i_{1n})(v_0 - v_1) + (v_0 - v_{0n})(-i_1).$$

One of the nice features of this control law is that it is independent of all circuit parameter values. The control is dependent only upon the state variables that are directly affected by the switch action, i.e. v_0, i_1, v_1, and the nominal values of these variables. Accurate information regarding the nominal state values is crucial for the success of this control scheme. In Chapter 6, we shall describe a self-tuning adaptation mechanism that permits stable on-line estimation of the nominal values required when using this scheme.

Note that the dependence upon only the above mentioned variables would hold even if the switch structure of Figure 2.5 were embedded in a larger network composed of (incrementally) passive elements. Such an embedding is illustrated in Figure 2.7. This feature is discussed further in Chapter 6.

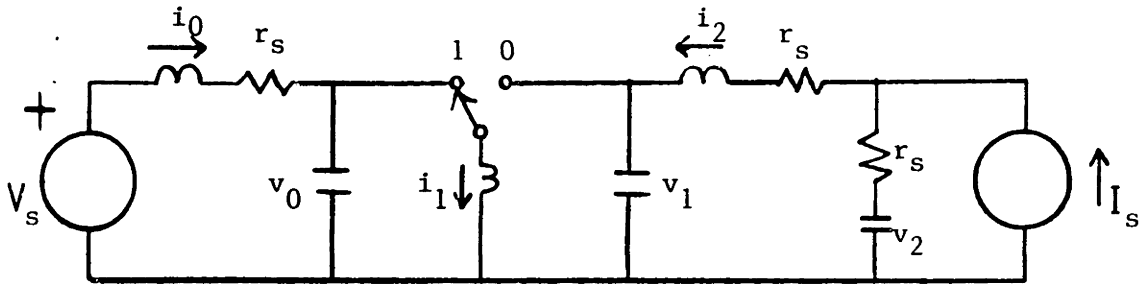

Figure 2.7: Up-Down Converter with Additional Filter Structures

This control scheme can easily be extended to switching power circuits that have numerous controllable switches with the duty ratios $\tilde{d}_1, \tilde{d}_2, \ldots, \tilde{d}_k$ being selected as functions of certain variables $y_1, y_2, \ldots, y_k$ (analogous to the single input case). This extension is considered in Chapter 5, along with other topics such as the control of switching converters containing nonlinear circuit elements.

The following section previews another approach for large signal control design that is taken in this thesis. This approach bases control designs on coordinate transformations.

2.5 Preview: Control Design Using Coordinate Transformations

In Chapter 7, we shall show how to obtain coordinate transformations for certain switching converters, which can facilitate control designs for these converters. The up-down converter of Figure 2.1 (modeled by (2.6)) will serve as our main example. For this converter, a useful state-space transformation takes the form

$$\begin{aligned} T_1 &= \frac{1}{2}C(v - V_s)^2 + \frac{1}{2}Li^2 \\ T_2 &= iV_s + (v/R - I_o)(V_s - v). \end{aligned} \tag{2.32}$$

If we were to use T_1 and T_2 as alternate state variables to model the converter, the state-space model would assume the form

$$\begin{aligned} T_1' &= T_2 \\ T_2' &= f(T_1, T_2, u) \end{aligned} \tag{2.33}$$

for some function $f(\bullet, \bullet, \bullet)$, for values of the state in the region of the state-space that corresponds to usual converter operation.

The utility of the transformation (2.32) for control design purposes is evident from the transformed model (2.33). With a model in the canonical form of (2.33), it is straightforward (if u enters $f(T_1, T_2, u)$ in an appropriate way) to make a feedback control design along the lines of the so-called *feedback linearization*. For this, we would need to consider the state-space averaged model corresponding to (2.33) (obtained by replacing u by d), and to select the duty ratio d such that

$$f(T_1, T_2, d) = -a_1(T_1 - T_1^{ref}) - a_2 T_2. \tag{2.34}$$

With this control, the variables T_1 and T_2 would exhibit the behavior of an LTI system, and the eigenvalues could be placed arbitrarily (at self-conjugate locations) by choice of a_1 and a_2.

Another route for the control design based on the transformed model (2.33) is through a sliding mode control design. This is the main control technique to

be explored in Chapter 7. It is possible to implement a sliding mode control design by using a sliding curve of the form

$$0 = s = c_1(T_1 - T_1^{ref}) + T_2. \tag{2.35}$$

Sliding behavior can be obtained on a portion of this curve by using a control that turns the transistor on ($u = 1$) if $s < 0$ and off ($u = 0$) if $s \geq 0$. A nice feature of this control is that each switch transition is commanded in a direct way. Such a control scheme can also be designed to yield excellent robustness properties, as will be demonstrated in Chapter 7.

In the next chapter, we review some of the relevant literature on fundamental limitations of switching converters, on averaged circuit representations, and on nonlinear control of switching converters.

Chapter 3

Literature Review

In this chapter, we examine the literature that is relevant to the topics investigated in this thesis. The chapter is divided into three sections. The first, Section 3.1, considers the literature on fundamental limitations of power conversion in electrical networks. Many of the network theoretic concepts introduced in Appendix A are essential for the early results on fundamental limitations discussed in Section 3.1. Section 3.2 studies previous work on the synthesis of averaged circuits that approximate the behavior of an underlying switched circuit. Previous work on nonlinear control for switching power converters is reviewed in Section 3.3. Note that many comments on the relation between the results of this thesis and those in the literature are distributed throughout the thesis.

3.1 Fundamental Constraints on Operation of Switching Converters

In the early work of Duffin [25], necessary conditions for the conversion of DC power to AC power were established. In particular, the article [25] applied Tellegen's theorem and concepts of passivity and incremental passivity to establish that at least one incrementally active resistance must be present in the *DC network* of a power conversion circuit. Here, the DC network is defined as the network obtained by open-circuiting capacitors and eliminating branches in series with the capacitors, and by short-circuiting inductors and combining the

nodes to which each inductor is connected. This result was extended in the doctoral thesis of Wolaver [26], as discussed below.

Wolaver [26] proved three very general theorems, later termed the *four-basket, three-basket,* and *two-basket* theorems in [27]. The proofs of these theorems relied mainly on Tellegen's theorem. These theorems were first applied to the steady state values of branch currents and voltages in a switching converter (or equivalently to the DC network) to determine fundamental constraints on the circuit resistances. Then, constraints on the reactances were deduced by first applying one of the basket theorems, and then time-averaging the obtained relations. We summarize some of the results of [26] in the following discussion.

To begin, we introduce some of the terminology from [26] for a circuit operating in the steady state. Let each branch variable (i.e. branch current and branch voltage) be represented as the sum of a constant time-averaged component and a zero-mean time-varying component. For instance, a branch voltage can be expressed in the form

$$v(t) = \overline{v} + \tilde{v}(t). \tag{3.1}$$

where $\overline{v}$ is the (constant) time-averaged value of the voltage and $\overline{\tilde{v}(t)} = 0$. A branch element in the converter is termed *DC active* if it supplies *average DC power* in the steady state, i.e.

$$\overline{v}\overline{i} < 0.$$

Note that an element that is DC active does not necessarily supply any average real power to the rest of the circuit. (An example is the diode in the up-down converter introduced in Chapter 2.) A branch element is termed *AC active* if it supplies *average AC power*, i.e.

$$\overline{\tilde{v}\tilde{i}} = \overline{(v-\overline{v})(i-\overline{i})} = \overline{vi} - \overline{v}\overline{i} < 0.$$

Among the results obtained in [26] is the fact that every operating DC-DC conversion circuit formed from interconnections of two-terminal devices must contain at least two nonlinear and/or time-varying resistances. In particular,

one of these must be DC active to supply average power to the load. This element is often a diode. The other nonlinear/time-varying resistance must be AC active to convert power from the DC source to AC power which in turn can be rectified by the DC active resistance. The second nonlinear/time-varying resistance is often a controlled switch such as a transistor. The necessity of an AC active resistance is equivalent to the result stated by Duffin [25]. (A time-invariant resistive element that is AC active is necessarily incrementally active.)

Further results of [26] on the resistances in a switching converter give lower bounds on the average DC power $(-\overline{vi})$ that must be supplied by the DC active resistances and on the average AC power $(-\overline{\tilde{v}\tilde{i}})$ that must be supplied by the AC active resistances. These bounds are stated in terms of the average real power delivered to the load and the DC current or voltage gain. Lower bounds on the magnitudes of the average currents and voltages of the DC active and AC active resistances (e.g. transistors and diodes) are also given. In a subsequent paper [69], Wolaver obtained lower bounds on the *peak* currents and *peak* voltages handled by the nonlinear/time-varying resistances in a DC-DC converter. These bounds are important for circuit design purposes when considering switching device stresses.

One of the results obtained for the reactances indicates a lower bound on the time-average of the magnitude of the power handled by the reactances. This bound is stated in terms of the average real power delivered to the load and the DC current or voltage gain. A consequence of this bound is that every operating DC-DC converter must contain at least one reactive element. Further, this bound allows the computation of a lower bound on the maximum total energy stored in the reactive elements in terms of the period and the number of zero crossings per cycle of the total reactive power. Similar lower bounds on the time-averaged magnitude of the currents and voltages in the reactive elements are given. These in turn permit computation of a lower bound on the maximum total current and voltage that must be handled by the reactive elements in terms

of the period and relevant zero crossing data.

In the following section, we examine the literature on averaged circuit representations for switched circuits.

3.2 Previous Work on Averaged Circuits

The earliest work on averaged circuit models for switching converters was that of Wester and Middlebrook [46]. In [46], the technique used to obtain an averaged circuit realization for a given switching converter could be termed an *in-place* averaging scheme, where the averaging is performed directly on the circuit. In particular, [46] suggested the construction of an averaged circuit model whose branch variables are one-cycle averages (see Chapter 2) of the corresponding branch variables of the underlying switched circuit. This very physical approach results in an averaged circuit that closely resembles the underlying circuit. However, [46] did not adequately realize the elements required to replace the switch branches. Rather, each ideal switch pair was simply replaced by an ideal transformer. A consequence of this is that the state-space model that governs the dynamics of the obtained averaged circuit is not always equivalent to the state-space averaged model for the underlying circuit.

The later synthesis method of Middelbrook and Cuk [23,44], termed 'hybrid modeling', is based on the state-space averaged model (and proceeds apparently by inspection). This technique results in circuit syntheses that do indeed realize the state-space averaged models for their underlying models. The development by Cuk and Middlebrook in [68] illustrated an analogous approach for synthesizing averaged circuits for switching converters operating in the discontinuous conduction mode. It is claimed in [23,44,68] that the technique is applicable to any converter; however, syntheses are only given for a set of example converters. A more recent paper of Tymerski et al. [45] reverts to the technique of simply replacing an ideal switch pair by an ideal transformer.

Averaged circuit models have also been developed for the analysis of switched capacitor filters. In particular, the paper of Tsividis [71] illustrates the replace-

ment of a capacitor and switch pair by a simple resistor. This equivalent circuit modeling involves a reduction of the order of the state-space, as is required in modeling a switching converter in the discontinuous conduction mode. Similar ideas were applied by other authors [72,73] for the analysis of switched capacitor circuits.

In Chapter 4, we shall apply the method of in-place averaging to obtain averaged circuit models that do indeed realize their appropriate state-space averaged models. Our approach will be based on compact network representations for various subnetworks in a given converter, and will typically permit the replacement of a switch pair with a simple non-switched two-port network. This development will also permit nonlinear circuit elements to be present in the converter.

3.3 Previous Work on Nonlinear Control of Power Circuits

This section is divided into two parts, one on switching law control, where each control input assumes a discrete value corresponding to a switch position, and a second on control design based on state-space averaged models, where each input takes on a value from a closed interval of the real line. The distinction between the two approaches is often blurred, however, since similar design methods may be applied with either approach. Further, practical implementation schemes of switching law controls may impose periodic switching patterns as is often done for state-space averaged control approaches. It is also possible that a control algorithm designed for the state-space averaged model may demand extreme values of the control inputs, and hence be indistinguishable from a switching law control.

3.3.1 Literature on Switching Law Control

A switching law control determines the discrete-valued input to the model (2.5) (or (2.7)) at each instant, using partial or full state information. This method of control is presently in use in various power electronic circuits. A relatively

simple application area is in the inductor current control loops of some DC-DC converters that use current mode programming [10,11,33]. Here, the position of a switch is set by comparing the current level in the inductor with a commanded current level. Different schemes may be used to decide the commanded current level, see for example [67] for a method based on 'power equalization'. A chattering (or sliding) type behavior can be effected if one switch position leads to increasing current while the other switch position causes the current to decrease. This control technique has been used to generate AC current waveforms by supplying a time-varying current command signal. More sophisticated methods of generating time-varying waveforms have been explored in the work of Sabonovic et al. [12]. The controls presented in [12] rely on full state information to effect the control decisions. The use of full state information has been considered in numerous other studies, as reported below.

In his doctoral thesis, Wood [1] developed a sliding mode control algorithm for down converters with second and fourth order output filters. He demonstrated the global stability of these power circuits under his sliding mode control algorithm, and proposed the extension to converters with higher order output filter stages. The class of down converters without an input filter stage is governed by state-space models that are essentially linear and controllable. It is a fact that all controllable linear state-space systems can be transformed to the phase canonical form (see (3.9)) via a linear change of coordinates [13]. Hence, it is not surprising that sliding mode control can be successfully implemented for the class of down converters. A sliding mode controller for a down converter was also proposed in the work of Venkataramanan, Sabanovic, and Cuk [8]. One interesting feature of the sliding curve proposed in [8] is that the switch (i.e. transistor, diode) current can be limited to a design value during transients if sliding operation is maintained.

The paper [8] also deals with the more involved problem of designing sliding surfaces for converters beyond the down converter. In particular, a sliding mode control law is derived for a boost converter. The sliding curve used is a straight

line in the $i - v$ plane that is designed using a dynamical model linearized about an equilibrium point. The authors show this sliding mode control algorithm results in a relatively large region of stability by considering large and small perturbations separately. It is also pointed out that this design method can be applied to other power circuits such as an up-down converter.

The development of sliding mode control laws for switching power electronic circuits is also treated in the recent papers of Sira-Ramirez [9], Sira-Ramirez and Ilic [70], and of the author [43]. (See Chapter 7 for details concerning [43].) Although the presentation in [9] is made in a more general setting, all of the sliding surfaces considered in [9] for DC-DC converters are of the form $x_j = K$, for some state variable x_j that is desired to be regulated at the level K. The restriction to this type of surface has disadvantages. Notably, the dynamical behavior on the surface cannot be tailored for a given application, and in some cases can be unstable (e.g. output voltage regulation of the up-down converter). (Results in [66] indicate that the presence of right-half plane zeros in the small signal transfer function from duty ratio to the variable s leads to instability in the sliding mode on the surface $s = K$.) The sliding mode control scheme of [70] uses the slow manifold of the open-loop state-space averaged model as the sliding surface. This control method requires that the open-loop switching converter circuit has a dominant *real* eigenmode, which is not always true. With such a scheme, the dynamical behavior in the sliding mode is governed by the same dynamics that asymptotically governs the open-loop behavior. This can be quite sluggish in many cases.

In another direction, [1] and [9] have considered the stabilization of lossless switched power electronic circuits whose states evolve on a generalized sphere. Wood [1] has given general theorems for controlling such a system on its manifold, while Sira-Ramirez [9] has proposed the use of sliding surfaces to govern the transition from one state configuration to another on the manifold. The possibility of generating AC waveforms by constraining the state of a lossless converter to evolve on a certain surface has also been considered in these references.

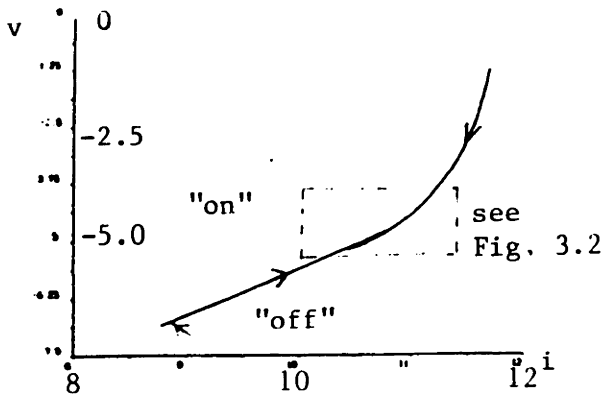

Figure 3.1: Switching Curve that Divides Current-Voltage State Plane into "On" (Above the Curve) and "Off" Regions. Trajectory Shown Begins in the "Off" Region.

Results on non-sliding switching law controls for converters with intrinsically nonlinear state-space models (e.g. up-down and up converters) have been obtained using state-plane methods [14,15]. In particular, Burns and Wilson [14] have made complete and detailed studies of state-plane control laws for three basic converters (down, up-down, and up converters). The following discussion will center on their approach to control of the up-down converter.

Figure 3.1 shows one state trajectory plotted in the inductor current - capacitor voltage ($i - v$) plane for the up-down converter of Figure 2.1 under a state trajectory control law as proposed in [14]. The dark curve is the switching curve that divides the state-plane into an "on" region ($u = 1$) and an "off" region ($u = 0$). For initial states in the "off" region (as shown in Figure 3.1), the trajectory using the control $u = 0$ runs into the switching curve, where the control switches to $u = 1$ so that the trajectory follows the switching curve to a final limit cycle. Analogous behavior occurs for initial states in the "on" region, but with the sequence of control reversed. Note that the steady state operation is a limit cycle determined by the switching curve. Figure 3.2 depicts the limit cycle behavior. The state follows the "on" section of the switching curve to point A where the control changes to "off" since the trajectory enters the "off" region. The state then cycles back to the switching curve at point B where the control changes to "on". Note that the size of the contour followed in the limit

cycle determines the switching frequency. Smaller contours (resulting in smaller peak-to-peak current and voltage ripple) require higher switching frequencies. This elegant control algorithm minimizes the number of switch transitions for a given transient, and precisely determines the steady state operation. However, there are drawbacks, as pointed out below.

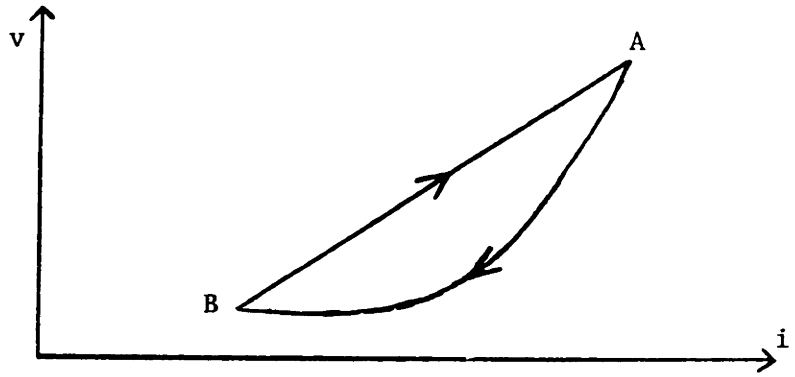

Figure 3.2: Limit Cycle Behavior

A serious problem lies in the necessity of accurate parameter and state information. The authors of [14] have demonstrated with simulations the relative insensitivity of the converter behavior under this control algorithm to variations in load conditions, and the same insensitivity was experimentally verified in [15]. However, if some circuit parameters are not very precisely known, behavior that appears to be chaotic can result. Figure 3.3 shows a simulation using the control law proposed in [14] with a capacitor value that is ten percent smaller than the design value. Note that the state trajectory does not settle to the desired steady state operation, but appears to approach a non-periodic steady state or *strange attractor*. Another drawback is in the complexity of the hardware and software required to implement the control law, since the stored switching curve consists of sections of spiral and exponential trajectories. In Chapter 7, where control designs based on state-space transformations are considered, we shall investigate a sliding mode control scheme that can solve these problems.

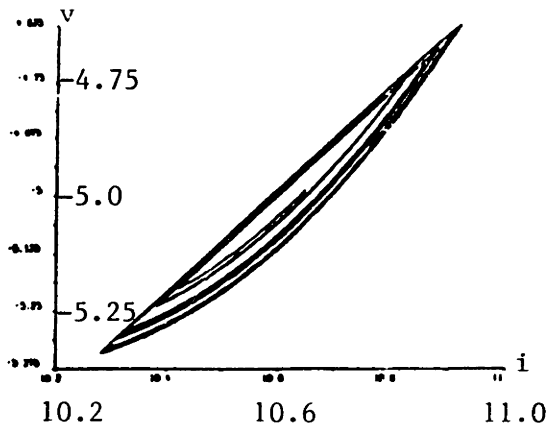

Figure 3.3: Instability that Results when the Circuit Value of the Capacitor is Ten Percent Smaller than the Nominal Value.

3.3.2 Literature on Control Design for Large Signal State-Space Averaged Models

As previously discussed in Chapter 2, some pitfalls of control designs based on small signal models obtained by linearizing large signal averaged models are outlined in the paper of Erickson, Cuk, and Middlebrook [16]. After discussing the development of large signal averaged models for switching converters, which take the form

$$x' = Ax + (Bx + b)d, \tag{3.2}$$

[16] considers the effects of the quadratic nonlinearity introduced into the bilinear state-space model (3.2) by linear state feedback (see (2.27)). It is noted that the transient response to a strong perturbation can be substantially different from the transient expected from the small signal design. One noted feature of the feedback system with quadratic nonlinearity is the possible presence of multiple equilibria, which prohibit global stability. The effect of saturation due to the constraints on the duty ratio is also noted in [16]; one obtains the dynamical behavior of a linear time-invariant system corresponding to (3.2) with the control d fixed at one of its extremes.

Control design for the large signal state-space averaged model using the so-called quantative feedback synthesis was explored in the paper of Horowitz, Sidi, and Erickson [92]. The method of [92] characterizes a class of plant inputs

(duty ratio waveforms) for each member of a set of possible plant models. The plant inputs are selected to produce a given desired output behavior (such as a start-up transient). The obtained input waveforms associated with the selected output waveforms are then used to determine approximate input-output transfer function relations. A control design is then based on these approximate input-output transfer functions. Simulation results in [92] indicate the feasibility of this approach.

Control Design Based on the Theory of Dissipative Systems One important approach to control of dynamical systems is via the theory of dissipative systems [28,29]. An n-input, n-output system modeled by

$$\begin{aligned} x' &= f(x,u) \\ y &= h(x,u) \end{aligned} \tag{3.3}$$

is said to be *dissipative* with respect to the *supply rate* $w(u,y)$ if there is a nonnegative definite internal storage function $V(x)$ such that

$$\frac{d}{dt}V - w(u,y) \leq 0. \tag{3.4}$$

The supply function that will be of main interest here is given by

$$w(u,y) = u^*y. \tag{3.5}$$

In the case where (3.3) models the immittance function of an n-port network, the supply function (3.5) corresponds to the power supplied to the network at its ports. For the purposes here, the immittance function of an n-port network modeled by (3.3) is passive (see Appendix A) if and only if the system (3.3) is dissipative with respect to the supply function (3.5). It is straightforward to demonstrate that a system that is dissipative with respect to this supply function is passive. The converse also holds although it is not always easy to explicitly determine a suitable internal storage function. (One such function is the available energy as defined in Appendix A.)

Some of the important features of dissipative systems are: (i) a point in the state space where the storage function attains a local minimum defines a stable equilibrium and the storage function is a Lyapunov function for this equilibrium; and (ii) feedback interconnections of dissipative systems are dissipative (the sum of the storage functions is a storage function for the interconnected system). See [28,29] for more details.

The theory of dissipative systems was applied by Wood [1] to obtain feedback control schemes for switching converters. The approach used in [1] was to view a closed-loop system (switching converter and controller) as the feedback interconnection of two dissipative systems. Wood [1] began with an input-output model for a given switching converter from duty ratio to a selected averaged output variable (although neither the term duty ratio nor state-space averaging were used). Such a model is not necessarily nor usually dissipative. In Chapter 6, we shall show how to pick an appropriate output variable that results in a dissipative model. The controller in [1] was selected to be linear, time-invariant, and such that its transfer function could be factored into two factors: one which combined with the plant input-output model to form a dissipative operator (passive system), and a second which combined with the saturation constraint to also result in a passive input-output model.

The stability of the resulting closed-loop system was concluded by using the Lyapunov function corresponding to the sum of the storage functions of the two interconnected dissipative systems. The set of passive, linear, time-invariant transfer functions which result in passive operators when cascaded with a monotone nonlinearity were termed *O'Shea functions* in [1]. (These functions were characterized in the paper of O'Shea [52].) Wood worked mainly with down converters for which input-output models are essentially linear. Some consideration of down converters which have essential nonlinearities in their state-space models (e.g. converters with series resistance in the DC source) was made in [1], but a thorough treatment was not given.

An intriguing approach to the control of the type of bilinear system that

arises in switching power circuits, i.e. (3.2), was explored in the work of Brockett and Wood [17]. In particular, a control scheme outlined in [17] is closely related to the dissipative system approach. The paper [17] notes that if the A matrix in the bilinear state-space model (3.2) is similar to a skew-symmetric matrix, and hence satisfies the Lyapunov-type equation

$$QA + A^*Q = 0, \quad Q = Q^* > 0, \tag{3.6}$$

then a feedback control law can be specified by examining the Lyapunov candidate $V = x^*Qx$. Differentiating V with respect to time, one finds

$$\frac{d}{dt}V = \{x^*(QB + B^*Q)x + (b^*Qx + x^*Qb)\}d, \tag{3.7}$$

which can always be made negative provided d can take on positive or negative values, and the quantity multiplying d does not become identically zero along trajectories of the system. The state-space model (2.6) for the example up-down converter of Figure 2.1 (Chapter 2) does not satisfy (3.6) for any matrix Q, but there does exist a matrix Q satisfying

$$QA + A^*Q \leq 0, \quad QB + B^*Q = 0, \quad Q = Q^* > 0. \tag{3.8}$$

In this case, it is still straightforward to take the approach to control design that is outlined above. In Chapter 4, we shall characterize the class of switching converters that have state-space models with A and B matrices that satisfy Lyapunov equations such as (3.8). The connection with dissipative systems is evident if the Lyapunov function $V(x)$ is thought of as a storage function. Of course, an appropriate input-output model with an associated supply function must be considered. We shall give this idea more consideration in Chapter 6.

Control Design Based on State-Space Transformations There has been significant work on the problem of characterizing systems that are controllable linear equivalents, i.e. those that can be brought to the phase canonical form

$$x_1' = x_2$$

$$
\begin{aligned}
x_2' &= x_3 \\
&\vdots \\
x_n' &= f(x_1, \ldots, x_n, u)
\end{aligned}
\qquad (3.9)
$$

via some nonlinear change of coordinates; see the develoments in [18,19,20,30] and in Chapter 7. The recent paper of Sira-Ramirez and Ilic [65] investigates the problem of feedback linearization for various DC-DC converters. With a system in the form (3.9), one can consider picking the feedback control $u(x_1, .., x_n)$ so that the system behaves as a prescribed linear time-invariant model. Other possibilities exist. For instance, in Chapter 7 we shall investigate a sliding mode control scheme that is based on a model of the form (3.9).

An approach to the feedback control problem for power electronic circuits along the lines of this so-called feedback linearization was taken in Salut et al. [21]. Rather than attempting to find alternate state variables so that the state-space model for the example boost converter can be transformed to the form of (3.9), [21] selects a simple feedback law so that the capacitor voltage obeys a stable first order linear, time-invariant differential equation. It is then demonstrated in [21] that the other state variables (i.e. inductor current) exhibit stable behavior. This approach along with that of [9] have the common feature of focusing on just one key state variable, and demonstrating overall stability through other considerations.

It turns out that many state-space systems including those modeling switching converters cannot be brought to the form (3.9) by some state-space transformation. A similar approach termed *pseudo linearization* that may have wider applications has been developed in [31]. This approach involves determining nonlinear transformations of the state and control inputs so that the tangent model (small signal linearization) of the transformed system is in phase canonical form (3.9). This approach to control has been applied by Sira-Ramirez [32] to second order up and up-down converters. One advantage of this approach (over simple linearization) is that a feedback control which stabilizes an entire class of equilibria can be specified. However, it is generally difficult to make

conclusions on the global stability and large signal behavior of control systems designed with this approach.

For a different application in the control of a series resonant converter, a nonlinear state transformation involving energy-like variables was developed in [33]. The method of [33] is to characterize each arc of the state plane trajectory by its radius which corresponds to an energy-like quantity. The instant of each controlled switch transition is then determined by continuously monitoring the radius of the trajectory arc of the subsequent circuit configuration, and comparing to the desired arc radius. The controlled switch transition is then commanded when the monitored quantity reaches the threshold value. This scheme results in very fast resonant tank control transients, transients that are time optimal in many cases. This approach has in common with the control schemes of [14,15,67] for switching converters the feature of using the desired state plane trajectory as the control law.

Chapter 4

General Properties of Switching Converter Dynamics

In this chapter, we examine some general properties of the dynamical behavior of switching power converters. In particular, we study the topic of existence and synthesis of non-switched circuits that exhibit the dynamics described by the state-space averaged model of a switched circuit. Then, the open-loop stability of switching converters is investigated.

4.1 Existence of Averaged Circuits for Switching Converters

In this section, we address an aspect of the question introduced in Chapter 2, namely:

> *Does there exist a non-switched "averaged" circuit that corresponds in a natural way to the state-space averaged model of a switching converter?*

By the phrase "in a natural way," it is meant that the state-space averaged model of the underlying converter exactly describes the dynamical behavior of the averaged circuit, and that the averaged circuit should topologically resemble as closely as possible the underlying switched circuit. Specific synthesis techniques for averaged circuit models will be considered in the following section.

The question of averaged circuit existence for a general switched power circuit that includes nonlinear circuit elements and an arbitrary, finite number of switch configurations will be considered here. Recall from Chapter 2 that the form of the switched state-space system modeling a switching converter with $m+1$ distinct switch configurations is

$$x' = (1 - u_1 - \ldots - u_m) f_0(x) + u_1 f_1(x) + \ldots + u_m f_m(x) \tag{4.1}$$

where the state x is typically the vector of inductor currents and capacitor voltages or the vector of inductor fluxes and capacitor charges. In the model (4.1), the control inputs u_k can take only the discrete values 0 and 1, with at most one input equal to 1 at a given time instant. The corresponding state-space averaged model takes the form

$$x' = (1 - d_1 - \ldots - d_m) f_0(x) + d_1 f_1(x) + \ldots + d_m f_m(x) \tag{4.2}$$

where the m duty ratios satisfy the constraints

$$\begin{gathered} 0 \le d_1 \le 1 \\ \vdots \\ 0 \le d_m \le 1 \\ 0 \le d_1 + \ldots + d_m \le 1. \end{gathered} \tag{4.3}$$

Note that the state-space averaged model (4.2) is a convex combination of the $m+1$ extreme models contained in (4.1) that correspond to the $m+1$ switch configurations.

Now consider the partitioning of a given switching converter system (including source and load) into nonlinear reactive and nonlinear resistive n-ports as shown in Figure 4.1. A nonlinear circuit element is indicated with a box surrounding the element. The resistive n-port includes the independent sources and is generally dependent upon the switch configuration determined by $u_1, \ldots, u_m$. We shall assume that the resistive n-port has a well defined hybrid representation $\mathcal{H}_u(\bullet)$ for each switch configuration with the current-controlled ports

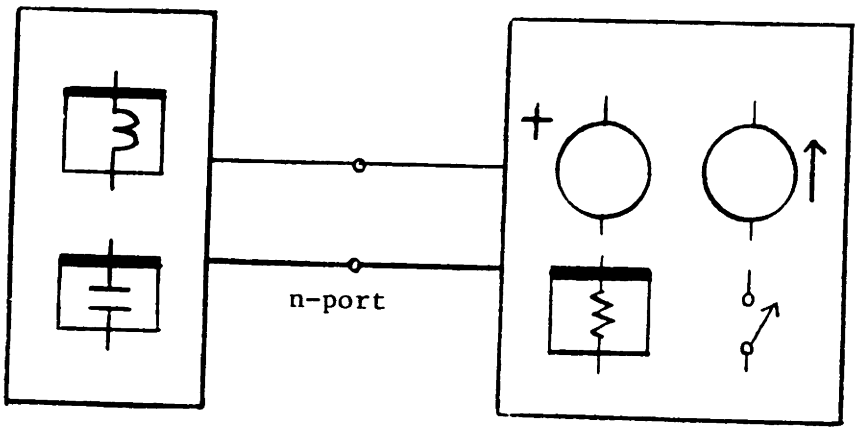

Figure 4.1: Reactance Extraction Partitioning of Switching Converter

connected to inductive ports and the voltage-controlled ports connected to capacitive ports. We also assume that all inductors are flux controlled and that all capacitors are charge controlled. These assumptions are consistent with the assumption that the switching converter has a well defined state-space model, with the state consisting of inductor fluxes and capacitor charges.

The state-space model governing the dynamical behavior of such a partitioned circuit is obtained by imposing Kirchhoff's Voltage Law (KVL) at the inductive ports and Kirchhoff's Current Law (KCL) at the capacitive ports, yielding

$$x' = -\mathcal{H}_u\{Q^{-1}(x)\} \tag{4.4}$$

where the elements of the vector x are inductor fluxes and capacitor charges. The function $Q^{-1}(\bullet)$ maps the inductor fluxes and capacitor charges to the inductor currents and capacitor voltages, respectively. Note that coupled inductances are permitted in the development here. By identifying the $m+1$ values of the hybrid resistive n-port function $\mathcal{H}_u(\bullet)$ with the $m+1$ distinct circuit configurations as follows

$$\begin{aligned} \mathcal{H}_0 &\leftrightarrow u_1 = \ldots = u_m = 0 \\ \mathcal{H}_1 &\leftrightarrow u_1 = 1 \\ &\vdots \\ \mathcal{H}_m &\leftrightarrow u_m = 1, \end{aligned} \tag{4.5}$$

we can write the state-space averaged model

$$x' = -(1 - d_1 - \ldots - d_m)\mathcal{H}_0\{Q^{-1}(x)\} - d_1\mathcal{H}_1\{Q^{-1}(x)\} - \ldots - d_m\mathcal{H}_m\{Q^{-1}(x)\}. \tag{4.6}$$

Note that (4.6) is equivalent to (4.2), and that (4.6) explicitly displays the form of the state-space averaged system. In particular, (4.6) could be rewritten in terms of a single *averaged* resistive hybrid n-port function, i.e.

$$x' = -\mathcal{H}_{avg}\{Q^{-1}(x)\} \tag{4.7}$$

where the form of $\mathcal{H}_{avg}(\bullet)$ is evident. The model (4.7) suggests the form of an averaged circuit synthesis, namely one that interconnects the original reactive n-port with a resistive n-port represented by $\mathcal{H}_{avg}(\bullet)$. If it is possible to synthesize a nonlinear resistive n-port with hybrid representation $\mathcal{H}_{avg}(\bullet)$, the question of average circuit existence is answered.

One of the interesting features of this approach to averaged circuit synthesis is that the structure of the reactive elements of the underlying circuit is preserved. The averaging is performed only on the resistive portion (including sources) of the circuit. This point will be brought out in the next section where a synthesis technique based on *in-place averaging* [46] is considered. Naturally, the approach here applies to circuits with time-varying sources and/or time-varying duty ratios. One would simply compute the averaged hybrid representation at each time instant. We now comment on some particular cases.

In the case where the non-reactive circuit elements include only passive linear resistances, independent sources, and switches, it is always possible to synthesize a circuit realization of $\mathcal{H}_{avg}(\bullet)$ using only passive linear resistive elements (including multiport transformers and gyrators) and independent sources [36]. Note that in this case, the hybrid function $\mathcal{H}_{avg}(\bullet)$ takes the form

$$\mathcal{H}_{avg}(x) = H_{avg}x + E_{avg}. \tag{4.8}$$

Methods for synthesizing a passive linear resistive network realizing H_{avg} are given in [36]. (Syntheses for linear, passive, resistive multiports were instrumental in [36] for the synthesis of dynamical, passive, LTI networks.) The constant

term E_{avg} in (4.8) can be realized by including appropriate sources in series and/or in parallel with the ports of the resistive network realizing H_{avg}. (Gyrators are only required in the case where nonreciprocal resistances are present.) In the more general case of nonlinear resistances, there is not a well known method for synthesizing a circuit realization of a given nonlinear hybrid representation. However, it is true that certain fundamental network properties that are common to each of the representations $\mathcal{H}_u(\bullet)$ are exhibited by the averaged hybrid representation $\mathcal{H}_{avg}(\bullet)$. For instance, if each of the resistive hybrid representations $\mathcal{H}_u(\bullet)$ is passive (respectively incrementally passive, reciprocal), then so is the average hybrid representation, and hence, so is a synthesis of $\mathcal{H}_{avg}(\bullet)$. (See Appendix A for definitions of these network properties.)

In the following section, we address the question of how one can synthesize an averaged circuit (namely the resistive portion of such a circuit), so that it is simply related to the underlying switched circuit.

4.2 Averaged Circuit Synthesis

Here, we develop a synthesis procedure for averaged circuit models using the method of *in-place averaging* pioneered by Wester and Middlebrook [46]. Our development will be rather broadbased at first, considering general nonlinear circuit elements, but will then focus on particular classes of circuits to ease the presentation. The in-place averaging method is outlined in the following paragraph.

The in-place averaging method is based on the application of the one-cycle averaging operation to each branch variable in a switched circuit, e.g.

$$\bar{i}(t) = \frac{1}{T}\int_{t-T}^{t} i(s)ds \tag{4.9}$$

for some branch current where the averaging interval T is selected to be equal to the fundamental period of the cyclic operation of the switches. A fundamental property of the resulting averaged branch variables is that these variables satisfy the same topological constraints (i.e. KCL and KVL) as in the non-averaged

circuit. This follows from the facts that the constraints imposed on the circuit branch variables by KCL and KVL are inherently linear algebraic constraints, and apply identically at each time instant. A first step in the synthesis of an averaged circuit is then to consider a circuit that is topologically equivalent to the underlying switched circuit. (For the present time, we can regard each switch as a two-terminal branch element. Later, the switch elements will be treated somewhat differently.) In order to complete the synthesis, we need to specify 'averaged' circuit elements that are consistent with the one-cycle averaged branch variables. We consider below the different types of circuit elements to clarify this procedure.

In the preceding section, we argued that if it is possible to obtain an averaged circuit model, such a model should include all the reactive elements of the underlying circuit. Here, we reconsider this, but from the viewpoint of inplace averaging. A nonlinear multiport capacitor can be represented by the state-space description (see Appendix A)

$$\begin{aligned} q' &= i \\ v &= f(q) \end{aligned} \tag{4.10}$$

where $f(\bullet)$ (assumed to be continuous) is the gradient of a scalar function, i.e. $f(q) = \nabla W(q)$ where $W(q)$ is the internal energy of the capacitor (to within an additive constant). Consider the application of the one-cycle averaging operation to this element, i.e.

$$\begin{aligned} \overline{q}(t) &= \frac{1}{T}\int_{t-T}^{t} q(s)ds \\ \overline{i}(t) &= \frac{1}{T}\int_{t-T}^{t} i(s)ds \\ \overline{v}(t) &= \frac{1}{T}\int_{t-T}^{t} v(s)ds. \end{aligned} \tag{4.11}$$

The averaging operation commutes with differentiation with respect to time since

$$\overline{q}'(t) = \frac{d}{dt}\frac{1}{T}\int_{t-T}^{t} q(s)ds = \frac{q(t)-q(t-T)}{T} = \frac{1}{T}\int_{t-T}^{t} q'(s)ds = \overline{q'(t)}, \tag{4.12}$$

and therefore, we have $\bar{q}' = \bar{i}$. In general $\bar{v} \neq f(\bar{q})$. However, because of the small ripple assumption and the continuity of $f(\bullet)$, this will be a good approximation (see the discussion in Chapter 2). For sufficiently small T, this approximation approaches equality arbitrarily closely. Since we are concerned with infinitesimally small T in the case of state-space averaging, it is an appropriate step in the construction of the averaged circuit model to include in the averaged circuit each nonlinear capacitor of the underlying circuit. An analogous argument applies for the nonlinear inductors. (Obviously, this argument is applicable to linear reactive elements.)

Let us note at this point that if it is possible to synthesize an averaged circuit via the method of in-place averaging, the resulting circuit will be a synthesis of the state-space averaged model. This follows from the facts that such a circuit will include all the reactive elements of the underlying circuit, and that the port variables of these elements will exhibit the one-cycle averaged waveforms. Therefore, the time derivatives of all inductor fluxes and all capacitor charges in the averaged circuit will coincide with those of the state-space averaged model that has as its state variables the fluxes and charges.

We have seen that the reactive elements do not pose any significant problems in the synthesis of an averaged circuit. However, the nonlinear resistive elements can present some difficulties. Assume that the constitutive relations for all nonlinear resistive elements are continuous, e.g. for a two-terminal resistor modeled by $v = r(i)$, the function $r(\bullet)$ is assumed to be continuous. In a given switched circuit, it is possible to identify two types of resistive branch elements: (i) those with continuous current or continuous voltage waveforms and (ii) those with discontinuities in both their current and their voltage waveforms. It is in the latter branch type that difficulties can arise. (Note that the switch branches can be thought of as elements of this type.)

To see that those resistive branch elements that have continuous current *and* continuous voltage waveforms present no difficulties, consider such a two-terminal resistor with constitutive relation $v = r(i)$. For such a resistor, the

approximation $\bar{v} \approx r(\bar{i})$ approaches an equality for infinitesimally small T. This is a consequence of the small ripple assumption and the continuity of $r(\bullet)$. Hence, the corresponding resistive element of the averaged circuit can be realized with a resistive component that is identical to that of the underlying circuit. This argument is applicable to a multiport resistor, as well. Any resistive branch that has a discontinuity in only one of its waveforms for all admissible operation must be a source, either independent or dependent. (If the element was not a source, the normally continuous waveform would necessarily exhibit a discontinuity for some discontinuity in the complementary waveform.) These source branches can be replaced with identical ones in the averaged circuit.

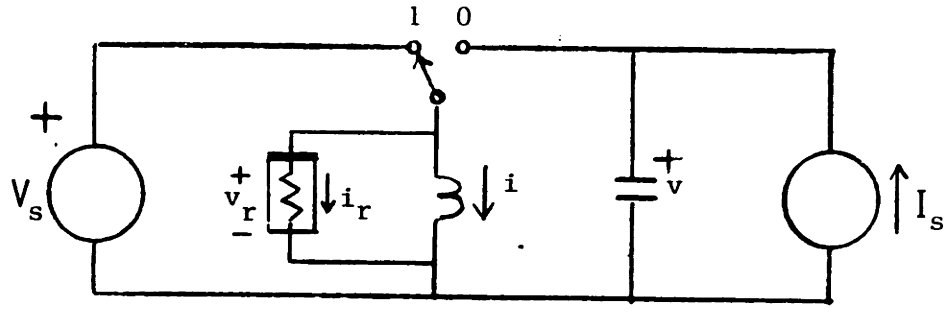

Figure 4.2: Switched Circuit that Violates Conditions for In-Place Averaging

In the case of nonlinear resistive branches that have discontinuities in both their current and voltage waveforms, there may not exist an approximate constitutive relation that is consistent with the one-cycle averaged waveforms. To see this, consider the up-down converter of Figure 4.2 that has a nonlinear resistor with relation $i = g(v)$, in parallel with the inductor. The average voltage across this resistor is given by

$$\bar{v}_r = (d)V_s + (1-d)\bar{v},$$

while the average current takes the form

$$\bar{i}_r = (d)g(V_s) + (1-d)g(\bar{v}).$$

It is clear that for this resistor $\bar{i}_r \neq g(\bar{v}_r)$, in general, and that there is no

general relationship between the average current and the average voltage. The relationship depends upon the particular values of the capacitor voltage and the voltage source voltage. Hence, for this example, it is not possible to construct an averaged circuit that simply replaces this two-terminal resistor with some other two-terminal element. Therefore, it is not possible in general to directly apply the in-place averaging procedure to switched circuits that contain nonlinear resistive elements that have discontinuities in both branch waveforms. Later, we shall demonstrate that it is typically possible to obtain averaged circuit models for switched circuits that violate this condition. We simply treat the nonlinear resistive branches that have discontinuous waveforms in the same manner as the switch branches are handled.

Note that any LTI resistive element can be replaced in the averaged model by an identical resistive element. This is a consequence of the fact that the one-cycle averaging operation commutes with any LTI constitutive relation. For the example above, if $g(\bullet)$ was linear, we would have obtained $\bar{i}_r = g(\bar{v}_r)$, despite the discontinuous waveforms.

Keeping the preceding discussion in mind, we can proceed to develop the in-place averaging synthesis technique. The crucial step in obtaining an averaged circuit synthesis is in modeling the elements that correspond to the switch branches. As mentioned earlier, it is possible to treat the switch branches as nonlinear resistive elements that have discontinuities in both their current and voltage waveforms. However, in our development, we shall treat the switch elements as being essentially different from the other circuit elements. This will facilitate the presentation, which will be divided into two subsections and one appendix (Appendix B). The first subsection will treat the case where all resistive elements are LTI and the circuit has one controlled switch pair (a two configuration circuit). The second subsection will consider the case where nonlinear resistive elements are present. Appendix B generalizes to the case where there are multiple switch configurations, but only LTI resistive elements.

4.2.1 Averaged Circuit Synthesis: LTI Resistive Elements, Ideal Sources, and One Controlled Switch

In this subsection, a rather simple and elegant result for a switched circuit with a single controlled switch will be demonstrated. However, the method to be used is not as rigorous as that of the following subsection (and Appendix B) since an assumption concerning the existence of a particular hybrid representation of a multiport network will be made. In Appendix B and in the following subsection, we give more general results on the synthesis of averaged circuits using constraint relations for multiports.

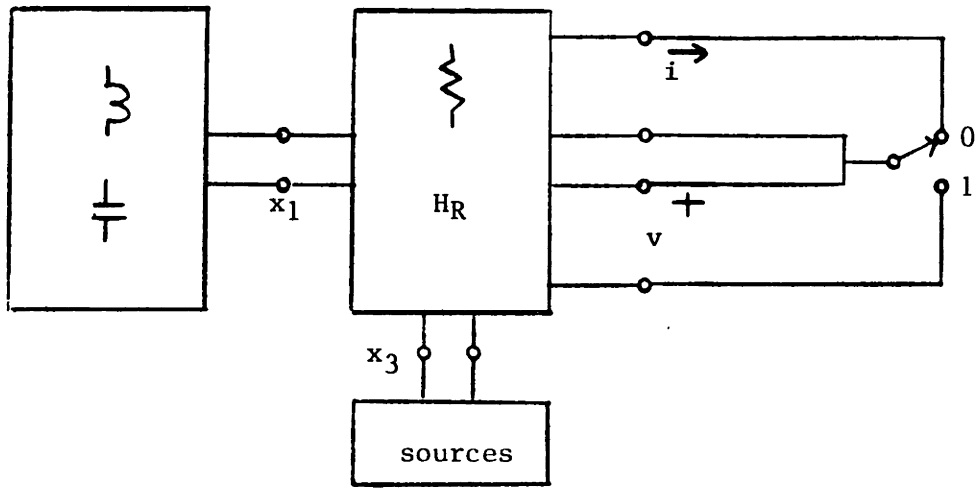

Figure 4.3: Partitioned Switching Converter

Here, we take an approach reminiscent of the method of reactance extraction [36] for impedance synthesis, where a given passive LTI circuit is partitioned into purely reactive and purely resistive multiports. However, the circuit diagram for a given switching converter will be partitioned further into reactive, resistive, source, and switch multiports as shown in Figure 4.3. It was already argued earlier in this section that an averaged circuit synthesis should include all the reactive elements, all the linear resistive elements, and all the source elements of the underlying switched circuit. The motivation for the partitioning in Figure 4.3 is to allow us to focus on the switch subnetwork, since it is no longer required to examine the internal behavior of any other subnetwork. All that remains is

to determine a resistive two-port network that can replace the switch two-port in Figure 4.3, and have the resulting circuit exhibit waveforms consistent with the one-cycle averaged waveforms of the underlying converter.

We proceed to derive a constitutive relation for a resistive two-port network that can replace the switch two-port in Figure 4.3. The derivation will demonstrate the existence of such a network. Assume that each branch voltage and current in the underlying switching converter circuit has a unique solution corresponding to each value of the state vector. In the approach outlined here, we shall require hybrid representations for some of the multiports of Figure 4.3. For this purpose, select the controlling port variables of the reactive multiport to be the inductor currents and the capacitor voltages (elements of vector x_1), the controlling port variables of the source multiport to be voltages for voltage sources and currents for current sources (elements of vector x_3), and select one of the two ports of the switch network to be current-controlled and the other to be voltage-controlled. The controlling variables of the two-port switch network form the vector x_2. Each port of the resistive multiport is designated to be of the same type (current- or voltage-controlled) as the port to which it is connected.

Next, let us determine the required hybrid representations for the multiports in the partitioned network. For the present, assume that for the selected set of controlling port variables, the resistive multiport has a well defined hybrid representation H_R. (This assumption is not generally valid, nor necessary for synthesis purposes as is demonstrated in Appendix B.) We partition H_R to reflect the three sets of ports to which it is connected, i.e.

$$H_R = \begin{bmatrix} H_{11} & H_{12} & H_{13} \\ H_{21} & H_{22} & H_{23} \\ H_{31} & H_{32} & H_{33} \end{bmatrix} \tag{4.13}$$

where the first set of ports are those connected to the reactive network, the second set consists of the ports connected to the switch network, and the third set corresponds to the ports connected to the source network. Now, for the two-port switch network, with the controlling variables and switch positions

$(u = 0, 1)$ indicated in Figure 4.3, we obtain for $u = 0$

$$H_s(0) = \begin{bmatrix} 0 & 0 \\ 0 & 0 \end{bmatrix}. \tag{4.14}$$

For $u = 1$, the hybrid representation is not well defined, but it is clear that the controlling port variables are constrained to be zero, i.e. $x_2 = 0$.

A first step in deriving the required constitutive relation is to determine the explicit solution for the vector of switch port variables for each switch configuration, i.e.

$$\begin{bmatrix} x_2|_u \\ y_2|_u \end{bmatrix},$$

where $x_2|_u$ is the vector of controlling port variables and $y_2|_u$ is the vector of complementary non-controlling port variables. (The subscript u indicates which switch configuration is present.) For this purpose, consider the application of the network constraints (KCL and KVL) at the switch ports, i.e.

$$H_{21}x_1 \;+\; [H_s(u) + H_{22}]x_2|_u \;+\; H_{23}x_3 \;=\; 0. \tag{4.15}$$

With (4.15) and the relations imposed by the hybrid model H_R for the resistive subnetwork in Figure 4.3, it is possible to solve for $x_2|_u$ and $y_2|_u$. In particular, for $u = 0$ we have

$$\begin{aligned} x_2|_{u=0} &= -H_{22}^{-1}[H_{21}x_1 + H_{23}x_3] \\ y_2|_{u=0} &= 0. \end{aligned} \tag{4.16}$$

The first line in (4.16) is obtained by noting that $H_s(0) = 0$ in (4.15), and that H_{22}^{-1} must exist, or else there would not exist an unique solution $x_2|_{u=0}$. The second line is a simple consequence of the fact that $H_s(0) = 0$, or equivalently, that $y_2|_{u=0}$ is constrained to be zero by the switch network. For $u = 1$, we obtain

$$\begin{aligned} x_2|_{u=1} &= 0 \\ y_2|_{u=1} &= H_{21}x_1 + H_{23}x_3 \end{aligned} \tag{4.17}$$

The first line in (4.17) is a consequence of the constraint imposed by the switch network, and the second line is obtained by considering the hybrid relationship for the resistive subnetwork.

With the above formulas for the switch port variables in each switch configuration, it is possible to determine the one-cycle averaged values for the switch port variables, i.e.

$$\begin{aligned} \bar{x}_2 &= (1-d)x_2|_{u=0} + (d)x_2|_{u=1} = -(1-d)H_{22}^{-1}w \\ \bar{y}_2 &= (1-d)y_2|_{u=0} + (d)y_2|_{u=1} = (d)w. \end{aligned} \tag{4.18}$$

where $w = [H_{21}x_1 + H_{23}x_3]$. Note that (4.18) gives an explicit parametrization of the subspace of $\mathcal{R}^4$ that contains the vector of one-cycle averaged switch port variables. This subspace is parametrized by the vector $w \in \mathcal{R}^2$. (This type of parametrization will be essential in the case where nonlinear resistive elements are present in the switched circuit.) In the actual operation of the circuit, the port variables may not attain any arbitrary point in the subspace parametrized by w in (4.18), since evidently w may not assume any arbitrary value in $\mathcal{R}^2$. For our purposes, it is adequate to characterize a two-port resistive network that constrains its port variables to lie in the defined subspace. Such a characterization is sufficient because it constrains the averaged switch port variables as required in the averaged circuit. It will be demonstrated that such a characterization will result in an averaged circuit that realizes the state-space averaged model.

A more familiar functional relationship can be obtained by elimination of w in (4.18), i.e.

$$\bar{y}_2 = -\frac{d}{1-d}H_{22}\bar{x}_2 \tag{4.19}$$

for $d \neq 1$. The relationship (4.19) suggests that the two-port switch network should be replaced in the averaged circuit by a resistive two-port with hybrid representation

$$H_s(d) = \frac{d}{1-d}H_{22} \tag{4.20}$$

for $d \neq 1$. (A sign reversal is required to account for the opposing polarities of the non-controlling port variables of the switch and resistive subnetworks in the original switched circuit.) *To obtain the averaged model, one therefore only*

needs to compute the hybrid immittance H_{22} seen by the switch two-port, and then determine a synthesis for a scaled version of this immittance function.

To see that the resulting averaged circuit model is a realization of the state-space averaged model, consider the following explicit solution for $\overline{y}_1$, the negative of the averaged vector of inductor voltages and capacitor currents (the non-controlling reactive port variables):

$$\begin{aligned} \overline{y}_1 &= H_{11}\overline{x}_1 + H_{12}\overline{x}_2 + H_{13}\overline{x}_3 \\ &= H_{11}\overline{x}_1 - (1-d)H_{12}H_{22}^{-1}[H_{21}\overline{x}_1 + H_{23}\overline{x}_3] + H_{13}\overline{x}_3 \end{aligned} \tag{4.21}$$

where the form of $\overline{x}_2$ in the second line of (4.21) is obtained from (4.18). The state-space averaged model can be obtained from (4.21) by simply writing

$$\overline{q}_1' = -\overline{y}_1 \tag{4.22}$$

since $\overline{y}_1$ can in turn be written in terms of $\overline{x}_1 = Q^{-1}(\overline{q}_1)$ and $\overline{x}_3$ using (4.21). This is readily verified to be the form of the state-space averaged model, by noting that it varies with d on the chord connecting the two extreme state-space models obtained by solving the network equations under $u = 0$ and $u = 1$. These two extreme models were assumed to be well defined at the outset.

Under the conditions mentioned above, we conclude that the two-port switch network in Figure 4.3 can be replaced by a linear resistive two-port so that the resulting network has the dynamical behavior of the state-space averaged model. Further, this linear resistive two-port is passive (reciprocal) if the resistive multiport H_R is also passive (reciprocal), since scaling a hybrid matrix by a positive real number preserves these properties. This result gives rise to a relatively simple approach to circuit-based analysis since one may use the non-switched average circuit model for analytical or computer-aided studies. There are many other ways to formulate the above problem by re-orienting the switch branches inside their two-port representation. We have used one of the possible orientations that leads to a relatively uncluttered result. The approach taken here for switched circuits with a single controlled switch can be generalized in a straightforward manner to switched circuits admitting more than two distinct switch

configurations. However, this development is omitted, since in Appendix B we present an alternative formulation that is applicable to the multi-switch case. The following subsection addresses the averaged circuit synthesis problem for the case where nonlinear resistive elements are present. The formulation used in the following subsection and in Appendix B is more rigorous since no assumptions concerning hybrid existence will be required. Before moving on, we study an example.

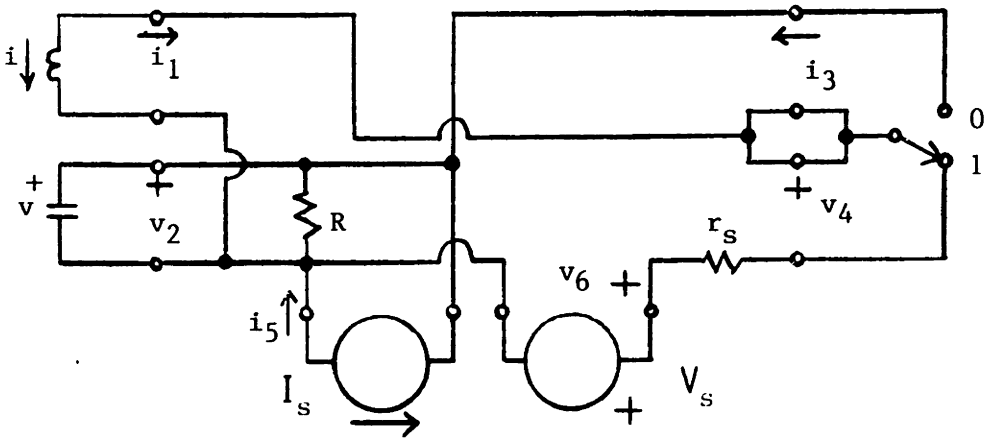

Figure 4.4: Partioning of Up-Down Converter with Source Resistance

Example: Up-Down Converter Figure 4.4 shows how we would partition a version of the up-down converter introduced in Chapter 2. This particular model includes parasitic resistance in series with the voltage source. It is straightforward to evaluate the immittance seen by the switch two-port:

$$H_{22} = \begin{bmatrix} r_s & -1 \\ 1 & 0 \end{bmatrix}. \tag{4.23}$$

To realize the resistive two-port that replaces the switch network, we synthesize a resistive two-port (see [36]) for $H_s(d) = \frac{d}{1-d} H_{22}$. The resulting averaged circuit is shown in Figure 4.5. Note that the averaged circuit includes one more two-terminal resistor than the original switched circuit. This 'extra' resistance is required to appropriately realize the one-cycle averaged behavior. Some previous work [45,46] on this problem resulted in averaged circuit models that did not include this resistance, but simply replaced the switch pair with an ideal

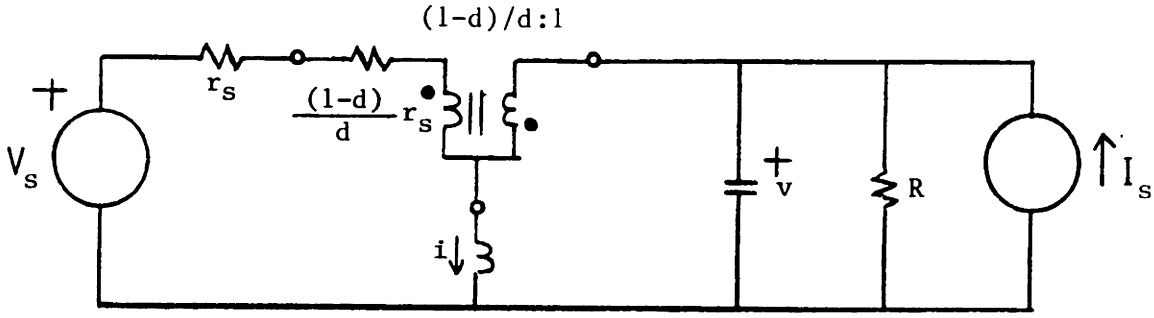

Figure 4.5: Averaged Circuit for Up-Down Converter with Source Resistance

transformer. Wester and Middlebrook [46] used a similar approach, but did not adequately model the averaged network required to replace the switch elements. Middlebrook and Cuk [23,44] synthesized averaged circuit models that included this resistance for certain example switched circuits, but their approach to averaged circuit synthesis was not as general as that given here.

Note that this averaged circuit can be used in applications where the duty ratio is a function of time (or other time-dependent variables) by inserting the appropriate time-varying value for d in the averaged circuit. One such application is in the simulation of a transient under a closed-loop control scheme.

•

4.2.2 Nonlinear Circuit Elements

Here we deal with the synthesis of a non-switched resistive network that can replace the switched resistive multiport in a partitioned switched circuit (see Figure 4.1) under more general conditions than considered in the previous subsection. In particular, nonlinear resistances (as well as nonlinear reactances) are permitted in the circuits to be considered. Our development will proceed along the lines of the in-place averaging method [46] outlined earlier in this section, and will rely on constraint relations (discussed below) for multiports whose internal behavior is not of interest. This will permit a simple replacement of the switch network in certain cases, as in the previous subsection, but when this is

not possible, we shall also consider replacement of a larger portion of the resistive network than that consisting of just the switch branches. In the interest of keeping the presentation uncluttered, we shall restrict attention to the case where there are only two distinct switch configurations. The extension to the case where there are more than two switch configurations can be treated in a straightforward manner, but will not be given here. See Appendix B for the multi-switch case where all resistive elements are linear.

A constraint relation is a rather general way to characterize a nonlinear (or linear) resistive multiport network. As an example, consider a two-terminal resistive element whose branch variables v and i are constrained by the element to lie on the unit circle in the $v - i$ plane, i.e. $v^2 + i^2 = 1$. Obviously, this element has neither a global current-controlled representation, nor a global voltage-controlled representation, and therefore illustrates the possible utility of the constraint representation. Constraint relations are also useful for LTI resistive multiport networks since it can be rather difficult to determine which subset of the port variables can serve as the controlling variables in a hybrid representation (see [47]). In general, the constraint relation for an n-port network takes the form

$$\mathcal{C}(x) = 0. \tag{4.24}$$

In the sequel, we shall consider only the case where the constraint relation (4.24) is continuous and possesses at least first partial derivatives, i.e. $\mathcal{C}(\bullet)$ is C^1. The constraint relation (4.24) is termed *regular* [81] if it imposes n independent constraints on the $2n$ components of x. That is, the Jacobian matrix

$$\left[\frac{d\mathcal{C}}{dx}\right]_{x_0}$$

has rank n at every x_0 that satisfies (4.24). The regularity condition essentially eliminates the possible presence of unusual network types such as norators and nullators. An equivalent way to characterize a nonlinear resistive network is with an explicitly parametrized manifold embedded in $\mathcal{R}^{2n}$ that contains the port variables. For the example above (the circular resistor), such a parametrization

takes the form

$$\begin{aligned} v &= sin(\sigma) \\ i &= cos(\sigma) \end{aligned} \tag{4.25}$$

where $\sigma \in [0, 2\pi)$. See [81] for more on this. This type of characterization will also be of use in our development.

To carry out the averaged circuit synthesis, we shall require the following three assumptions:

1. The state-space model for the switching converter is well defined in each switch configuration.

2. For each switch configuration and for any admissible state and source values, each branch voltage and current in the converter circuit has a unique solution.

3. All network constitutive relations are C^1.

Note that the first assumption is weaker than (but similar in nature to) the assumption of the preceding subsection concerning the existence of a particular hybrid representation for the resistive multiport in Figure 4.3.

We can now proceed to develop an averaged circuit synthesis procedure for those converters that do not contain nonlinear resistive branches having discontinuous current and discontinuous voltage waveforms. For these converters, we shall obtain a sufficient condition (necessary in the case where all the resistive elements in the switched circuit are reciprocal) for there to exist a non-switched resistive network that can replace the switch branches in the underlying converter, and maintain consistency with the in-place averaged circuit variables. Later, we treat the case where nonlinear resistive elements having discontinuous current and discontinuous voltage waveforms are present in the switching converter, by grouping these with the switches.

Case Where All Nonlinear Resistive Branches Have at Least One Continuous Branch Waveform

As previously discussed, in the synthesis of an averaged circuit model for a given switching converter, we would include all the reactive elements, all the linear resistive elements, and all the resistive branch elements which have a continuous current waveform, a continuous voltage waveform, or both waveforms continuous. Therefore, in the case where the converter has no nonlinear resistive branches with discontinuous current and discontinuous voltage waveforms, the only work to be done involves the switch branches. Our task is to determine if there is a non-switched resistive two-port that can be inserted in the place of the switch branches, and have the resulting averaged circuit exhibit the one-cycle averaged waveforms. Such a resistive two-port can be characterized by a constraint relation or an explicitly parametrized manifold, as discussed above. Now our development can follow along the lines of the preceding subsection, but with the various subnetworks of the switching converter modeled by constraint relations. We organize the relevant constraint relations for a switching converter below.

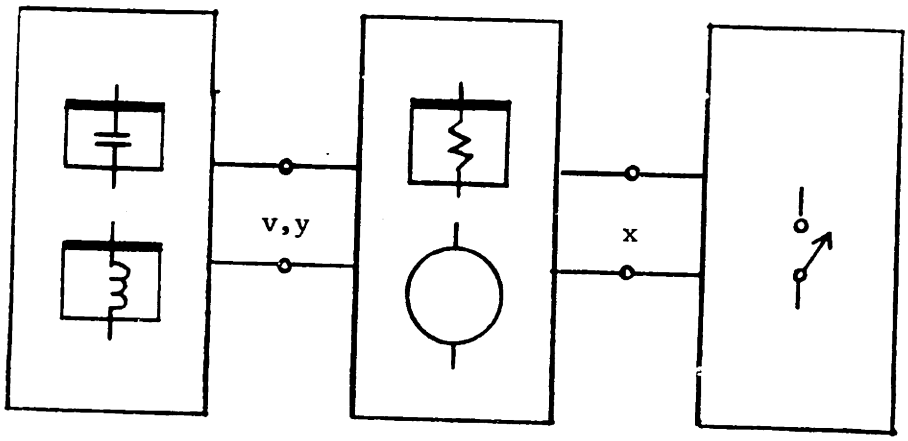

Figure 4.6: Partitioned Nonlinear Switched Network

Consider the partitioned switched circuit of Figure 4.6 where all sources are absorbed into the nonlinear resistive multiport. Let x denote the vector of switch port variables, v denote the vector of inductor currents and capacitor voltages, and y denote the vector of inductor voltages and capacitor currents.

We shall construct the constraint relation for the nonlinear resistive multiport in two stages. Firstly, denote the constraints imposed by this network on the switch port variables with the relation

$$\mathcal{C}_2(v, x) = 0 \tag{4.26}$$

where the vector of controlling reactive port variables v is viewed as a parameter. Secondly, let the constraints imposed by the resistive multiport on the reactive port variables (v, y) be written in the form

$$-y = \mathcal{C}_1(v, x). \tag{4.27}$$

This can be done by hypothesis since we have assumed that the state-space model for the switched circuit is well defined, and this necessitates an explicit solution of y, the vector of inductor voltages and capacitor currents. The constraint imposed by the switch multiport will be represented by the relation

$$\mathcal{C}s_u(x) = 0 \tag{4.28}$$

where the dependence upon the switch configuration is noted with the subscript u. The constraint imposed by the interconnection of the three multiport networks can be represented by the composite constraint relation

$$\begin{aligned} -y &= \mathcal{C}_1(v, x) \\ 0 &= \mathcal{C}_2(v, x) \\ 0 &= \mathcal{C}s_u(x). \end{aligned} \tag{4.29}$$

The composite constraint relation (4.29) determines the state-space model since for each value of v, this constraint determines a unique value of y. Further, this set of constraints uniquely determines the vector x of switch variables for each value of v.

With the in-place averaging method, the one-cycle averaged switch variables take the form

$$\overline{x} = d\,x|_{u=1} + (1-d)x|_{u=0} \tag{4.30}$$

where $x|_u$ is the value of the vector of switch branch variables when the switch configuration is u. Since, by hypothesis, each branch variable in the circuit is well defined for each switch configuration, we can determine the functional form of $x|_u$ in terms of the vector v from the constraints (4.29), i.e.

$$x|_u = g_u(v). \tag{4.31}$$

We conclude that the averaged switch vector $\bar{x}$ assumes the functional form

$$\bar{x} = g_d(\bar{v}) = d\,g_1(\bar{v}) + (1-d)g_0(\bar{v}). \tag{4.32}$$

Now we require conditions under which we can characterize a manifold in which the vector $\bar{x}$ is constrained to lie. Such a characterization can be made implicitly via a constraint relation, i.e.

$$\mathcal{C}s_d(\bar{x}) = 0, \tag{4.33}$$

or with an explicit parametrization. Recall that in the previous subsection where we considered the case in which the resistances were linear, this manifold was a subspace of $\mathcal{R}^4$.

A sufficient condition for the construction of an explicit characterization of the manifold in which the averaged switch vector $\bar{x}$ must lie is that the function $\mathcal{C}_2(v,x)$ that appears in the second constraint of (4.29) is separable into two additive terms, i.e.

$$0 = \mathcal{C}_2(v,x) = \mathcal{C}_{2v}(v) + \mathcal{C}_{2x}(x). \tag{4.34}$$

Note that the representation for $\mathcal{C}_2(v,x)$ is not unique, and the separability property may depend upon the particular choice for this representation. However, our statement holds as long as there exists some representation $\mathcal{C}_2(v,x)$ that is separable. This separability condition is necessary as well as sufficient in the case where all resistances in the circuit are reciprocal. We shall consider the necessity after demonstrating the sufficiency ot this condition. To demonstrate that this condition is sufficient, we shall give a procedure for characterizing the desired manifold. Begin by forming the two functions $g_0(\bullet)$ and $g_1(\bullet)$ which give

the explicit solution x for each value of v. Note that these functions take the form (for $u = 0, 1$)

$$g_u(v) = \mathcal{D}_u^{-1}\left(\begin{bmatrix} w \\ 0 \end{bmatrix}\right) \tag{4.35}$$

where

$$\mathcal{D}_u(x) = \begin{bmatrix} \mathcal{C}_{2x}(x) \\ \mathcal{C}s_u(x) \end{bmatrix} \tag{4.36}$$

and $w = -\mathcal{C}_{2v}(v)$. Next, compute the function $g_d(\bullet)$ according to (4.32) which takes the form

$$g_d(\overline{v}) = \tilde{g}_d(\overline{w}) = \mathcal{D}_d^{-1}\left(\begin{bmatrix} \overline{w} \\ 0 \end{bmatrix}\right) = \{(1-d)\mathcal{D}_0^{-1} + (d)\mathcal{D}_1^{-1}\}\left(\begin{bmatrix} \overline{w} \\ 0 \end{bmatrix}\right). \tag{4.37}$$

The image of $\tilde{g}_d(\bullet)$ where $\overline{w}$ ranges over $\mathcal{R}^2$ (more properly the subset of $\mathcal{R}^2$ where $\tilde{g}_d(\bullet)$ is well defined) is typically a two dimensional manifold embedded in $\mathcal{R}^4$. This is certainly true for the extreme cases $d = 0, 1$. For those values of d for which this holds true, we obtain an explicit parametrization of the two dimensional manifold in which the vector $\overline{x}$ of averaged switch port variables must lie. In many cases, it is possible to determine a global implicit representation for this two dimensional manifold of the form (4.33) by eliminating the parameter $\overline{w}$ in (4.37). We illustrate this procedure with an example, and then discuss the necessity of the separability condition for obtaining an explicit characterization of the constraint manifold.

Example: Up-Down Converter with Nonzero Source Impedance The purpose of this example is only to illustrate the procedure for constructing the constitutive relation for the vector of averaged switch variables. We use the example of Figure 4.7, previously considered in Subsection 4.2.1, although it only contains linear resistive elements. We shall give a more interesting example when we consider synthesis procedures for circuits that have nonlinear resistances with discontinuous waveforms. For the circuit of Figure 4.7, we obtain the following constraint relations imposed by the resistive portion of the circuit, including the sources:

$$-i_C = -I_s + i_{s2}$$

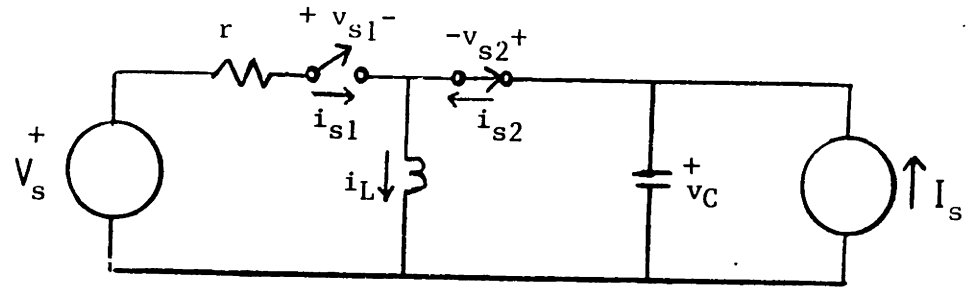

Figure 4.7: Up-Down Converter with Nonzero Source Impedance

$$\begin{aligned} -v_L &= -v_C + v_{s2} \\ 0 &= i_L - i_{s1} - i_{s2} \\ 0 &= V_s - v_C - v_{s1} - r i_{s1} + v_{s2}. \end{aligned} \tag{4.38}$$

As is evident from the final two lines of (4.38), this example satisfies the sufficient condition given above. These two lines can be recast in the form

$$\begin{aligned} i_{s1} + i_{s2} &= i_L = w_1 \\ v_{s1} + r i_{s1} - v_{s2} &= V_s - v_C = w_2 \end{aligned} \tag{4.39}$$

To proceed, we form the constraint relations imposed by the switch network:

$$\begin{aligned} \mathcal{C}s_0 \ &: \ i_{s1} = 0 \\ & \quad v_{s2} = 0 \end{aligned} \tag{4.40}$$

$$\begin{aligned} \mathcal{C}s_1 \ &: \ v_{s1} = 0 \\ & \quad i_{s2} = 0. \end{aligned} \tag{4.41}$$

Next form the two functions $\mathcal{D}_0^{-1}(\bullet)$ and $\mathcal{D}_1^{-1}(\bullet)$ by combining (4.39) and (4.40) and by combining (4.39) and (4.41), respectively. We obtain

$$\mathcal{D}_0^{-1}(\bullet) \ : \ i_{s1} = 0$$

$$
\begin{aligned}
v_{s1} &= w_2 \\
i_{s2} &= w_1 \\
v_{s2} &= 0
\end{aligned} \tag{4.42}
$$

$$
\begin{aligned}
\mathcal{D}_1^{-1}(\bullet) \;:\; & i_{s1} = w_1 \\
& v_{s1} = 0 \\
& i_{s2} = 0 \\
& v_{s2} = -w_2 + r w_1 .
\end{aligned} \tag{4.43}
$$

The function

$$
\mathcal{D}_d^{-1}(w_1, w_2) = (1-d)\mathcal{D}_0^{-1}(w_1, w_2) + (d)\mathcal{D}_1^{-1}(w_1, w_2)
$$

gives an explicit parametrization of the desired two dimensional manifold in terms of the parameters w_1 and w_2. This function takes the form

$$
\begin{aligned}
i_{s1} &= (d) w_1 \\
v_{s1} &= (1-d) w_2 \\
i_{s2} &= (1-d) w_1 \\
v_{s2} &= (d)(-w_2 + r w_1).
\end{aligned} \tag{4.44}
$$

The characterization (4.44) in terms of the variables w_1 and w_2 is an adequate representation of the two-dimensional manifold (vector space here) to which the average switch variables are constrained. However, it is possible to eliminate the parameters by combining the lines of (4.44) to obtain an implicit representation of the manifold, i.e. a constraint relation. The constraint relation takes the form

$$
\begin{aligned}
(1-d) i_{s1} - (d) i_{s2} &= 0 \\
(d) v_{s1} + (1-d) v_{s2} - (1-d) r i_{s1} &= 0.
\end{aligned} \tag{4.45}
$$

Now a synthesis of a two-port realizing the constraint (4.45) can be obtained in various ways, but we shall omit any further details since this example was already treated in Subsection 4.2.1. The objective here was to demonstrate a method for characterizing a constraint manifold. •

Necessity of Separability Condition In the case where the resistive subnetwork obtained by extracting the reactive and switch multiports is reciprocal, the separability condition given above is necessary as well as sufficent for the existence of a constraint manifold in which the vector of averaged switch port variables must lie. This is demonstrated here. We begin by obtaining a simple necessary condition on the first constraint of the composite constraint relation (4.29), i.e. $-y = \mathcal{C}_1(v, x)$.

It turns out that $\mathcal{C}_1(\bullet, \bullet)$ must be linear in its second argument. This is a consequence of the fact that the state-space averaged model for duty ratio d can be expressed in terms of the variable y via

$$\overline{q}' = \overline{y} = -(1-d)\mathcal{C}_1\{\overline{v}, g_0(\overline{v})\} - (d)\mathcal{C}_1\{\overline{v}, g_1(\overline{v})\} \tag{4.46}$$

and equivalently by

$$\overline{q}' = \overline{y} = -\mathcal{C}_1\{\overline{v}, (d)g_1(\overline{v}) + (1-d)g_0(\overline{v})\} \tag{4.47}$$

where q is the vector of inductor fluxes and capacitor charges. Equation (4.46) results by forming a convex combination of the two extreme state-space models, while (4.47) is obtained by substituting the form of the averaged switch port vector $\overline{x}$ into the first line of (4.29). The separability condition on the second constraint of (4.29) is a consequence of this condition and the reciprocity of the resistive network modeled by the first two lines of (4.29).

To see this, consider the manifold determined by the second constraint of the constraint relation (4.29). Recall that this is the manifold to which the vector of switch port variables is constrained by the resistive subnetwork, with the vector v of controlling reactive port variables viewed as a constant parameter. At any given point in the configuration space, such a manifold must locally have at least one hybrid description of the form

$$x_2 = h(v, x_1) \tag{4.48}$$

where the dependence on the parameter vector v is noted explicitly. (This follows from the analogous property of linear resistive networks [82,83]. The tangent

space of the constraint manifold at the point (x_1, x_2) is a local approximation to this manifold.) With these coordinates, we can obtain a hybrid representation (at least locally) for the resistive network described by the first two constraints in (4.29). Such a representation takes the form

$$\begin{aligned} -y &= \tilde{C}_1(v, x_1) = C_1\{v, (x_1, x_2)\} \\ x_2 &= h(v, x_1). \end{aligned} \tag{4.49}$$

Now the hybrid relation (4.49) must retain the property that the first line involving the variable y is linear in x, or x_1 in this case. The reciprocity of the resistive network implies that the Jacobian matrix for this hybrid representation has certain symmetry properties, as discussed in Appendix A. In particular, this Jacobian H must satisfy

$$H\Sigma = \Sigma H^* \tag{4.50}$$

where Σ is a diagonal (signature) matrix with all its diagonal elements either $+1$ or -1. Consider partitioning the relationship (4.50) commensurately with the two sets of ports, i.e.

$$\begin{bmatrix} \tilde{C}_{1v} & \tilde{C}_{1x} \\ h_v & h_x \end{bmatrix} \begin{bmatrix} \Sigma_1 & 0 \\ 0 & \Sigma_2 \end{bmatrix} = \begin{bmatrix} \Sigma_1 & 0 \\ 0 & \Sigma_2 \end{bmatrix} \begin{bmatrix} \tilde{C}_{1v}^* & h_v^* \\ \tilde{C}_{1x}^* & h_x^* \end{bmatrix}. \tag{4.51}$$

An implication of this symmetry constraint is that

$$\tilde{C}_{1x}\Sigma_2 = \Sigma_1 h_v^*. \tag{4.52}$$

Because of the linearity of $\tilde{C}_1(\bullet, \bullet)$ in its second argument, the corresponding entry of the Jacobian matrix, i.e. $\tilde{C}_{1x}$, is not dependent on x_1 (or x). The symmetry constraint (4.52) guarantees that h_v is also independent of x_1, i.e.

$$\frac{d}{dx_1} h_v = 0.$$

A consequence of this is that $h(v, x_1)$ which appears in (4.49) can be expressed as the sum of two additive terms, namely as

$$h(v, x_1) = h^v(v) + h^x(x_1).$$

(This can be seen by considering the first two terms in a Taylor series expansion for $h(v, x_1)$.) The result is the separability condition above.

Next, we shall consider synthesis of averaged circuit realizations for switched circuits that contain nonlinear resistances with discontinuous current and voltage waveforms.

Switched Circuits Containing Nonlinear Resistances with Discontinuous Waveforms

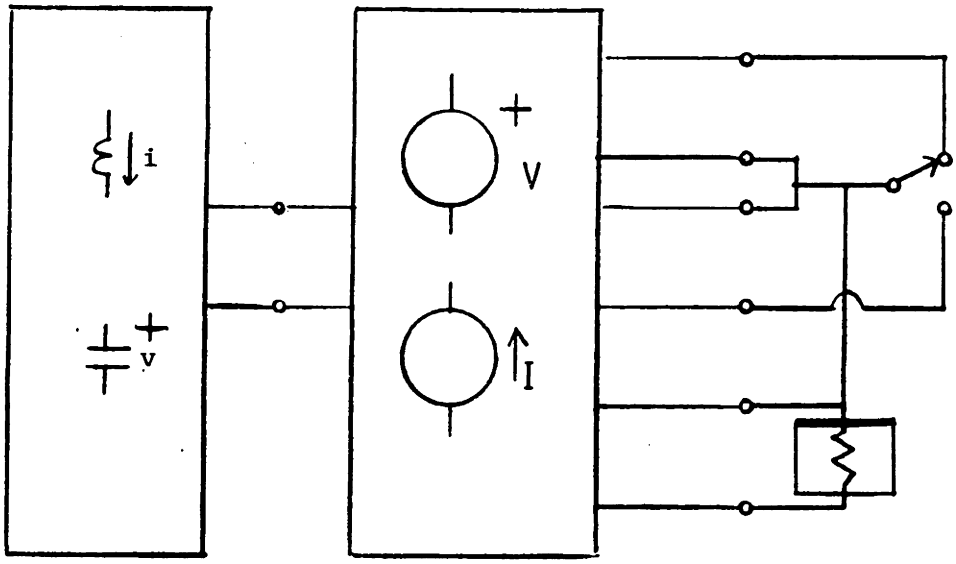

Figure 4.8: Partitioned Converter

Earlier in this subsection, we illustrated the difficulty that arises from nonlinear resistive branches that have discontinuities in both current and voltage waveforms. We noted that these resistive branches could not be simply treated with the in-place averaging scheme. However, it is possible to extract these resistive branches, and to lump them into a multiport network with the switch branches. With this modified partitioning, the result based on the separability condition carries over, as could be shown with an analogous argument. Rather than repeating the details, we study some examples.

Note that in the case where a nonlinear multiport resistor is present in the switched circuit, and only a subset of its ports have both discontinuous current and discontinuous voltage waveforms, it may be advantageous to extract the

entire multiport resistor and to include it with switch network. If this was not done, it may turn out the separability condition does not hold. Of course, one could first check to see if the separability did hold when only some of the resistive branches were extracted. In any case, the presence of a nonlinear multiport resistor in a switching converter is not at all common, and we shall not study any examples of this type.

Examples: Converters with Nonlinear Elements having Discontinuous Waveforms For the example of Figure 4.2 given in the beginning of this subsection, we would partition the circuit as shown in Figure 4.8. We would then apply the procedure given above, but with the three-port network playing the role of the extracted switch network. It turns out that for this example the necessary computations are extremely difficult, and so we shall treat an easier one. In some cases, it is possible to lump the nonlinear resistive branches that have discontinuous waveforms with the switch network, but without increasing the number of ports of this network. Such an example is the up-down converter with nonlinear source resistance that is shown in Figure 4.9. For the circuit of

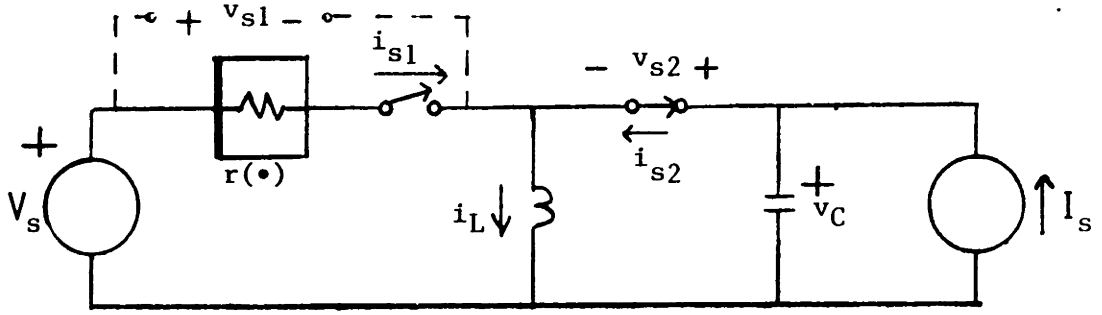

Figure 4.9: Up-Down Converter with Nonlinear Source Resistance

Figure 4.9, we can lump the nonlinear source resistance with its series switch branch. This is illustrated in the figure. With the modified port variables, we obtain the following constraint relation imposed by the remainder of the circuit:

$$-i_C = -I_s + i_{s2}$$

$$\begin{aligned} -v_L &= -v_C + v_{s2} \\ 0 &= i_L - i_{s1} - i_{s2} \\ 0 &= -V_s + v_C + v_{s1} - v_{s2}. \end{aligned} \tag{4.53}$$

The first two lines in (4.53) form the constraint $-y = C_1(v, x)$. The last two lines of (4.53) form the constraint relation $0 = C_2(v, x)$ which can clearly be expressed in the form $C_{2x}(x) = -C_{2v}(v) = w$, as follows:

$$\begin{aligned} i_{s1} + i_{s2} &= i_L = w_1 \\ v_{s1} - v_{s2} &= V_s - v_C = w_2. \end{aligned} \tag{4.54}$$

To proceed, we form the constraint relations imposed by the modified switch network:

$$\begin{aligned} Cs_0 \ : \ & i_{s1} = 0 \\ & v_{s2} = 0 \end{aligned} \tag{4.55}$$

$$\begin{aligned} Cs_1 \ : \ & v_{s1} - r(i_{s1}) = 0 \\ & i_{s2} = 0. \end{aligned} \tag{4.56}$$

Next, form the two functions $\mathcal{D}_0^{-1}(\bullet)$ and $\mathcal{D}_1^{-1}(\bullet)$ by combining (4.54) and (4.55) and by combining (4.54) and (4.56), respectively. We obtain

$$\begin{aligned} \mathcal{D}_0^{-1}(\bullet) \ : \ & i_{s1} = 0 \\ & v_{s1} = w_2 \\ & i_{s2} = w_1 \\ & v_{s2} = 0 \end{aligned} \tag{4.57}$$

$$\begin{aligned} \mathcal{D}_1^{-1}(\bullet) \ : \ & i_{s1} = w_1 \\ & v_{s1} = r(w_1) \\ & i_{s2} = 0 \\ & v_{s2} = -w_2 + r(w_1). \end{aligned} \tag{4.58}$$

The function

$$\mathcal{D}_d^{-1}(w_1, w_2) = (1-d)\mathcal{D}_0^{-1}(w_1, w_2) + (d)\mathcal{D}_1^{-1}(w_1, w_2)$$

gives an explicit parametrization of the desired two dimensional manifold in terms of the parameters w_1 and w_2. This function takes the form

$$\begin{aligned} i_{s1} &= (d)w_1 \\ v_{s1} &= (1-d)w_2 + (d)r(w_1) \\ i_{s2} &= (1-d)w_1 \\ v_{s2} &= (d)(-w_2 + r(w_1)). \end{aligned} \tag{4.59}$$

By combining the lines of (4.59), we can eliminate the parameters w_1 and w_2 to obtain a representation for this manifold with a constraint relation, i.e.

$$\begin{aligned} 0 &= (1-d)i_{s1} - (d)i_{s2} \\ 0 &= (1-d)v_{s2} + (d)v_{s1} - (d)r\left(\frac{i_{s1}}{d}\right). \end{aligned} \tag{4.60}$$

We can obtain an equivalent hybrid representation for the resistive network described by (4.60) as follows:

$$\begin{aligned} i_{s2} &= \frac{1-d}{d} i_{s1} \\ v_{s1} &= -\frac{1-d}{d} v_{s2} + r\left(\frac{i_{s1}}{d}\right). \end{aligned} \tag{4.61}$$

The hybrid representation suggests a synthesis involving an ideal transformer and a two terminal nonlinear resistor. This synthesis is shown in Figure 4.10.

• The following example shows how to apply our method to obtain an averaged circuit model for a converter operating in the discontinuous conduction mode. This problem was addressed in the paper of Cuk and Middlebrook [68] using the so-called 'hybrid modeling' technique, which apparently proceeds by inspection. Our approach is somewhat more systematic.

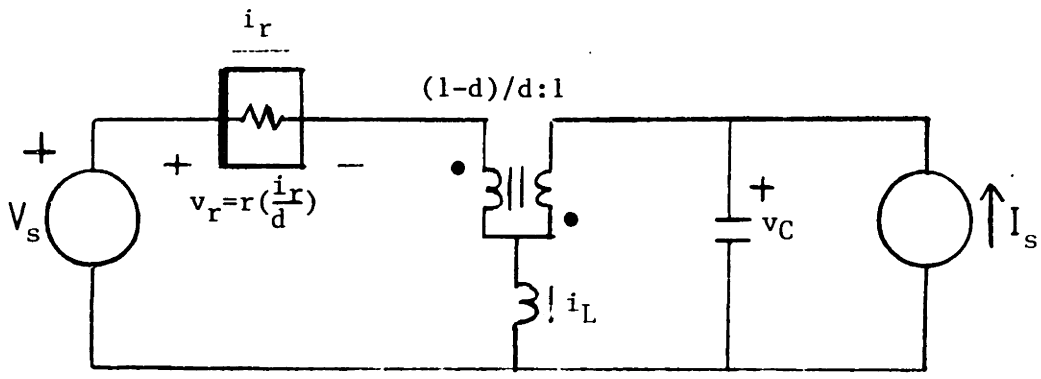

Figure 4.10: Average Circuit Realization for Up-Down Converter with Nonlinear Source Resistance

Example: Converter Operating in the Discontinuous Conduction Mode

Consider the up-down converter and the typical inductor current waveform for operation in the discontinuous conduction mode shown in Figure 4.11. The other state varible waveforms exhibit relatively small ripple, and so are not shown. The diode in the figure is necessary to capture the circuit behavior in the discontinuous conduction mode. If the diode was not present, the L_1 inductor current could reverse, violating a basic constraint for this circuit (that this inductor current remains nonnegative at all times). In order to apply any averaged circuit synthesis technique for such a circuit, we need to recognize that a switching converter operating in the discontinuous conduction mode is governed by a reduced order state-space averaged model. This is a consequence of the fact that the L_1 inductor current is identically zero during a portion of each cycle. Therefore, in our scheme, we would treat this inductor as a nonlinear resistive element. We depart slightly from our usual framework because the waveforms for the L_1 inductor are so different from those of other resistive elements that typically appear in a converter. Even though this inductor has a continuous current waveform, we lump it with switch branches and diode into a modified two-port switch network as shown in Figure 4.11. (If this was not done, it would not be possible to obtain an averaged circuit model.) With the indicated partitioning, it is now straightforward to apply our procedure.

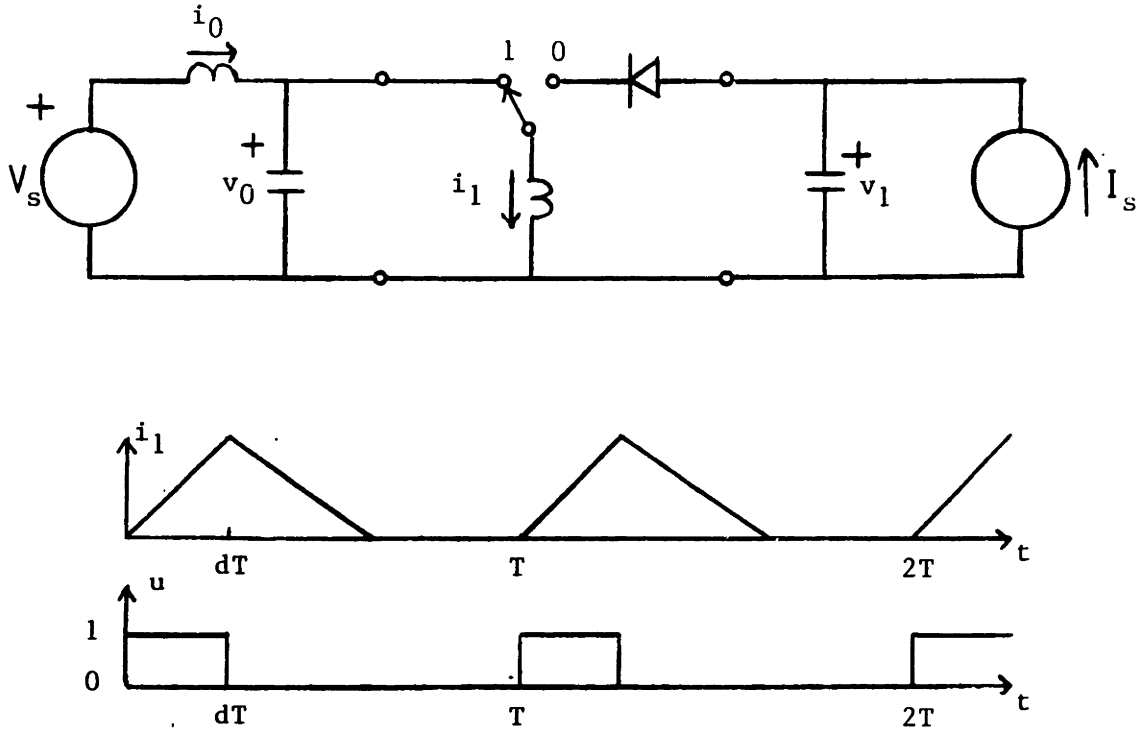

Figure 4.11: Model and Waveforms for Discontinuous Conduction Mode of Up-Down Converter

The constraint $\mathcal{C}_2(v,x) = 0$ takes the form

$$\begin{aligned} v_{s1} - v_0 &= 0 \\ v_{s2} - v_1 &= 0. \end{aligned} \tag{4.62}$$

This constraint clearly satisfies the separability condition, and can easily be expressed in the form $\mathcal{C}_{2x}(x) = -\mathcal{C}_{2v}(v) = w$ as follows

$$\begin{aligned} v_{s1} &= v_0 = w_1 \\ v_{s2} &= v_1 = w_2. \end{aligned} \tag{4.63}$$

The next step is to obtain the constraints imposed by the extracted and modified switch network for each of the two switch configurations. Since the inductor current i_1 varies significantly over each cycle, we shall compute an averaged constraint for each of the two configurations. When the switch is in the 0

position during an interval $[t_j, t_j + dT)$, the current $i_{s2} = 0$ and the current i_{s1} is equal to the L_1 inductor current. The average value of the latter current over this interval can readily be seen to be $\frac{v_0 dT}{2L_1}$ from the form of the waveform in Figure 4.11. Hence, we obtain the averaged constraint for this interval as

$$\begin{aligned} \mathcal{C}s_0 \quad : \quad & i_{s1} - \frac{v_{s1} dT}{2L_1} = 0 \\ & i_{s2} = 0. \end{aligned} \tag{4.64}$$

With a similar calculation for the interval $[t_j + dT, t_j + T)$ when the switch is in the 1 position, we obtain

$$\begin{aligned} \mathcal{C}s_1 \quad : \quad & i_{s1} = 0 \\ & i_{s0} + \frac{v_{s1}^2 d^2 T}{2v_{s2} L_2 (1-d)} = 0. \end{aligned} \tag{4.65}$$

Next, we form the two funtions $\mathcal{D}_0^{-1}(\bullet)$ and $\mathcal{D}_1^{-1}(\bullet)$ by combining (4.63) and (4.64) and by combining (4.63) and (4.65), respectively.

$$\begin{aligned} \mathcal{D}_0^{-1}(\bullet) \quad : \quad & v_{s1} = w_1 \\ & v_{s2} = w_2 \\ & i_{s1} = \frac{w_1 dT}{2L_1} \\ & i_{s2} = 0 \end{aligned} \tag{4.66}$$

$$\begin{aligned} \mathcal{D}_1^{-1}(\bullet) \quad : \quad & v_{s1} = w_1 \\ & v_{s2} = w_2 \\ & i_{s1} = 0 \\ & i_{s2} = -\frac{w_1^2 d^2 T}{2w_2 L_1 (1-d)} \end{aligned} \tag{4.67}$$

We can then form the function $\mathcal{D}_d^{-1}(w_1, w_2)$ as in the previous example, i.e.

$$\begin{aligned} \mathcal{D}_d^{-1}(\bullet, \bullet) \quad : \quad & v_{s1} = w_1 \\ & v_{s2} = w_2 \\ & i_{s1} = \frac{w_1 d^2 T}{2L_1} \\ & i_{s2} = -\frac{w_1^2 d^2 T}{2w_2 L_1}. \end{aligned} \tag{4.68}$$

The function $\mathcal{D}_d^{-1}(w_1, w_2)$ gives an explicit parametrization of the manifold in which the modified switch port variables are constrained to lie. It is possible to obtain a voltage controlled representation for this two-port network by eliminating w_1 and w_2 in (4.68). This representation takes the form

$$\begin{aligned} i_{s1} &= \frac{v_{s1} d^2 T}{2L_1} \\ i_{s2} &= -\frac{v_{s1}^2 d^2 T}{2 v_{s2} L_1}. \end{aligned} \tag{4.69}$$

With this type of representation for a resistive two-port network that replaces the modified switch network in Figure 4.11, we readily obtain the averaged circuit representation shown in Figure 4.12.

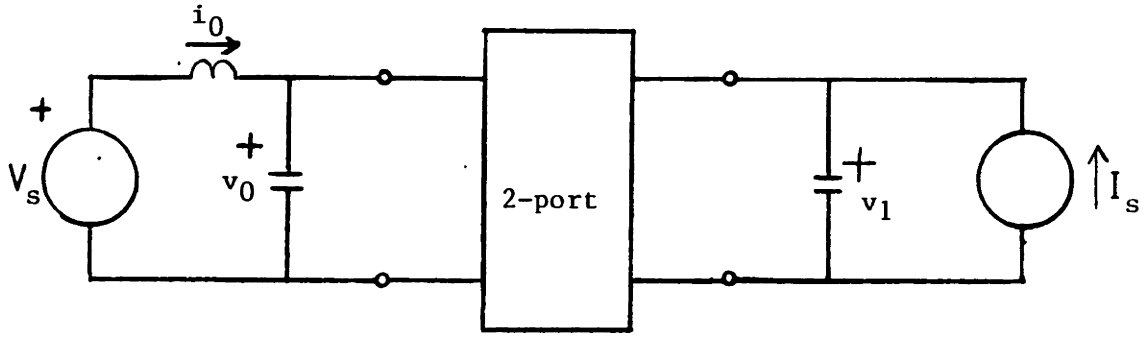

Figure 4.12: Averaged Circuit Model for Discontinuous Conduction Mode

It is of interest that the resistive two-port model (4.69) is an incrementally passive model. This can be seen by evaluating the Jacobian matrix for this model, i.e.

$$\begin{bmatrix} \frac{di_s}{dv_s} \end{bmatrix} = \begin{bmatrix} \frac{d^2 T}{2L_1} & 0 \\ -\frac{v_{s1} d^2 T}{v_{s2} L_1} & \frac{v_{s1}^2 d^2 T}{2 v_{s2}^2 L_1} \end{bmatrix}. \tag{4.70}$$

This Jacobian matrix is evidently positive semi-definite (where it is well defined), leading to the conclusion that the two-port is incrementally passive. This fact will be of some importance in Chapter 5 (Section 5.6) where we consider control design for this converter operating in the discontinuous conduction mode.

4.3 Open-Loop Stability of Switching Converters

In this section, switching converter systems (understood to include source and load) that consist of an interconnection of ideal DC sources, ideal switches, incrementally passive resistors, and linear reactive elements that are strictly relatively passive (see Appendix A) are considered. Multiport circuit elements are included in the development here. This class of switching converters is shown to be stable by exhibiting a Lyapunov function that corresponds to the *energy in the increment* with respect to an arbitrary, nominal state trajectory. The argument is extended to include nonlinear reactive elements that are strictly relatively passive in the case where the switching frequency becomes infinite, and stability with respect to an equilibrium point is considered. Essential background on network theoretic issues for the development in this section is given in Appendix A.

To motivate this work, we first present an example of a periodic time-varying system in which the system switches between two stable linear, time-invariant models. This example system exhibits unstable behavior. We shall be able to contrast this example with the result to be obtained for switching converter circuits.

Example of an Unstable Switched System Consider the periodically time-varying linear system

$$x' = A(t)x \tag{4.71}$$

with period $T = 0.1$, and where for each integer k

$$\begin{aligned} A(t) = A_0 &= \begin{bmatrix} -1 & 10 \\ 0 & -1 \end{bmatrix}, \quad kT \le t < (k+0.5)T \\ A(t) = A_1 &= \begin{bmatrix} -1 & 0 \\ 10 & -1 \end{bmatrix}, \quad (k+0.5)T \le t < (k+1)T \end{aligned} . \tag{4.72}$$

The stability of such a system can be assessed by examining the eigenvalues of the transition matrix for one period of operation, i.e. the eigenvalues of

$\Phi(T,0) = exp(0.5A_1T)exp(0.5A_0T)$. Here, we have

$$\Phi(T,0) = \begin{bmatrix} 0.9048 & 0.4524 \\ 0.4524 & 1.1310 \end{bmatrix}. \tag{4.73}$$

The eigenvalues of the transition matrix are approximately 1.48 and 0.55; since one of these is outside the unit circle, the conclusion is that the system is unstable. Note that this instability results despite the fact that each of the two matrices A_0 and A_1 is asymptotically stable.

Another route for this analysis is via the method of state-space averaging in which we would have assessed the stability properties of the average system matrix $A_{avg} = [(1/2)A_0 + (1/2)A_1]$. The eigenvalues of the average matrix A_{avg} are computed to be 4 and -6, leading to the conclusion that the averaged system is unstable. In this case, we observe that the average of two asymptotically stable matrices is an unstable matrix. In the remainder of this section, we examine the stability properties of periodically switched circuits, and investigate the special features that permit relatively strong conclusions on the stability of these systems. •

4.3.1 Switching Converter Stability Under Finite Switching Frequency

Let the switching converter be composed of ideal DC sources, ideal switches, incrementally passive resistors, and linear reactive elements that are **strictly** relatively passive. We suppose the switches are operated in accord with a given arbitrary switching pattern and suppose that we are given a nominal solution corresponding to the given switching pattern.

For each branch of the network, denote the nominal trajectory by $\{\tilde{v}(t), \tilde{i}(t)\}$, and form the (not necessarily small) *increments* with respect to the nominal trajectory for each network branch, i.e.

$$\begin{aligned} \delta i(t) &= i(t) - \tilde{i}(t) \\ \delta v(t) &= v(t) - \tilde{v}(t) \end{aligned} \tag{4.74}$$

By applying Tellegen's theorem to the increments in all the network branches when the circuit is in any one of its topologies, we obtain

$$0 = \sum_{DC sources} \delta i\, \delta v + \sum_{Switches} \delta i\, \delta v + \sum_{Res.} \delta i\, \delta v + \sum_{Ind.} \delta i\, \delta v + \sum_{Cap.} \delta i\, \delta v \qquad (4.75)$$

The summation involving DC sources is always zero since the increment in either voltage or current of each term is necessarily zero. The terms involving switches also add zero contribution to the sum in (4.75) for the same reason. The third summation on the right-hand side of (4.75) is always nonnegative since each term is individually positive or zero as a result of the incremental passivity of the resistors. In fact, this summation can be thought of as the dissipated *power in the increment* with respect to the given nominal trajectory. The remaining two summations represent the time rate of change of the *stored energy in the increment*. Combining these facts, we can write:

$$\frac{d}{dt}\mathbf{V}(\delta x) = \sum_{Ind.} \delta i\, \delta v + \sum_{Cap.} \delta i\, \delta v = -\sum_{Res.} \delta i\, \delta v, \text{ where} \qquad (4.76)$$

$$\mathbf{V}(\delta x) = \sum_{Ind.} (1/2)(\delta i_k)^* L_k(\delta i_k) + \sum_{Cap.} (1/2)(\delta v_k)^* C_k(\delta v_k). \qquad (4.77)$$

Because of the assumption on strict relative passivity of the reactive elements, the quantity $\mathbf{V}(\delta x)$ which we shall from now on refer to by the suggestive name *energy in the increment*, is a positive definite quadratic function of the incremental state variables. Since equation (4.75) holds identically for any of the possible circuit topologies, the energy in the increment is a Lyapunov function for the dynamical system. In particular, we have

$$\frac{d}{dt}\mathbf{V}(\delta x) = -\sum_{Res.} \delta v\, \delta i \leq 0. \qquad (4.78)$$

In conclusion, the energy in the increment is a Lyapunov function for the given nominal trajectory, and we see that the nominal trajectory is stable in the large. Since the nominal trajectory selected above can be taken as any solution trajectory, this statement implies that any two solution trajectories do not diverge.

Typically, asymptotic stability in the large can be concluded as well since at least some parasitic loss is always associated with each energy storage element, i.e. series resistance with inductors and parallel leakage resistance with capacitors. An argument for asymptotic stability appears in [34] for circuits that have a DC equilibrium point, and consist of only two-terminal elements. In [34], lossiness is guaranteed to be associated with each state variable by excluding inductor-capacitor-voltage source loops and inductor-capacitor-current source cutsets. (In this case, we would require that all resistors be strictly incrementally passive.)

A special case of the above result is when the switches are operated with a periodic switching pattern, and there exists a nominal periodic steady state solution. In this case, the result states that the given periodic steady state trajectory is stable in the large. This result is of particular interest for the case of a DC-DC converter operating with constant switching frequency. Note that this result holds up for DC-DC converters operating in both the continuous conduction and *discontinuous* conduction modes. This can be seen by redrawing the schematic for the DC-DC converter of interest with an ideal SPDT switch and incrementally passive resistive device (i.e. diode) replacing each transistor-diode pair. For example, we would redraw the up-down converter of Figure 2.1 as shown in Figure 4.13. The circuit of Figure 4.13 satisfies the conditions for its nominal periodic trajectory to be stable in the large, and it makes no difference whether or not the nominal trajectory contains a portion where the inductor current is identically zero.

4.3.2 Stability under Infinite Switching Frequency and Constant Duty Ratio

The result to be stated here is based on the fact that a switching converter operating at infinite switching frequency has dynamics governed by its state-space averaged model. In such a case, where the duty ratio is constant, the switching converter is equivalent to a time-invariant circuit because of the re-

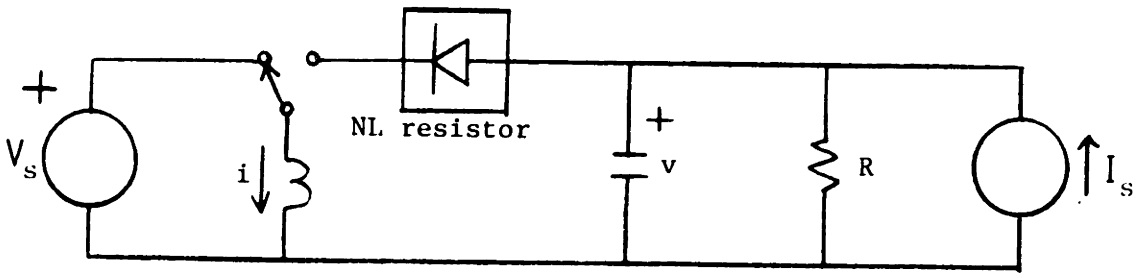

Figure 4.13: Up-Down Converter Redrawn to Illustrate Stability in Case of Discontinuous Conducion

sult of Section 4.1. Hence, we can replace the multiport network consisting of all non-reactive elements with a constant resistive multiport with hybrid representation $\mathcal{H}_{avg}(\bullet)$. Suppose that the switching converter is constructed from ideal switches, ideal DC sources, incrementally passive resistors, and reactive elements that are strictly relatively passive. In this case, the resistive multiport with hybrid representation $\mathcal{H}_{avg}(\bullet)$ is incrementally passive. This is a result of the following two facts. Firstly, each of the hybrid representations $\mathcal{H}_u(\bullet)$ that corresponds to a particular switch configuration is incrementally passive if each of the resistive elements in the converter is incrementally passive (see Appendix A for properties of interconnected networks). Secondly, a convex combination of a set of incrementally passive hybrid representations is also incrementally passive.

Under the above mentioned conditions, if the averaged model has an equilibrium point, then the equilibrium is stable in the large. The argument for stability is analagous to the one given in the previous subsection. Here, we can permit **nonlinear** relatively passive reactive elements since the energy in the increment is well defined with respect to a given DC operating point. If the reactive elements of the converter are assumed to have a composite representation of the form

$$\begin{aligned} x' &= u \\ y &= y(x), \end{aligned} \tag{4.79}$$

the total energy in the increment with respect to the equilibrium point x_{eq} takes

the form

$$\begin{aligned}
\mathbf{V}_{x_{eq}}(x) &= \sum_{Reactive} \int_0^T u(t)^* \{y(x(t)) - y(x_{eq})\}\, dt \\
&= \sum_{Reactive} \int_0^T x'(t)^* \{y(x(t)) - y(x_{eq})\}\, dt \\
&= \sum_{Reactive} \oint_{x_{eq}}^{x(T)} (dv)^* \{y(v) - y(x_{eq})\}. \qquad (4.80)
\end{aligned}$$

Once again, asymptotic stability in the large can be concluded in many practical cases because of parasitic losses. Further topological constraints can be imposed as in [34] to guarantee global asymptotic stability. See the discussion in the preceding subsection.

4.3.3 Summary: Energy in the Increment

The main point of this section has been that for a given circuit that satisfies the conditions of Sections 4.3.1 or 4.3.2, there exists a Lyapunov function, the energy in the increment, that enables one to conclude stability for nominal open-loop operation. The energy in the increment, although essentially different from physical stored energy, has units of energy and is a property of the reactive elements in a given circuit. For the case of Section 4.3.1 where all reactive elements were linear and time-invariant, the energy in the increment takes the form of a positive definite quadratic form in the incremental state values with the coefficients determined by the values of the capacitances and inductances. The incremental state values are defined with respect to a given time-varying nominal state trajectory. For the case of Section 4.3.2 where nonlinear reactive elements and averaged circuit models were considered, the energy in the increment is again a positive definite function of the incremental state. However, in this case, this quantity can be defined only with respect to a constant equilibrium state, rather than an arbitrary nominal trajectory.

The concept of the energy in the increment will be essential in the following two chapters of the thesis.

Chapter 5

Lyapunov-Based Control Design: Static Compensators

In this chapter, an approach to control of switching power converters based on the use of Lyapunov functions will be introduced. The main focus will be on control design based on the state-space averaged model for a given switching converter. The converters of interest are those that satisfy the conditions guaranteeing that nominal state trajectories are globally stable under open-loop operation, specifically converters constructed from incrementally passive resistors, ideal sources, ideal switches, and reactive elements that are strictly relatively passive (see Chapter 4 and Appendix A). (For the most part, the reader can keep in mind the case where all resistive and reactive elements are linear and passive.) One particular choice of Lyapunov function for control design purposes that will be of interest is the energy in the increment.

We shall begin by illustrating the Lyapunov-based control method with an application to the up-down converter introduced in Chapter 2. Then, we shall demonstrate how such a control design can be obtained in a more general way. There is typically some freedom in the choice of Lyapunov function for the control design, but we shall exhibit some particular advantages of using the energy in the increment. Generalizations to converters containing nonlinear circuit elements, to converters that handle time-varying input-output waveforms, and to converters operating in the discontinuous conduction mode will be given.

A method (dual to the control design approach) for designing state observers will be considered.

5.1 Example: Up-Down Converter

Consider the up-down converter of Figure 2.1 which has a state-space averaged model of the form

$$x' = Ax + (Bx + b)d, \tag{5.1}$$

where the two-component state x consists of the deviation of the inductor current from its nominal value ($x_1 = i - i_n$) and the deviation of the capacitor voltage from its nominal ($x_2 = v - v_n$), and where the input d is the deviation in the duty ratio from its nominal value ($d = d_t - d_n$). (Note that d_t indicates the total duty ratio here.) The parameter values listed below were selected for operation at a switching frequency of 50KHz.

$$\begin{aligned} C &= 5.4\mu\text{F} \\ L &= 0.18\text{mH} \\ R &= \infty \\ d_n &= 3/8 \\ V_s &= 15\text{volts} \\ I_o &= 2\text{amps} \\ v_n &= -9\text{volts} \\ i_n &= 3.2\text{amps} \end{aligned}$$

For the parameters listed above, the relevant matrices of the system are as follows:

$$
\begin{aligned}
A &= \begin{bmatrix} 0 & (1-d_n)/L \\ -(1-d_n)/C & 0 \end{bmatrix} = \begin{bmatrix} 0 & 3472.2 \\ -115740. & 0 \end{bmatrix} \\
B &= \begin{bmatrix} 0 & -1/L \\ 1/C & 0 \end{bmatrix} = \begin{bmatrix} 0 & -5555.6 \\ 185185. & 0 \end{bmatrix} \\
b &= \begin{bmatrix} (V_s - v_n)/L \\ i_n/C \end{bmatrix} = \begin{bmatrix} 133.33 \\ 592.59 \end{bmatrix} \\
Q &= \begin{bmatrix} L & 0 \\ 0 & C \end{bmatrix} = \begin{bmatrix} 180. & 0 \\ 0 & 5.4 \end{bmatrix} \bullet 10^{-6}
\end{aligned}
$$

The result on open-loop stability in Chapter 4 guarantees that the energy in the increment is a Lyapunov function for open-loop operation of this circuit. For the up-down converter, the energy in the increment takes the form

$$V = \frac{1}{2}L(i - i_n)^2 + \frac{1}{2}C(v - v_n)^2, \tag{5.2}$$

or

$$V = \frac{1}{2}x^*Qx. \tag{5.3}$$

Differentiating V along the system trajectories, we obtain

$$\frac{d}{dt}V(x) = \frac{1}{2}x^*(QA + A^*Q)x + d\frac{1}{2}\{x^*(QB + B^*Q)x + 2b^*Qx\}. \tag{5.4}$$

It turns out that $QA + A^*Q = 0$ for this example, which verifies that the energy in the increment is a Lyapunov function for open-loop operation ($d = 0$). In this example, it is also true that $QB + B^*Q = 0$. These relationships hold because of the lossless nature of the example converter, i.e. the lack of resistive elements in the converter. Considering these relationships, (5.4) simplifies considerably to

$$\frac{d}{dt}V(x) = (b^*Qx)d. \tag{5.5}$$

Many stabilizing control schemes can be obtained by inspection of (5.5). We shall consider the simple control law $d = -\alpha b^*Qx$ with α real and positive, modified to handle the duty ratio saturation constraint $-d_n \le d \le 1 - d_n$, i.e.

$$d = \begin{cases} -\alpha y, & -d_n \le d \le 1 - d_n \\ -d_n, & -\alpha y < -d_n \\ 1 - d_n, & -\alpha y > 1 - d_n \end{cases} \tag{5.6}$$

where $y = b^*Qx$. Here, the variable y takes the form

$$\begin{aligned} y &= (V_s - v_n)(i - i_n) + i_n(v - v_n) \\ &= (V_s - v)(i - i_n) + i(v - v_n). \end{aligned} \tag{5.7}$$

Note that the only dependence on circuit parameters is on the nominal values of the inductor current, the capacitor voltage, and the source voltage. This property is shared by analagous control schemes based on the energy in the increment for many other switching converters, as will be demonstrated in Section 5.3.

To investigate the closed-loop behavior, we examine the derivative of the Lyapunov function $V(x)$ along the closed-loop system trajectories:

$$\begin{aligned} \frac{d}{dt}V(x) &= yd \\ &= \begin{cases} -\alpha y^2, & -d_n \le d \le 1 - d_n \\ -d_n y, & -\alpha y < -d_n \\ (1 - d_n)y, & -\alpha y > 1 - d_n \end{cases} \end{aligned} \tag{5.8}$$

In the saturated regions (the second and third lines of (5.8)), the time derivative of $V(x)$ is strictly negative since either $V' < -\alpha d_n^2$ or $V' < -\alpha(1 - d_n)^2$. As a result, state trajectories quickly enter the unsaturated region. In the unsaturated region (the first line in (5.8)), $V(x)$ is strictly decreasing if $y \neq 0$, and asymptotic stability can be concluded by LaSalle's theorem since $y \equiv 0$ is not a system trajectory unless $x \equiv 0$. To see this, note that $y \equiv 0$ implies $d \equiv 0$ and the following:

$$\begin{aligned} b^*Qx &= 0 \\ b^*QAx &= 0, \end{aligned} \tag{5.9}$$

with the last line in (5.9) obtained by noting that $y' = 0$. The existence of a nonzero solution x to (5.9) is equivalent to the statement that the pair $\{b^*Q, A\}$ is unobservable. However, this pair is observable in this example, and therefore there are no system trajectories that do not converge to the origin.

In this example, we have not considered the effect of lossiness due to parasitic and/or load resistances. The effect of such passive resistances would only

enhance our stability result, by causing additional nonpositive terms of the form $-x^*Rx$ (with R positive semi-definite) to be added to the terms on the right-hand sides of (5.8).

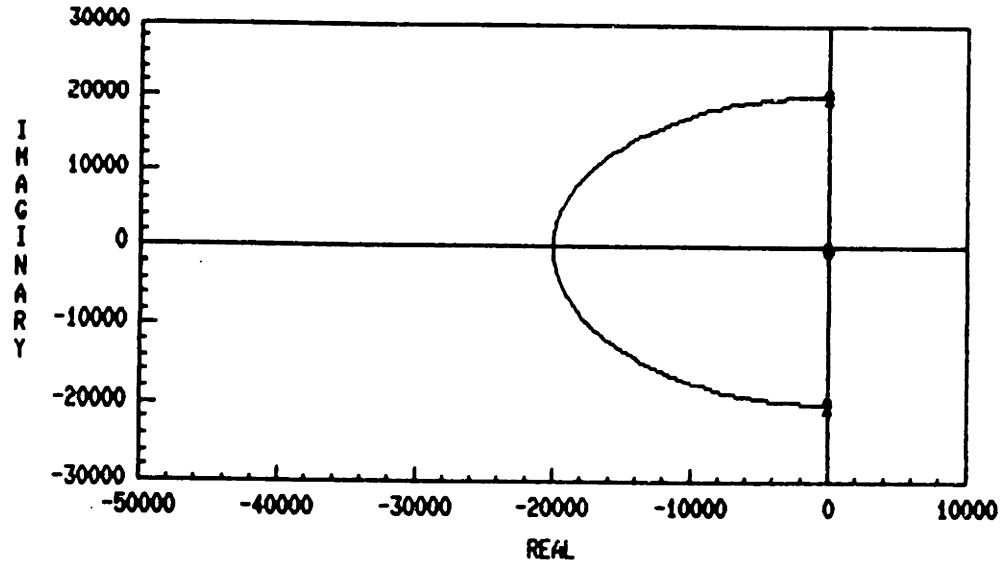

Figure 5.1: Root-Locus for Linearized Closed-Loop Control System

Asymptotically, the decay of the Lyapunov function $V(x)$ is controlled by the eigenvalues of the small signal model obtained by linearizing the closed-loop system about $x = 0$. In this example, there is some freedom in placing the eigenvalues of the linearized closed-loop system by choice of the gain α. A root locus of the closed-loop eigenvalues of the small-signal model is shown in Figure 5.1. To minimize the maximum of the real parts of the eigenvalues, for example, the gain should be selected so that the two eigenvalues coincide on the real axis at -20.05Krad/sec. An easy calculation indicates that the value of the gain required to obtain this eigenvalue placement is approximately $\alpha = .00785$. In the remainder of the discussion of this example, a value of the gain of $\alpha = .008$ will be used. The resulting closed-loop eigenvalues are at about -16.7Krad/sec and -24Krad/sec. Note that in this example the dynamical behavior of the small signal closed-loop dynamics is limited by the natural resonant frequency $(1 - d_n)/\sqrt{LC}$ of the open-loop state-space averaged system. Since the bandwidth

of the closed-loop dynamics is usually designed to be approximately an order of magnitude below the switching frequency, and since this is also a typical resonant frequency of the open-loop dynamics for a reasonably designed converter, the preceding limit on attainable closed-loop bandwidth is acceptable.

We expect the closed-loop system to be very well behaved, and this is confirmed by the digital computer simulation shown in Figure 5.2. In the next section, we present a derivation of a class of control schemes to which the above example belongs.

5.2 A Basic Approach to Lyapunov-Based Control Design

In this section, we show how to derive a class of control laws for a switching converter model of the form (5.1), to which the example (5.6) belongs. Note that the open-loop stability of the system (5.1) is crucial for this approach, and hence we shall restrict attention to switching converters that satisfy the conditions (see Chapter 4) guaranteeing stability under nominal duty ratio operation. A basic first step in this approach, as illustrated above, is the specification of a Lyapunov function for open-loop operation. The model (5.1) is linear and time-invariant in the case of open-loop operation under a constant nominal duty ratio, i.e. $d = 0$. Since the open-loop model is known a priori to be stable, it is generally possible to determine a family of suitable quadratic Lyapunov functions. In fact, in the case where the matrix A is asymptotically stable, it is possible to parametrize the family of such quadratic functions with the Lyapunov equation

$$A^*Q_1 + Q_1A = -P_1P_1^* \tag{5.10}$$

where $\{P_1^*, A\}$ is an observable pair. The existence of a positive definite, symmetric solution Q_1 to (5.10) is guaranteed by the stability of the matrix A and the observability of the pair $\{P_1^*, A\}$. Later in this section, we shall consider the selection of a suitable matrix Q_1 for the case where the matrix A has (simple) eigenvalues on the $j\omega$-axis.

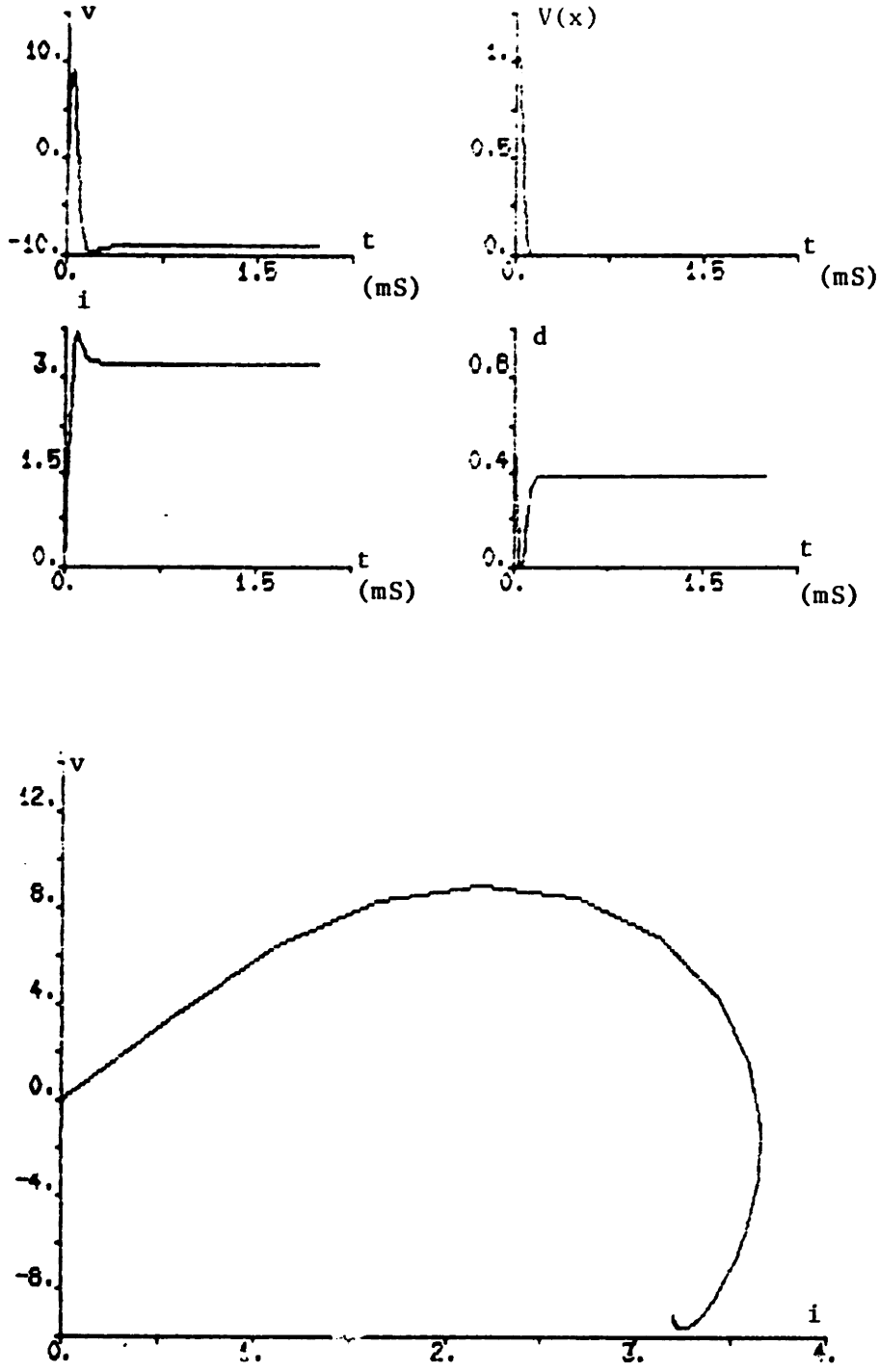

Figure 5.2: Digital Simulation of Up-Down Converter under Nonlinear Feedback Control Scheme

Having determined the form of a suitable matrix Q_1, it is straightforward to specify a globally stabilizing control law for the model (5.1) of the form (5.6), but based on the Lyapunov function $V(x) = \frac{1}{2}x^*Q_1x$, as follows:

$$d = \begin{cases} -\alpha y, & -d_n \leq -\alpha y \leq 1 - d_n \\ -d_n, & -\alpha y < -d_n \\ 1 - d_n, & -\alpha y > 1 - d_n \end{cases} \tag{5.11}$$

where $y = (Bx+b)^*Q_1x$. One particular choice for Q_1 is Q where $V(x) = \frac{1}{2}x^*Qx$ is the energy in the increment, and it turns out that this choice leads to certain nice features, which will be elaborated in the next section. First, we consider a second example that is somewhat more complex than the second order up-down converter.

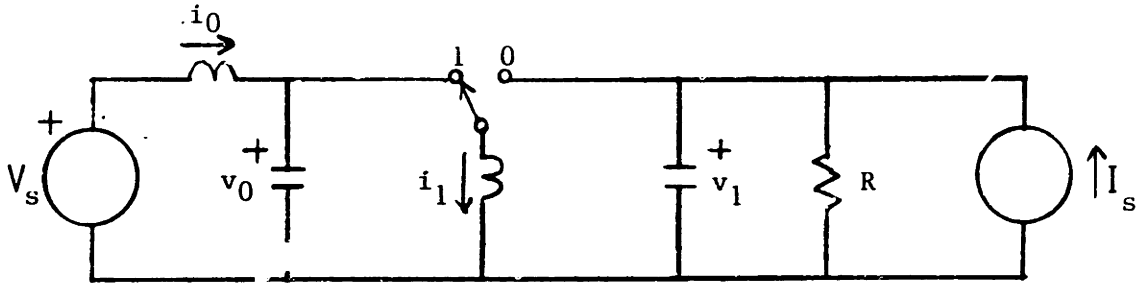

Figure 5.3: Up-Down Converter with Input Filter

Example 2: Up-Down Converter with Input Filter Section Consider the up-down converter of Figure 5.3, which includes a section of input filter to reduce current ripple in the line, generated by the switching action of the converter. Such a converter would be modeled by a fourth order state-space averged system of the form (5.1). For the following parameter values:

$$\begin{aligned} C_0 = C_1 &= 5.4\mu\text{F} \\ 5L_0 = L_1 &= 0.18\text{mH} \\ R &= \infty \end{aligned}$$

$$
\begin{aligned}
d_n &= 3/8 \\
V_s &= 15\text{volts} \\
I_o &= 2\text{amps} \\
v_{0n} &= 15\text{volts} \\
i_{0n} &= 1.2\text{amps} \\
v_{1n} &= -9\text{volts} \\
i_{1n} &= 3.2\text{amps},
\end{aligned}
$$

the relevant matrices of the fourth order system corresponding to (5.1) are given by

$$
A = \begin{bmatrix} 0 & -0.2778 & 0 & 0 \\ 1.8519 & 0 & -0.6944 & 0 \\ 0 & 0.0208 & 0 & 0.0347 \\ 0 & 0 & -1.1574 & 0 \end{bmatrix} \bullet 10^5
$$

$$
B = \begin{bmatrix} 0 & 0 & 0 & 0 \\ 0 & 0 & -1.8519 & 0 \\ 0 & 0.0556 & 0 & 0.0556 \\ 0 & 0 & 1.8519 & 0 \end{bmatrix} \bullet 10^5
$$

$$
b = \begin{bmatrix} 0 \\ 5.9259 \\ 1.3333 \\ -5.9259 \end{bmatrix} \bullet 10^5
$$

$$
Q = diag\{36\ 5.4\ 180\ 5.4\} \bullet 10^{-6}
$$

We shall first consider the control scheme (5.11) where $y = (Bx + b)^*Qx$ and $\frac{1}{2}x^*Qx$ is the energy in the increment. Because of the lack of resistive elements in the model, it turns out that $A^*Q + QA = 0$ and $B^*Q + QB = 0$. Once again, the control law (5.11) takes a simple form since the quantity y depends only on some state values and some nominal state values:

$$
y = -i_1(v_0 - v_{0n}) + (v_0 - v_1)(i_1 - i_{1n}) + i_1(v_1 - v_{1n}). \tag{5.12}
$$

Computation of the derivative of the Lyapunov function $V(x) = (1/2)x^*Qx$ along system trajectories results in the relation (5.8) as computed above.

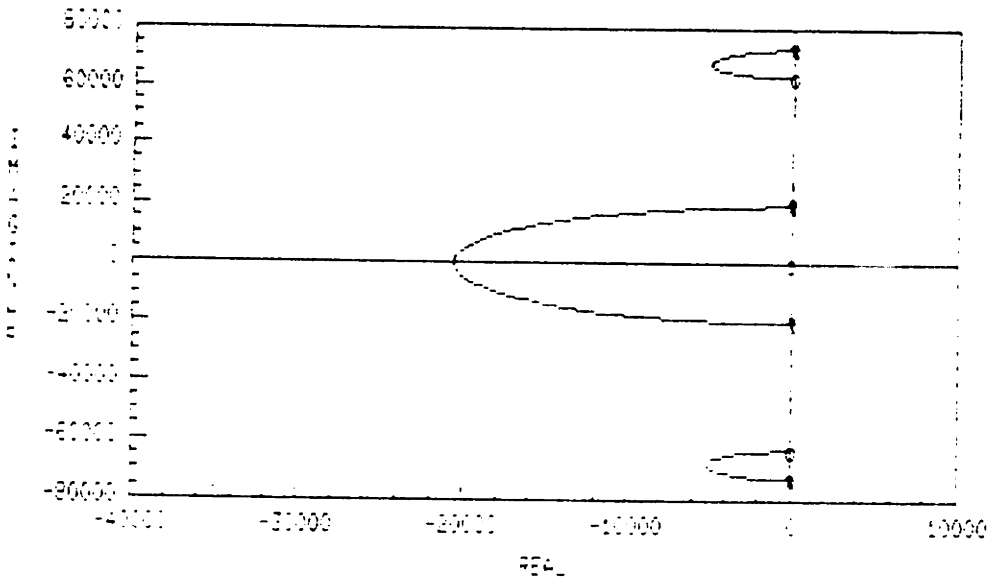

Figure 5.4: Root Locus for Fourth Order Converter

The same reasoning as used in the argument above for globally satisfactory dynamical behavior of the second order example can be applied here. In the unsaturated region, the rate of decay is governed asymptotically by the greatest of the real parts of the eigenvalues of the small signal model. The main difference from the second order case is that the eigenvalues cannot be placed so well by varying the gain α. A value of the gain that approximately minimizes the maximum of the real parts of the small signal eigenvalues is given by $\alpha = .0094$, which places the eigenvalues at $-5.08 \pm j68$Krad/sec, -9.6Krad/sec, -46Krad/sec. A root locus for the small signal eigenvalues parametrized by the gain α is shown in Figure 5.4. Figure 5.5 shows a digital simulation of a start-up transient in the fourth order converter under the control law (5.11) with gain $\alpha = .0094$.

In this fourth order example, it is possible by choice of an alternative matrix Q_1 to obtain a globally stabilizing control law of the form (5.11), but where the small signal behavior is governed by significantly faster dynamics. This is of interest for large signal behavior, since the dynamics in the unsaturated region is controlled asymptotically by the small signal behavior. For this example the set of positive definite, symmetric matrices Q_1 that satisfy (5.10) can be parametrized by two real scalars (and an arbitrary scaling factor). Note that

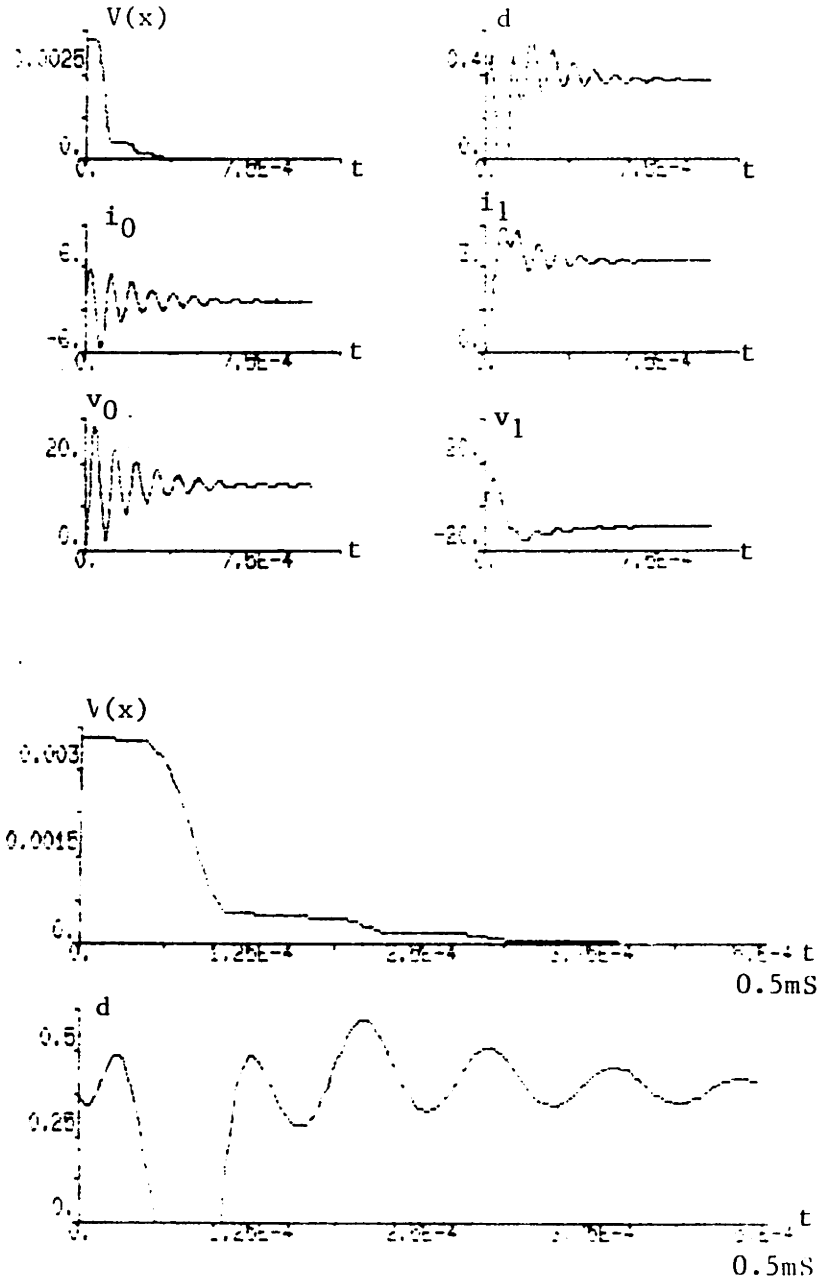

Figure 5.5: Digital Simulation of Fourth Order Up-Down Converter under Nonlinear Feedback Control Law

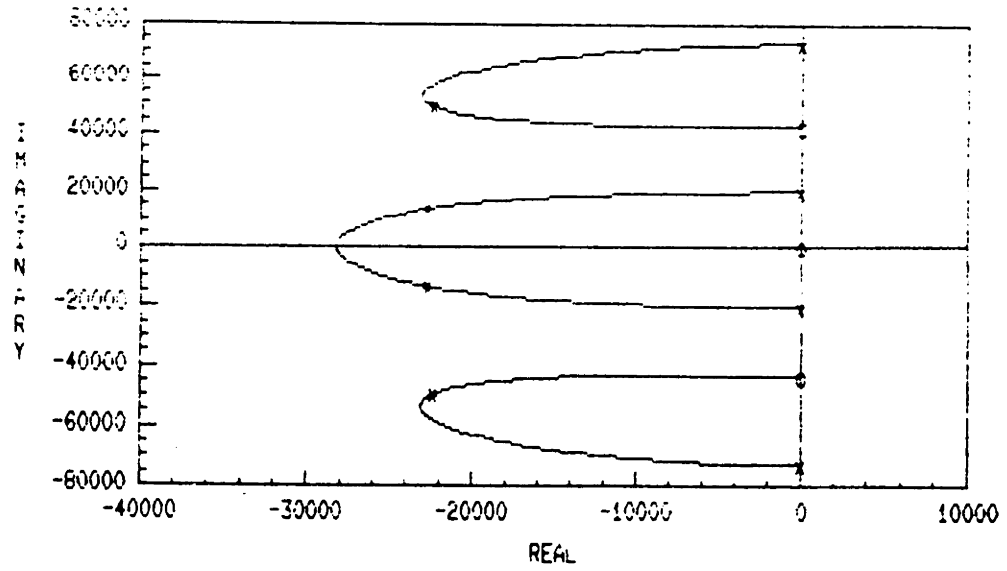

Figure 5.6: Root Locus for Fourth Order Converter Using Alternative Matrix Q_1

because of the lossless nature of the circuit model of Figure 5.3, all eigenvalues of the matrix A are on the $j\omega$-axis, and all solutions to (5.10) require $P_1 = 0$. To see that all solutions Q_1 can be parametrized by two scalars, note that the modal form for A is given by

$$J = \begin{bmatrix} 0 & -\omega_0 & 0 & 0 \\ \omega_0 & 0 & 0 & 0 \\ 0 & 0 & 0 & -\omega_1 \\ 0 & 0 & \omega_1 & 0 \end{bmatrix}. \tag{5.13}$$

Hence all solutions to the transformed Lyapunov equation

$$Q_J J + J^* Q_J = 0 \tag{5.14}$$

take the form $Q_J = diag\{a_1\ a_1\ a_2\ a_2\}$ where a_1 and a_2 are real constants. Since all solutions to the original Lyapunov equation (5.10) can be obtained by transformation from this diagonal structure, it follows that all solutions are parametrized by a_1 and a_2. Another way to view the specification of the matrix Q_1 will be considered in Chapter 6 (Section 6.5). There, we shall relate the selection of Q_1 to the specification of the zeros of a certain small signal transfer function.

As an example of an alternative selection of the matrix Q_1 for the present example, consider the matrix

$$Q_1 = \begin{bmatrix} 1.0410 & 0 & -0.3589 & 0 \\ 0 & 0.1602 & 0 & 0.0067 \\ -0.3589 & 0 & 0.9281 & 0 \\ 0 & 0.0067 & 0 & 0.0238 \end{bmatrix} \tag{5.15}$$

and the associated control law (5.11). The small signal dynamics of this control scheme is governed by the eigenvalues of the system matrix

$$A - \alpha bb^* Q_1.$$

The root locus shown in Figure 5.6 displays the closed loop eigenvalues as a function of α. The value $\alpha = .05$ results in eigenvalues located in the positions shown in Figure 5.6, with the real parts of all eigenvalues less than -22Krad/sec.

•

Another route for the derivation of the control law (5.11) is through the formulation of an optimal control problem. In particular, it is possible to obtain this control scheme by minimizing the cost index

$$J(x) = \min_{d(t)} \int_0^\infty \{q(x) + rd^2\}\, dt \tag{5.16}$$

where

$$q(x) = \begin{cases} -x^*(A^*Q_1 + Q_1A)x + r(y/r)^2, & -d_n \le -y/r \le 1 - d_n \\ -x^*(A^*Q_1 + Q_1A)x - r(1-d_n)^2 - 2y(1-d_n), & -y/r > 1 - d_n \\ -x^*(A^*Q_1 + Q_1A)x - rd_n^2 - 2yd_n, & -y/r < d_n, \end{cases} \tag{5.17}$$

$r > 0$, Q_1 is a solution of (5.10), and $y = (Bx + b)^*Q_1x$. We shall not give any more details on this development, but note that it is a common approach in the literature on control of bilinear systems of the form (5.1). In particular, this method was applied in [39], for an application in induction motor control. Another example is the result of Derese and Noldus [49], where a virtually identical development is given, except that constraints on the input variables are

not considered. As mentioned in Chapter 3, Brockett and Wood [17] suggested Lyapunov-based control schemes for switching converter circuits in their early work on state-space averaging. Many of the Lyapunov-based control strategies for bilinear systems have been neatly unified in the recent note [50].

5.3 Advantages of the Use of the Energy in the Increment for Control Purposes

As noted in the previous section, there is typically some freedom in the choice of the Lyapunov function that can be used in the control designs described there. In this section, we outline three advantages obtained by using the energy in the increment as the Lyapunov function in these control schemes.

One advantage of the choice of the energy in the increment as the Lyapunov function for control design purposes arises in the computation of the variable $y = (Bx + b)^* Qx$ which is used in these control schemes. In particular, one can always (indirectly) measure the vector $Q(Bx + b)$. To see this, consider the modification of (5.1) where we multiply this equation on the left by the matrix Q, giving

$$Qx' = QAx + Q(Bx + b)d. \tag{5.18}$$

Now the vector on the left-hand side of (5.18) is composed of the time derivatives of the inductor fluxes and the time derivatives of the capacitor charges. The elements of this vector are necessarily inductor voltages and capacitor currents. The vector $Q(Bx + b)$ is the amount by which this vector changes when the duty ratio steps from $-d_n$ to $1 - d_n$, or equivalently, the amount this vector changes when the switch configuration is changed. In general, it is possible and feasible to determine the vector $Q(Bx + b)$ during each cycle. To do this, for each inductor branch one would measure the voltage across the branch in each of the two switch configurations, and then form the difference of the two measurements. This difference constitutes the element of $Q(Bx + b)$ corresponding to the particular inductor port. In the case of a capacitor, one would measure the current flowing into the capacitor in each of the two switch configurations, and

form the difference of the two measured currents. This difference constitutes the element of $Q(Bx + b)$ corresponding to the particular capacitor. By performing the described measurement process, it is possible to obtain an accurate measurement of the vector $Q(Bx + b)$. Consequently, one can compute the variable $y = x^* Q(Bx + b)$ by forming the inner product of x and $Q(Bx + b)$. The only parametric dependence in y is therefore on the nominal state values required to determine x, the deviation in the states from their nominal values.

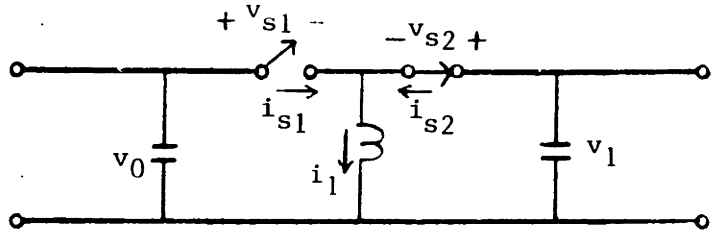

Figure 5.7: Switch Structure

In certain cases, it is possible to further simplify the measurement of $Q(Bx + b)$. For these cases, it is possible to directly measure the vector $Q(Bx + b)$ by measuring certain branch voltages and branch currents in the circuit (at one time instant). Consider a switching converter that has a switch structure like that of the up-down converter, as shown in Figure 5.7. (It is convenient for our purposes here to represent the switches with individual branches, rather than an SPDT switch.) A switch structure in some such form, termed a canonical cell in [48], is common to all (square-wave) switching power converters. Two conditions that are simultaneously necessary and sufficient for the direct measurement of $Q(Bx + b)$ are:

1. The two switch branches participate in a loop containing only capacitors and voltage sources.

2. The two switch branches participate in a cutset containing only inductor

branches and current sources.

The first condition guarantees that the change in voltage on the inductor branch caused by a change of the switch configuration is the sum (modulo sign) of the voltages of the two switch branches. The second condition concerns the capacitor node (or cutset) to which each of the switch branches belongs. It guarantees that the change in current flowing into each capacitor node (or cutset) due to a change in switch position is the sum (modulo sign) of the switch branch currents. In the case where the two conditions hold, it is possible to obtain the nontrivial elements of the vector $Q(Bx + b)$ in a direct manner. (Typically, many elements of the vector $Q(Bx + b)$ are zero since the switching action does not directly affect all the states. For instance, the state x_1 of Example 2 corresponding to the L_0 inductor current has a derivative that is instantaneously independent of the switch position.) To obtain the nontrivial elements of this vector that correspond to inductor voltages, one would simply measure the sum of the switch branch voltages (modulo sign). Similarly, to obtain the nontrivial elements that correspond to capacitor currents, one would measure the sum of the switch currents (modulo sign). For the example of Figure 5.7, with states $x_1 = v_0 - v_{0n}$, $x_2 = i_1 - i_{1n}$, and $x_3 = v_1 - v_{1n}$, the vector $Q(Bx + b)$ takes the form:

$$Q(Bx + b) = \begin{bmatrix} -i_{s1} - i_{s2} \\ v_{s1} - v_{s2} \\ i_{s1} + i_{s2} \end{bmatrix} = \begin{bmatrix} -i_1 \\ v_0 - v_1 \\ i_1 \end{bmatrix}. \tag{5.19}$$

Clearly the components of this vector can be directly measured from the circuit. The above conditions lead to the possibility of obtaining the variable y in a direct way that involves parametric dependence only on the nominal values of certain state variables. There is no dependence in y on other circuit parameters such as values of capacitances, inductances, or resistances.

A second potential advantage of the choice $Q_1 = Q$ in (5.11) is that it is possible to use a nearly linear version of this control algorithm by replacing $y = (Bx + b)^* Qx$ in (5.11) with $y_{lin} = b^* Qx$, and still maintain global stability. (Of course, the saturation constraints are still in effect.) To see that global stability

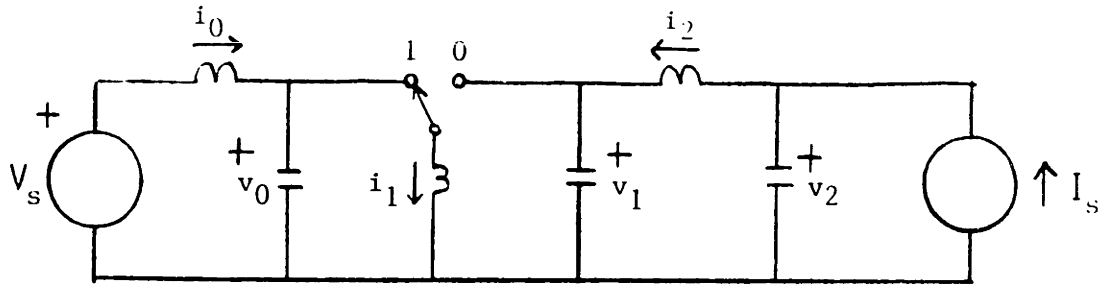

Figure 5.8: Up-Down Converter with Additional Filter Sections

is maintained, consider the following Lyapunov analysis with $V(x) = \frac{1}{2}x^*Qx$:

$$\frac{d}{dt}V(x) = \frac{1}{2}x^*[(A+dB)^*Q + Q(A+dB)]x + (b^*Qx)d. \qquad (5.20)$$

Now the first term on the right-hand side of (5.20) is always nonpositive. This follows from the fact that the energy in the increment takes the form $\frac{1}{2}x^*Qx$ for any nominal duty ratio, with the fixed matrix Q. The choice of the control in (5.11) (using y_{lin}) forces the second term on the right-hand side of (5.20) to be nonpositive. Global stability results from the nonpositivity of the right-hand side of (5.20). Hence, the choice of $Q_1 = Q$ in (5.11) permits the use of a feedback control that requires only the computation of the linear variable y_{lin}.

A third advantage of the use of the energy in the increment as a Lyapunov function for control design is that a control law of the form (5.11) with $Q_1 = Q$ can result in global stability of a more complex power system in which the original converter is embedded. In particular, if the converter is interconnected only with (relatively) passive circuit elements, the resulting interconnected system is always guaranteed to be stable. For example, if an additional section of output filter is added to the up-down converter of Example 2, as shown in Figure 5.8, the control law designed for the original converter stabilizes the modified circuit. We shall reserve a more detailed discussion of this feature for Chapter 6, where ideas concerning interconnected passive networks are applied.

In the following sections, we shall show how to extend the method of Lyapunov-

based control design to converters containing nonlinear resistive and/or nonlinear reactive elements, to converters that handle time-varying input-output waveforms, to converters that operate in the discontinuous conduction mode, and to an approach to observer design (for converters).

5.4 Switching Converters Containing Nonlinear Circuit Elements

Here, we shall demonstrate how to apply the Lyapunov-based method of control design to DC-DC converters constructed from ideal switches, DC sources, incrementally passive resistors, and reactive elements that are strictly relatively passive. As shown in Chapter 4, the energy in the increment is a Lyapunov function for constant nominal duty ratio operation of such a converter in the case of infinite switching frequency. As introduced in Chapter 2, the state-space averaged model for a switching converter containing nonlinear circuit elements takes the form

$$x' = f(x) + g(x)d. \tag{5.21}$$

For the purposes here, it will be most convenient to take the state x as the deviations from nominal in the inductor fluxes and the capacitor charges. (This is because we have defined the energy in the increment in (4.80) in terms of fluxes and charges, as a result of assuming flux-controlled inductors and charge-controlled capacitors.) Differentiating the energy in the increment $V(x)$ along the system trajectories, we obtain

$$\frac{d}{dt}V(x) = \nabla V(x)f(x) + \nabla V(x)g(x)d. \tag{5.22}$$

The first term on the right-hand side of (5.22) is nonpositive as a result of the fact that the energy in the increment is a Lyapunov function for constant nominal duty ratio operation of the converter. It is possible to obtain a stabilizing control of the form (5.11) by taking $y = \nabla V(x)g(x)$. In general, it is difficult to obtain alternate Lyapunov functions for the nominal open-loop system

$x' = f(x)$. Hence, for Lyapunov-based control design purposes, one may be practically limited to the energy in the increment.

Note that the control scheme outlined above shares the three advantages discussed in the previous section with the analagous control scheme for a converter constructed from linear reactive and resistive elements. It is easy to see that the first advantage is shared, by noting that the vector $g(x)$ is analogous to the vector $Q(Bx + b)$ of the linear elements case. This follows since we are working with a model in which the states are inductor fluxes and capacitor currents, and $g(x)$ is precisely the amount by which the time-derivative of the state vector varies when the switch configuration is changed. Hence, $g(x)$ is composed of voltages and currents which are either directly or indirectly measurable. The gradient of the energy in the increment takes the very simple form

$$\nabla V(x) = [\ i_1 \quad \dots \quad i_m \quad v_1 \quad \dots \quad v_p\ ] \tag{5.23}$$

where the components of this vector correspond to deviations from nominal in the inductor currents and in the capacitor voltages. As in the case where the resistive and reactive elements are linear, it is possible to determine the variable y with uncertainty limited by knowledge of nominal operating conditions.

To see that the second advantage of control designs based on the energy in the increment discussed in the previous section carries over to the case where nonlinear circuit elements are present, consider the control scheme (5.11) with y replaced by

$$y_{lin} = \nabla V(x) g(0). \tag{5.24}$$

The function $g(\bullet)$ is evaluated at the steady state value of the state $x = 0$ (or equivalently in the total variable notation $x_t = x_n$). It is clear from (5.23) that y_{lin} is linear in the deviations from nominal in the inductor currents and capacitor voltages. Consider the closed-loop system obtained by applying (5.11) to (5.21) with y replaced by $y_{lin} = \nabla V(x) g(0)$. Differentiating $V(x)$ along the system trajectories yields

$$\frac{d}{dt} V(x) = \nabla V(x)[f(x) + d(x)\{g(x) - g(0)\}] + \nabla V(x) g(0) d(x). \tag{5.25}$$

The second term on the right-hand side of (5.25) is nonpositive as a result of the choice of the control. The first term on the right-hand side is nonpositive because the system $x' = f(x) + d(t)\{g(x) - g(0)\}$ is the state-space model for a modified circuit consisting of the interconnection of the (nonlinear) reactive elements of the original circuit with a time-varying, incrementally passive, resistive multiport. As a consequence, the original form of the energy in the increment is a Lyapunov function for the modified circuit.

To see this, consider a state-space model that uses mixed variables, namely derivatives of fluxes and charges on the left-hand side and functions of inductor currents and capacitor voltages on the right-hand side. A general model of this type has the form:

$$q_t' = -\mathcal{H}_0(x_t) - d_t\{\mathcal{H}_1(x_t) - \mathcal{H}_0(x_t)\} \tag{5.26}$$

where the variables with subscript t represent total variables (as opposed to deviations). Such a model is expressed explicitly in terms of the hybrid resistive representations for the circuit in each of its switch configurations. Now consider any nominal operating point $\{q_n, x_n, d_n\}$ for (5.26), and form an equation for the increments with respect to this nominal condition ($q = q_t - q_n$, etc.) :

$$\begin{aligned} q' \;=\; & -\{[(1-d_t)\mathcal{H}_0 + d_t\mathcal{H}_1](x_t) - [(1-d_t)\mathcal{H}_0 + d_t\mathcal{H}_1](x_n)\} - \\ & \{\mathcal{H}_1(x_n) - \mathcal{H}_0(x_n)\}d. \end{aligned} \tag{5.27}$$

The first term on the right-hand side of (5.27) corresponds to the model for a hybrid representation for a time-varying, incrementally passive, resistive multiport. Therefore, the energy in the increment (4.80) carries over as a suitable Lyapunov function for a circuit consisting of such a time-varying resistive multiport that is interconnected with the reactive multiport of the original circuit model. Therefore, the first term on the right-hand side of (5.25) is guaranteed to be nonpositive. Hence, it is possible to pick d as a linear function of y_{lin} (in the absence of control saturation), and obtain global stability.

We shall leave for Chapter 6 a discussion of the third advantage, namely preservation of stability in interconnected systems. Before moving on, we shall

consider an example where this control method is applied to a circuit containing nonlinear circuit elements. The example to be considered arises in the application of active filtering methods to switching power circuits.

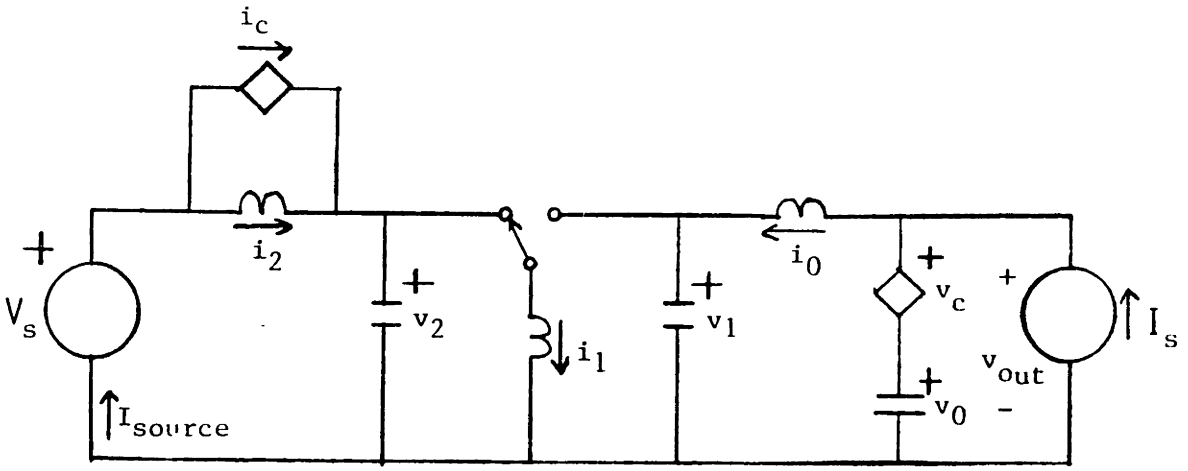

Figure 5.9: Up-Down Converter with Active Filter Stages

Example: Converter with Active Ripple Filters Consider the up-down converter depicted in Figure 5.9, with controlled sources associated with the input and output filters. The output filter configuration (dependent voltage source) corresponds to the so-called voltage drive enhancement method of [40,41] for enlarging the effective capacitance of C_0. The dependent current source in parallel with L_2 corresponds to the current drive method of [40,41] for enhancing the current filtering action of L_2 in the input filter. The state-space averaged model for the converter of Figure 5.9 is given by

$$x' = [A + dB]x + Gw, \tag{5.28}$$

where the components of the state vector x represent variations about an equilibrium corresponding to nominal duty ratio d_n and $v_c = i_c = 0$. The elements of x are as follows:

$$\begin{aligned} x_1 &= i_0 - I_s \\ x_2 &= v_0 - \frac{-d_n}{1-d_n} V_s \\ x_3 &= i_1 - \frac{1}{1-d_n} I_s \end{aligned}$$

$$
\begin{aligned}
x_4 &= v_1 - \frac{-d_n}{1-d_n} V_s \\
x_5 &= i_2 - \frac{d_n}{1-d_n} I_s \\
x_6 &= v_2 - V_s.
\end{aligned} \tag{5.29}
$$

The components of the control vector w are d (variation in the duty ratio), v_c, and i_c. A typical constraint on the duty ratio is $-d_n \leq d \leq 1 - d_n$, while constraints on v_c and i_c are implementation dependent. The matrices in the model (5.28) are given by

$$
A = \begin{bmatrix}
0 & 1/L_0 & 0 & -1/L_0 & 0 & 0 \\
-1/C_0 & 0 & 0 & 0 & 0 & 0 \\
0 & 0 & 0 & (1-d_n)/L_1 & 0 & d_n/L_1 \\
1/C_1 & 0 & -(1-d_n)/C_1 & 0 & 0 & 0 \\
0 & 0 & 0 & 0 & 0 & -1/L_2 \\
0 & 0 & -d_n/C_2 & 0 & 1/C_2 & 0
\end{bmatrix}
$$

$$
B = \begin{bmatrix}
0 & 0 & 0 & 0 & 0 & 0 \\
0 & 0 & 0 & 0 & 0 & 0 \\
0 & 0 & 0 & -1/L_1 & 0 & 1/L_1 \\
0 & 0 & 1/C_1 & 0 & 0 & 0 \\
0 & 0 & 0 & 0 & 0 & 0 \\
0 & 0 & -1/C_2 & 0 & 0 & 0
\end{bmatrix}
$$

$$
G = \begin{bmatrix}
0 & 1/L_0 & 0 \\
0 & 0 & 0 \\
\frac{V_s}{(1-d_n)L_1} & 0 & 0 \\
\frac{I_s}{(1-d_n)C_1} & 0 & 0 \\
0 & 0 & 0 \\
\frac{-I_s}{(1-d_n)C_2} & 0 & 1/C_2
\end{bmatrix} \tag{5.30}
$$

In the spirit of [40,41], the two control inputs corresponding to the controlled sources can be designed so as to increase the apparent value of the associated reactive element. For instance, the input v_c can be chosen as follows:

$$
v_c = \begin{cases}
-10\text{volts}, & -\gamma x_2 < -10\text{volts} \\
10\text{volts}, & -\gamma x_2 > 10\text{volts} \\
-\gamma x_2 = -\gamma(v_0 - v_0^{\text{desired}}), & \text{otherwise}
\end{cases} \tag{5.31}
$$

With this choice of control for positive γ, the function of the dependent voltage source in Figure 5.9 is as a negative capacitor for small values of x_2 (that is for

small values of the perturbation in v_0 from the nominal). However, the series impedance of the dependent voltage source and C_0 remains that of a positive capacitance for values of γ less than one. This can be seen by writing

$$\begin{aligned} v_{series} &= v_c + v_0 \\ &= -\gamma(v_0 - v_0^{desired}) + v_0 \\ &= \gamma v_0^{desired} + (1-\gamma)v_0. \end{aligned} \tag{5.32}$$

Considering the saturation constraints on v_c (see (5.31)), the series combination of v_c and C_0 can be given a representation as a nonlinear capacitor whose charge-voltage relation is shown in Figure 5.10. Note that the characteristic shown is that of a capacitor that is strictly relatively passive. For values of voltage near the nominal, the capacitor has an amplified incremental value, while for large voltage swings ($>$ 10volts) the capacitor has the incremental value of C_0.

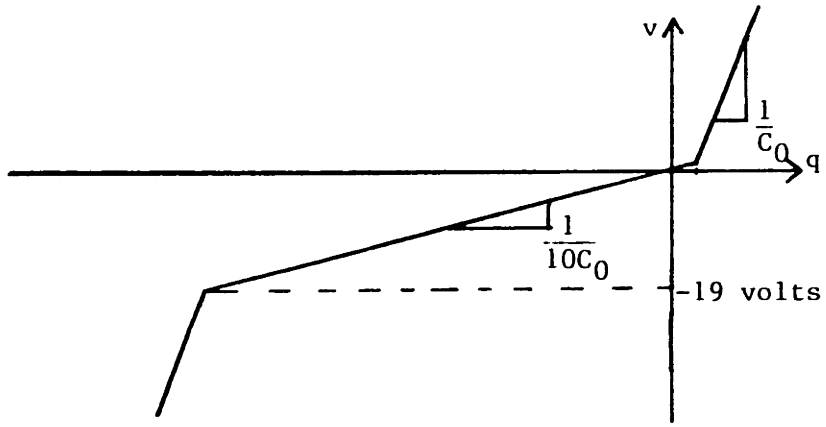

Figure 5.10: Representation of Series Combination of C_0 and v_c as a Nonlinear Relatively Passive Capacitance

Note that many other choices of the control v_c are possible and are worth investigating. For the purposes here, we shall carry on with the choice (5.31), and shall pick a similar control strategy for i_c to increase the incremental inductance of L_2 for small current variations. One possible choice is

$$i_c = \begin{cases} -.1\text{amps}, & -\gamma(i_2 - i_2^{nominal}) < -.1\text{amps} \\ .1\text{amps}, & -\gamma(i_2 - i_2^{nominal}) > .1\text{amps} \\ -\gamma(i_2 - i_2^{nominal}), & \text{otherwise} \end{cases} \tag{5.33}$$

With this choice of control strategy for the input i_c, the parallel combination of L_2 and the dependent current source i_c takes the form of an inductor that is strictly relatively passive to infinity. The shape of the flux-current relation for this inductor is analogous to the charge-voltage relation of Figure 5.10. For small variations in the current from the nominal, the incremental value of the inductance is amplified by $\frac{1}{1-\gamma}$. For large deviations in the current from the nominal ($>$ .1amps), the incremental inductance is L_2.

Since we now have an equivalent circuit model that contains DC sources, ideal switches, incrementally passive resistors, and (nonlinear) reactive elements that are strictly relatively passive to infinity, it is possible to make a control design based on the energy in the increment. The control law takes the form of (5.11).

A digital simulation of the converter of Figure 5.9 under the control strategies (5.11, 5.31, 5.33) with $\gamma = .9$ and $\alpha = .003$ is shown in Figure 5.11. Figure 5.11a) shows a start-up transient where all the states are initially at zero. A comparison of the ripple in the external waveforms (V_{out} and I_{source}) with and without the active ripple filter stages is depicted in Figure 5.11b). In this figure, the steady state converter operation is simulated for 0.2 msec with the active filter stages operational, and then for 0.2 msec without the active filter function. •

5.5 Switching Converters that Handle Time-Varying Source and/or Load Waveforms

Here, we shall consider the control of switching power converters that operate with time-varying source and/or load waveforms. Typical application areas are in rectifiers, inverters, and cycloconverters. In order to set a foundation for the discussion, we shall introduce an example of a converter that operates from a rectified single phase AC line. The front end of the circuit in Figure 5.12 is a full-wave bridge rectifier that ideally provides a rectified sinusoidal voltage waveform to the rest of the circuit. The remainder of the circuit is a boost

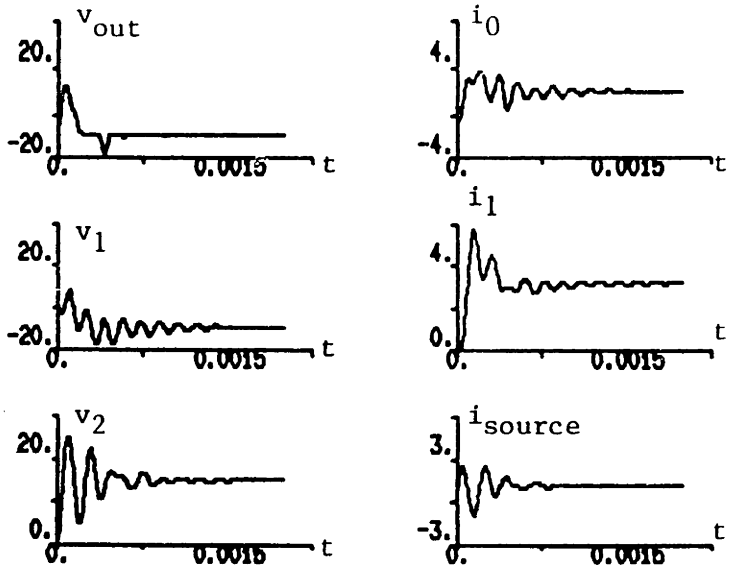

a)

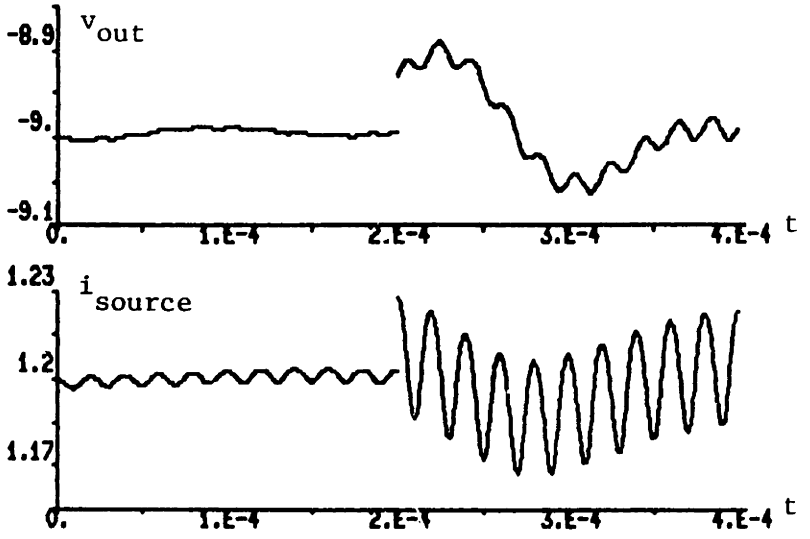

b)

Figure 5.11: Digital Simulation of Converter with Active Filter Stages

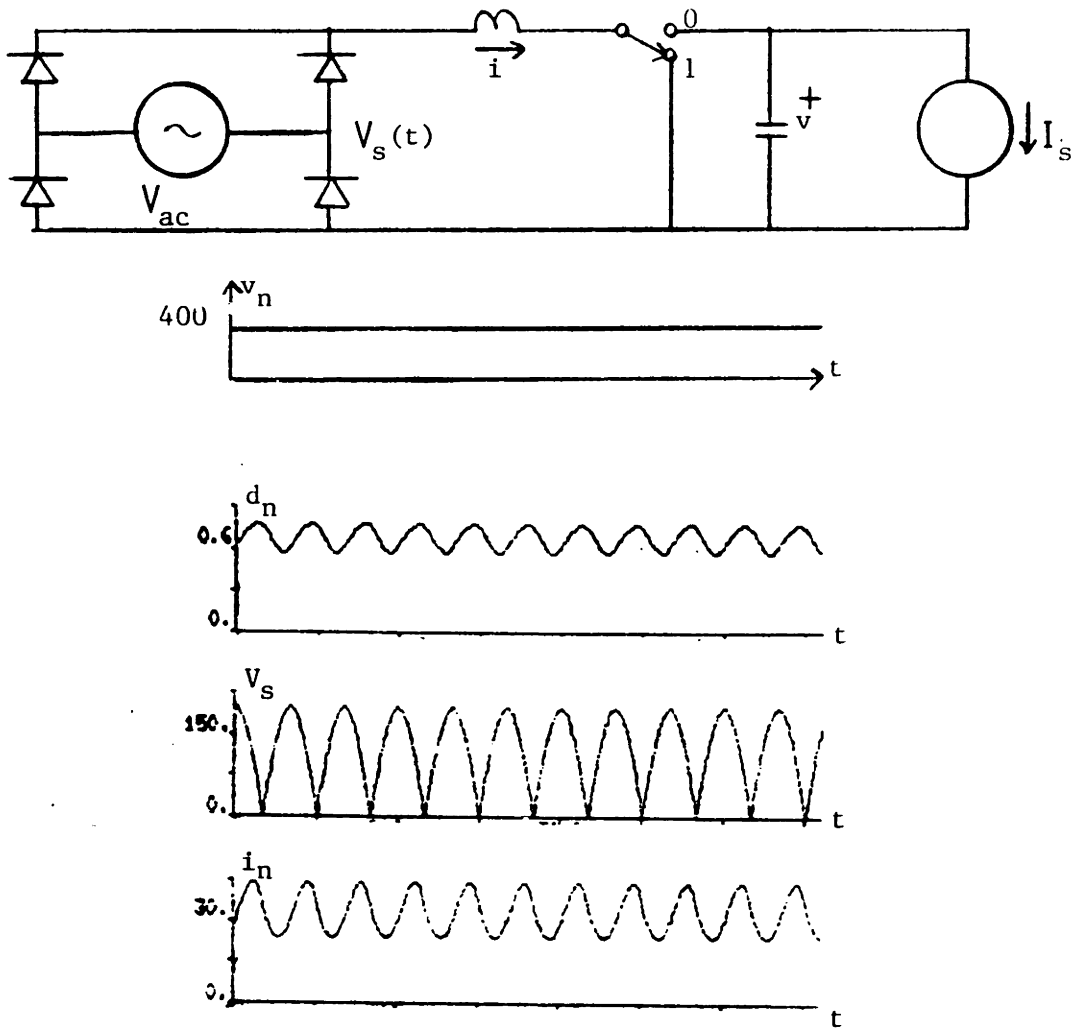

Figure 5.12: Converter that Operates Off Rectified Line

converter. A possible design objective for this circuit is to provide a constant output voltage on the capacitor. Typical steady state (averaged) waveforms for this application are shown in Figure 5.12.

The state-space averaged model for such a converter takes the general form

$$x' = Ax + \{Bx + b(t)\}d + f(t) \tag{5.34}$$

in the case where the converter is constructed from linear resistive and linear reactive elements, ideal switches, and time-varying sources. The theory presented here is directly applicable to the case where nonlinear resistive elements

are present, but to simplify notation we shall restrict attention to the case of linear circuit elements. We shall consider the case where the source waveforms are periodic with period T, and there exists a nominal periodic state and duty ratio trajectory that corresponds to a desired behavior. For the example boost converter designed to operate off the rectified AC line voltage, the nominal trajectory includes a constant capacitor voltage and periodic inductor current and duty ratio waveforms.

In the case where all resistive elements are incrementally passive and all linear reactive elements are strictly relatively passive, the energy in the increment is a Lyapunov function for the nominal trajectory. With respect to the nominal periodic state trajectory $x_n(t)$, the energy in the increment takes the form

$$V(x(t),t) = \frac{1}{2}\{x(t) - x_n(t)\}^* Q\{x(t) - x_n(t)\}. \tag{5.35}$$

where Q is the matrix of inductor and capacitor values. It is possible to design globally stabilizing control laws based on this time-varying Lyapunov function with a method analogous to that presented earlier in this chapter. Differentiating the energy in the increment with respect to time, we obtain

$$\begin{aligned}\frac{d}{dt}V(x(t),t) &= \frac{1}{2}(x - x_n)^*[Q(A + d_nB) + (A + d_nB)^*Q](x - x_n) + \\ &\quad (x - x_n)^*Q\{Bx + b(t)\}(d - d_n).\end{aligned} \tag{5.36}$$

The first term on the right-hand side of (5.36) is always nonpositive since the energy in the increment is a Lyapunov function for nominal open-loop operation (i.e. $d = d_n$). It is possible by choice of d to force the second term on the right-hand side of (5.36) to also be nonpositive, guaranteeing global stability. One particular choice satisfying this requirement takes the form

$$d(t) = d_n(t) - \alpha\{x - x_n(t)\}^*Q\{Bx + b(t)\} \tag{5.37}$$

subject to the saturation constraint $0 \leq d(t) \leq 1$. Note that it is generally difficult to base a globally stabilizing control scheme on an alternate quadratic Lyapunov function $(x - x_n)^*Q_1(x - x_n)$ since the matrix Q_1 is required to satisfy

$$Q_1(A + dB) + (A + dB)^*Q_1 \leq 0 \tag{5.38}$$

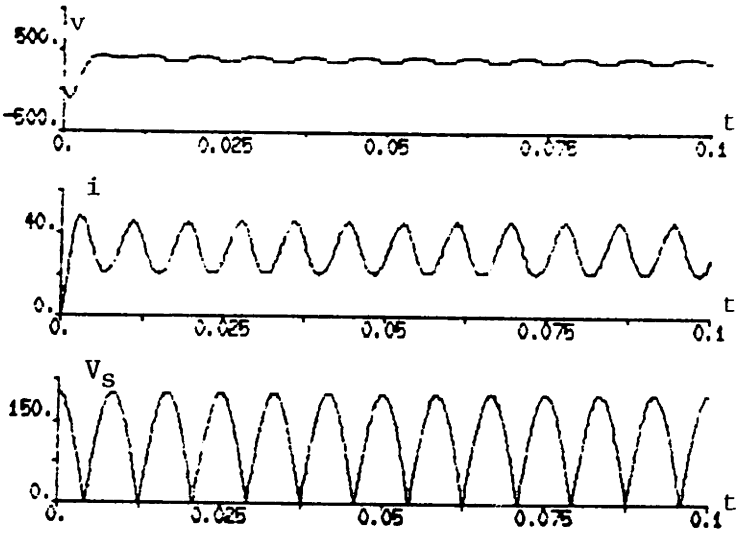

Figure 5.13: Numerical Simulation of Closed-Loop Off-Line Converter

for all values of $d \in [0,1]$. (It is possible to obtain alternate Lyapunov functions for the periodic system via Floquet theory, but it is difficult to make conclusions for the behavior on a time scale smaller than one period.)

The control scheme (5.37) shares many of the previously discussed advantages of control laws designed for DC-DC converters based on the energy in the increment. In particular, it is possible to determine the gain vector $Q\{Bx + b(t)\}$ by measurements performed directly on the circuit. The main difficulty is in obtaining the nominal steady state waveforms that correspond to a given operating condition. The nominal waveforms for a new operating condition are required in essentially real time in order to implement this (or any other) control algorithm. Note that in the case of a DC-DC converter, the nominal waveforms are constant, and therefore, considerably less difficult to compute.

For the example of Figure 5.12, the state-space averaged model takes the form (5.34) with state $x = [i \;\; v]^*$ and the following system matrices:

$$A = \begin{bmatrix} 0 & -1/L \\ 1/C & 0 \end{bmatrix}$$

$$B = \begin{bmatrix} 0 & 1/L \\ -1/C & 0 \end{bmatrix}$$

$$b(t) = \begin{bmatrix} 0 \\ 0 \end{bmatrix}$$
$$f(t) = \begin{bmatrix} V_s(t) \\ I_o \end{bmatrix} \tag{5.39}$$

A numerical simulation of a start up transient of this converter under the control scheme (5.37) is shown in Figure 5.13 where the circuit parameters used were $L = 10\text{mH}$, $C = 50\mu\text{F}$, $I_o = 10\text{amps}$, and $V_s(t) = 200|cos(377t)|$ volts, and $\alpha = 1.6 \bullet 10^{-5}$. The nominal duty ratio and inductor current waveforms were approximated as sinusoidal waveforms (with DC pedestals). It is evident that a fast transient response results. There is considerable 120 Hz ripple in the output waveform, but this is attributed to the errors in the nominal waveforms which were crudely approximated.

The application here is closely related to the earlier work of Schlecht [51] on a line interfaced inverter. The approach of [51] was to select time-varying feedback gains so that the eigenvalues of the quasi-static small signal model were located in fixed locations in the left-half plane. Approximate nominal waveforms for the inverter were obtained with a heuristic approach. In [51], the sensitivity of the output waveform to disturbances and/or uncertainties was reduced by the selection of the feedback gains (in the pole placement scheme). The method of control design based on the energy in the increment provides a simple feedback that is inherently stabilizing. However, the reduction of sensitivity to uncertainties and/or disturbances is an area that requires further work. In Chapter 6, we shall describe some methods for reducing sensitivity in DC-DC converters.

5.6 Control of Converters Operating in Discontinuous Conduction Mode

An application area related to the topic of the previous section is the control of DC-DC converters operating in the discontinuous conduction mode. Such a converter can be viewed as a circuit constructed from ideal switches, DC sources, linear reactive elements, and nonlinear incrementally passive resistors. In par-

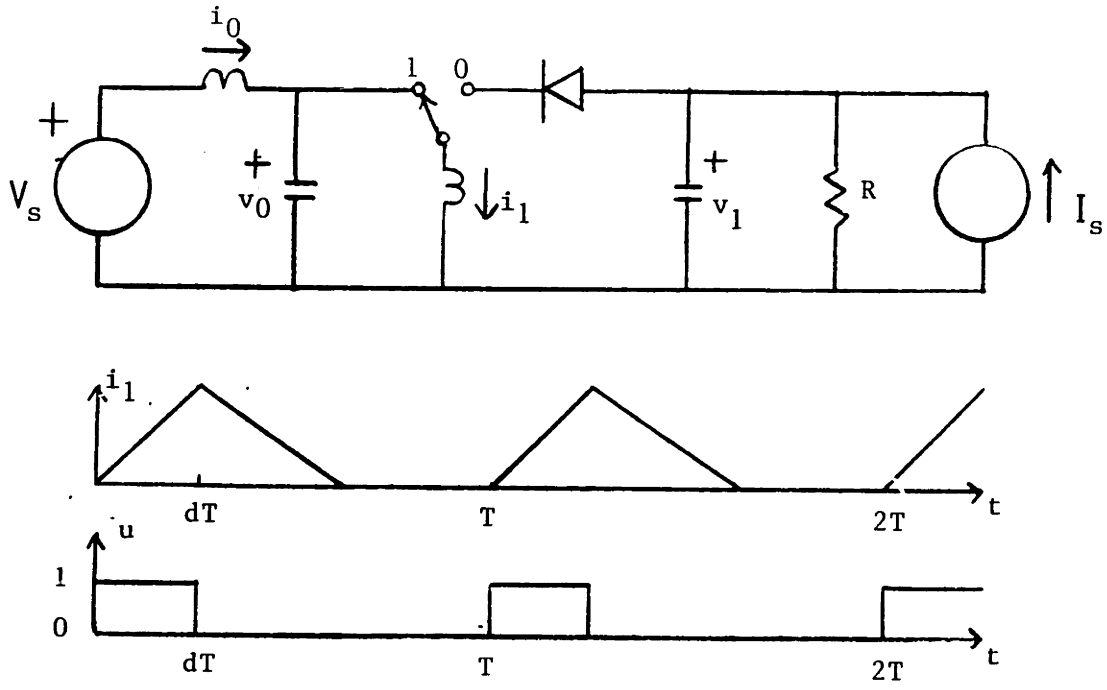

Figure 5.14: Model and Waveforms for Discontinous Conduction Mode of Up-Down Converter

ticular, for the example up-down converter of Figure 5.14, the diode functions as a nonlinear incrementally passive resistor. As a consequence, the result on open-loop stability of nominal trajectories given in Chapter 4 (Section 4.3.1) is directly applicable. The energy in the increment, which has the form (5.35), is thus a Lyapunov function for the nominal trajectory $x_n(t)$.

One route for the application of a Lyapunov-based control scheme to the converter operating in the discontinuous conduction mode, is based on the non-averaged state-space model. We shall outline this approach, and then describe a more practical control method that is based on the state-space averaged model for operation in the discontinuous conduction mode [68,48]. For convenience, we shall express the non-averaged state-space model in a mixed form with derivatives of flux and charge on the left-hand side, and a function of inductor current and capacitor voltage on the right-hand side, i.e.

$$Qx' = -\mathcal{H}_0(x) - u(\mathcal{H}_1 - \mathcal{H}_0)(x) \tag{5.40}$$

where $Q = diag\{L_0\ C_0\ L_1\ C_1\}$ and where $\mathcal{H}_j(\bullet)$ is a hybrid representation for the (nonlinear) resistive portion of the circuit when the switch is in position j. If a nominal periodic trajectory $\{x_n(t), u_n(t)\}$ satisfies (5.40), it is possible to form a model for the deviation of a given trajectory from this nominal, i.e.

$$\begin{aligned} Q(x' - x_n') &= -\{[(1-u_n)\mathcal{H}_0 + u_n\mathcal{H}_1](x) - [(1-u_n)\mathcal{H}_0 + u_n\mathcal{H}_1](x_n)\} - \\ &\quad (u - u_n)[\mathcal{H}_1 - \mathcal{H}_0](x). \end{aligned} \tag{5.41}$$

To form a Lyapunov-based control strategy, we differentiate the energy in the increment $V(x,t) = \frac{1}{2}(x - x_n)^* Q(x - x_n)$ along the system trajectories:

$$\begin{aligned} \frac{d}{dt}V(x,t) &= (x - x_n)^* Q(x' - x_n') \\ &= -(x - x_n)^*\{[(1-u_n)\mathcal{H}_0 + u_n\mathcal{H}_1](x) - \\ &\quad [(1-u_n)\mathcal{H}_0 + u_n\mathcal{H}_1](x_n)\} - \\ &\quad (u - u_n)(x - x_n)^*[\mathcal{H}_1 - \mathcal{H}_0](x). \end{aligned} \tag{5.42}$$

The first term on the right-hand side of (5.42) (involving the curly bracket) is nonpositive since the resistive network with hybrid representation $[(1-u_n)\mathcal{H}_0 +$

$u_n\mathcal{H}_1](\bullet)$ is incrementally passive. In the case where $u = u_n$, this statement is equivalent to the statement that any system trajectory does not diverge from the nominal trajectory x_n. The second term on the right-hand side of (5.42) can be made nonpositive by choice of control. Obviously, the choice $u = u_n$ is one that satisfies this requirement. The control design problem is quite complex since u and u_n take only the values 0 and 1, and we would typically like to limit the number of switch transitions to two per cycle. One practical approach to the control design is to base the design on the state-space averaged model for discontinuous operation, as described below.

The rationale for the use of a state-space averaged model for a converter operating in the discontinuous conduction mode is that the state variables of interest usually exhibit small ripple. The state-space averaged model for a converter operating in the discontinuous conduction mode, such as that of Figure 5.14, has a lower order than that of the exact state-space model. This is a result of the fact that there is no dynamical behavior associated with the L_1 inductor current. This current is constrained to be zero during a portion of each cycle because of the operating mode of the circuit. The averaged value for this current can be computed in terms of the duty ratio, certain circuit parameters, and the averaged values for the other state variables, see [68]. For the converter of Figure 5.14, the state-space averaged model has the form

$$\begin{aligned} i_0' &= (V_s - v_0)/L_0 \\ v_0' &= i_0/C_0 - \frac{v_0 T}{2L_1 C_0} d^2 \\ v_1' &= I_s/C_1 + \frac{v_0^2 T}{2v_1 L_1 C_1} d^2 \end{aligned} \tag{5.43}$$

where T is the period of one cycle.

It turns out that the energy in the increment (appropriately modified for the reduced order model) is still a Lyapunov function for the averaged model (i.e. (5.43)). This can be seen from the averaged circuit model obtained for this example in Chapter 4 (see Figure 4.12)). Note that in Section 4.2.2, it was demonstrated that the two-port network used to replace the combined switch-

inductor-diode network is incrementally passive. Hence, the modified Lyapunov function takes the form

$$V(x) = \frac{1}{2}L_0(i_0 - i_{0n})^2 + \frac{1}{2}C_0(v_0 - v_{0n})^2 + \frac{1}{2}C_1(v_1 - v_{1n})^2. \tag{5.44}$$

It is straightforward to base a control scheme on the Lyapunov function (5.44) for the model (5.43), as was done in Sections 5.1 and 5.2. We illustrate this below.

For the purposes of a control design to regulate the converter at a specified steady state operating point, it is convenient to express the model (5.43) in coordinates that represent deviations about a nominal operating point, i.e. in the form

$$x' = f(x) + g(x)(d^2 - d_n^2.) \tag{5.45}$$

Note that we regard the deviation away from nominal in the *square* of the duty ratio as the input in this model, because of the way the duty ratio enters the model (5.43). The function $g(x)$ in (5.45) takes the form

$$g(x) = \begin{bmatrix} 0 \\ -\frac{v_0 T}{2L_1 C_0} \\ \frac{v_0^2 T}{2v_1 L_1 C_1} \end{bmatrix}. \tag{5.46}$$

Since the function (5.44) is a Lyapunov function for open-loop operation of (5.45), we have that

$$[\nabla V(x)]^* f(x) \leq 0. \tag{5.47}$$

A natural implementation of the Lyapunov-based control would specify the duty ratio in terms of its square as follows

$$\begin{aligned} d^2 &= d_n^2 - \alpha[\nabla V(x)]^* g(x) \\ &= d_n^2 - \alpha\{(v_0 - v_{0n})\frac{v_0 T}{2L_1} + (v_1 - v_{1n})\frac{-v_0^2 T}{2v_1 L_1}\}, \end{aligned} \tag{5.48}$$

subject to the saturation constraint $0 \leq d \leq 1$. A numerical simulation of a transition from steady state operation in the continuous conduction mode (with load current of 1amp) to the discontinuous conduction mode (with load current

of 0.05amps) using this control scheme is shown in Figure 5.15). The circuit parameters (aside from the load current) were taken to be identical to those of Example 2 in Section 5.2, and the gain $\alpha = 0.15$ was selected. Note that this simulation exhibits a graceful recovery for this transient. ♦

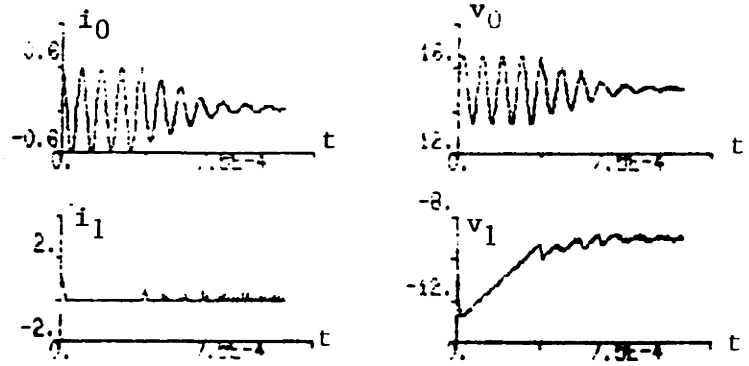

Figure 5.15: Transition from Continuous Conduction Mode to Discontinuous Conduction Mode

5.7 Design of State Observers for Switching Power Circuits

In some applications it necessary to obtain an accurate estimate of the state of a switching converter without directly measuring each state variable. In other situations, the available measurements may be so noisy that some filtering is required in order for the data to be of any use. The use of a state observer is a natural approach to filtering and/or reconstructing the state of a dynamical system. Here, we shall illustrate an approach to designing state observers for switching power circuits. Consider for now a switching converter constructed from ideal sources, ideal switches, linear passive resistors, and linear reactive elements that are strictly relatively passive. The (non-averaged) state-space model for such a converter takes the form

$$x' = Ax + (Bx + b)u + f. \tag{5.49}$$

Suppose the available measurements contained in the vector y are linear in the state, i.e.

$$y = C(u)x \tag{5.50}$$

where we have allowed dependence on the switch configuration in the measurement equation. A state observer for the system described by (5.49) and (5.50) can take the form

$$z' = Az + (Bz + b)u + f + H(u)[C(u)z - C(u)x] \tag{5.51}$$

where $H(u)$ is the observer gain, and the measurement y is incorporated in a linear fashion. The error system associated with this observer structure is given by

$$e' = (A + uB)e + H(u)C(u)e \tag{5.52}$$

where $e = z - x$. The free design parameters are contained in the observer gain matrix $H(u)$.

Note that for a general time-varying linear system, it is generally not possible to obtain a stable observer with a constant gain matrix. (A method for obtaining stable observer designs with time-dependent gains is via the Kalman-Bucy filter.) We shall illustrate how to obtain stable observer behavior with a simple gain $H(u)$ for the special case where the system (5.49) models a switching converter (as described above). The method to be used is dual to the approach for feedback design based on the energy in the increment. Here, we shall consider as a Lyapunov function $V(e) = \frac{1}{2}e^*Qe$ for the error system (5.52), where Q is the matrix used in the definition of the energy in the increment. This Lyapunov function takes the form of the energy in the increment between the observer state z and the underlying system state x.

To proceed, we examine the time-derivative of $V(e)$:

$$\frac{d}{dt}V(\epsilon) = \frac{1}{2}e^*[Q(A + uB) + (A + uB)^*Q]\epsilon + e^*QH(u)C(u)\epsilon. \tag{5.53}$$

The first term on the right-hand side is nonpositive (as in previous results) and the second term can be made nonpositive through the choice of $H(u)$. A

potential choice that results in stable observer dynamics is given by

$$H(u) = -Q^{-1}C^*(u)R \tag{5.54}$$

where R is a nonnegative definite matrix. (R need not be symmetric.) Note that in the case where the measurement vector does not depend on the switch configuration, i.e. $C(u) = C$, the gain H is also independent of u. Some of the considerations in the selection of the gain $H(u)$ are the steady state filter performance in eliminating (wideband) noise, the steady state sensitivity to measurement biases and model uncertainties, and the small signal dynamical behavior.

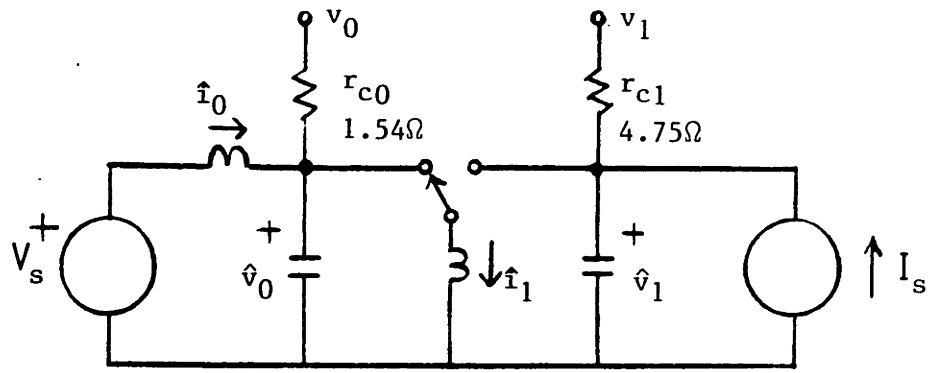

Figure 5.16: Observer Realization for Example Converter

Example: Observer Design for Converter of Example 2 Suppose we would like to construct a state observer for the circuit of Example 2 (Figure 5.3) that uses measurements of only the input voltage V_s, the capacitor voltages v_0 and v_1, and the load current I_s. A first step in realizing the observer is through a circuit that is identical to the underlying converter circuit. It is possible to scale the parameters so that the observer circuit handles only a fraction of the power handled by the power circuit (as in the MIT Parity Simulator [24]). For simplicity of presentation, suppose the observer circuit is identical to the power

circuit with state-space model

$$z' = Az + (Bz + b)u + f. \tag{5.55}$$

The output measurement y is a two component vector of the two capacitor voltages (independent of the switch position), of the form (5.50) with C constant. One possible choice for the observer gain takes the form (5.54) with the matrix R diagonal and positive definite. With this form of the gain, the circuit realization for the observer can be completed by the simple addition of two resistors as shown in Figure 5.16. The measured capacitor voltages v_0 and v_1 are introduced to the observer circuit through low impedance buffers. Note that the switch is operated synchronously with the switch of the underlying power circuit. With the resistive elements r_{c0} and r_{c1} chosen to have the values in the figure, and circuit parameter values taken as those in Section 5.2, the eigenvalues of the small signal, state-space averaged model for the observer error are approximately $-19.7 \pm j2.03$ Krad/sec and $-59.8 \pm j41.1$ Krad/sec. Note that the global stability of this scheme is evident from the passive circuit structure.

It turns out that this observer scheme can be applied to switched circuits that contain nonlinear resistive elements. This is a consequence of the result of Chapter 4 which states that any two solution trajectories of a given circuit do not diverge, provided the circuit is constructed from incrementally passive resistive and reactive elements. (The circuit is not permitted, in general, to contain nonlinear reactive elements since these are never incrementally passive, see Appendix A.) Since we have constructed the initial observer circuit model (without any observer update gain) to be identical to the underlying switched circuit, the solution trajectories of this circuit obey the same dynamical equations as those of the underlying circuit. It follows that the trajectories of the initial observer circuit do not diverge from those of the underlying circuit. The observer update gain $H(u)$, which can be implemented with some resistive elements, can still be selected to enhance the observer stability, as done above.

A nontrivial example of a converter circuit that contains a nonlinear resistive element is the up-down converter, operated in the discontinuous conduction

mode, as depicted in Figure 5.14. As discussed in Section 5.5, it is possible to view a converter operating in the discontinuous conduction mode as a switched circuit that has a diode (nonlinear resistive device) in series with one of its switch branches. Consequently, it is possible to use the observer structure shown in Figure 5.16 to handle operation in both the continuous and the discontinuous conduction modes. This is illustrated in Figure 5.17 with a numerical simulation of a transient where the observer states are initially zero, but the initial converter states are close to their steady state values for operation in the discontinuous conduction mode. Figure 5.17a) shows the transient in the observer error $e = z - x$, while Figure 5.17b) displays waveforms for the actual switching converter. To illustrate some detail in the observer behavior, Figure 5.17c) shows an expanded segment of the first 100μsec of the converter current waveform, the observer estimate of the current waveform, and the observer error in the current waveform. •

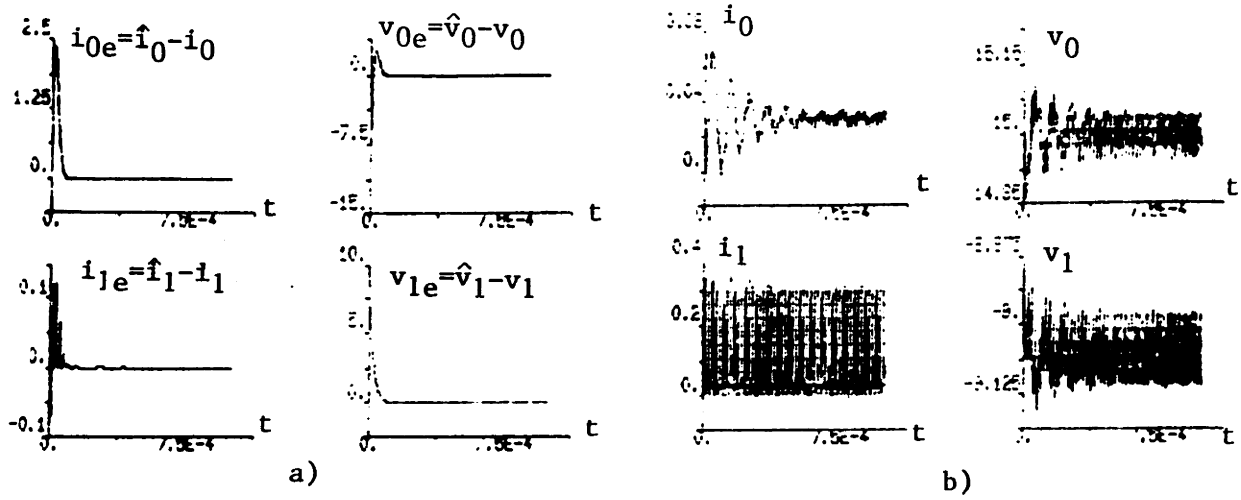

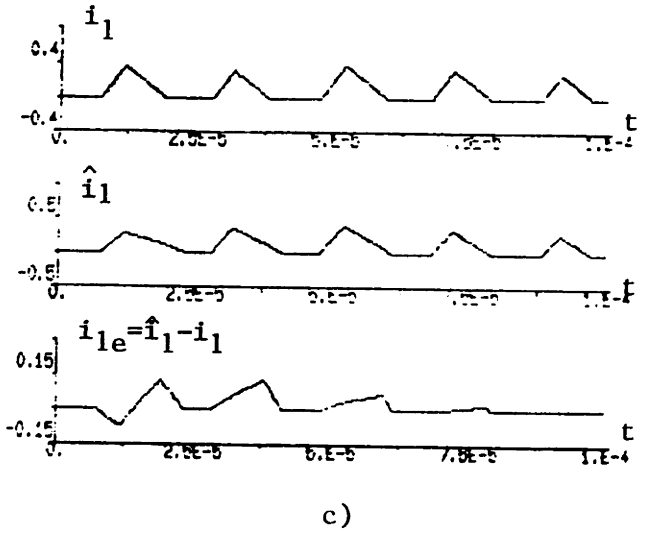

Figure 5.17: Observer Waveforms for Operation in Discontinuous Conduction Mode

Chapter 6

Lyapunov-Based Control Design: Dynamical Compensators

In this chapter, we shall build upon the results of Chapter 5 by viewing the Lyapunov-based feedback control schemes considered there as network interconnections of (incrementally/relatively) passive circuit elements. In particular, this point of view suggests the replacement of the static feedback schemes introduced in Chapter 5 with dynamical compensators that offer more flexibility in the resulting closed-loop systems. The approach is easily extended to converters admitting more than two switch configurations (with associated multi-input state-space averaged models). To gain some insight into this method, we shall first give an interpretation of the Lyapunov-based control strategy of Sections 5.1 and 5.2 as an interconnection of (incrementally/relatively) passive circuit elements. Then, in the subsequent sections, we study the performance (sensitivity, robustness, transient response) that can be obtained using passive dynamic compensation.

6.1 Introduction: Feedback Systems as Interconnected Networks

Consider the closed-loop system obtained by interconnecting the system

$$x' = Ax + (Bx + b)d$$

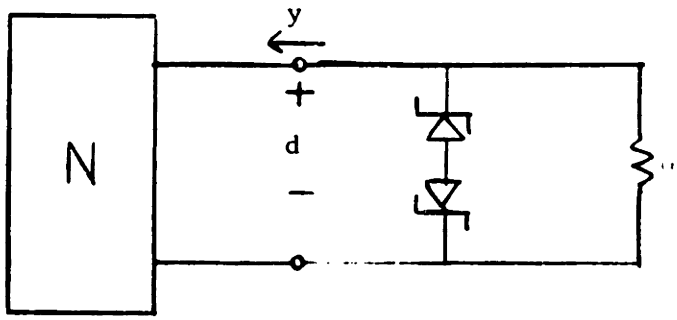

Figure 6.1: Network Representation of Feedback Control Scheme

$$y = (Bx + b)^* Q_1 x \tag{6.1}$$

where Q_1 is positive definite, symmetric, and satisfies $Q_1 A + A^* Q_1 \leq 0$ with the saturating control law $d = -\alpha(y)$ defined by

$$d = \begin{cases} -\alpha y, & -d_n \leq -\alpha y \leq 1 - d_n \\ -d_n, & -\alpha y < -d_n \\ 1 - d_n, & -\alpha y > 1 - d_n \end{cases} \tag{6.2}$$

This closed-loop system is identical to the one considered in Sections 5.1 and 5.2, and can be given a *network interpretation* as shown in Figure 6.1. The network N, which corresponds to the system (6.1), represents a nonlinear one-port that operates on a "voltage" waveform $d(t)$ to produce a "current" waveform $y(t)$. The linear "resistor" of value α corresponds to the unsaturated feedback control law applied to (6.1), while the saturation constraints are imposed by the "Zener diodes."

The stability of the closed-loop system can be concluded from the passivity properties of this network interconnection. There is a well developed theory of input-output stability for interconnected passive systems [37]. However, the Lyapunov function approach to stability remains the most useful tool for our purposes here, since we are interested in the *internal* stability of the closed-loop converter system. The passivity of the "circuit" elements in Figure 6.1 immediately suggests as a Lyapunov function the sum of the internal energy functions (e.g. available energy) of the circuit elements participating in the

interconnection. This approach to stability of dissipative dynamical systems was taken by Willems [28], and by Wood [1] for switching converters, as discussed in Chapter 3. Wood noted that the input-output stability theory for dissipative (passive) systems was considerably more difficult to apply than the internal (Lyapunov) stability method; however, Wood did indicate the utility of the approach via passivity for generating Lyapunov functions.

Returning to our example, the resistor of value α is strictly incrementally passive for finite positive values of α, and the pair of Zener diodes constitutes an incrementally passive resistive element. We shall demonstrate that **N** (modeled by (6.1)) is strictly relatively passive at the origin to infinity. Here, we evaluate a lower bound on $W_0(x)$, the energy in the increment with respect to the nominal trajectory $\{d = 0, x = 0, y = 0\}$ for a trajectory beginning at $x(0) = 0$.

$$\begin{aligned} W_0(x(T)) &= \int_0^T y(t)d(t)\,dt \\ &= \int_0^T (Bx + b)^* Q_1 x d(t)\,dt \\ &= \int_0^T \frac{1}{2}\left\{\frac{d}{dt}(x^* Q_1 x) - x^*(Q_1 A + A^* Q_1)x\right\} dt \\ &\geq \int_0^T \frac{d}{dt}\left(\frac{x^* Q_1 x}{2}\right) dt \\ &= \frac{1}{2}x(T)^* Q_1 x(T) \end{aligned} \tag{6.3}$$

Since Q_1 is a positive definite matrix, the network **N** is strictly relatively passive at the origin to infinity. The stability of the interconnection is most easily seen by taking as a Lyapunov function the sum of the internal energy functions, which in this example takes the form $\mathbf{V}(x) = \frac{1}{2}x^* Q_1 x$. We have already performed the stability analysis with this Lyapunov function in Chapter 5.

The main purpose of introducing the concept of interconnected passive systems is the simplicity with which a large class of globally stabilizing control schemes can be obtained. In particular, replacing the static compensator (6.2) with any element **C** that is strictly relatively passive and that satisfies $\mathbf{C}(0) = 0$ preserves the global stability properties of the interconnection. A compensator having this property can be selected to yield some desirable performance fea-

tures, as will be demonstrated in Sections 6.4, 6.5, and 6.6. In the following section, we extend the approach to switching converters that have multiple inputs (more than one controllable switch) and nonlinear circuit elements. Using the formulation given here, Section 6.3 applies some general stability robustness results for interconnected passive networks. Before moving on, we shall contrast this approach with that taken by Wood in [1].

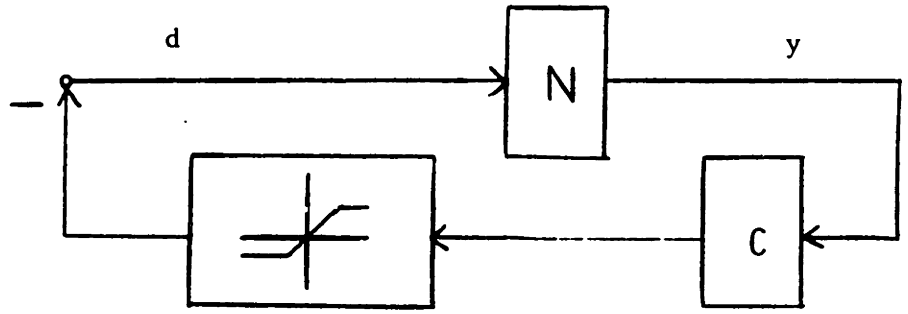

Figure 6.2: Block Diagram with Series Saturation Element

There is a difference between the scheme of Figure 6.1 and the method used by Wood in [1]. The control schemes considered in [1] can be represented by the block diagram of Figure 6.2. In the case where the operator **N** in the forward path is passive, a sufficient condition for finite gain stability (used in [1]) is that the operator in the feedback path is strictly passive, and has finite gain. In the scheme of Figure 6.2, this requires that the cascade of the compensator **C** with the saturation operator is strictly passive. The class of linear compensators satisfying this constraint is specified in the paper of O'Shea [52], and termed O'Shea functions in [1]. This class of functions is a subclass of the strictly positive real functions, and hence, the method of [1] is more restrictive than the approach considered here.

For purposes of comparison, a block diagram equivalent to the network interconnection of Figure 6.1 is shown in Figure 6.3. The static nonlinear element connected in parallel with **N** realizes the limiting function of the Zener diodes by injecting enough "current" into the compensator **C** to clamp the compensator

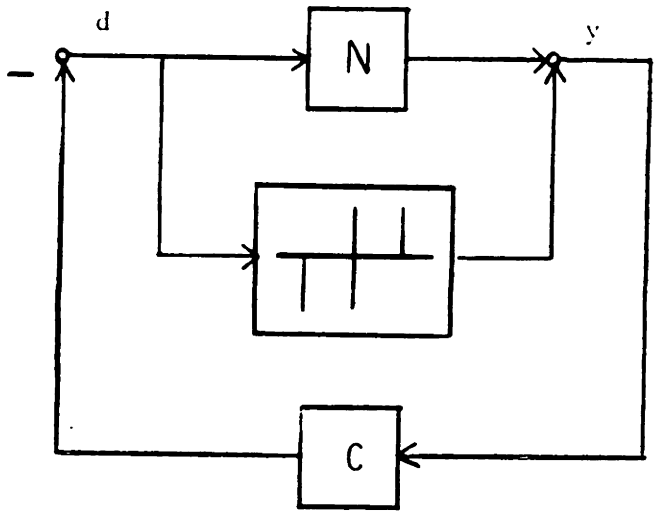

Figure 6.3: Block Diagram Equivalent to Network Interconnection

output. The distinct advantage of our scheme (Figure 6.3) over that of Figure 6.2 is that any compensator that is strictly relatively passive may be used.

The approach outlined here is related to that of Kapasouris et al. [53] for multivariable linear systems containing saturating nonlinearities at the inputs. The more sophisticated method of [53] would insert a gain $\lambda(t) \in [0,1]$ in front of the compensator C that would guarantee that the control output never saturated. However, it is not evident that a positive real compensator modified by the scheme of [53] to prevent saturation remains a positive (incrementally passive) operator.

6.2 Switching Converters Containing Nonlinear Elements and Admitting Multiple Switch Configurations

Here we shall consider the development of control strategies for converters containing nonlinear circuit elements and admitting multiple switch configurations. The method to be used is a generalization of that of the previous section. The open-loop stability result of Section 4.3.2 is applicable only to the state-space

averaged models for DC-DC converters constructed from ideal switches, DC sources, incrementally passive resistors, and nonlinear reactive elements that are strictly relatively passive. We shall therefore restrict attention to these models. The general form of the state-space averaged model for such a converter with multiple controlled switches is as follows:

$$x' = f(x) + G(x)D. \tag{6.4}$$

The variable x represents the deviation in the state from a nominal equilibrium point. The control input D is a vector of duty ratios satisfying constraints such as $-d_{jn} \leq d_j \leq 1 - d_{jn}$, and $G(x)$ is a matrix whose elements may depend upon the state x. For such a system, there exists a positive definite function $\mathbf{V}(x)$ corresponding to the energy in the incremental state x. Further, because of the result on open-loop stability in Chapter 4, the function $\mathbf{V}(x)$ has a unique minimum at $x = 0$ (say $\mathbf{V}(0) = 0$) and satisfies

$$\nabla \mathbf{V}(x) f(x) \leq 0. \tag{6.5}$$

In order to apply the method of the previous section, we require an appropriate input-output model. To this end, we append the output equation

$$Y = G(x)^* [\nabla \mathbf{V}(x)]^* \tag{6.6}$$

to (6.4). The resulting input-output model is strictly relatively passive at the origin to infinity. To see this, consider the following calculation of a lower bound on $W_0(x)$, the energy in the increment with respect to the nominal constant trajectory ($D = 0, x = 0, Y = 0$) for a trajectory beginning at $x = 0$.

$$\begin{aligned} W_0(x(T)) &= \int_0^T Y(t)^* D(t)\, dt \\ &= \int_0^T [\nabla \mathbf{V}(x)] G(x)\, D\ dt \\ &= \int_0^T \left\{ \frac{d}{dt}\mathbf{V}(x) - \nabla \mathbf{V}(x) f(x) \right\} dt \\ &\geq \int_0^T \frac{d}{dt}\mathbf{V}(x)\, dt \\ &= \mathbf{V}(x(T)) \end{aligned} \tag{6.7}$$

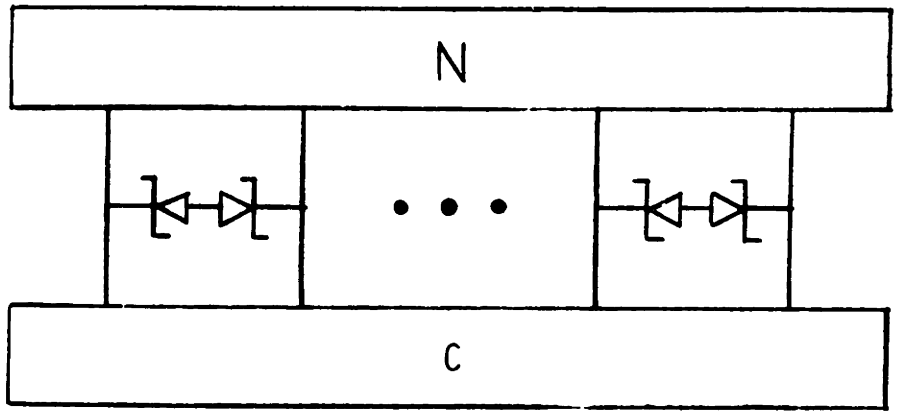

Figure 6.4: Network Representation of Multi-Input Multi-Output Incrementally Passive Feedback

It is straightforward to extend the approach to control described in the previous section to the system model of (6.4) and (6.6). Consider the network representation of a multi-input, multi-output compensator that is strictly relatively passive and that takes saturation into account as shown in Figure 6.4. It is easy to conclude global stability of the system shown in Figure 6.4 because of the (relative/incremental) passivity of each of the elements participating in the network interconnection. A Lyapunov function for the system can be obtained by summing the internal energy functions for each of the multiports participating in the interconnection.

In the next section, we shall study the third advantageous feature of Section 5.3 for control designs based specifically on the energy in the increment. This choice leads to a robustness property in the case of an arbitrary interconnection of a given switching converter with incrementally passive circuit elements.

6.3 Interconnected Networks

In this section, we shall apply some results on interconnected passive networks to switching converter systems. In particular, we shall elaborate on the third advantageous feature (of Section 5.3) of the use of the energy in the increment as a Lyapunov function for control design. To begin, we paraphrase a theorem from the recent thesis of Colgate [54]:

A necessary and sufficient condition to ensure the stability of the interconnection of a given LTI n-port network N with an arbitrary passive LTI n-port P is that the n-port N be passive.

It is evident from the discussions in the preceding sections and Appendix A that the passivity of N is sufficient for the stability of the network interconnection. However, the theorem indicates that it is always possible to specify some passive network P that destabilizes an interconnection of P with N if N is not passive. The proof in the 1-port case is easy to make via Nyquist diagram arguments. However, the proof of necessity for the n-port case in [54] is unsatisfactory, but an alternative proof proceeds by reducing the problem to the 1-port case (using the method in [75]).

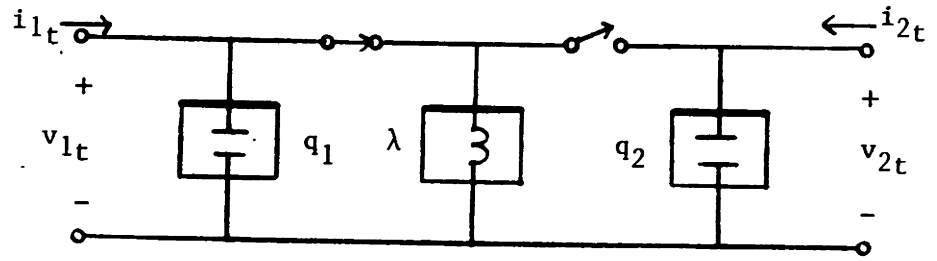

Figure 6.5: Nonlinear Canonical Cell

This theorem has some implications for large interconnected systems of switching power converters. In particular, if one compensates each switching converter subsystem so that at its electrical terminals, it is a relatively passive network, then an arbitrary interconnection of such subsystems with other relatively passive networks is always guaranteed to be stable. (Of course, interconnections are typically not made arbitrarily, but accidents do occur and ill conceived system configurations can arise.) The control schemes based on the energy in the increment (introduced in Sections 5.1 and 5.2) achieve this feature, as discussed below. Note that with other control strategies, there are generally no such guarantees. In particular, consider a control law for the canonical cell

of Figure 6.5, under which the resulting small signal impedance matrix of the closed-loop two-port is not positive real. Then, the theorem of Colgate [54] assures that there is some passive LTI two-port that can be connected with the closed-loop canonical cell, and cause the resulting interconnection to be unstable.

To see that the canonical cell of Figure 6.5 remains strictly relatively passive to infinity under a control law based on the energy in the increment (such as (6.2) with $Q_1 = Q$), first consider the following state-space averaged model for the network of Figure 6.5:

$$\begin{aligned} x' &= f(x) + g(x)d + Fi \\ y &= g(x)^*[\nabla \mathbf{V}(x)]^* \\ v &= F^*[\nabla \mathbf{V}(x)]^* \end{aligned} \tag{6.8}$$

where

$$F = \begin{bmatrix} 1 & 0 \\ 0 & 0 \\ 0 & 1 \end{bmatrix},$$

$x = [q_1 \ \lambda \ q_2]^*$ is the vector of the deviations from nominal in the capacitor charges and inductor flux, $\mathbf{V}(x)$ is the energy in the increment, $i = [i_1 \ i_2]^*$ is the vector of the deviations from nominal in the port currents, and $v = [v_1 \ v_2]^*$ is the vector of the deviations from nominal in the port voltages. (Note that $\nabla \mathbf{V}(x) = [v_1 \ i \ v_2]$.) The model (6.8) is strictly relatively passive at the origin to infinity. This can be verified by a straightforward calculation for a lower bound on $W_0(x)$, the energy in the increment with respect to the nominal constant trajectory $\{i = 0, d = 0, x = 0, v = 0, y = 0\}$ for a trajectory with initial state $x = 0$. The calculation is nearly identical to (6.7) of the previous section, and so will not be given here.

The point is that the model (6.8) represents a three-port network that is strictly relatively passive to infinity, and hence, if we terminate one of its ports in a strictly incrementally passive one-port, the resulting two-port network remains strictly relatively passive to infinity (see Appendix A). A control law based on the energy in the increment, such as (6.2), is a strictly incrementally passive

termination for the (non-electrical) port whose variables are d and y. Hence, under a control law of this form, the two-port shown in Figure 6.5 is strictly relatively passive to infinity.

The result given above is a type of robustness result. Other issues concerning performance under the closed-loop control with the passivity-based compensation scheme outlined in Section 6.1 are investigated in the following three sections.

6.4 Performance: Sensitivity Reduction

In this section, we study the effects of perturbations and uncertainties on closed-loop switching converter systems that have control schemes based on the interconnection of (relatively) passive elements, as introduced in Section 6.1. The disturbances that affect a switching converter system are generally highly structured, usually entering in the form of uncertain parameter information, which in turn leads to imprecisely known nominal state values. Note that time-dependent variations in the source and/or load waveforms can be viewed as parametric disturbances. Here, we shall investigate the design of positive real compensators to be used in the scheme outlined in Sections 6.1 and 6.2, chosen to produce closed-loop systems that have reduced sensitivity to parametric disturbances and uncertainties. In these control designs, the speed of the transient behavior is considered as well. This is crucial for rejecting time-varying disturbances arising in the source and load. A related issue is the stability robustness of the closed-loop system; this will be addressed in the next section.

To begin, we examine how parametric disturbances affect the switching converter control systems. The state-space averaged model for a switching converter built from LTI circuit elements, an ideal switch pair, and DC sources takes the form

$$x_t' = A_t x_t + (B_t x_t + b_t) d_t + f_t \tag{6.9}$$

where the subscript t indicates that the associated variables and parameters belong to a model in which the variables are *total* variables as opposed to devi-

ations with respect to nominal variables. In a typical application, the nominal value for one given output is defined a priori. For instance, the desired output voltage of the converter may be specified. This typically translates to having one component of the nominal state x_n known exactly. The other components of the nominal state along with the nominal duty ratio may be unknown. With this type of uncertainty, we are led to consider a perturbed version of the model (6.1):

$$\begin{aligned} x' &= Ax + (Bx + b)(d + \delta d_n) \\ y &= (Bx + b)^* Q_1 (x - \delta x_n) \end{aligned} \tag{6.10}$$

where uncertainty in the nominal duty ratio enters in the term δd_n and uncertainty in the nominal state enters in the term δx_n. The resulting error in the output map can be summarized by the term

$$\delta y = (Bx + b)^* Q(-\delta x_n). \tag{6.11}$$

We omit consideration of uncertainties arising in the circuit parameters. These model uncertainties would affect the specification of Q_1, which would be reflected in the output map of (6.10). The justification for this omission is that the resulting error could have been included as an additional term in δy in (6.11). Therefore, we have effectively summarized the total error due to parametric uncertainties. In Section 6.6, we shall address the stability robustness issue that arises due to uncertainty in determining $Q_1(Bx + b)$.

A block diagram for a closed-loop control system with the model (6.10) as the plant **P** is shown in Figure 6.6. The saturation constraint is represented with a static, passive nonlinearity associated with the plant. There is a well developed theory of sensitivity minimization for *linear* control systems of the form shown in Figure 6.6 (e.g. [63]), based on an explicit parametrization of all the controllers **C** that stabilize **P**. Although the theory for sensitivity minimization is not applicable to the nonlinear case, some parallels exist. A parametrization of all stabilizing compensators for a given stable nonlinear plant is given in the paper of Desoer and Liu [62].

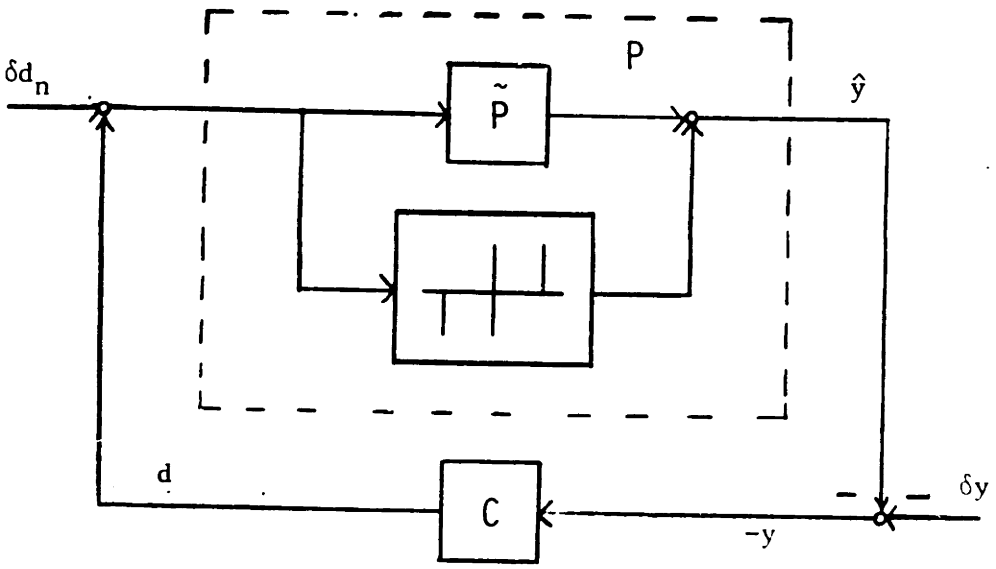

Figure 6.6: General Feedback Connection

The parametrization of [62] has some potential in applications to our problem since the switching converter models of interest are open-loop stable. Actually, the theory in [62] requires that the plant **P** be *finite gain stable* and *incrementally stable*. We shall not go into details on this theory, but note that for such a plant **P**, the set of all stabilizing compensators is given by $\mathbf{C} = \mathbf{Q}(I - \mathbf{PQ})^{-1}$ where **Q** is any finite gain stable operator.

This parameterization and its associated input-output maps afford some insight into the sensitivity reduction problem. In particular, if we consider the respective small signal models $p(s)$, $q(s)$, and $c(s)$ for the operators **P**, **Q**, and **C**, the small signal input-output maps for the signals in Figure 6.6 take the form:

$$\begin{aligned} d &= q\,\delta y - pq\,\delta d_n \\ \hat{y} &= pq\,\delta y + (p - pqp)\,\delta d_n. \end{aligned} \tag{6.12}$$

As an example, for the case where the nominal duty ratio is known ($\delta d_n = 0$), we can impose zero sensitivity to the disturbance δy at a given frequency s_0 by requiring that $q(s)$ satisfy $q(s_0) = 0$. (In the case where $p(s)$ has no pole at s_0, the small signal linearization of the corresponding compensator would have a

zero at s_0.) This situation will be considered in Subsection 6.5.1.

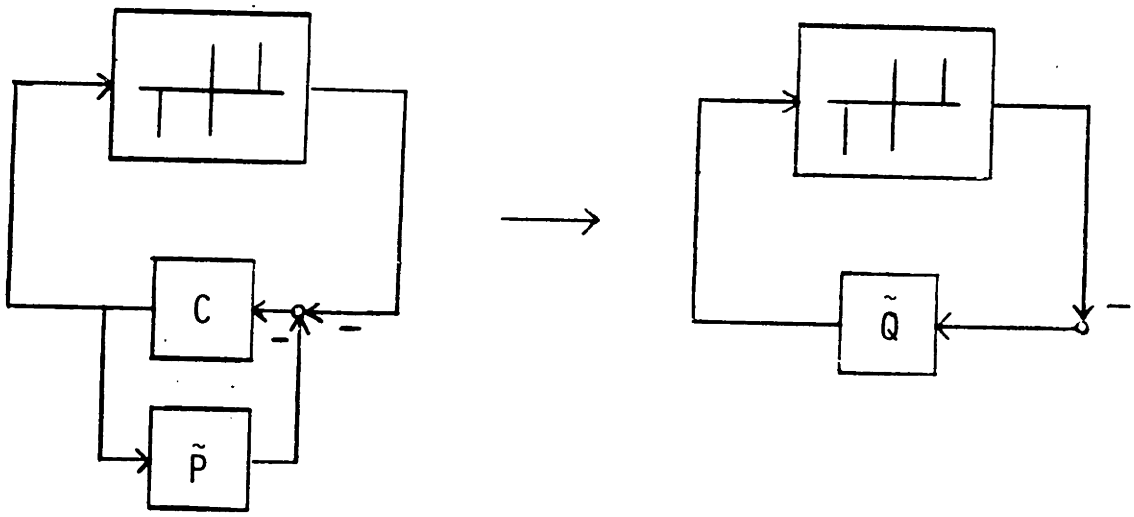

Figure 6.7: Transformed Diagram to Illustrate Constraint on **Q**

Another result of the parametrization described above is that it is possible to relax the constraint that the compensator be positive real. One reason for imposing this constraint was so that stability would be preserved in the presence of the saturating nonlinearity. It is possible to transform the diagram of Figure 6.6 to that of Figure 6.7 in the case where $\delta d_n = \delta y = 0$. From the transformed diagram of Figure 6.7, it is evident that the only requirement on the controller **C** to obtain stability can be stated in terms of the input-output map

$$\tilde{\mathbf{Q}} = \mathbf{C}(I + \tilde{\mathbf{P}}\mathbf{C})^{-1}.$$

In particular, $\tilde{\mathbf{Q}}$ must be stable assuring that **C** stabilizes $\tilde{\mathbf{P}}$, and the interconnection of the map $\tilde{\mathbf{Q}}$ with the static saturating nonlinearity must be stable. One sufficient condition for this is that the operator $\tilde{\mathbf{Q}}$ be strictly relatively passive at the origin to infinity; there are undoubtedly still more relaxed conditions analogous to the Popov and Circle Criteria [37] that apply in the case where $\tilde{\mathbf{Q}}$ is LTI. However, we shall consider only the situation where **C** is designed to be incrementally passive (or positive real), and consequently so is $\tilde{\mathbf{Q}}$.

The remainder of this section is divided into two subsections. The first deals with the case in which the nominal duty ratio is known, and the second addresses the situation where the nominal duty ratio is unknown.

6.4.1 Sensitivity Reduction for Case of Unknown Nominal State Values

Here we consider the case where the nominal duty ratio is assumed to be known exactly. This assumption is relavent to the case where the output voltage of a DC-DC converter is specified and the input voltage is measured. In this case, the required nominal duty ratio can be accurately computed. For instance, for the up-down converter introduced in Chapter 2, we have $d_n = v_n/(v_n - V_s)$. (Note that this formula is valid only in the absence of parasitic resistances, but will usually result in a good approximation.) It is generally difficult to accurately determine the nominal state vector, particularly the components corresponding to inductor currents, since these scale with the load current. Even in the case where the load current is accurately measured, there may be unmodeled dynamics associated with the load that prohibit inference of its constant nominal value. (Identification schemes may be applicable, but will not be considered here.)

With the parametric uncertainty arising only in the nominal state value, the input-output model (6.10) for the converter can be modified as:

$$\begin{aligned} x' &= Ax + (Bx + b)d \\ y &= (Bx + b)^* Q_1(x - \delta x_n). \end{aligned} \tag{6.13}$$

The net effect of the uncertainty in the nominal state value is reflected in the output map in (6.13). We shall take a rather simple approach, noting that it is mainly low frequency (e.g. unknown constant nominal state value) disturbances that drive the control system. It is possible to decouple the closed-loop system from *constant* disturbances of the form indicated in (6.13) by requiring that the controller C block DC signals. (See the discussion following Figure 6.6.) In the framework introduced in Section 6.1, the design can be accomplished by

specifying a LTI controller $C(s)$ that is positive real and satisfies $C(s)|_{s=0} = 0$. In making such a control design, it is desirable to also obtain fast transient behavior. This will permit the closed-loop system to (approximately) reject time-varying disturbances arising from load and source variations. This problem is addressed below.

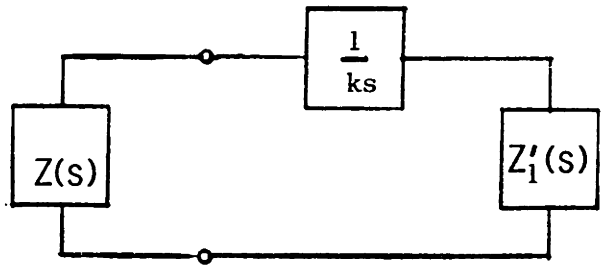

Figure 6.8: Network Interpretation of Control Design

We attack the design problem with a two-step procedure. First, we demonstrate how to obtain a family of positive real compensators $C(s)$ satisfying $C(s)|_{s=0} = 0$. Then, we select from this family one compensator that yields fast small signal transient behavior. One way to view the procedure is by the analogy with interconnected circuit elements given in Section 6.1. Consider an impedance representation $Z(s)$ for the small signal input-output behavior of the plant P. The control design problem can be interpreted as that of specifying a terminating impedance $Z_1(s)$ that has a pole at the origin and that results in "fast" closed-loop behavior. Note that $Z_1(s)$ corresponds to the reciprocal of $C(s)$ and hence the requirement that $C(s)|_{s=0} = 0$ is equivalent to requiring that $Z_1(s)$ have a pole at the origin. To introduce a family of such terminating impedances, consider

$$Z_1(s) = \frac{1}{ks} + Z_1'(s). \tag{6.14}$$

Note that $Z_1(s)$ is guaranteed to be positive real if $k > 0$ and $Z_1'(s)$ is positive real. The constant k is a free design parameter. The design can be completed by specifying k and the impedance $Z_1'(s)$ to terminate the impedance $Z(s) + \frac{1}{ks}$ with

satisfactorily fast dynamical behavior. In Section 6.6, we shall demonstrate an ad hoc, but practically effective method for obtaining a terminating impedance that results in reasonably fast closed-loop behavior. A network representation of the control scheme using this design method is illustrated in Figure 6.8. We apply this design procedure to the fourth order up-down converter (Example 2) of Chapter 5. The details on obtaining the particular compensator will be saved for Section 6.6 (Example 3).

Example: Reduced Sensitivity Control Design for Example 2 Consider the interconnection of the model (6.13) with the compensator $C(s)$ that has a zero at the origin given by

$$2382\frac{s(s+30.2-j15.2)(s+30.2+j15.2)}{(s+38.01-j43.96)(s+38.01+j43.96)(s+31.06)(s+4.488)} \tag{6.15}$$

with all poles and zeros reported in Krad/sec. The model (6.13) here corresponds to the fourth order up-down converter (Example 2) of Chapter 5 with $Q_1 = Q$ corresponding to the matrix that defines the energy in the increment. The eigenvalues of the small signal linearization of this interconnected system are given by (approximately)

$$\begin{aligned} -9.09 \pm j75.42 \quad & \text{Krad/sec,} \\ -11.66 \pm j3.98 \quad & \text{Krad/sec,} \\ -13.60 \pm j7.73 \quad & \text{Krad/sec, and} \\ -21.77 \pm j63.78 \quad & \text{Krad/sec.} \end{aligned}$$

Note that slowest mode of this small signal model is almost twice as fast as the slowest mode that was obtained in Chapter 5 using only static compensation. Details on obtaining the compensator will be given in Section 6.6 (Example 3).

The results of a numerical simulation of a start-up transient using the controller $C(s)$ are shown in Figure 6.9a). Note that the trace corresponding to the energy in the increment is not monotonically decreasing; this follows because the energy in the increment is not a Lyapuonov function for closed-loop operation. Some additional "energy" is associated with the controller $C(s)$. To study

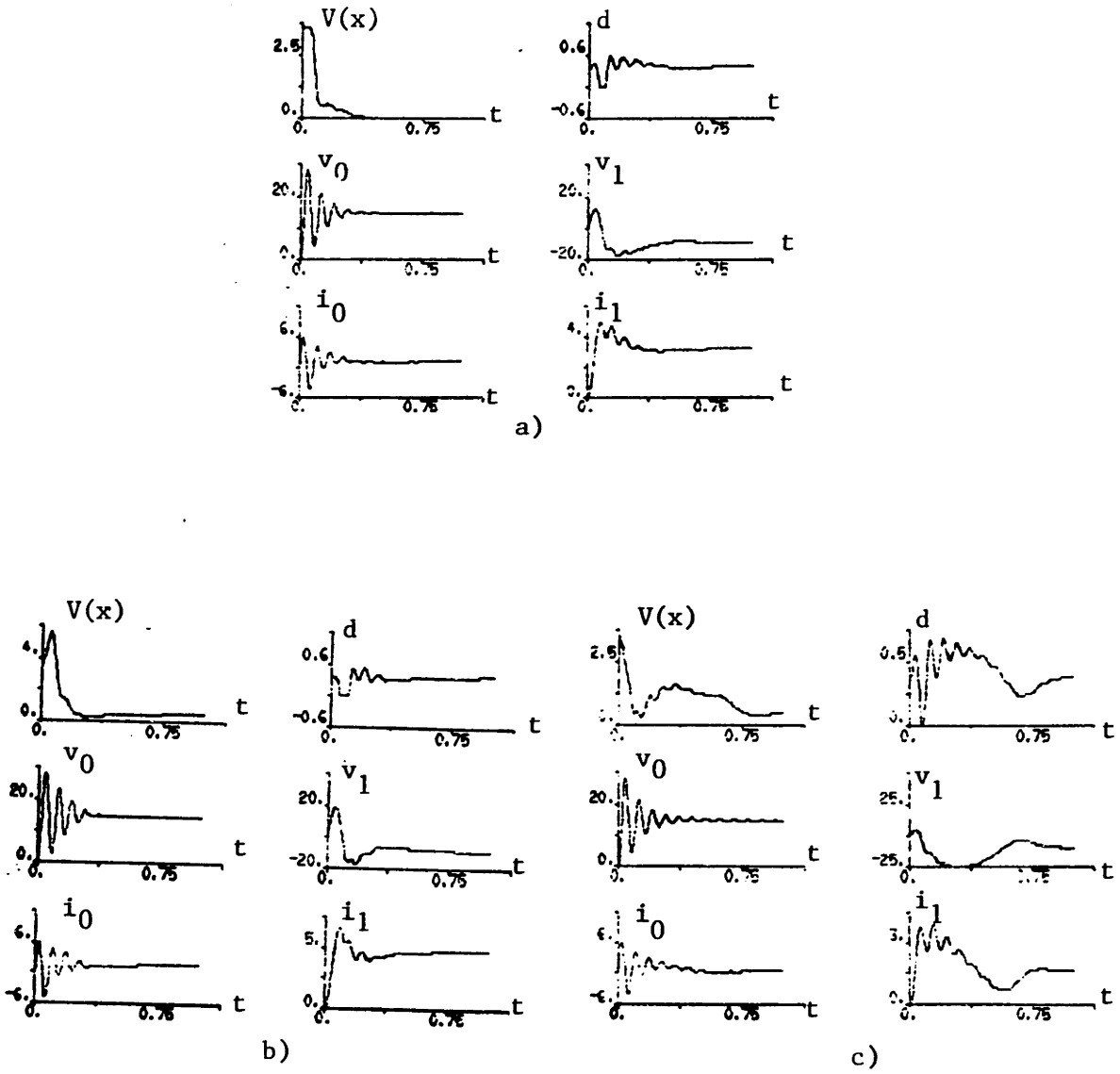

Figure 6.9: Numerical Simulation of Control System with Reduced Sensitivity

the effects of unknown nominal parameters, a second run was made with the load current increased by 50%. Traces for this run are shown in Figure 6.9b). Waveforms for a third run with the load current reduced by 50% are shown in Figure 6.9c). Note that the system is quite well behaved in the presence of these significant disturbances. •

In the next subsection, we study the case where the nominal duty ratio is also considered an unknown parameter. In the context of Figure 6.6, this corresponds to the case where $\delta d_n \neq 0$.

6.4.2 Unknown Nominal Duty Ratio

Now we shall examine the case where the nominal duty ratio of a DC-DC converter is not precisely known, and the only known nominal value corresponds to a specified output variable. A natural way to handle this case is with integral control. This problem can be cast in the framework of the **Q**-parametrization described earlier in this section, but we shall not pursue that here. To implement the integral control scheme, we append an integrator to the plant to integrate the error in the specified output variable, i.e. we construct the auxiliary state z such that

$$z' = cx$$

where cx is the error in the output variable. We then proceed to design a stabilizing controller for the modified plant using the technique developed earlier in this chapter and in Chapter 5. For this purpose, consider the augmented system

$$\tilde{x}' = \tilde{A}\tilde{x} + (\tilde{B}\tilde{x} + \tilde{b})d \tag{6.16}$$

where $\tilde{x} = \begin{bmatrix} x \\ z \end{bmatrix}$,

$$\tilde{A} = \begin{bmatrix} A & 0 \\ c & 0 \end{bmatrix}, \text{ and}$$

$$\tilde{B}\tilde{x} + \tilde{b} = \begin{bmatrix} (Bx + b) \\ 0 \end{bmatrix}.$$

The first step is the specification of a symmetric, positive definite matrix $\tilde{Q}$ satisfying $\tilde{Q}\tilde{A} + \tilde{A}^*\tilde{Q} \leq 0$. Such a matrix can be determined in the case where $\tilde{A}$ is stable. Two conditions that are sufficient for this are that (i) the converter be constructed from DC sources, passive LTI circuit elements, and one ideal switch pair and (ii) any mode of A at the origin (with eigenvector η) is unobservable through c, i.e. $c\eta = 0$. (In the case where the second condition does not hold, there is no reason for augmenting the system model, since the system already contains an 'internal model' of the constant disturbance.) The first condition is our generic open-loop stability condition. In the case where $\tilde{A}$ is stable, we determine an appropriate matrix $\tilde{Q}$ and associate the output equation

$$y = (\tilde{B}\tilde{x} + \tilde{b})^*\tilde{Q}\tilde{x} \tag{6.17}$$

with the system model (6.16) to obtain an augmented input-output model that is strictly relatively passive at the origin to infinity. A control design for the model (6.16) and (6.17) can now be made as done earlier in this chapter.

Example: Second Order Up-Down Converter of Example 1 Consider the problem of output voltage regulation of the second order up-down converter whose model parameters are given in Section 5.1. The parameters for the augmented model with $z' = v - v_n$ are given by

$$\begin{aligned}
\tilde{A} &= \begin{bmatrix} 0 & (1-d_n)/L & 0 \\ -(1-d_n)/C & 0 & 0 \\ 0 & 1 & 0 \end{bmatrix} \\
\tilde{B} &= \begin{bmatrix} 0 & -1/L & 0 \\ 1/C & 0 & 0 \\ 0 & 0 & 0 \end{bmatrix} \\
\tilde{b} &= \begin{bmatrix} (V_s - v_n)/L \\ i_n/C \\ 0 \end{bmatrix}.
\end{aligned}$$

The set of positive definite, symmetric matrices $\tilde{Q}$ that satisfy

$$\tilde{Q}\tilde{A} + \tilde{A}^*\tilde{Q} \leq 0 \tag{6.18}$$

can be parametrized with two scalars in this example. Note that, because of the lossless nature of our model (i.e. all modes of $\tilde{A}$ are on the imaginary axis), the only solutions to (6.18) satisfy (6.18) with equality. To see that all solutions $\tilde{Q}$ can be parametrized with two scalars, note that the modal form for $\tilde{A}$ has the form

$$\tilde{J} = \begin{bmatrix} 0 & -\omega_0 & 0 \\ \omega_0 & 0 & 0 \\ 0 & 0 & 0 \end{bmatrix}. \tag{6.19}$$

Hence all the solutions to the Lyapunov equation

$$\tilde{Q}_J \tilde{J} + \tilde{J}^* \tilde{Q}_J = 0 \tag{6.20}$$

take the form $\tilde{Q}_J = diag\{a_1 \; a_1 \; a_2\}$. Since all the solutions $\tilde{Q}$ to the original Lyapunov equation can be obtained by transformation from this diagonal structure, it follows that all solutions are determined by a_1 and a_2. (This approach to characterizing all solutions to the Lyapunov equation (6.18) was discussed in Chapter 5 (Section 5.2).)

Another way to think about the design procedure of selecting $\tilde{Q}$ is to realize that we are specifying the zeros of the transfer function corresponding to the small signal model for (6.16) and (6.17). Of course, the poles of this transfer function are determined by $\tilde{A}$. The problem is to specify zeros that result in a positive real small signal transfer function. For the case of purely imaginary poles and a strictly proper transfer function, the zeros must also be purely imaginary, and alternate with the poles [75]. For this third order example, we see that the choice of $\tilde{Q}$ amounts to specifying the location of a pair of imaginary zeros. The two parameters a_1 and a_2 then determine this zero location along with a simple scaling factor. This is a general way of characterizing all solutions of the Lyapunov equation in the case where the eigenvalues of the (stable) A-matrix are purely imaginary.

For the particular example with numerical parameters given in Section 5.1, we have determined a suitable solution

$$\tilde{Q} = \begin{bmatrix} 0.6872 & 0 & -576.4 \\ 0 & 0.01563 & 0 \\ -576.4 & 0 & 2.0 \bullet 10^6 \end{bmatrix}.$$

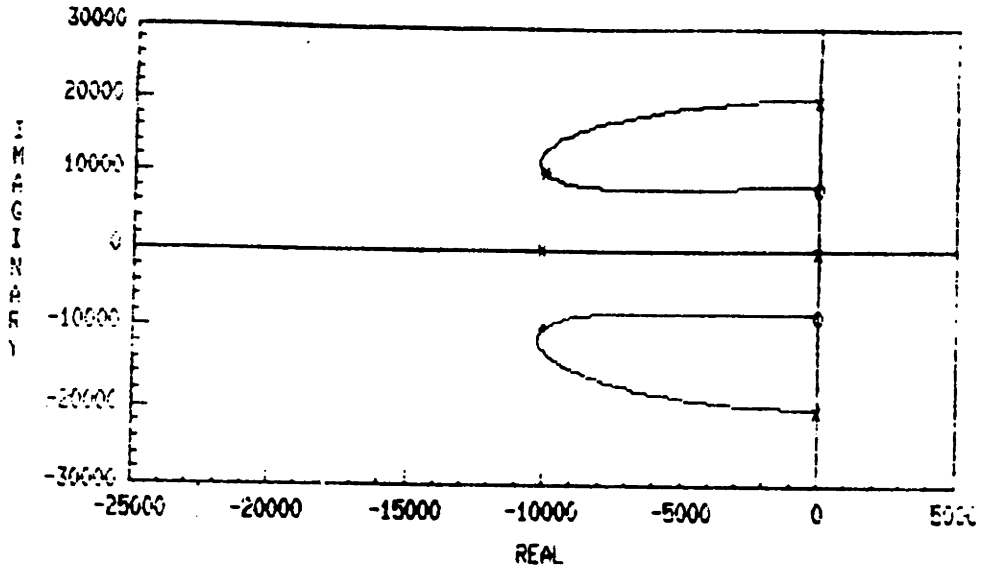

Figure 6.10: Root Locus for Small Signal Behavior of Closed-Loop System that Includes Integral Control Action

A root locus for the eigenvalues of the small signal model of the control system where a simple feedback gain is applied to the model (6.16) and (6.17) is shown in Figure 6.10. Note that with a simple gain of $1.7 \bullet 10^{-6}$, the resulting small signal eigenvalues are given by $-10.0 \pm j9.98$ Krad/sec and -10.1 Krad/sec. We shall reserve a numerical simulation for the fourth order example below. We have limited consideration here to the use of nondynamic feedback in conjunction with the constructed input-output model (6.16) and (6.17), but dynamical passive compensation techniques can be applied. See Section 6.6 for this. The reason for not considering dynamical feedback in this example is that we have obtained reasonably fast small signal behavior with the nondynamic approach. This holds true for the fourth order example discussed below, as well. •

Example: Fourth Order Converter of Example 2 Here we consider the problem of regulating the output voltage of the fourth order up-down converter in Example 2 of Section 5.2. To implement the integral control action, we augment the system model with the variable z satisfying $z' = v_1 - v_{1n}$, just as in the previous example. To design a globally stabilizing control for the

augmented system, we first specify the matrix $\tilde{Q}$. In this example, the five poles of the small signal model are purely imaginary, and hence, the selection of $\tilde{Q}$ reduces to specifying two pairs of purely imaginary zeros and a scaling factor. We have obtained one choice of $\tilde{Q}$ that can result in satisfactory small signal dynamics with a nondynamic compensator. The root locus for the small signal eigenvalues of the closed-loop system using a simple gain is shown in Figure 6.11. With this scheme, the small signal eigenvalues can be placed at $-11.86 \pm j1.66$Krad/sec,$-14.98 \pm j61.75$ Krad/sec, and -14.87Krad/sec by a constant scalar gain. This is the gain that will be used in the numerical simulations discussed below.

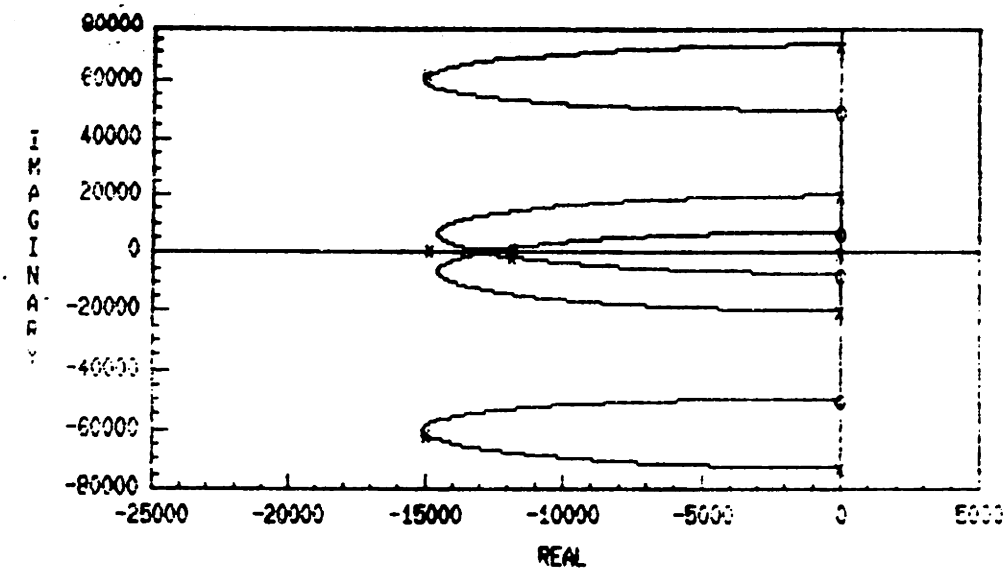

Figure 6.11: Root Locus for Fourth Order Converter Control System that Uses Integral Control

Waveforms for numerical simulations of some start-up transients are displayed in Figure 6.12. Figure 6.12a) shows waveforms for a start-up transient in the case where all circuit parameters are considered known. A simulation for the case where the load current is reduced by 50% is shown in Figure 6.12b). Note that in this case, some of the nominal state values differ from those programmed into the controller, but satisfactory behavior prevails. Figure 6.12c) exhibits waveforms for the case where the input voltage V_s is 33% less than its

nominal value. In this situation, the nominal duty ratio as well as some nominal state values are different from those used by the controller. The closed-loop system remains stable, but there appears to be a dominant slow mode. •

To summarize this section, we have demonstrated two approaches for the reduction of sensitivity to disturbances arising from uncertain parameter information. In so doing, we have also shown how to maintain reasonably fast dynamics. The methods fit the framework of the Lyapunov-based control schemes outlined earlier in the thesis, and hence result in globally stable dynamical behavior for the nominal models. However, in the presence of perturbations due to parametric uncertainty, the input-output models (6.10) and (6.16,6.17) can lose their property of being strictly relatively passive to infinity. In this case, although we have not observed instability in the examples, there is not an a priori guarantee for global (or even small signal) stability. This is the subject of the next section where stability robustness is examined.

6.5 Performance: Stability Robustness

In this section, we investigate the large signal stability robustness of the control strategies introduced earlier in this and the preceding chapter. This topic is closely related to the issue of system sensitivity discussed in the previous section, but differs in that here we study conditions under which global stability is maintained in the presence of uncertainties and disturbances. We shall develop schemes similar to those of the previous section for sensitivity reduction, but that also have excellent robustness properties. The presentation here is divided into three main subsections, and a summarizing subsection.

The first subsection investigates the effects of uncertain or unknown circuit parameters such as inductor, capacitor, and resistor values. The focus is on how to select an appropriate quadratic Lyapunov function $\frac{1}{2}x^*Q_1x$ that results in large signal stability robustness of the Lyapunov-based control scheme. We emphasize the fact that the choice $Q_1 = Q$, where Q defines the form of the energy in the increment, results in excellent robustness properties. The second

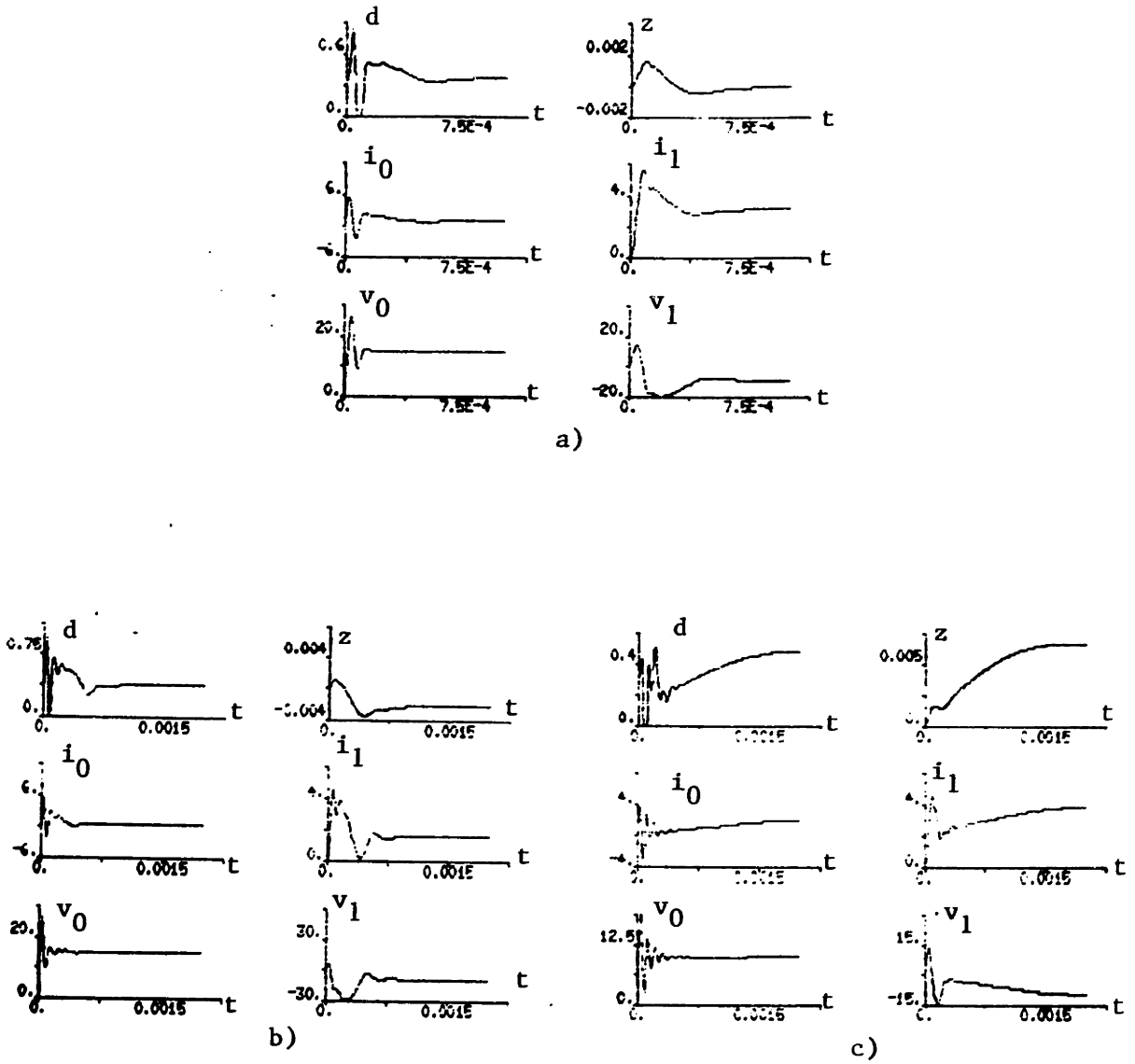

Figure 6.12: Numerical Simulations of Start-Up Transients with Controller that Incorporates Integral Control Action

and third subsections deal with uncertainties in the nominal state values and the nominal duty ratio. These are often the dominant uncertainties that need to be considered in robust control design since these are generally due to factors external to the converter (such as the load). To handle these uncertainties, we develop a *self-tuning adaptive control* algorithm that stably estimates unknown nominal state values required in the Lyapunov-based control schemes. The resulting behavior can be guaranteed to be globally asymptotically stable, and the small signal dynamics can be made adequately fast as demonstrated in examples.

A general framework for studying the stability robustness of control systems of the type considered here was suggested in [62], using the parametrization of all stabilizing controllers for a given stable plant. The robustness result of [62] is based on the small gain theorem (see [37]), and requires that the perturbations in the plant input-output map satisfy a certain bound. Such a bound is difficult to obtain for the plant models that we consider for two reasons. Firstly, it is generally difficult to compute the gain (or incremental gain) for any nonlinear operator. Secondly, the perturbations that need to be considered are generally large, as can be seen by considering a small signal linearization for the plant. For instance, uncertainty in the position of a pole near the $j\omega$-axis leads to a large perturbation in the linearized plant model for frequencies near the perturbed pole. Because of the structured nature of the uncertainties affecting the nominal plant models of interest here, and the difficulty in applying the framework of [62], we study the effects of these uncertainties as outlined in the preceding paragraph.

6.5.1 Uncertainties Arising in Circuit Parameters

In this subsection, we deal with uncertainties that prohibit accurate knowledge of the matrices A, B, and b in the model (6.1) introduced in Section 6.1. For the Lyapunov-based control schemes of this chapter and the previous one, the ramification of this type of uncertainty emerges in the specification of the matrix

Q_1 that appears in (6.1). In particular, we shall investigate conditions under which the model (6.1) remains strictly relatively passive to infinity when the available data for control design consists of imperfect model data, i.e. $\tilde{A}$, $\tilde{B}$, and $\tilde{b}$. Since we are not concerned with uncertainties in the nominal state values, we assume that x is precisely known. Hence, uncertainty in determining y arises only in determining the vector $Q_1(Bx+b)$. In evaluating the vector $Q_1(Bx+b)$, we would normally first determine $Q(Bx+b)$ and then multiply on the left by $Q_1\tilde{Q}^{-1}$ where $\tilde{Q}$ is the model value of Q. It was demonstrated in Section 5.3 that it is generally possible to determine the vector $Q(Bx+b)$ quite accurately. We shall give some attention to the situation where parasitic resistances affect the measurement of $Q(Bx+b)$, below.

With the assumption that $Q(Bx+b)$ is known, the underlying input-output model takes the form

$$\begin{aligned} x' &= Ax + (Bx+b)d \\ y &= (Bx+b)^* Q\tilde{Q}^{-1}Q_1 x. \end{aligned} \tag{6.21}$$

The simplest and strongest condition for the model (6.21) to be strictly relatively passive to infinity is that the control design is based on the energy in the increment. In this case we would take $Q_1 = \tilde{Q}$ (since the best we can do is to use the model data). Then, $\frac{1}{2}x^*Qx$ is a storage function for (6.21), leading to the conclusion that the model is strictly relatively passive to infinity. Note that such a storage function gives an explicit lower bound on the energy in the increment between a given trajectory with initial condition $x(0) = 0$ and the nominal constant trajectory with $x = 0$. To see this, consider the calculation:

$$\begin{aligned} W_0 &= \int_0^T y d\, dt \\ &\geq \int_0^T \frac{d}{dt}\left(\frac{1}{2}x^*Qx\right) dt \\ &= \frac{1}{2}x(T)^*Qx(T). \end{aligned} \tag{6.22}$$

See Appendix A and preceding sections for more details on this type of calculation. We shall discuss more general conditions for the perturbed model to

remain strictly relatively passive to infinity in the case where an alternative storage function is selected. (Recall that one of the main reasons for selecting an alternative storage function was to obtain faster transient behavior.) First, we study the effects of parasitic resistances on the measurement of the vector $Q(Bx+b)$, and the resulting implications for the model (6.21) in the case where $Q_1 = \tilde{Q}$.

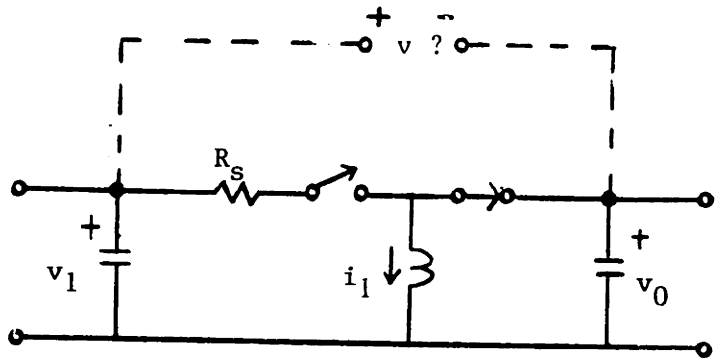

Figure 6.13: Effect of Parasitics on Measurement of $Q(Bx + b)$

In order to study errors in the measurement of the vector $Q(Bx + b)$, we need to recognize how this vector is measured. In Section 5.3 we discussed two methods for this. The second and supposedly preferred method involved a simple measurement of circuit state variables associated with the switch branches. This scheme was based on two topological conditions requiring the absence of resistances participating in a certain loop and in a certain cutset involving the switch branches. In a typical (idealized) switching converter model, there are no resistances aside from those associated with the load. Hence, we would usually like to apply this second method for measuring $Q(Bx + b)$. However, parasitic resistances (e.g. switch resistance and capacitor equivalent series resistance (ESR)) will often lead to the violation of the necessary topological conditions. It will be argued that these parasitics typically do not destroy the passivity property of the model (6.21) in the case where $Q_1 = \tilde{Q}$. First, we illustrate with an example the type of measurement errors that arise because of parasitic resistances.

Example: Effect of Parasitic Resistance on Measurement of $Q(Bx+b)$
Consider the canonical cell shown in Figure 6.13. Recall that $Q(Bx+b)$ is the amount (modulo sign) that the vector of the derivatives of the inductor fluxes and capacitor currents changes at the instant of a switch transition. In the absence of the switch resistance R_s, the vector $Q(Bx+b)$ takes the form $[-i_1 \ (v_1 - v_0) \ i_1]^*$ as previously calculated in Section 5.3. However, in the presence of the parasitic switch resistance, $Q(Bx+b)$ becomes

$$[-i_1 \ \ (v_1 - R_s i_1 - v_0) \ \ i_1]^*.$$

If we attempted to measure the elements of this vector directly on the canonical cell as shown in Figure 6.13, ignoring the presence of the parasitic resistance, our measurement would result in the original unperturbed value of $Q(Bx+b)$. The point illustrated by this example is that the error incurred can be summarized with the error term

$$Q(\delta B)x = Q(\tilde{B}x+b) - Q(Bx+b). \tag{6.23}$$

Note that the term δB in (6.23) need not necessarily be the perturbation in the B matrix in the model (6.21). In fact, the obtained measurement can depend upon the instantaneous switch position. To overcome this difficulty, we shall assume a form for a bound on δB in terms of the perturbation in the B matrix, as discussed below. •

Recall from Chapter 4 where the structure of the state-space averaged model was studied that the matrices A and B in (6.21) are given by

$$A = -Q^{-1}[(1-d_n)H_0 + d_n H_1] \tag{6.24}$$

$$B = -Q^{-1}[H_1 - H_0] \tag{6.25}$$

where H_0 and H_1 are hybrid representations for the resistive multiport in the partitioned circuit corresponding to the two switch configurations. Suppose that our design (and measurement scheme) is based on the *model* values

$$\tilde{A} = -\tilde{Q}^{-1}[(1-d_n)\tilde{H}_0 + d_n \tilde{H}_1] \tag{6.26}$$

$$\tilde{B} = -\tilde{Q}^{-1}[\tilde{H}_1 - \tilde{H}_0] \tag{6.27}$$

which neglect all parasitic resistances. We shall make two assumptions on the hybrid matrices H_0, $\tilde{H}_0$, H_1, and $\tilde{H}_1$, and on the measurement that is obtained. Firstly, we assume that the effect of the parasitic resistances is only to increase (in the positive definite sense) the value of the hybrid matrices, i.e.

$$\begin{aligned} \tilde{H}_0 &\leq H_0 \\ \tilde{H}_1 &\leq H_1. \end{aligned} \tag{6.28}$$

This holds in the case where the nominal converter model is lossless, i.e. where $\tilde{H}_0$ and $\tilde{H}_1$ are skew-symmetric. The second assumption is that the effect of parasitic resistance is to force the actual measurement to be somewhere in between the true value $-[H_1 - H_0]x + Qb$ and the model value for this measurement $-[\tilde{H}_1 - \tilde{H}_0]x + Qb$. That is, measurement error can be summarized in the form

$$Q(\delta B)x = [\delta H_1 - \delta H_0]x \tag{6.29}$$

where δH_1 and δH_0 are bounded in the positive definite sense as follows

$$\begin{aligned} 0 \leq \delta H_1 &\leq H_1 - \tilde{H}_1 \\ 0 \leq \delta H_0 &\leq H_0 - \tilde{H}_0 \end{aligned} \tag{6.30}$$

(The right-hand sides of (6.30) are positive semi-definite as a result of the first assumption.) One case for which the second assumption holds is where the actual measurement obtained is given by

$$-[\tilde{H}_1 - \tilde{H}_0]x + Qb. \tag{6.31}$$

This was the case in the example of Figure 6.13. Note that although we have not given general conditions for these two assumptions to hold, we have not discovered a reasonable example where parasitic resistances cause the assumptions to be violated. Furthermore, in the process of making a control design, it is possible to check that these conditions are not violated for a certain set of parasitics.

With the groundwork in place, we examine the model given by

$$\begin{aligned} x' &= Ax + (Bx + b)d \\ y &= (Bx + b)^* Qx - [Q(\delta B)x]^* x. \end{aligned} \tag{6.32}$$

It turns out that the model (6.32) is strictly relatively passive to infinity, if the two conditions above are satisfied. This can be verified by considering $\frac{1}{2}x^*Qx$ as a storage function. In particular, by differentiating this function along the system trajectories, we find

$$\begin{aligned}\frac{d}{dt}\left(\frac{1}{2}x^*Qx\right) &= \frac{1}{2}x^*[QA + A^*Q]x + [Q(\delta B)x]^*xd + yd \\ &= -x^*[(1-d_n)H_0 + d_nH_1]x - x^*[\delta H_1 - \delta H_0]xd + yd \\ &= -x^*[(1-d_n)H_0 - (\delta H_0)d + d_nH_1 + (\delta H_1)d]x + yd\end{aligned} \tag{6.33}$$

Because of the bounds (6.30) and the duty ratio constraint $-d_n \leq d \leq 1 - d_n$, the first term on the right-hand side of the last line of (6.33) is nonpositive, and hence we have demonstrated that the model (6.32) is strictly relatively passive to infinity. The conclusion is that parasitic resistances cannot destroy the passivity property of the model (6.1) in the case where we take the energy in the increment as a storage function, and we use the simplest measurement scheme to determine $Q(Bx + b)$. Now we return to the general case $Q_1 \neq \tilde{Q}$, and ignore the uncertainty in determining $Q(Bx + b)$.

A sufficient condition for the model (6.21) to be strictly relatively passive to infinity is that there exist a positive definite quadratic storage function $\frac{1}{2}x^*\tilde{Q}_1x$ (with $\tilde{Q}_1$ symmetric) for the system (6.21). The notation here (tilde) is meant to suggest that $\tilde{Q}_1$ approximates Q_1 since $\frac{1}{2}x^*Q_1x$ would have been a valid storage function in the case of perfect parameter information. Such a quadratic form would necessarily satisfy

$$\frac{d}{dt}(\frac{1}{2}x^*\tilde{Q}_1x) = \frac{1}{2}x^*[\tilde{Q}_1A + A^*\tilde{Q}_1]x + x^*[\tilde{Q}_1 - Q_1\tilde{Q}^{-1}Q](Bx + b)d + yd. \tag{6.34}$$

In order for $\frac{1}{2}x^*\tilde{Q}_1x$ to be a storage function for (6.21), it must be true that $\tilde{Q}_1$ is positive definite and that the sum of the first two terms on the right-hand side of (6.34) is nonpositive for all admissible values of d and x. Note that x is permitted to take on any value in $\mathcal{R}^n$, but d is confined to a closed interval of the real line. Two constraints on the matrix $\tilde{Q}_1$ emerge from this requirement,

namely

$$[\tilde{Q}_1 - Q_1\tilde{Q}^{-1}Q]b = 0, \text{ and} \tag{6.35}$$

$$\frac{1}{2}(\tilde{Q}_1 A + A^*\tilde{Q}_1) + (\tilde{Q}_1 - Q_1\tilde{Q}^{-1}Q)Bd \leq 0 \tag{6.36}$$

where (6.36) holds for all admissible values of d. In general, there is an open set of positive definite, symmetric matrices that satisfy the first constraint (6.35). With some linear algebraic manipulation, it can be shown that the symmetric matrix $\tilde{Q}_1$ that most closely approximates $M = Q_1\tilde{Q}^{-1}Q$ in the Frobenius norm and satisfies (6.35) is given by

$$\tilde{Q}_1 = \frac{Mbb^*M}{b^*Mb} + \left[I - \frac{bb^*}{b^*b}\right]\left(\frac{M + M^*}{2}\right)\left[I - \frac{bb^*}{b^*b}\right] \tag{6.37}$$

Note that $\tilde{Q}_1 = M$ if M is symmetric. Furthermore, it is clear from this formula that $\tilde{Q}_1$ is positive definite if M is positive definite. In general, we expect this to be the case since it is typically possible to have accurate parameter information on the elements of Q, which correspond to the values of the inductors and the capacitors in the switching converter. In the case where Q is known, we would have $M = Q_1$ which is positive definite by design. We shall focus on the second constraint (6.36) with the idea that the matrix $\tilde{Q}_1$ closely approximates Q_1.

In the case where there is no uncertainty arising from the reactive portion of the converter circuit, i.e. $\tilde{Q}_1 = Q_1$, the satisfaction of the second constraint (6.36) depends solely on the uncertainty in the resistive portion of the circuit. The second constraint reduces essentially to the Lyapunov equation

$$\tilde{Q}_1 A + A^*\tilde{Q}_1 \leq 0. \tag{6.38}$$

In the remainder of the discussion, we shall consider issues in the selection of the matrix Q_1 which lead to robust satisfaction of the constraint (6.36). Note that the selection of Q_1 is necessarily based on the model parameters $\tilde{A}$, $\tilde{B}$, and $\tilde{b}$. It is well known [13] that, in the case where $\tilde{A}$ is asymptotically stable, there exists a symmetric, positive definite solution Q_1 to the Lyapunov equation

$$Q_1\tilde{A} + \tilde{A}^*Q_1 = -P \tag{6.39}$$

where P is positive definite and symmetric. In the case where $\tilde{A}$ differs from the underlying matrix A by an additive term, i.e. $\tilde{A} = A + \delta A$, the Lyapunov equation (6.39) readily leads to the following bound on the permissible uncertainty δA:

$$\sigma_{max}\{\delta A\} \leq \frac{\sigma_{min}\{P\}}{2\sigma_{max}\{Q_1\}} \tag{6.40}$$

where $\sigma\{\bullet\}$ refers to the indicated singular value. The relation (6.40) gives an explicit bound on the size of perturbations (due to resistive uncertainty) in A that do not destroy the passivity property of (6.21).

One of the main reasons for selecting a matrix $Q_1 \neq Q$ would be to shape the small signal transient behavior. The above result indicates that in so doing, it is generally possible to pick Q_1 to permit some margin of uncertainty in $\tilde{A}$. Note that this result does not apply to control designs that use integral control since the augmented A-matrices that arise in those designs are never asymptotically stable. In many cases the most significant perturbations in the A-matrix are highly structured. We discuss a robustness result for these perturbations, below.

The perturbations due to resistive uncertainty in the converter circuit are generally (i) minor perturbations due to parasitics and (ii) large perturbations associated with load uncertainty. Here we focus on the large perturbations. In particular, there may be a single diagonal entry in A that corresponds to a load resistance. This element may take on a range of values depending on how heavy the load is and to what extent the load is resistive. In any case for a particular uncertainty that manifests itself as a rank one perturbation in A, we can write the perturbed A-matrix in the form

$$A_\epsilon = A + \epsilon A_1 \tag{6.41}$$

where $\epsilon \in [0, 1]$. Now the problem is to solve a family of simultaneous Lyapunov equations given by

$$Q_1(A + \epsilon A_1) + (A + \epsilon A_1)^* Q_1 = -P_\epsilon \tag{6.42}$$

where Q_1 is symmetric and positive definite, and P_ϵ is symmetric and nonnegative definite for each ϵ.

A sufficient condition for the existence of a solution to (6.42) can be stated in terms of a factorization for A_1, i.e. $A_1 = bc$ where b is a column vector and c is a row vector. It turns out that if the transfer function $-c(sI - A_1)^{-1}b$ is positive real, then (6.42) has a solution. This follows from the fact that if $-c(sI - A)^{-1}b$ is positive real, there exists a positive definite matrix Q_1 such that

$$\begin{aligned} Q_1 A + A^* Q_1 &\leq 0 \\ c &= -b^* Q_1. \end{aligned} \tag{6.43}$$

It then follows that $Q_1(A+\epsilon A_1)+(A+\epsilon A_1)^* Q_1 \leq 0$ for all nonnegative ϵ. (Note that, because of the result of Chapter 4 on open-loop stability, the matrix Q that defines the form of the energy in the increment is always a solution to (6.43).) The equations (6.43) give a straightforward method to check if a given matrix Q_1 generates a control scheme that is robust to a large structured perturbation of A. We illustrate this with one of our earlier examples.

Example: Integral Control of Up-Down Converter with Uncertain Load Consider the integral control scheme applied to the second order up-down converter as done in Section 6.4. In the case where the load consists of a current source and a linear resistor of value R, the augmented A-matrix takes the form

$$A = \begin{bmatrix} 0 & (1-d_n)/L & 0 \\ -(1-d_n)/C & -1/RC & 0 \\ 0 & 1 & 0 \end{bmatrix}.$$

Suppose the value of R is not known because it is uncertain what fraction of the load current is due to the current source. This leads to structured uncertainty in A of the form

$$A_1 = \begin{bmatrix} 0 & 0 & 0 \\ 0 & -1 & 0 \\ 0 & 0 & 0 \end{bmatrix} = \begin{bmatrix} 0 \\ -1 \\ 0 \end{bmatrix} \begin{bmatrix} 0 & 1 & 0 \end{bmatrix} = b_1 c_1.$$

When we first studied this example, we selected a matrix Q_1 that was given by

$$Q_1 = \begin{bmatrix} 0.6872 & 0 & -576.4 \\ 0 & 0.01563 & 0 \\ -576.4 & 0 & 2.0 \bullet 10^6 \end{bmatrix}.$$

For this selection it is already known that $Q_1 A + A^* Q_1 \leq 0$ where A corresponds to the case $R = \infty$, and hence the first condition of (6.43) is satisfied. It turns that the second condition of (6.43) is also satisfied (to within a scaling factor). We conclude that this choice of Q_1 leads to robustness with respect to uncertainties in the load character. In particular, the control scheme of Section 6.4 (reconsidered here) will result in globally stable behavior, regardless of the composition of the load. The load current may be due to any combination of resistive and current source components; all that is required is that the nominal value of the load is known. (The case where the nominal value of the load current is unknown is considered below.) •

To summarize this subsection, we have investigated the effects of uncertain circuit parameters on the passivity property of the model (6.1). The strongest result available is that designs that are based on the energy in the increment are inherently robust to these uncertainties. Some care is needed in choosing alternative Lyapunov functions. However, the preservation of the passivity property of (6.1) is undoubtedly a stronger condition than is necessary for the preservation of large signal stability. In the next subsection, we investigate the effects of unknown nominal state values, and methods for dealing with these. Most of the following discussion will assume the use of control based on the energy in the increment.

6.5.2 Adaptive Control Method to Handle Uncertain Nominal State Values

Here we consider control design for the model (6.13) introduced in the previous section for the case where the nominal state vector is unknown, but constant. It is assumed that the nominal duty ratio is exactly known. The 'self-tuning' method to be used is very similar to that of Section 6.4 where a blocking zero at DC was introduced into the controller, but will permit the conclusion of global asymptotic stability in the presence of uncertain nominal state values. The presentation to be given selects a form for the adaptation mechanism at the

outset, and subsequently justifies it. It is possible to motivate the use of this adaptation mechanism by a Lyapunov argument, but this will be omitted.

To implement the self-tuning scheme, we shall include as part of an augmented state vector, an estimate $\tilde{x}_n(t)$ of the constant nominal value of the state vector for the original plant. We can equivalently represent this estimate by its error, i.e. $\delta x_n(t) = \tilde{x}_n(t) - x_n$. The update law for $\delta x_n(t)$ is selected to be

$$\frac{d}{dt}(\delta x_n) = -K^{-1}Q_1(Bx + b) \tag{6.44}$$

where K is a symmetric positive definite matrix and Q_1 is as previously specified. The rationale for this adaptation mechanism arises from the augmented state-space model for the perturbed model (6.13) that includes the error in the estimate of the nominal converter state vector as a part of its state, i.e.

$$\begin{aligned} x' &= Ax + (Bx + b)d \\ (\delta x_n)' &= -K^{-1}Q_1(Bx + b)d \\ y &= (Bx + b)^*Q_1(x - \delta x_n) \end{aligned} \tag{6.45}$$

Note that y can now be determined without any uncertainty arising from the unknown nominal state values since

$$x - \delta x_n = (x_t - x_n) - (\tilde{x}_n - x_n) = x_t - \tilde{x}_n,$$

and x_t can be measured while $\tilde{x}_n$ is stored in the controller. Recall that it is generally possible to obtain an accurate measure of $Q(Bx + b)$ (see Section 5.3), which in turn can be used in the computation of $Q_1(Bx + b)$, as discussed earlier in this section. It turns out that the model (6.45) is strictly relatively passive at the origin to infinity, as can be seen by taking as storage function

$$V = \frac{1}{2}x^*Q_1x + \frac{1}{2}(\delta x_n)^*K(\delta x_n). \tag{6.46}$$

Therefore, it is possible to embed the augmented plant model (6.45) in a control loop with an incrementally passive compensator that takes saturation into account, as done elsewhere in this chapter. Before studying some examples, we comment on certain features of this augmented model.

As previously noted, this scheme is very similar to the method introduced in Section 6.4 for reducing DC sensitivity by introducing a blocking zero at DC into the compensator. The method of Section 6.4 for introducing a DC zero into the compensator was actually to place a simple integrator in parallel with the input-output model for the plant. Recall that in the analogy with circuit models, we placed an impedance $1/ks$ in series with the impedance model $Z(s)$ for the plant. Since the "current" is the input for this model, the additional term $1/ks$ amounts to a parallel element if one considers a block diagram representation. Here, we use a slightly more sophisticated version of this idea by replacing the simple integrator with a vector of integrators whose rates are controlled by the state x through the vector $Bx + b$.

One possible choice for the matrices Q_1 and K in (6.45) is $Q_1 = Q$ and $K = kI$ where Q is the matrix composed of inductance and capacitance parameters that defines the energy in the increment. In this case, we would require a measurement of the vector $Q(Bx + b)$, and as noted in Section 5.3, it is usually possible to accurately measure the vector $Q(Bx + b)$. Errors due to parasitic resistances, as discussed in Subsection 6.5.1, do not destroy the relative passivity property of (6.45). To see this, consider the perturbed version of (6.45) that takes into account this type of parasitic:

$$\begin{aligned} x' &= Ax + (Bx + b)d \\ (\delta x_n)' &= -k^{-1}Q(\tilde{B}x + b)d \\ y &= (\tilde{B}x + b)^*Q(x - \delta x_n). \end{aligned} \tag{6.47}$$

Differentiating the storage function (6.46) along the trajectories of (6.47), we obtain

$$\frac{d}{dt}V = \frac{1}{2}x^*[QA + A^*Q]x - \frac{1}{2}x^*[Q(\delta B) + (\delta B)^*Q]xd + yd. \tag{6.48}$$

The first two terms on the right-hand side of (6.48) are nonpositive when the parasitic resistances satisfy the conditions outlined in Subsection 6.5.1. The result of this choice for Q_1 and K will be excellent stability robustness. In the examples to be studied, we shall make these particular selections for Q_1 and K.

Example: Estimation of Nominal Inductor Current in Simple Up-Down Converter In this example, we apply the adaptive control scheme to the second order up-down converter whose parameters are given in Section 5.1. We now assume, however, that the load is unknown but constant in the steady state. As a consequence, the nominal inductor current is also unknown. This is the parameter that our self-tuning mechanism will estimate. In this example, it is assumed that the input voltage V_s is known (i.e. measured), the nominal output voltage v_n is defined by the regulation problem, and the nominal duty ratio d_n is known. (The nominal duty ratio can usually be determined from V_s and v_n.) For the choices $Q_1 = Q$ and $K = kI$, we work with the augmented model

$$\begin{bmatrix} i' \\ v' \\ (\delta i_n)' \end{bmatrix} = \begin{bmatrix} 0 & (1-d_n)/L & 0 \\ -(1-d_n)/C & 0 & 0 \\ 0 & 0 & 0 \end{bmatrix} \begin{bmatrix} i \\ v \\ (\delta i_n) \end{bmatrix} + \begin{bmatrix} (V_s - v_t)/L \\ i_t/C \\ -k^{-1}(V_s - v_t) \end{bmatrix} d$$

$$y = (V_s - v_t)\{i - (\delta i_n)\} + i_t(v - v_n). \tag{6.49}$$

Note that in this model, the quantities without subscripts are deviations from nominal, the quantities with subscript t are total variables that can be measured, and the quantities with subscript n are nominal variables. We only attempt to estimate the nominal inductor current since the other nominal state variable (the capacitor voltage) is known. The output y of this model can be determined exactly since $i - (\delta i_n)$ is precisely $i_t - \tilde{i}_n$, i.e. the difference between the actual inductor current and the present estimate of the nominal value of this current. The control design can be completed by specifying $k > 0$ and a positive real compensator for the system (6.49). The issues concerning small signal transient behavior are analogous to those dealt with in Section 6.4.

For this example, we can obtain reasonably fast behavior with a simple static feedback that incorporates the saturation constraint. For example, with a nominal load current of 2amps, the eigenvalues of the small signal linearized model can be placed at $-7.713 \pm j12.9$Krad/sec and -11.36Krad/sec by selecting $k = 2778$

and the unsaturated gain $\alpha = .004$. Other parameter choices can result in still faster small signal behavior. A numerical simulation of a start-up transient using these parameters is shown in Figure 6.14. Note that the initial condition for the estimate of the nominal inductor was taken as zero. •

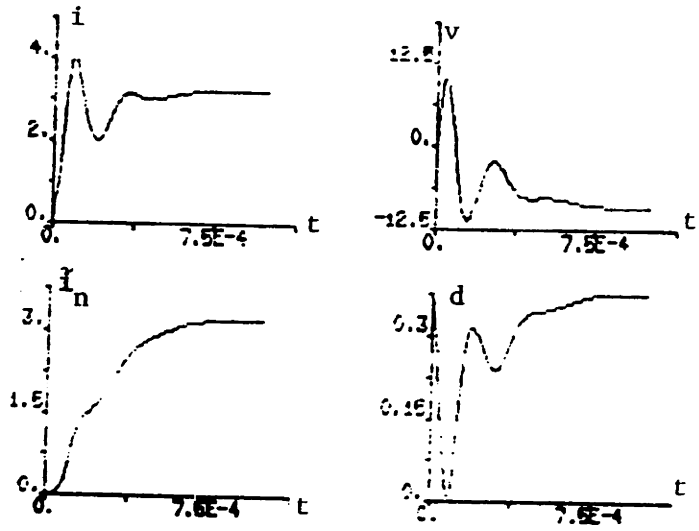

Figure 6.14: Start-Up Transient in Second Order Converter Using Adaptive Control Scheme

A potential problem of the adaptation scheme (6.44) for the case where more than one parameter is to be estimated is that there may be redundant parametrization. A consequence of this is that the small signal model of (6.45) becomes unobservable. This can result in nondecaying (unobservable) modes associated with the adaptation mechanism. Of course, since the nondecaying modes are unobservable, these will have no effect on the internal behavior of the converter circuit. We would like to be assured, however, that we do not have a problem with divergence in the adaptation mechanism.

A first step toward this end is to recognize redundant parameters in the adaptation scheme, and to eliminate them. This was done in the previous example by not attempting to estimate v_n. However, there are cases where the model including the adaptation mechanism does not have parameter redundancy, but the small signal linearization is nevertheless non-minimal. It is possible in this case

for the stable closed-loop system to come to rest with $\delta x_n \neq 0$. We shall need to assure that, in the presence of wideband disturbances that drive the closed-loop system, the estimates of the nominal state parameters do not diverge.

One route for proving that parameter estimates do not diverge is to demonstrate that the governing dynamics for the estimates is exponentially stable when (persistently exciting) external driving terms are present [64]. This is indeed the case for our adaptation mechanism, as can be seen by considering the error dynamics that govern the behavior of δx_n (with unsaturated duty ratio):

$$\begin{aligned}\frac{d}{dt}(\delta x_n) &= -Q(Bx+b)d \\ &= -Q(Bx+b)C(s)\{(Bx+b)^*Q(\delta x_n)\} + \\ &\qquad Q(Bx+b)C(s)\{(Bx+b)^*Qx\}. \qquad (6.50)\end{aligned}$$

The mixed notation involving both time domain and frequency domain variables is becoming standard in the literature on adaptive control, see [64]. What is meant by this notation is that $C(s)$ is a LTI (convolution) operator. The model (6.50) is obviously not a complete state-space model, but only a model for the dynamics that govern the behavior of the estimation error with the other states viewed as time-varying parameters. The compensator $C(s)$ in our design methodology is LTI and positive real. Consider a homogeneous system governing the behavior of δx_n composed of only the first term on the right-hand side of (6.50). It is well known [64] that two conditions that are simultaneously sufficient for the boundedness of δx_n in (6.50) is that the homogeneous system is exponentially stable, and that the second (driving) term on the right-hand side of (6.50) is bounded. Note that the driving term is bounded since the converter states converge to their steady state values ($x = 0$). This was argued at the outset.

Sufficient conditions [64] for the exponentially stability of the homogeneous system are that $C(s)$ be strictly positive real and that the vector $Q(Bx + b)$, viewed as a function of time, be persistently exciting. The compensator will be strictly positive real in all practical designs with our framework. We expect that

the elements of the vector $Q(Bx + b)$ will contain a broad spectrum of frequencies because of the switching action of the converter and because of external disturbances (e.g. time-dependent load disturbances) that drive the converter system. The conclusion is that the parameter estimates will not diverge.

Despite this argument for parameter non-divergence, we explore below an alternative method for guaranteeing parameter convergence. The alternative method will become essential in the next subsection, where we consider adaptive schemes to handle an unknown nominal duty ratio. With these schemes, there will be no a priori global stability results available, and so local exponential stability will be required.

There is a way to guarantee parameter convergence in our self-tuning scheme in the absence of persistently exciting signals. In particular, we can modify the adaptation mechanism (6.44) as follows:

$$\frac{d}{dt}(\delta x_n) = -K^{-1}Q_1(Bx + b) - \gamma(\tilde{x}_n - x_t) \tag{6.51}$$

with $\gamma > 0$. (Recall that $\tilde{x}_n - x_t = (\delta x_n) - x$.) The effect of the additional term is to impose exponentially stable behavior on those modes of the parameter estimator that are unobservable in the small signal model. For the remainder of the discussion, we shall take $Q_1 = Q$ and $K = kI$, as done in the example above. With this update law the associated augmented state-space model takes the form

$$\begin{aligned} x' &= Ax + (Bx + b)d \\ (\delta x_n)' &= -\frac{1}{k}Q(Bx + b)d - \gamma\{(\delta x_n) - x\} \\ y &= (Bx + b)^*Q(x - \delta x_n) \end{aligned} \tag{6.52}$$

In the case where there is some loss associated with each state in the converter circuit, i.e. $QA + A^*Q < 0$, the associated augmented state-space model can be guaranteed to be strictly relatively passive to infinity by picking γ small enough. To see this, consider the derivative of the storage function $V = \frac{1}{2}x^*Qx +$

$\frac{1}{2}k(\delta x_n)^*(\delta x_n)$ along the system trajectories:

$$\frac{d}{dt}V = \frac{1}{2}x^*(QA + A^*Q)x + k\gamma(\delta x_n)^*x - k\gamma(\delta x_n)^*(\delta x_n) + yd. \qquad (6.53)$$

Now the input-output model (6.52) is strictly relatively passive if the sum of the first three terms in (6.53) is nonpositive. This can be assured by making γ small enough if $QA + A^*Q < 0$.

Note that the small signal linearization of (6.52) will generally be unobservable, but the unobservable modes will be exponentially stable in the absence of any excitation. The issues concerning small signal transient behavior are essentially the same as those for the model (6.45). In particular, we can generally place the significant (i.e. observable) modes reasonably well with a positive real compensator $C(s)$, while the unobservable modes do not affect the behavior of the internal converter states. We illustrate the use of this modified adaptive scheme below.

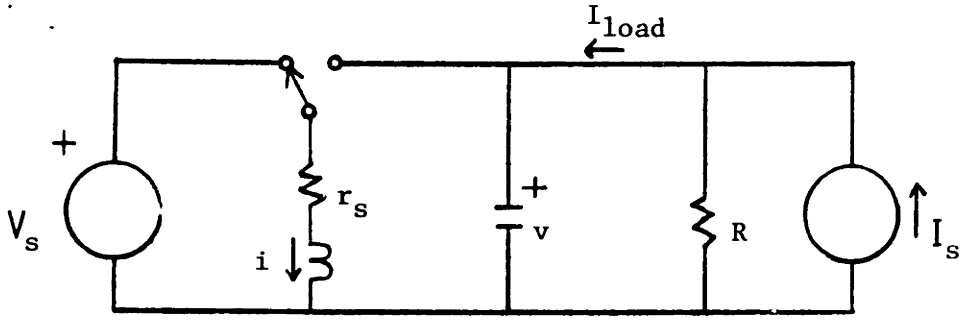

Figure 6.15: Up-Down Converter with Parasitic Resistance

Example: Adaptation Scheme for Two Unknown Nominal States in the Up-Down Converter Here we consider the application of the adaptive control scheme outlined above to the up-down converter of Figure 6.15. It will be assumed that the input voltage V_s is known, and that the nominal duty ratio is calculated using an idealized model that omits parasitics, i.e.

$$d_n = \frac{v_n}{v_n - V_s}.$$

However, because of the parasitic series resistance r_s associated with the inductor, the steady state capacitor voltage becomes

$$v_n = -\frac{d_n}{1-d_n}V_s + \frac{r_s I_{load}}{(1-d_n)^2} \tag{6.54}$$

where I_{load} is the total steady state load current. Because of the dependence on the load current and the value of the parasitic resistance, it is not generally possible to know the value v_n. We are then led to consider an adaptive scheme that estimates values for both i_n and v_n. Since the converter is assumed to have some resistive component in its load, we can be sure that $QA + A^*Q < 0$. Therefore, we can apply the modified adaptive scheme (6.52). We shall use the same gain parameters as in the previous example. The resulting small signal eigenvalues are nearly identical, except for an additional mode controlled by the constant γ.

We first study the large signal behavior of the converter under this adaptive control algorithm. Figure 6.16a) shows a start-up transient of the converter with this control scheme for the case where all initial states in the controller are set at zero. Note that the converter states i and v rapidly approach their steady state values, while the states corresponding to the adaptation mechanism $\tilde{i}_n$ and $\tilde{v}_n$ exhibit a slow mode. This slow mode does not affect the converter states. Note that the steady state value for v (and for $\tilde{v}_n$) is approximately -8.95 volts, which is slightly off from the design value of -9 volts. A longer simulation is required to show that $\tilde{v}_n$ and $\tilde{i}_n$ actually approach their steady state values. To see that these parameter estimates do indeed converge, Figure 6.16b) shows a trace of the sum of the squared error in these two quantities, obtained in a longer term (one second) simulation. •

The adaptive control scheme presented here combines nearly all the best features of the Lyapunov-based control design methodology studied in this and the previous chapter. In particular, by choosing to base the control design on the energy in the increment, the closed-loop control systems that result are inherently robust to circuit parameter uncertainty. This follows because the model (6.45) is guaranteed to be strictly relatively passive to infinity for any set of

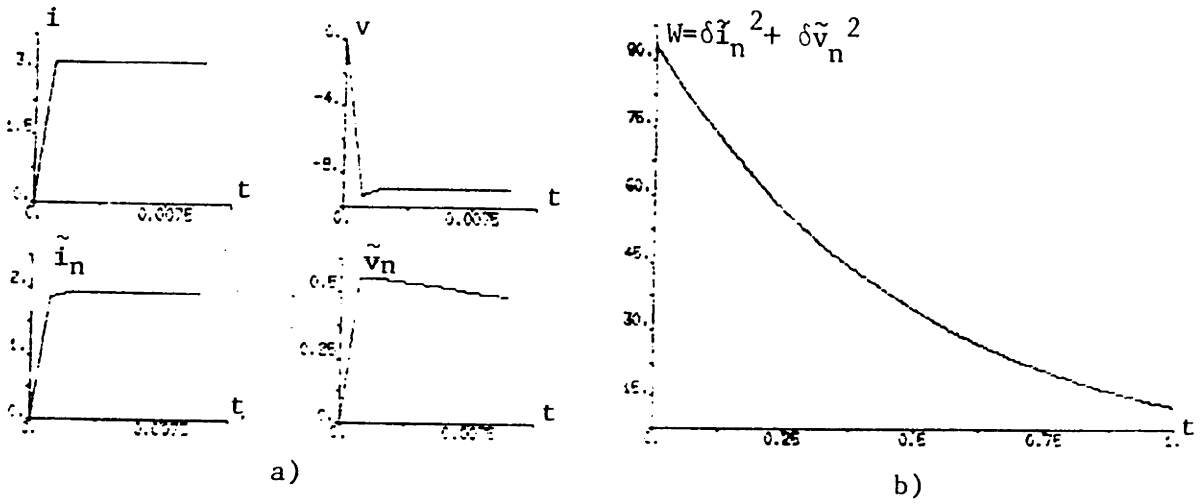

Figure 6.16: Start-Up Transients Under Adaptive Control Scheme that Estimates Two Unknown Parameters

(passive) circuit parameter values. (The model (6.52) can also be guaranteed to be strictly relatively to infinity for any set of passive circuit parameters, provided $QA + A^*Q < 0$. That is, there is some dissipation associated with each state in the open-loop converter.) Further, with this choice for the Lyapunov function, the closed-loop converter system is robust to arbitrary interconnection with other incrementally passive circuit elements. The additional elements would simply be integrated into a modified and/or augmented system model, but the form of the variable y would remain unchanged. (Recall that the variable y depends only upon the states that form the canonical cell of the converter.) Sensitivity to unknown nominal state values is not an issue since these are explicitly estimated, and incorporated into the control scheme. Finally, it is possible to obtain adequately fast small signal transient behavior by applying a positive real, dynamical compensator with the model (6.45) or (6.52). See the following

subsection for an approach to designing such a positive real compensator.

The method mentioned above is based on a particular small signal linearization for the model (6.45). Since this small signal linearization is dependent upon a nominal circuit model *including* the load, it is possible that the small signal dynamical behavior will vary widely with the steady state operating condition. To compensate for this, it is possible to design a family of parametrized compensators that is applied to the model (6.45) or (6.52). The appropriate member of the family can be selected via a gain scheduling technique, possibly implemented with a look-up table. To assure that the resulting time-varying compensator is incrementally passive, we can require that it has a circuit synthesis with a fixed set of reactive elements, but programmable resistors. This topic remains as a subject for future work.

The main shortcoming of the method described above is the requirement that the nominal duty ratio be known. How restrictive this requirement is depends on the application. In the following subsection, we consider adaptive methods for handling an unknown nominal duty ratio. First, we examine some of the issues involved in determining the nominal duty ratio for a specific example.

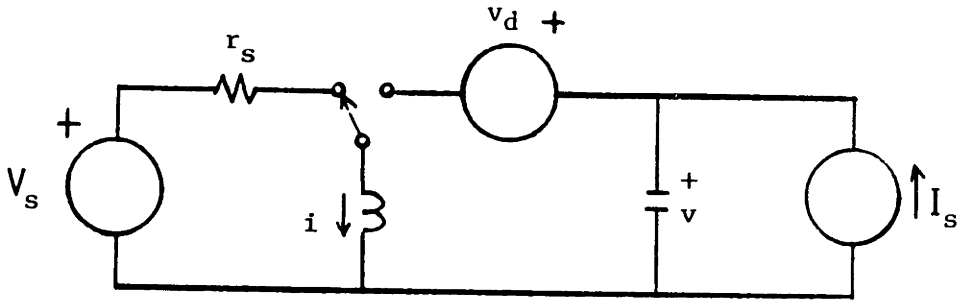

Figure 6.17: Up-Down Converter with Parasitic Elements

Example: Effects of Parasitics on Determining Nominal Duty Ratio
The up-down converter shown in Figure 6.17 includes a linear resistance r_s to model the on-resistance of the actively controlled switch (e.g. MOSFET), and a

voltage source to model the drop across the passive switch (e.g. rectifier). These models for the parasitic elements are only selected for the purpose of illustration. With the modeled parasitic elements, the nominal capacitor voltage v_n takes the form

$$v_n = -\frac{d_n}{1-d_n}\left(V_s - r_s\frac{I_s}{1-d_n}\right) + v_d. \tag{6.55}$$

It is possible to solve (6.55) for d_n to obtain a functional relationship for d_n in terms of the parameters V_s, r_s, I_s, and v_d and the desired capacitor voltage v_n. Naturally, this relationship will be sensitive to errors in the parameters and to erroneous modeling in Figure 6.17. The algorithms outlined in this subsection will result in regulation at the operating point determined by the commanded nominal duty ratio, and hence static errors can result from imperfect modeling. For those applications that cannot tolerate such errors, we consider in the following subsection an adaptive control scheme that can handle uncertainties in the nominal duty ratio, as well as in the nominal state values. •

6.5.3 Adaptive Control Methods for Uncertain Nominal Duty Ratio and Uncertain Nominal State Values

In the light of the preceding subsection and Section 6.4, two approaches for the robust regulation problem involving uncertainties in the nominal duty ratio and in the nominal states are evident. Firstly, it is possible to append the adaptive mechanism (6.44) or (6.51) to the state-space model that is already augmented to realize integral control action. The purpose of the additional augmentation is to robustly stabilize the system at a set of feasible operating points. Secondly, it is possible to implement a self-tuning adaptive control scheme that estimates the nominal duty ratio along with the nominal state values. It turns out that we cannot conclude global stability (in general) for either of these schemes. However, the first approach, using integral control, can be shown to lead to robust stability for small signal operation, while no conclusions are available for the second approach. This will be elaborated in the comparison of the two approaches below.

Integral Control with Adaptation for Unknown Nominal States

One possibility for obtaining robustly stable behavior in the presence of uncertainties in the nominal duty ratio and in the nominal states of a switching DC-DC converter is by appending the adaptive mechanism (6.51) to the integral control algorithm introduced in Section 6.4.2. The appropriate input-output model that needs to be considered for this approach is given by

$$\begin{aligned} x' &= Ax + (Bx + b)(d + \delta d_n) \\ z' &= cx \\ (\delta x_n)' &= -\frac{1}{k} Q_1 (Bx + b)d - \gamma(\delta x_n - x) \\ y &= (Bx + b)^* Q_1 (x - \delta x_n) + (Bx + b)^* qz \end{aligned} \tag{6.56}$$

where we have selected the estimator update gain as $K = kI$. In the model (6.56), the variable z is the integral of the error in the variable cx, and the matrix $\tilde{Q}$ of Section 6.5.2 is split into its various components, i.e.

$$\tilde{Q} = \begin{bmatrix} Q_1 & q \\ q^* & \theta \end{bmatrix}. \tag{6.57}$$

θ is a scalar entry in the matrix $\tilde{Q}$, which previously had not been partitioned as required here. (Recall that $\tilde{Q}$ is selected to satisfy $\tilde{Q}\tilde{A} + \tilde{A}^*\tilde{Q} \leq 0$ where

$$\tilde{A} = \begin{bmatrix} A & 0 \\ c & 0 \end{bmatrix}$$

is the A-matrix augmented to account for the integral control action.) Naturally, we would only attempt to estimate nominal values for the converter states contained in x, and in many cases only a small subset of these nominal values. Note that the purpose of the integral control action is to make the system insensitive to static (and low frequency) disturbances that arise from uncertainty in the nominal duty ratio.

It turns out that a control system that interconnects an incrementally passive feedback with the model (6.56) will lead to globally stable behavior in the presence of uncertainties in the nominal operating condition provided the nominal duty ratio is known, i.e. $\delta d_n = 0$. No general conclusions can be made for

globally stable operation in the case where the nominal duty ratio is unknown. However, local stability is preserved for small enough perturbations δd_n. These comments are elaborated below.

Firstly, it is easy to see that a control scheme that applies incrementally passive feedback around the model (6.56) (realizing the saturation constraint as in Section 6.1) results in globally stable behavior for the case where $\delta d_n = 0$. This follows from the fact that in this case this model is strictly relatively passive to infinity, which is verified by taking as a storage function

$$\frac{1}{2}\tilde{x}^*\tilde{Q}\tilde{x} + \frac{1}{2}k(\delta x_n)^*(\delta x_n) = \frac{1}{2}(x^*Q_1x + 2x^*qz + \theta z^2) + \frac{1}{2}k(\delta x_n)^*(\delta x_n). \quad (6.58)$$

Note that in implementing such a control scheme, it is important to supply the best possible a priori estimate of the nominal duty ratio since this has implications on the stability properties. This is an essential difference from the case of linear feedback control where the addtional state z would be scaled and combined linearly with any arbitrary a priori estimate of the nominal duty ratio.

Secondly, in the case where the nominal duty ratio is imprecisely known, the model (6.56) generally loses its (relative) passivity property. However, it is possible to design the control system assuming the nominal duty ratio is known, and to make the resulting system with known duty ratio exponentially stable. Note that in making the small signal model asymptotically stable in the preceding subsection, we actually made the system exponentially stable. For this reason, the modified adaptation mechanism (6.51) (rather than (6.44)) is required to assure exponential stability for the case where the duty ratio is known. In this case, the local stability of the system is robust to small structured perturbations, namely those perturbations that do not change the order of the system. (This is a general property of dynamical systems [76].) Note that it is generally not possible to guarantee global asymptotic stability.

A theory for determining the region of attraction in the state-space for a locally stable equilibrium point (or other limit set) has emerged recently in the literature [77,78,79]. A consequence of this theory for a system that has a unique stable equilibrium point is that the equilibrium is stable in the large if there

are no other limit sets, and no trajectories diverge (asymptotically approach infinity). It is often possible to conclude that a system that incorporates integral control has a unique equilibrium, but it is generally difficult to rule out the existence of nonstationary limit sets such as limit cycles and strange attractors. We shall discuss this further in Chapter 8 where directions for future research are considered. Next, we study an example that applies a control based on the model (6.56).

Example: Combined Integral and Adaptive Control for Second Order Up-Down Converter Here we consider the application of the control method outlined above to the second order up-down converter of Example 1 in Section 5.1. The route to be followed will append the adaptation mechanism (6.51) to the state-space model that is already augmented to realize integral control action. The integral control design of Section 6.4.2 for this example will be used as the base model to which the adaptive mechanism will be added. In this example, the adaptive mechanism will be used only to estimate the nominal value for the inductor current, with the goal of making the closed-loop system robust to uncertain nominal load conditions. The other nominal parameter values are typically known fairly accurately, and therefore can only cause relatively small perturbations in the closed-loop system. With the integral control, the system will be insensitive to static uncertainty in the nominal duty ratio (although not necessarily globally stable in the presence of such uncertainty).

In our design, we take $k = 50$ and $\gamma = 10$ in the adaptation mechanism (6.51). These gain parameters are selected with regard to the small signal dynamics obtained for a nominal load current of 2 amps. With the above parameters, with the matrix $\tilde{Q}$ of Subsection 6.4.2, and with a constant feedback gain $\alpha = 1.7 \bullet 10^{-6}$ applied to the model (6.56), the eigenvalues of the corresponding small signal model are $-9.4 \pm j9.8$Krad/sec, -11.6Krad/sec, and -10rad/sec. Note that γ controls the slowest mode, which does not affect the small signal transient behavior of the converter states. This results from the non-minimality of the

small signal model. The selection of $\gamma > 0$ assures that the system will remain stable in the presence of small parametric perturbations that are not accounted for in the adaptation scheme. We verify this control design with numerical simulations.

Figure 6.18a) shows a start-up transient in the up-down converter for a load current of 2 amps with the closed-loop control described above. Since this is the nominal load current that was used in the design, we obtain a stable transient with decay asymptotically governed by the eigenvalues computed above. In particular, the converter states i and v exhibit a fast transient since the slow mode at -10rad/sec does not affect these states. However, there is a slow transient (due to the slow mode) in the variables z and $\tilde{i}_n$ that is not evident in the figure. This slow behavior has no consequence for the converter performance. To study the behavior in the case where the load current varies from the nominal, we simulated a transient that occurs when the converter is approximately in steady state, and the load current steps from 2 amps to 5 amps. This is shown in Figure 6.18b). Note that the converter remains stable, and comments similar to those above are applicable to this case. To study the sensitivity properties of this control design, the simulations in Figures 6.18c) and d) show the behavior when a 100Hz sinusoidal component is added to the load and to the source, respectively. In these simulations, after an initial start-up transient, the inductor current i begins to exhibit a sinusoidal component in its waveform, while the capacitor voltage remains nearly constant at -9 volts. Once again, the variables z and $\tilde{i}_n$ have a slow stable behavior that is not clear from the figure because of the relatively short simulation run. •

Adaptive Control Scheme for Uncertain Nominal Duty Ratio and Uncertain Nominal State Values

Here we illustrate a fundamental problem that arises in an adaptive control scheme that attempts to estimate the nominal duty ratio and some nominal state values. The basic model for a DC-DC converter that accounts for uncertainties

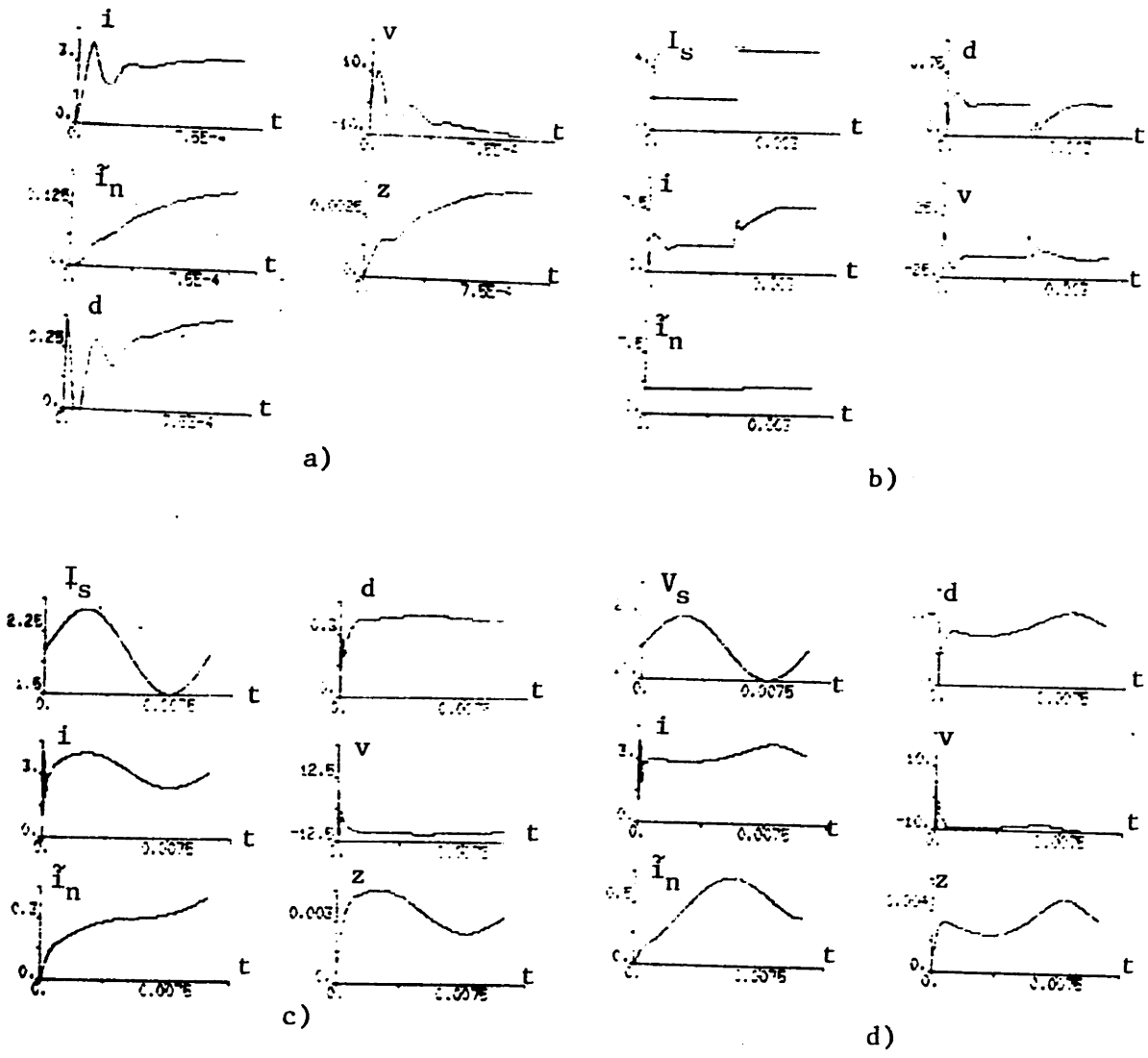

Figure 6.18: Simulation Waveforms for Combined Integral and Adaptive Control of Up-Down Converter

in the nominal duty ratio and in the nominal state values is (6.10) of Section 6.4. To realize the adaptive control, we would append to the model (6.10) the nominal state estimator (6.44) and an update mechanism for the estimate of the nominal duty ratio. The update mechanism for the nominal duty ratio might take the form

$$(\delta d_n)' = -\frac{1}{r}(Bx + b)^* Q(x - \delta x_n) \tag{6.59}$$

where r is a free gain parameter. Note that the quantity $x - \delta x_n$ is the controller's estimate of the deviation from nominal in the state. This update mechanism is motivated by the choice of

$$V = \frac{1}{2}x^* Q x + \frac{1}{2}k(\delta x_n)^*(\delta x_n) + \frac{1}{2}r(\delta d_n)^2 \tag{6.60}$$

as a storage function. With the above adaptation mechanisms, the resulting input-output model is given by

$$\begin{aligned} x' &= Ax + (Bx + b)(d + \delta d_n) \\ (\delta x_n)' &= -\frac{1}{k}Q(Bx + b)d - \gamma(\delta x_n - x) \\ (\delta d_n)' &= -\frac{1}{r}(Bx + b)^* Q(x - \delta x_n) \\ y &= (Bx + b)^* Q_1(x - \delta x_n) + (Bx + b)^* qz. \end{aligned} \tag{6.61}$$

Differentiating the candidate storage function (6.60) along the trajectories of (6.61), we obtain

$$\frac{d}{dt}V = \frac{1}{2}x^*[QA + A^*Q]x + yd + (\delta x_n)^* Q(Bx + b)(\delta d_n). \tag{6.62}$$

The final term on the right-hand side of (6.62) prevents V in (6.60) from being a valid storage function for the system (6.61). There is apparently no clearcut method for specifying an update mechanism for an estimate of the nominal duty ratio that can result in a dissipative input-output model of the form (6.61). One might decide to implement a control scheme based on the model (6.61), despite the difficulty that will be encountered in concluding global stability. However, such a control system will have a small signal model that has at least one mode at

the origin. (This results from the non-minimality of the small signal linearization of (6.61), and the fact that there seems to be no simple way to modify the update mechanism (6.59) to make the overall system asymptotically stable.) Because of the inherent nondecaying mode of the small signal model, and the lack of a Lyapunov function, there is no a priori guarantee of local (or global) stability. Hence, this approach is not recommended.

6.5.4 Summarizing Remarks

This subsection presented an approach to handling uncertainties arising in the parameters required to implement the Lyapunov-based control schemes. The main trade-off that emerges is between the adaptive scheme of Subsection 6.5.2 that can be based on the energy in the increment, and the integral control scheme of Subsection 6.5.3 that also adapts for uncertain nominal state values. The first would always be preferred in the case where the nominal duty ratio is known to within sufficient accuracy, since this scheme combines all the best robustness features, as discussed in that section. The only disadvantage of this scheme is sensitivity to errors in the nominal duty ratio. In the case where the nominal duty ratio cannot be obtained with sufficient accuracy, the integral control method of Subsection 6.5.3 can yield satisfactory performance.

In the following section, we explore methods for obtaining fast transient behavior using control schemes based on the concept of interconnected (relatively) passive networks.

6.6 Performance: Transient Behavior

In this section, we examine methods for obtaining fast transient behavior using control schemes based on the concept of interconnected passive networks. The objective here will be to explore limits on the small signal transient behavior (since this problem is somewhat tractable), keeping in mind that the small signal behavior asymptotically governs all stable behavior. Recall that in Chapter 5, for the second order up-down converter (Example 1), it was possible with a static

control law based on the energy in the increment to place the eigenvalues of the small signal model at about -20Krad/sec. This was quite satisfactory in view of the 50KHz (or 314Krad/sec) switching frequency and the open-loop resonant frequency of approximately 20Krad/sec. However, in the case of the fourth order up-down converter (Example 2) with the same approach, it was only possible to place the closed-loop eigenvalues of the small signal model at approximately -5.1 ± 68Krad/sec, -9.6Krad/sec, -46Krad/sec. The asymptotic behavior is then governed by the complex pair with real part at -5.1Krad/sec which is considerably slower than that of the second order case. (Note that the fourth order converter was also intended to operate with a switching frequency of 50KHz.) It was also demonstrated that with an alternative quadratic Lyapunov function for the fourth order example, one could obtain considerably faster behavior in the small signal model, with eigenvalues having real part less than -22Krad/sec. However, because of the numerous advantageous features of control design based on the energy in the increment (outlined in Section 5.3), we might like to obtain faster behavior with such a control scheme. In other applications, it may not be possible to obtain adequately fast behavior with any static, Lyapunov-based feedback law. We are then led again to consider alternative design methods.

The basic limitation of the static feedback schemes based on a fixed Lyapunov function (e.g. the energy in the increment) introduced in Sections 5.1 and 5.2 is that these schemes afford only one degree of freedom, namely the choice of the gain α. There are various ways to introduce additional degrees of freedom in the control design including time-varying (possibly periodic or state-dependent) positive feedback gains and dynamic positive real compensation schemes. In the sequel, we shall investigate the use of dynamic LTI positive real compensators in conjunction with the system modeled by (6.1) with an appropriate fixed matrix Q_1, such as that determined by the form of the energy in the increment. Since we are interested in small signal behavior, it suffices to consider the (strictly proper) positive real system that models the small signal behavior of (6.1).

For our purposes here, a basic question concerning the small signal behavior

can be posed as follows:

> *Given an arbitrary passive LTI network with impedance $Z(s)$, is there a limit on the speed of the dynamical behavior that can be obtained with a termination in a positive real impedance $Z_1(s)$? If so, how does one determine a passive LTI termination $Z_1(s)$ that results in fastest behavior?*

The speed of the dynamical behavior can be defined in terms of the asymptotically dominant mode(s) determined by the closed-loop eigenvalue(s) with least negative real part. It appears that the answer to this question depends upon the complexity of the network $Z(s)$. In the case where $Z(s)$ models a single capacitor, it is possible to resistively terminate the capacitor and obtain an arbitrarily small time constant. However, in the case where $Z(s)$ represents a higher order network, it is considerably more difficult to terminate the network for optimal speed. There is some literature on closely related problems, which will be discussed shortly. First, we shall present an *ad hoc*, but practically effective scheme based on the optimal matching problem [60].

Consider the situation where the network represented by $Z(s)$ is nearly lossless. (This is typical of the impedance functions arising in switching converter applications because of the inherent lack of resistive elements in these circuits.) An optimal control problem related to that of obtaining fast transients is that of minimizing the internal energy of the network $Z(s)$ at the end of a time interval $[0, T]$ with an arbitrary initial condition, i.e.

$$\inf_{i(t)} \left\{ \frac{1}{2} x(T)^* Q x(T) \right\} \tag{6.63}$$

where $x(t)$ is the state vector of a realization for $Z(s)$, $x(0)$ is the specified initial condition, and the input and output wavforms ($i(t)$ and $v(t)$) are consistent with the network. The relationship to fast transient behavior, although not precisely given here, could be seen by evaluating any quadratic form (such as that in (6.63)) along the system trajectories of a LTI system. Such a quadratic form exhibits behavior governed by the pair-wise sums of the eigenvalues of

the corresponding system. Hence, "fast" eigenvalues result in fast decay of the quadratic form. Since the quadratic form in (6.63) is positive definite, the optimal control solution that minimizes $\frac{1}{2}x(T)^*Qx(T)$ also results in certain bounded decay of each system mode. In the case where $Z(s)$ is lossless, the optimal control problem above is equivalent to maximizing the energy extracted over the interval $[0,T]$. Although this problem can be solved quite easily [74], it does not have a time-invariant solution.

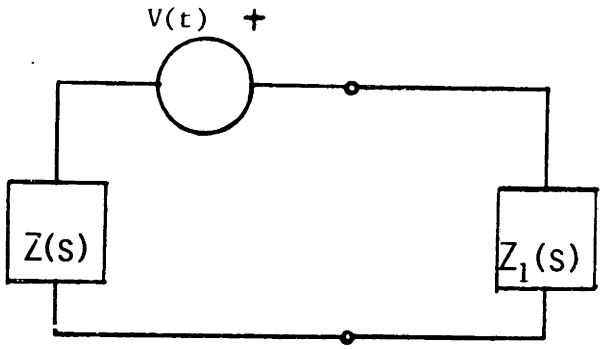

Figure 6.19: General Matching Problem

We shall consider the optimal control problem on an infinite interval for two reasons. Firstly, it is a well known result from optimal control theory [74] that the infimal value (6.63) of the problem described above with $T_1 > T$ is less than or equal to that obtained by solving two consecutive optimal control problems on the intervals $[0,T]$ and $[T,T_1]$. (It is understood that the boundary conditions for the consecutive problems must be consistent.) We would therefore expect superior performance by making the interval arbitrarily large. Secondly (and more significantly), in the case where the interval becomes infinite, the optimal control problem provides a relatively simple result. In particular, the optimal solution can be generated by a LTI system (i.e. terminating network). The paper [60] solves the problem of determining the LTI terminating network that absorbs the maximum average power over the doubly infinite interval $(-\infty,\infty)$, from an arbitrary voltage source excitation with series Thevenin impedance $Z(s)$ (see Figure 6.19). The classical result of [60] (also evident in [59]) is that the

optimal terminating network has impedance $Z(-s)$.

To relate this to our problem, consider the case where the voltage source is identically zero except for some impulsive behavior at $t = 0$. Given a controllable realization for $Z(s)$, any initial state $x(0^+)$ can be obtained through appropriate impulsive action of the voltage source. Hence, the result of [60] is applicable to this case. Unfortunately, in the case where $Z(s)$ is positive real, a causal realization of $Z(-s)$ is anti-stable, and of no use here. However, many methods for approximating the optimal termination with positive real impedances are available, e.g. the broadband matching problem [56,57,58,59,61]. The approximation schemes used for the broadband matching problem are based on frequency domain methods that seek to maximize the average power transfer over an interval of the $j\omega$-axis.

We would like to obtain a positive real terminating impedance $Z_1(s)$ that results in a network interconnection that approximates the *stable time domain* behavior of the interconnection of $Z(s)$ with $Z(-s)$. Note that the natural frequencies of the network interconnection of $Z(s)$ and $Z_1(s)$ are determined by the zeros of $Z(s) + Z_1(s)$ and by the common poles of $Z(s)$ and $Z_1(s)$. The situation where the two networks have a common pole is analogous to that where a pole-zero cancellation occurs in a single-input, single-output feedback control system. For the cases of interest here, the two networks $Z(s)$ and $Z_1(s)$ will generally not have any common poles, and hence we can usually obtain the natural frequencies by examining the zeros of $Z(s) + Z_1(s)$. As a result of the symmetry of the expression, the negative of a zero of $Z(s) + Z(-s)$ is also a zero of this quantity. ($Z(s)$ and $Z(-s)$ will not have any common pole if all poles of $Z(s)$ are in the open left-half plane.) A possible goal is then to determine a positive real impedance function $Z_1(s)$ that when interconnected with $Z(s)$ results in natural freqencies at the left-half plane zeros of $Z(s) + Z(-s)$. (We would first examine these left-half plane zeros to see if they are sufficiently "fast". This is the case in the examples to be studied.) Our approximation scheme uses

the scattering parameter

$$\rho_1(s) = \frac{1 - Z_1(s)}{1 + Z_1(s)}. \tag{6.64}$$

for the network with impedance $Z_1(s)$. Note that $\rho_1(s)$ is bounded real if and only if $Z_1(s)$ is positive real [36]. The following procedure will be used to determine an approximating network.

1. Determine the left-half plane zeros $\{s_l\}$ of $Z(s) + Z(-s)$.

2. Determine the constraints on $Z_1(s)$ to place eigenvalues at the $\{s_l\}$, i.e. $Z_1(s_l) = Z(-s_l)$, and the corresponding constraints on $\rho_1(s)$.

3. Define a region of the complex plane $Re\{s\} \geq -a$ (a real and positive) over which the impedance function $Z_1(s)$ is to be positive real. (The corresponding scattering parameter is bounded real in the same region where $Z_1(s)$ is positive real.)

4. Solve the H^∞ optimization problem [63]:

$$\inf_{\rho_1}\{\sup_{\omega} |\rho_1(-a + j\omega)|\} \tag{6.65}$$

subject to the constraints on $\rho_1(s)$ determined in step 2. If the resulting optimal solution has value less than one, the obtained scattering parameter is bounded real in the defined region of the complex plane, and the corresponding impedance function has all singularities to the left of the line $s = -a$. If the resulting optimal solution has value greater than one, pick a smaller value of a and return to step 3.

Upon determining the impedance $Z_1(s)$ with the above procedure (if it can be done), the network interconnection of $Z(s)$ with $Z_1(s)$ is guaranteed to have natural frequencies at the $\{s_l\}$. However, there are additional natural frequencies introduced. By picking the value of a in step 3 to be sufficiently large, we *might* expect the additional natural frequencies to be relatively fast (by a time scale separation argument). To illustrate the procedure, we shall apply it to Examples 1 and 2 of Chapter 5, and to an example that arose in designing a control for reduced sensitivity in Section 6.4.

Example 1: Second Order Up-Down Converter The impedance function $Z(s)$ arises from the linearization of the state-space averaged model (6.1) for the second order up-down converter of Section 5.1 with d taken as the "current" and y as the "voltage." The resulting impedance function has the form

$$Z(s) - \frac{s}{s^2 + \omega_0^2} \tag{6.66}$$

with $\omega_0 \approx 20$Krad/sec. Since $Z(s) + Z(-s) = 0$, we are led to consider a perturbed version of the impedance in which all singularities are perturbed to the left by the small parameter ϵ. Consider

$$Z(s+\epsilon) = \frac{s+\epsilon}{s^2 + 2\epsilon s + \epsilon^2 + \omega_0^2}. \tag{6.67}$$

It turns out that in the limit as $\epsilon \to 0$, the zeros of $Z(s+\epsilon) + Z(-s+\epsilon)$ are given by $s_r = \pm\omega_0$. The procedure outlined above leads us to determine a terminating impedance that results in an interconnected network with one of its natural frequencies at $-\omega_0$. The resulting terminating impedance is a constant resistor of value $\frac{1}{2\omega_0}$ which results in two closed-loop eigenvalues at $-\omega_0$. This is the solution that was used in Section 5.1 where the example was first studied. o

Although this example did not provide an interesting result, the following example based on the fourth order up-down converter does lead to a nontrivial result.

Example 2: Fourth Order Up-Down Converter The impedance function arising from the linearized state-space averaged model (6.1) (with $Q_1 = Q$ corresponding to the form of the energy in the increment) for the fourth order up-down converter introduced in Section 5.2 takes the form

$$Z(s) = \frac{s(s^2 + \omega_z^2)}{(s^2 + \omega_1^2)(s^2 + \omega_2^2)} \tag{6.68}$$

where $\omega_1 = 19.75$Krad/sec, $\omega_2 = 72.81$Krad/sec, and $\omega_z = 63.47$Krad/sec. Since this is the impedance function of a lossless network, we have $Z(s) + Z(-s) = 0$. We are again led to consider the perturbed impedance $Z(s+\epsilon)$. For an infinitesimally small value of the parameter ϵ, the six finite zeros of $Z(s+\epsilon) +$

$Z(-s+\epsilon)$ occur at ± 20.6Krad/sec and at $\pm 22.6 \pm j62.6$Krad/sec. Applying the procedure outlined above with a value of $a = 50$Krad/sec, we obtain the terminating impedance

$$Z_1(s) = 2.83 \bullet 10^3 \frac{(s+50.0+j40.0)(s+50.0-j40.0)}{(s+822)(s+52.1)} \tag{6.69}$$

where all poles and zeros are reported in Krad/sec. The resulting natural frequencies of the network interconnection of $Z(s)$ with $Z_1(s)$ are $-22.5 \pm j62.7$Krad/sec, -20.8Krad/sec, $-11.7 \pm j75.4$Krad/sec, and -15.8Krad/sec. Note that the additional modes (the last three listed) are somewhat slower than the target modes, namely the left-half plane zeros of $Z(s+\epsilon) + Z(-s+\epsilon)$. However, the slowest mode is still more than twice as fast as the slowest mode that was obtained with the static compensation in Section 5.2. Further, if we scale the impedance $Z_1(s)$ by a factor of 0.96, we can obtain closed-loop natural frequencies at $-20.7 \pm j64.0$Krad/sec, -23.9Krad/sec, $-13.3 \pm j75.5$Krad/sec, and -13.4Krad/sec which are still a little faster. •

In the following, we continue the example of Section 6.4.1 that attempted to make a control design for the converter of Example 2 (Section 5.2) that resulted in reduced low frequency sensitivity to certain disturbances, and in adequately fast dynamical behavior. Recall that in this example we required that the controller $C(s)$ have a zero at the origin. (This is the only difference from the preceding example.) As discussed in Section 6.4.1, the requirement that $C(s)$ have a zero at the origin is equivalent to requiring that the terminating impedance $Z_1(s)$ have a pole at the origin. A family of such impedances was introduced:

$$Z_1(s) = \frac{1}{ks} + Z_1'(s). \tag{6.70}$$

Note that $Z_1(s)$ is guaranteed to be positive real if $k > 0$ and $Z_1'(s)$ is positive real. The constant k is a free design parameter. The design can be completed by specifying k and the impedance $Z_1'(s)$ to terminate the impedance $Z(s) + \frac{1}{ks}$ with satisfactorily fast dynamical behavior. A network representation of the control scheme using this design method is illustrated in Figure 6.8 of Section 6.4.1.

Example 3: Reduced-Sensitivity Control Design for Example 2 of Section 5.2 The first step in the design is the selection of the parameter k. It may appear that one achieves the most freedom in the second stage of the design by selecting k very large, since the positive real term $Z_1'(s)$ is to be added to $1/ks$. However, the second stage will restrict $Z_1'(s)$ to have all singularities in some region $Re\{s\} < -a$ with a positive and real. One way to gauge a choice of k is by evaluating the zeros of

$$Z(s) + \frac{1}{ks} + Z(-s) + \frac{1}{-ks},$$

since the stable roots will define the target closed-loop modes. In our example, this quantity is zero, so we consider the zeros for a perturbed impedance function (as done before). The choice $k = 8$ results in stable roots of the perturbed version of $Z(s) + \frac{1}{ks} + Z(-s) + \frac{1}{-ks}$ at approximately $-21.77 \pm j63.8$ Krad/sec and $-11.66 \pm j3.98$ Krad/sec. The procedure described in this section can now be applied to determine a positive real terminating impedance $Z_1'(s)$ for $Z(s) + \frac{1}{ks}$ that yields four closed-loop poles at the locations specifed above. With the choice $a = 50$ Krad/sec which forces all singularities of $Z_1'(s)$ to lie in the closed region to the left of the line $s = -50$Krad/sec, the procedure breaks down; there is no such $Z_1'(s)$. However, the choice $a = 30$ Krad/sec yields a successful result. The resulting closed-loop poles are located at

$$\begin{aligned} -9.09 \pm j75.42 \quad & \text{Krad/sec,} \\ -11.66 \pm j3.98 \quad & \text{Krad/sec,} \\ -13.60 \pm j7.73 \quad & \text{Krad/sec, and} \\ -21.77 \pm j63.78 \quad & \text{Krad/sec.} \end{aligned}$$

The compensator $C(s) = (Z_1'(s) + \frac{1}{ks})^{-1}$ takes the form

$$4.723 \bullet 10^{-4} \frac{s(s + 30.2 - j15.2)(s + 30.2 + j15.2)(s + 5043)}{(s + 38.01 - j43.96)(s + 38.01 + j43.96)(s + 31.06)(s + 4.488)} \tag{6.71}$$

with all poles and zeros specified in Krad/sec. The high frequency zero in $C(s)$ has a negligible effect on the closed-loop performance, and will complicate

any implementation or simulation. For these reasons, we are led to consider a reduced model that omits this zero, and replaces it with the constant gain 5,043 Krad/sec. It turns out that the modified compensator is also positive real, and the closed-loop poles that result are nearly identical. This reduced model for the compensator was used in the example of Section 6.4.1. •

Returning to our original question, an answer to a closely related problem is available in the paper of Chan and Kuh [55]. In [55], conditions are given for an arbitrary active (possibly unstable) LTI one-port $Z(s)$ to be stably terminated in a passive LTI one-port $Z_1(s)$. Suppose it is desired to determine whether the passive one-port $Z(s)$ can be passively terminated so that all the resulting eigenvalues λ_j satisfy $Re\{\lambda_j\} \leq -a$ for some positive real number a. We could attempt to stabilize the (active) network with impedance $Z(s-a)$ by termination in a passive network $Z_1'(s)$ using the approach of [55]. If this can be done, the interconnection of $Z(s)$ with $Z_1(s) = Z_1'(s+a)$ results in a network with all its eigenvalues $\{\lambda_j\}$ satisfying $Re\{\lambda_j\} \leq -a$. Note that the resulting $Z_1(s)$ is analytic and positive real in the region of the complex plane defined by $Re\{s\} > -a$ which is more restrictive than the requirement that $Z_1(s)$ be positive real. Although this approach offers a solution to a closely related problem, the computation involved even in simple examples is usually intractible.

Another closely related problem is the classical broadband matching problem studied by Bode [56], Fano [57,58], Youla [59], Carlin [61] and numerous others. In the broadband matching problem, the goal is to design a lossless, passive, LTI two-port equalizer that couples a resistive generator (time-varying voltage source with Thevenin resistance r) to a specified LTI passive load $Z(s)$ so that the average power transfer from the source to the load is maximized. In the paper of Youla [59], the problem is reduced to specifying $Z_1(s)$, the impedance seen by the load looking into the two-port equalizer terminated in the resistance r. (It is asserted in [59] that one can always synthesize the desired $Z_1(s)$ with a lossless two-port terminated in a resistor.) The broadband matching problem is then equivalent to the optimal matching problem of Rohrer [60] in the case

where the terminating network impedance $Z_1(s)$ is restricted to being positive real.

There are numerous interesting and unanswered questions pertaining to the problem discussed above. We have demonstrated one approach to the problem that appears to be promising. In the next chapter, we consider an entirely different approach to control design for switching converters.

Chapter 7

Control Design Based on Coordinate Transformations

In this chapter, we take an entirely different tack for the development of control designs for switching converters. The focus here is on control designs based implicitly or explicitly on coordinate transformations. The main approach proceeds along the lines of the so-called feedback linearization; however, the method to be illustrated does not require explicit computation of a linearizing feedback. Rather, the state-space transformation required in a feedback linearization is used to directly realize a sliding mode control algorithm. The second order up-down converter introduced in Chapter 2 is used as a vehicle to illustrate the technique.

As discussed in the literature review of Chapter 3, there has been much work on the problem of determining when a given nonlinear system is equivalent to a linear system in some sense, and how to find a transformation that makes the equivalence explicit. The book of Isidori [30] discusses various types of exact linear equivalence including input/output linearization and state-space linearization. The method has been applied to switching converters in the recent work of the author [43], and in a recent paper by Sira-Ramirez and Ilic [65]. The basic idea of the method is presented in the following section.

7.1 Feedback Linearization Problem

In order to introduce the method of feedback linearization, we shall consider a nonlinear state-space model that is linear in the control (as in [30] and other related literature), i.e.

$$x' = f(x) + G(x)u \tag{7.1}$$

where $f(0) = 0$ and $G(x)$ denotes an $n \times m$ matrix whose elements may depend on the state x. Consider an open neighborhood U of the origin in $\mathcal{R}^n$. The system (7.1) is **feedback equivalent** on U to a linear system if there exists a nonlinear state feedback

$$u = \alpha(x) + \beta(x)v, \tag{7.2}$$

defined on U, with $\alpha(\bullet)$ and $\beta(\bullet)$ sufficiently smooth and $\beta(\bullet)$ nonsingular on U, such that the resulting system

$$\begin{aligned} x' &= (f + G \circ \alpha)(x) + G \circ \beta(x)v & (7.3)\\ &= \tilde{f}(x) + \tilde{G}(x)v & (7.4) \end{aligned}$$

is diffeomorphic to a controllable, linear, time-invariant system. That is, there exists a sufficiently smooth, locally invertible nonlinear transformation

$$\tau : U \to V \subset \mathcal{R}^n \tag{7.5}$$

mapping $x \in U$ to $z \in V$, such that

$$\begin{aligned} \frac{d\tau}{dx}\tilde{f}(\tau^{-1}(z)) &= Az, & (7.6)\\ \frac{d\tau}{dx}\tilde{G}(\tau^{-1}(z)) &= B, & (7.7) \end{aligned}$$

and in V, the transformed system takes the form

$$z' = Az + Bv. \tag{7.8}$$

Before stating conditions for a nonlinear system to be feedback equivalent to a linear system, we shall give some background and standard notation. A *vector*

field is a map from a manifold to its tangent space, and on $\mathcal{R}^n$ is a map from $\mathcal{R}^n$ to $\mathcal{R}^n$. The *Lie derivative* of a scalar function $\phi(\bullet)$ with respect to a vector field $f(\bullet)$ is the directional derivative of the function along the vector field, i.e.

$$\mathcal{L}_f(\phi)_x = \left[\frac{d\phi}{dx}\right]_x f(x). \tag{7.9}$$

Note that the Lie derivative of a function is also a function. The *Lie bracket* of two vector fields is another vector field, represented in coordinates on $\mathcal{R}^n$ by

$$[f,g] = \frac{df}{dx}g - \frac{dg}{dx}f. \tag{7.10}$$

The Lie bracket can also be written using the *ad* notation as

$$ad_f^1(g) = [f,g], \tag{7.11}$$

and by induction we define

$$ad_f^k(g) = [f, ad_f^{k-1}(g)]. \tag{7.12}$$

A set of vector fields $\{f_1,\ldots,f_n\}$ is *involutive* if for any two elements of the set, the Lie bracket is contained in the span of the set. That is, we have

$$[f_i,f_j] = \sum_{k=1}^{n} a_k^{ij} f_k. \tag{7.13}$$

For more background on manifolds and related ideas, we refer the reader to [42,30].

Necessary and sufficient conditions for the system (7.1) to be feedback equivalent to a linear system were given in [19,20] for the single input case ($m = 1$). (This case and the multi-input case are treated in [30].) For simplicity, we shall shall state necessary and sufficient conditions for the single input case. The single input version of system (7.1) with $G(x) = g(x)$, and with equilibrium at the origin, is locally feedback equivalent to a linear system if and only if the set of vector fields $\{g, ad_f^1(g), ad_f^2(g),\ldots,ad_f^{n-1}(g)\}$ spans $\mathcal{R}^n$ about the origin and the set $\{g, ad_f^1(g),\ldots,ad_f^{n-2}(g)\}$ is involutive. The open neighborhood U of the

origin in which the system is a linear equivalent is determined by the region over which the above conditions hold.

An equivalent necessary and sufficient condition that is given in [19,20,30] is that there exist a scalar function $T_1(x)$ such that

$$\begin{aligned} \mathcal{L}_g(T_1) &= 0 \\ \mathcal{L}_{ad_f^1(g)}(T_1) &= 0 \\ &\vdots \\ \mathcal{L}_{ad_f^{n-2}(g)}(T_1) &= 0 \qquad (7.14) \\ \mathcal{L}_{ad_f^{n-1}(g)}(T_1) &\neq 0 \qquad (7.15) \end{aligned}$$

This set of conditions will facilitate our computation of a transformation which makes explicit the feedback equivalence of an example up-down converter to a controllable linear, time-invariant system. In particular, after determining a suitable solution T_1 to (7.14,7.15) (if it can be done), we would obtain $n-1$ additional transformed state variables by computing

$$\begin{aligned} T_2 &= \mathcal{L}_f(T_1) \\ &\vdots \\ T_n &= \mathcal{L}_f(T_{n-1}). \qquad (7.16) \end{aligned}$$

It is also possible to compute a transformed input variable, i.e. $T_{n+1} = \mathcal{L}_f(T_n)$, which makes explicit the equivalence to a linear system. The conditions (7.14,7.15) guarantee that $T_j' = T_{j+1}$ for $j = 1, \ldots, n$, and further that $\frac{\partial T_{n+1}}{\partial u} \neq 0$. The variables $T_1, \ldots, T_{n+1}$ therefore belong to the controllable LTI system

$$\begin{aligned} T_1' &= T_2 \\ &\vdots \\ T_n' &= T_{n+1}. \qquad (7.17) \end{aligned}$$

In the following subsection, we consider the application of feedback linearization to the up-down converter.

7.1.1 Example: Up-Down Converter

Here, we consider the feedback linearization of the second order up-down converter modeled by (2.6), but in state variables that represent perturbations from an equilibrium corresponding to a constant value of the duty ratio d_n. This type of description is useful for analyzing the behavior with respect to a desired steady state operating point, but with the input still constrained to take on one of two discrete values. In the following, the variables with subscript t represent *total* variables while an unsubscripted variable represents the perturbation in a quantity with respect to its nominal value. With this notation, the model for the up-down converter takes the form

$$x' = Ax + (Bx + b)u \tag{7.18}$$

where the states are $x_1 = i = i_t - i_n$ and $x_2 = v = v_t - v_n$, the control input u can take on the discrete values $-d_n$ and $1 - d_n$, and the relevant matrices are given by

$$\begin{aligned} A &= \begin{bmatrix} 0 & (1-d_n)/L \\ -(1-d_n)/C & -1/RC \end{bmatrix}, \\ B &= \begin{bmatrix} 0 & -1/L \\ 1/C & 0 \end{bmatrix}, \\ b &= \begin{bmatrix} (V_s - v_n)/L \\ i_n/C \end{bmatrix}. \end{aligned}$$

In this case the vector field $f(x) = Ax$ is linear and the vector field $g(x) = Bx + b$ is affine in the state. To determine if this second order example is a feedback linear equivalent, we need to check

1. if the vector fields $g(x)$ and $ad_f^1(x)$ are linearly independent about the origin, and

2. if the vector field $g(x)$ is involutive.

It is a trivial fact that a set consisting of a single vector field is always involutive. It turns out that the first condition is also satisfied. Note that the first condition

is guaranteed to hold in a neighborhood of the origin since the small signal linearization of the large signal state-space averaged model is controllable. This follows since the set of vector fields $\{g, ad_f^1(g)\}$ is given by $\{Bx + b, [AB - BA]x + Ab\}$ which reduces to the controllability matrix $[b\ Ab]$ for $x = 0$. We shall address the issue of the region of existence of a linearizing transformation after determining the form of such a transformation.

To find a transformation which makes explicit the feedback equivalence, consider the conditions (7.14) which for this system reduce to

$$\frac{dT_1}{dx}(Bx + b) = 0, \tag{7.19}$$

or equivalently

$$\frac{\partial T_1}{\partial i}(-v - v_n + V_s) + \frac{\partial T_1}{\partial v}(i + i_n) = 0. \tag{7.20}$$

A solution of the partial differential equation (7.20) can be obtained by separation of variables and is given by

$$T_1(x) = \frac{1}{2}C(v + v_n - V_s)^2 + \frac{1}{2}L(i + i_n)^2, \tag{7.21}$$

or

$$T_1 = \frac{1}{2}C(v_t - V_s)^2 + \frac{1}{2}Li_t^2. \tag{7.22}$$

Note that the variable T_1 has the form of the energy in the increment with respect to the point $(v_n, i_n) = (V_s, 0)$, but there is no evident connection with our earlier results in Chapter 4 concerning the energy in the increment. (It also turns out that if the procedure here is applied to a model for a boost converter, the corresponding variable T_1 can take the form of the total stored energy.) Having obtained the scalar function T_1, it is straightforward to determine a linearizing transformation. We can readily compute a second state variable in the transformed system by differentiating T_1 along the vector field $f(x) = Ax$, as noted after (7.14,7.15). We obtain

$$T_2 = \mathcal{L}_f(T_1) = i_t V_s + (v_t/R - I_o)(V_s - v_t). \tag{7.23}$$

A third variable corresponding to the transformed input variable can be computed by differentiating T_2 along the vector field $f(x)$, giving

$$\begin{aligned} T_3(x,u) &= \mathcal{L}_f(T_2) \\ &= [(V_s - v_t)/R + (I_o - v_t/R)][(I_o - v_t/R - i_t)/C] + v_t V_s/L + \\ &\quad u_t\{[(V_s - v_t)/R + (I_o - v_t/R)]i_t/C + (V_s - v_t)V_s/L\}. \end{aligned} \tag{7.24}$$

At this point, some comments on the region of existence of the linearizing transformation are in order. Note that the transformed system (in coordinates T_1, T_2, and T_3) loses controllability at the set of points where the quantity multiplying u_t in (7.24) is zero. This is the set where the system is not equivalent to a controllable linear system. (See [65] for more on this.) However, the state-space transformation $\tau : U \to V$ which maps i and v to T_1 and T_2 is a diffeomorphism in the neighborhood of the origin, where the Jacobian matrix

$$\frac{d\tau}{dx} = \begin{bmatrix} Li_t & C(v_t - V_s) \\ V_s & I_o + \frac{V_s - v_t}{R} \end{bmatrix} \tag{7.25}$$

is nonsingular. This neighborhood contains the region where $i_t > 0$ and $V_s - v_t > 0$ which corresponds to usual operation of the up-down converter. Our development of a control design will be based on this state-space transformation, rather than a linearizing feedback, so that we only need to be concerned with the invertibility of this transformation.

Another issue concerning explicit feedback linearization is that the input variable in our model u_t can take on only two discrete values. In a true feedback linearization where the input could take on a continuum of values, we would obtain the linearizing feedback (i.e. $\alpha(x)$ and $\beta(x)$) by solving (7.24) explicitly for u_t. (This could be done if we were considering the state-space averaged model for the converter, but our development will not require an explicit feedback linearization.) With the transformed system, there are many control possibilities including linear state feedback (for the averaged model) and sliding mode control algorithms. We have investigated the sliding mode approach, as discussed in the following section.

7.2 Sliding Mode Control Design with Transformed State Variables

One particular class of switching control laws for the stabilization of certain nonlinear (and linear) systems invokes the theory of sliding mode control, see [4,5,6,7,66]. This method of control can be most readily applied to systems in the canonical form

$$\begin{aligned} x_1' &= x_2 \\ x_2' &= x_3 \\ &\vdots \\ x_n' &= f(x_1, \ldots, x_n, u). \end{aligned} \tag{7.26}$$

A sliding mode control forces the state to move to, and subsequently lie on a certain (specified by design) sliding surface in the state-space ($\mathcal{R}^n$). The surface is chosen to divide the state-space into two regions, with a separate control law used in each of the two regions. The control laws are picked to drive the state toward the sliding surface. In the case of infinitely fast switching between the two control laws, the state is constrained to lie on the sliding surface (once it reaches the surface), and the system is governed by an averaged control law. The sliding surface is always designed so that a prescribed dynamical behavior results when the state lies on the surface. For instance, for the system (7.26), one might use the function

$$s = c_n x_n + \ldots + c_1 x_1 \tag{7.27}$$

to define the sliding surface via

$$s = 0 \tag{7.28}$$

or

$$c_n x_1^{(n-1)} + \ldots + c_1 x_1 = 0, \tag{7.29}$$

where $x^{(j)}$ denotes the j-th derivative of x with respect to time, and the c_j satisfy Hurwitz conditions that guarantee that the linear differential equation (7.29) is

asymptotically stable. Another route to analyzing the dynamics in the sliding mode is to solve for the *equivalent* (or averaged) feedback control $u_{eq}(x_1, \ldots, x_n)$ as in [4,8,9], by (in effect) differentiating (7.29) and solving for u. This equivalent control, when employed in (7.26), produces dynamical behavior identical to that which occurs in the sliding mode, provided the initial condition is on the sliding surface.

The main advantage of a sliding mode control scheme over a linear feedback scheme that would provide the same equivalent control on the sliding surface is the invariance of the sliding motion to certain disturbances and uncertainties [4,5,6,7,66,80]. In the case of an additive disturbance on the right-hand side of (7.26), the closed-loop system would be entirely insensitive to sufficiently bounded (but possibly state and time dependent) disturbances of the form

$$\begin{bmatrix} 0 \\ \vdots \\ 0 \\ 1 \end{bmatrix} w(x,t).$$

Furthermore, in the case of arbitrary impulsive disturbances, the state of the closed-loop system would first jump from the surface, and then return to the sliding surface where the dynamics are constrained. This feature is particularly useful in second order systems since the sliding surface is a curve in the plane that exactly determines the closed-loop trajectories. The result is excellent robustness. The invariance properties outlined here are not features of standard linear feedback control system.

One of the noted disadvantages of sliding mode control is the inherent chattering or switching action. In a mechanical system, the chattering can excite unmodeled dynamics, leading to degraded or unsatisfactory behavior. In [6], Slotine and Sastry studied methods for reducing the effects of chattering in a sliding mode control system. However, in the case of a switching converter, the switching action is an intrinsic property of the operation of the circuit. In fact, it is possible to implement a sliding mode control for a switching converter where the function of the control algorithm is simply to dictate each switch transition.

This is the approach that we take here (and the reason why we have not considered explicit feedback linearization for the averaged model of the up-down converter).

Example: Sliding Mode Control of Up-Down Converter Using Transformed Coordinates In the previous section, we determined a coordinate transformation for the up-down converter model (2.6) that results in a state-space model with the form (7.26), i.e.

$$\begin{aligned} T_1' &= T_2 \\ T_2' &= T_3 = f(T_1, T_2, u). \end{aligned} \tag{7.30}$$

With the model (7.30), a sliding mode control law can be designed by specifying a sliding criterion of the form

$$s = c_1(T_1 - T_1^{ref}) + T_2 \tag{7.31}$$

with $c_1 > 0$. The control law

$$u = \begin{cases} 1 - d_n, & s \leq 0 \\ -d_n, & s > 0 \end{cases} \tag{7.32}$$

will then result in sliding behavior on a portion of the curve defined by (7.31). To investigate the extent of sliding behavior, the criterion s is differentiated along the system trajectories. We find

$$s' = c_1 T_1' + T_2' = c_1 T_2 + f(T_1, T_2, u). \tag{7.33}$$

For the region of the state-space where $i_t > (I_o - v_t/R)$ (the region where the inductor current exceeds the total load current), the expression $f(T_1, T_2, u)$ is negative for $u = -d_n$ and is positive for $u = 1 - d_n$. It then follows that for sufficiently small values of the parameter c_1, the control law (7.32) will result in sliding behavior on the portion of the curve (7.31) that lies in the region $i_t > (I_o - v_t/R)$. This region corresponds to normal operation of the converter. We study the resulting performance with numerical simulations and an experiment, as discussed below.

Figure 7.1 shows a simulation of a discrete-time version of this control law for $c_1 = 100$Krad/sec with initial conditions $v = -7$volts and $i = 10$amps. The converter parameters used were selected for a nominal switching frequency of approximately 50KHz. The simulated controller made a decision every 0.1μsec, and held the control constant in between decision times. (This permitted the possibility of extremely fast switching operation (relative to the design parameters), but the objective here was only to study the idealized behavior.) Note that the trajectory shown in Figure 7.1 exhibits two phases. First, in the reaching phase, the trajectory approaches and actually crosses the sliding curve (see Figure 7.1(f)). The trajectory crosses the sliding curve because there is a finite time delay until the required switch transition is executed. In the second phase, the sliding phase, the trajectory is constrained to approximately follow the sliding curve toward the desired operating condition. During the sliding phase, the sliding criterion s stays at approximately zero, so that T_1 and T_2 must obey

$$0 \approx c_1(T_1 - T_1^{ref}) + T_2. \tag{7.34}$$

Since $T_1' = T_2$, we expect from (7.34) that T_1 will exhibit an exponential decay with exponent $-c_1$ during the sliding phase. This is confirmed in Figure 7.1(d), where the temporal evolution of the variable T_1 is displayed. Note that the trajectory apparently does not reach a final limit cycle, which may be undesirable. The absence of limit cycle behavior is a result of the discrete-time nature of the control law. It is possible to use a constant frequency version of this control law that results in a stable limit cycle, as will be discussed below. First, we study the sensitivity and stability robustness with regard to parameter uncertainty.

The closed-loop converter system that uses the sliding mode control algorithm introduced above is relatively immune to parameter uncertainties. The only effect of unknown circuit parameters on the closed-loop system is to perturb the shape of the sliding curve in the $i - v$ plane. Note that the computation of s is based on the variables T_1 and T_2, and the parameter T_1^{ref}. The nominal inductor current i_n required in the computation of T_1^{ref} might be obtained by supposing that the instantaneous value of the load current is its steady state

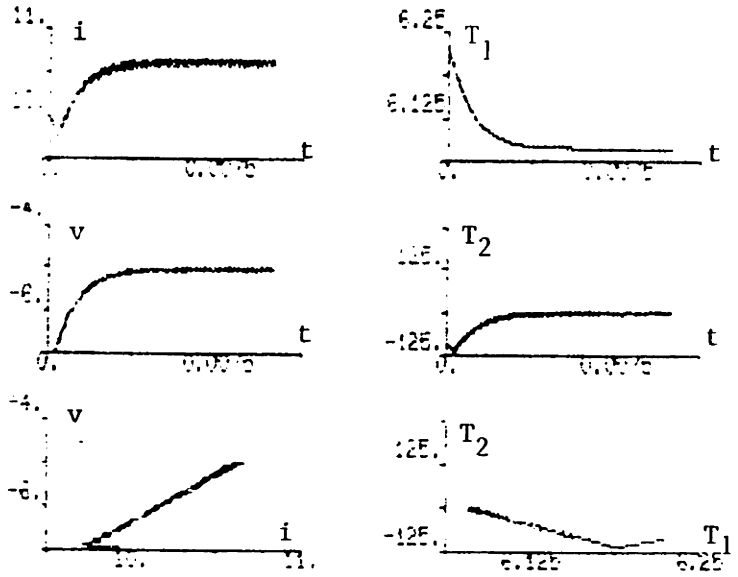

Figure 7.1: Digital Simulation of Sliding Mode Control Scheme Using Transformed Coordinates

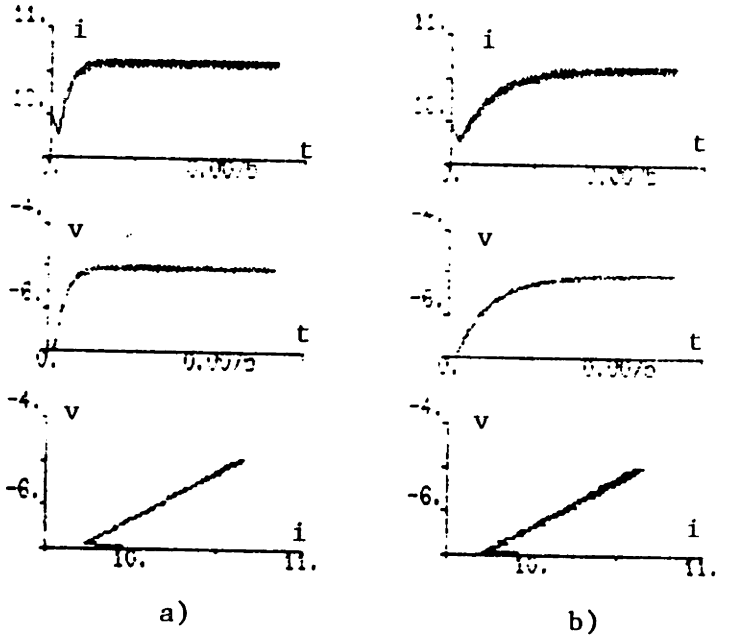

Figure 7.2: Digital Simulations of Sliding Mode Control Scheme with Actual Value of Capacitor a) Reduced by 30% and b) Increased by 30%

value. (Although this assumption does not hold in general, it is valid in the steady state.) In the case where the total load current $I_{load} = I_o - v_t/R$ and the source voltage V_s are measured and used in the computation of T_1 and T_2, and T_1^{ref} is obtained using a value for i_n based on the instantaneous load current, the sliding curve will intersect the desired steady state operating point even in the presence of parametric uncertainty. A consequence of this is a lack of steady state error. To see this, consider the computation of s with imprecisely known model parameters $\tilde{C}$ and $\tilde{L}$, i.e.

$$\begin{aligned} \tilde{s} &= c_1(\tilde{T}_1 - \tilde{T}_1^{ref}) + T_2 \\ &= c_1\left(\{\frac{1}{2}\tilde{C}(v_t - V_s)^2 + \frac{1}{2}\tilde{L}i_t^2\} - \{\frac{1}{2}\tilde{C}(v_n - V_s)^2 + \frac{1}{2}\tilde{L}i_n^2\}\right) + \\ &\quad i_t V_s - I_{load}(V_s - v_t). \end{aligned} \tag{7.35}$$

Consider ideal stable sliding behavior, i.e. $\tilde{s} \equiv 0$. In the steady state $T_2 = T_1' \equiv 0$, and so $\tilde{s} \equiv 0$ implies $\tilde{T}_1 = \tilde{T}_1^{ref}$. Because the same incorrect model parameters are used to compute both $\tilde{T}_1$ and $\tilde{T}_1^{ref}$, it follows that an equilibrium is defined by $i_t = i_n$ and $v_t = v_n$. Therefore, in the presence of parametric uncertainty, the system may come to rest at the desired equilibrium if stable sliding behavior occurs. The stability robustness is addressed below.

A closely related issue concerns the stability of the sliding motion in the presence of parametric uncertainty. It turns out that any smooth sliding curve defined by

$$s(T_1, T_2) = 0 \tag{7.36}$$

will result in stable sliding motion if sliding behavior is obtained, and if

$$\left(\frac{\partial s}{\partial T_1}\right)\left(\frac{\partial s}{\partial T_2}\right) > 0 \tag{7.37}$$

for points on the curve (7.36). Since the product (7.37) for the unperturbed sliding curve is $c_1 > 0$, this product will generally remain positive in the presence of small perturbations. This topic is perhaps best studied with simulations. Numerical simulation using the same control algorithm as that used for the simulation of Figure 7.1, but with the actual circuit value of the capacitor reduced

by 30% and increased by 30%, are shown in Figure 7.2. Behavior similar to that with the nominal parameters is exhibited, with the main difference appearing in the rate of the asymptotic decay. We shall give more attention to the sensitivity and robustness issues in the experimental segment of this work.

The preceding numerical simulations incorporated a discrete time controller that used the state information to make a control decision every 0.1μsec. The control input was held constant in between sampling/decision times. As previously mentioned, this control method typically does not result in a stable limit cycle behavior. The absence of periodic behavior results from the fact that an integral multiple of the 0.1μsec control cycle typically does not equal the period of a feasible limit cycle. However, this discrete-time control proved relatively economical in digital simulation time, and hence was preferred for most simulations. The resulting (and apparently chaotic) behavior may be undesirable in practice because of the broadband frequency spectrum generated by the circuit waveforms. The audible noise generated by a circuit operating in this mode has been described as that of frying bacon [22]!

It is possible to implement another variation of the desired control law that uses a constant frequency switching. At the beginning of each control period, the control can be set "on" if $s \leq 0$. Then the control is set "off" when and if the criterion s crosses zero during the control period. If the criterion s remains negative for the entire period, the control remains "on". At the other extreme, if the criterion is positive at the beginning of the period, the control is set "off" for the entire period. In this way, the control is limited to at most two switch transitions per control period. The simulation in Figure 7.3 and experimental results discussed below suggest that a stable limit cycle may indeed be reached.

Although this control based on transformed variables is in principle an effective approach to the control problem, the control law requires some nontrivial computation. Simplified control laws can be obtained by examining the state plane trajectories and the switching curves derived above. We have constructed

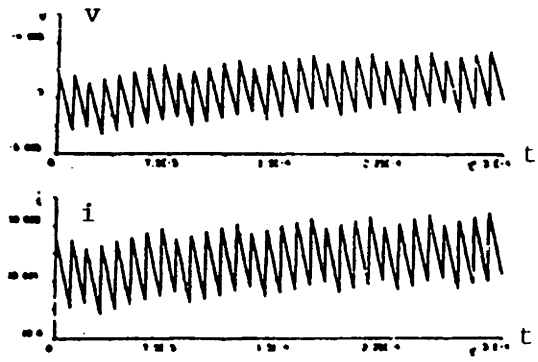

Figure 7.3: Asymptotic Behavior under Constant Switching Frequency Switching Scheme

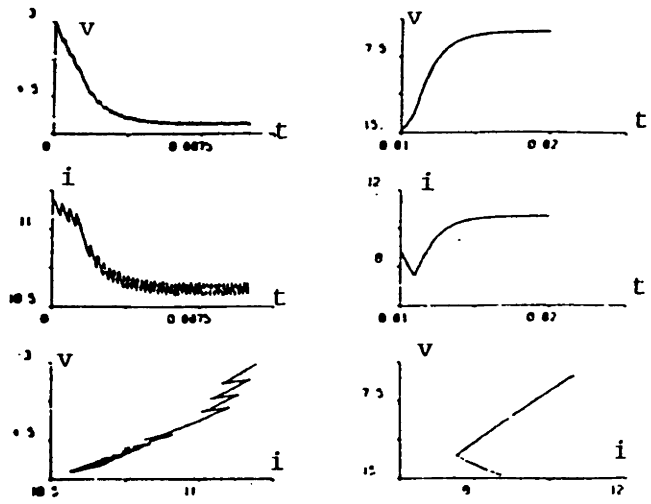

a) b)

Traces in a) are for initial values v=-3volts and i=11.2amps, while those in b) are for initial values v=-14.5volts and i=8.8amps.

Figure 7.4: Simulation of Sliding Mode Control Using Sliding Curve Constructed from Straight Line Segments in the $i - v$ Plane

a switching curve composed of straight line segments in the inductor current-capacitor voltage ($i - v$) plane that results in stable behavior as demonstrated by digital simulation. The curve constructed from line segments loosely approximates the switching line based on the $T_1 - T_2$ coordinates, and the local behavior in a neighborhood of the desired operating condition is similar to that obtained with the previously specified control law. Figure 7.4 shows state-plane and time domain waveforms for this control law. Note that the linear switching curves and surfaces proposed in [8] and [9] would also result in simple implementation schemes. Of course, a crucial step in implementing a sliding mode control with a linear sliding surface is in determining the nominal state values, that permit operation at the desired steady state operating point. (This is one issue that is conveniently handled using the transformation based implementation.)

In the following subsection, we present the results of an experimental implementation of the sliding mode control scheme that is based on the coordinate transformation into the variables T_1 and T_2.

7.2.1 Experimental Results

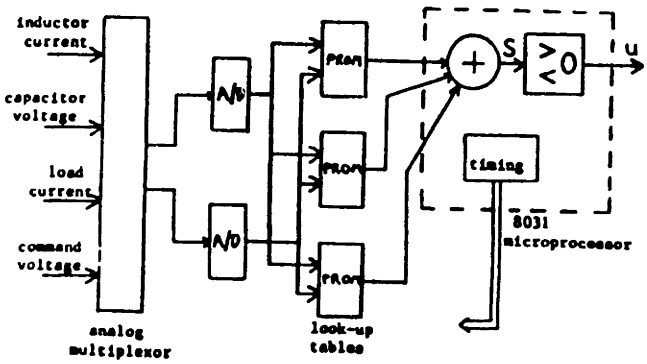

Figure 7.5: Block Diagram of Prototype Controller

A prototype digital controller for an up-down converter was built, using PROM look-up tables and an 8031 microprocessor to perform housekeeping and timing functions. The implemented control algorithm consisted of the sliding mode control scheme using the transformed state variables T_1 and T_2. A block diagram

of the hardware realization is exhibited in Figure 7.5. The up-down converter circuit was realized on the MIT Parity Simulator [24]. The Parity Simulator was used to implement a low-power, time-scaled version of the circuit in Figure 2.1 as well as modifications of it (see below). The circuit parameters of Example 2 of Chapter 5 were scaled for operation at a switching frequency of 50Hz (as opposed to 50KHz). Note that our objective here was to test the proposed control laws under ideal conditions or under prescribed deviations from the ideal; the issue of real-time implementation is of great importance ultimately, but is beyond the scope of what is attempted here.

The behavior under the sliding mode controller with sliding time constant of $\frac{1}{\pi}$sec is displayed in Figure 7.6a). Figure 7.6a) shows a transient in the state variables due to a step change in the command voltage from approximately -6volts to approximately -9volts, and back to -6volts. Note that after a short reaching phase, a well behaved first order type transient with time constant of approximately 0.3sec is exhibited in the sliding phase. The switching operation of the circuit was run at a constant frequency of 50Hz, with the transistor on for the start of each cycle and the turn-off determined by the sliding criterion. (See the discussion on switching operation above.)

To investigate the effects of model uncertainties on the circuit behavior, we considered certain perturbations in circuit parameters. Figures 7.6b) and c) show the responses to the same step change in command voltage as in Figure 7.6a), but with the circuit value of the capacitor 20 percent larger and 20 percent smaller, respectively. Note that the transients are qualitatively identical, with apparently equal time constants governing the decay in the sliding mode. The most prominent difference among the traces in Figure 7.6 is the amplitude of the voltage ripple. Figure 7.6b), which corresponds to a greater value of capacitance than nominal, displays a slightly smaller amplitude of voltage ripple, while Figure 7.6c), which corresponds to a smaller value of capacitance than nominal, displays a slightly greater voltage ripple; this is to be expected.

One interesting feature of the switching scheme manifested itself in the ex-

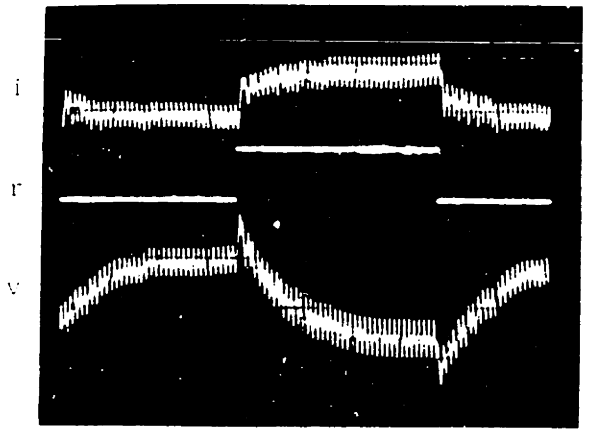

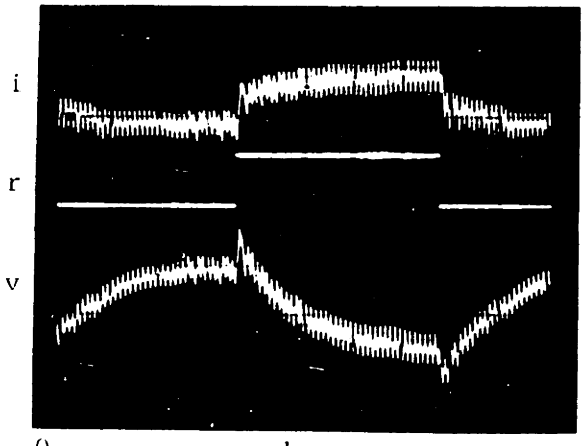

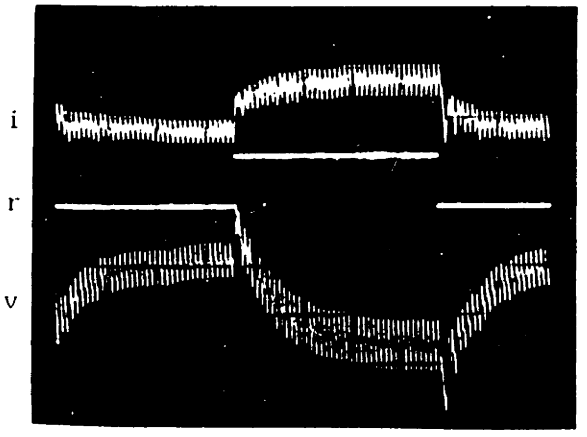

Figure 7.6: Step Response: a) With Ideal Circuit Parameters, b) Capacitor 20% Larger, c) Capacitor 20% Smaller

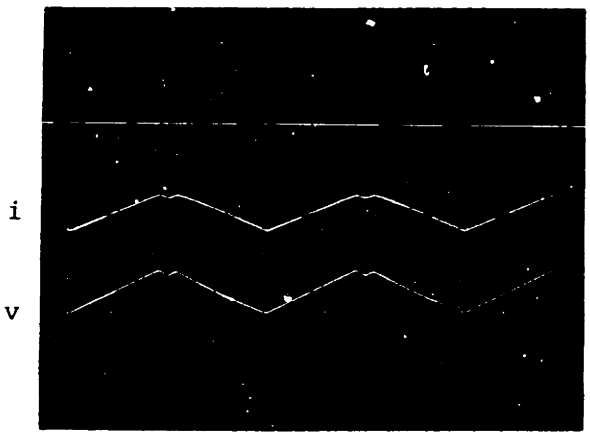

Figure 7.7: Two-Cycle Oscillation

periments. The constant frequency switching scheme did not result in stable limit cycle behavior for nominal duty ratios greater than 50 percent. This result may have been predicted from previous work on current mode control [10,11] where similar switching schemes have been utilized, and the same phenomenon observed. The loss of stable limit cycle behavior in current mode programming applications has been remedied with the use of a so-called compensation ramp. We have yet to attempt such a solution. The most interesting behavior occurred for a nominal duty ratio of approximately 50% (command voltage of -15volts). At this operating condition, a stable *two-cycle* oscillation was observed, as depicted in Figure 7.7. Note that each apparent period exhibited in the waveforms is composed of two cycles, one where the transistor is on for most of the cycle followed by one where the transistor is off for most of the cycle; the two-cycle average corresponded to a 50% duty ratio.

7.3 Summarizing Remarks

The method of exact state-space linearization is evidently an effective approach for the design of nonlinear control schemes for our example up-down converter. It is apparent that all locally controllable second-order systems are exact linear equivalents (at least locally); the procedure used for the up-down converter in

Section 7.1 is applicable for these systems. A second-order boost converter is one power electronic circuit for which we have been able to determine a linearizing transformation. For this converter, the variable T_1 in the linearizing transformation can be taken as the total stored energy in the reactive elements of the converter. Related results have been developed in Sira-Ramirez and Ilic [65].

The case of higher order (> 2) converters that have essential nonlinearities may not be easily treated with this approach. One possibility is the method of multiple time-scales, where certain states are viewed as "slowly varying" (i.e. quasi-static) and the model consisting of the "fast states" is an exact linear equivalent. Other potential approaches for these converters along the lines of exact linearization are the so-called pseudolinearization [31,32] and exact input-output linearization (model matching) via dynamic feedback [30].

Chapter 8

Contributions of Thesis and Suggestions for Future Research

In this final chapter, the main results and contributions of this thesis will be summarized. Directions for future research will also be outlined.

8.1 Contributions of Thesis

Averaged Circuit Models An important contribution of this thesis has been to extend earlier results on averaged circuit models for switching power converters. In particular, in Chapter 4, we applied the intuitive in-place averaging method of Wester and Middlebrook [46] to devise a methodical procedure for synthesizing averaged models. Earlier results on averaged circuit synthesis were either not entirely correct or based on examples. For a converter constructed from LTI circuit elements, sources, and one controlled switch pair, we showed in Section 4.2.1 that one could obtain the averaged circuit model essentially by finding the hybrid immittance function seen by the two switch branches. Section 4.2.2 applied the averaged circuit synthesis technique to converters containing nonlinear circuit elements. This gave an entirely new result which may prove very useful in the analysis of switched converter circuits as nonlinear circuit elements are incorporated into future converter designs.

One consequence of the result on averaged circuit models for DC-DC converters containing nonlinear circuit elements is the open-loop stability result of

Section 4.3.2. For such a circuit containing nonlinear reactive elements, it is typically not possible to obtain a stability result for a nominal periodic trajectory. However, it was possible to demonstrate that an equilibrium for the averaged circuit model was stable in the large. This stability result was then applied in Section 5.4 to aid in the design of controllers for DC-DC converters containing nonlinear circuit elements.

Unification of Network Theoretic Principles with Control Design Perhaps the most important contribution of this thesis has been the unification of certain network theoretic principles with a framework for control design for switched converters. This theme has been developed in a number of different ways. The form of a natural internal energy function, the energy in the increment, was first determined in Chapter 4 for a converter constructed from incrementally passive circuit elements and switches. It was then demonstrated in Chapter 5 how one can base a globally stabilizing control design on this energy function. Chapter 5 laid the foundation for this approach, and showed how it can be applied to various classes of switching power circuits, including converters containing nonlinear circuit elements, converters that handle time-varying source and/or load waveforms, and converters that operate in the discontinuous conduction mode. The approach was also applied to the design of state observers that estimate the state of a given converter from incomplete or noisy measurement data.

Chapter 6 built upon the approach of Chapter 5 by recognizing that the behavior of the converter from its control input u or d to a properly defined synthetic output y was that of a passive circuit. This allowed us to view a closed-loop control system (for a switching converter) as an interconnection of circuit elements. The result of this is a generic global stability result based on the passivity properties of the "circuit elements" that could be applied in all the schemes considered in that chapter. This approach has been taken by numerous other authors in the context of general feedback control systems (e.g.[28,29,37])

and for switching power converters by Wood [1]. Most of the earlier results in the literature are concerned with demonstrating stability. However, the results in this thesis are distinguished from the earlier works by the control performance that has been demonstrated here. In particular, the self-tuning adaptive control scheme developed in Section 6.5 permits robustly stable operation for any feasible operating point. The analogy between closed-loop control systems and network interconnections also proved useful in designing controllers that permit adequately fast transient behavior. In particular, Section 6.6 borrowed certain ideas from the optimal matching problem to aid in the design of closed-loop systems that exhibit fast transient behavior.

It is appropriate to note a potential limitation of the Lyapunov-based control designs that are obtained using averaged models. The stability argument used in Chapters 5 and 6 applies directly for the averaged model, but in practice, the control schemes would be implemented with finite switching frequency. Although results that relate the stability of an underlying time-varying model to that of an averaged model are available (e.g. [84]), it still remains to determine an explicit lower bound on the switching frequency for which such a conclusion can be made. This remains as a subject for future study.

The Lyapunov-based approach to control is evidently applicable to other types of control systems. The main requirement is that the underlying system (or possibly the closed-loop system) can be modeled with incrementally passive circuit elements. An example of the application of this approach to control for a robotic manipulator is in the recent work of Slotine [85]. Although the form of the control input for the robotic manipulator is quite different from that in a switching power converter, reference [85] developed a self-tuning adaptive control scheme much like that of Section 6.5 that was also based on an internal energy function. It was also suggested in [85] that this approach would have applications in many other types of control systems.

Control Design Using Coordinate Transformations Another approach to control design investigated in this thesis was based on the use of coordinate transformations. In particular, in Chapter 7, we determined the form of a state-space transformation that could be used in a feedback linearization for an example up-down converter. It was noted that such a transformation can facilitate various types of control designs, and this transformation was used in Chapter 7 to design a sliding mode controller for the up-down converter. It was noted that the sliding mode control could be made to command each switch transition in the converter circuit, whereas schemes based on the state-space averaged model do not share this feature. The sliding mode controller was shown to yield satisfactory closed-loop behavior with numerical simulations and experimental results. In particular, using this scheme, relatively fast transient behavior and robustness to uncertain circuit parameters were obtained. This approach to control is apparently applicable to other second order converters, but may not be easily applied to higher order converters.

8.2 Suggestions for Future Research

There are many questions that are addressed, but not entirely answered in this thesis. Further, many new questions arise in the light of the results that are obtained. Here, we shall outline some of these as possibilities for future research.

8.2.1 Averaged Circuit Models

The results on averaged circuit models in this thesis and in the literature are applicable only to the class of switching converters that have well defined state-space averaged models. These converters have switching frequencies that are significantly higher than the bandwidth of the averaged circuit dynamics. The class of resonant converters [2,48] can be modeled with neither the usual state-space averaging techniques nor the available averaged circuit representations. It is of interest to develop an averaged circuit modeling technique for resonant converter circuits. This development might possibly follow along the lines of the

in-place averaging scheme used in this thesis and in [46]. In this case, it would be necessary to replace not only the switch network, but also the L - C resonant tank elements. Because the resonant tank exhibits nontrivial low frequency dynamical behavior [2], it would be necessary to replace the tank and switch elements with a dynamical network, rather than a resistive network. This topic remains as a subject for future research.

8.2.2 Limit Cycle Existence in Switched Circuits

The result of Section 4.3.1 on open-loop stability applied for any given nominal trajectory that corresponded to a given switching pattern. It is of interest to determine when it can be concluded that there *exists* a nominal periodic trajectory for the case where all switches are operated periodically with period T. Work that is presently being carried out indicates a route for proving the existence and uniqueness of a nominal periodic trajectory, for a switched circuit of the form considered in Section 4.3.1 where all switches are operated periodically with period T. These results rely on the incremental passivity of the circuit elements, and will appear in future publications. Some previous researchers [89,90] who studied this question have restricted attention to second order systems.

8.2.3 Lyapunov-Based Control

Experimental Verification of Control Designs An important topic that was not treated in this thesis is the experimental verification of the Lyapunov-based control schemes. It will be of great interest to implement in hardware some of the control schemes introduced in Chapters 5 and 6. These control designs, based on averaged models, can probably be best implemented with standard integrated circuit (IC) chips used to implement pulse-width modulation schemes in existing controllers. Some additional signal processing functions will be needed to compute the nonlinear feedback control laws. Experimental work will undoubtedly generate new research directions, and expose limitations.

Time-Varying Source and/or Load Waveforms We demonstrated in Section 5.5 how the method of control that was based on the energy in the increment could be applied to a converter that operated with nominally periodic input and/or output waveforms. Typical applications are in rectifiers, inverters, and cyclo-converters. The greatest difficulty encountered in this application is in obtaining the nominal periodic state trajectories for use in the feedback control. (This problem was significantly easier to handle in the case of a DC-DC converter, as demonstrated in Sections 6.4 and 6.5.) There is a theory currently being developed in the literature on so-called repetitive control systems (see [86] and references contained therein) where the control system is designed to have an internal model of the periodic disturbance or reference trajectory. This approach is a natural generalization of the use of integral control to handle unknown constant nominal operating points. It would be extremely useful to incorporate the methods of repetitive control systems with our Lyapunov-based control approach to obtain control schemes for rectifiers, inverters, and cyclo-converters that permit globally stable operation and robustness to unknown nominal source and/or load waveforms. This remains as a topic for future work.

Converters that Operate in Both Continuous and Discontinuous Conduction Modes In Section 5.6, we showed how the Lyapunov-based control approach could be applied to a converter operating in the discontinuous conduction mode. However, the particular control law required for nominal operation in the discontinuous conduction mode differed from that required for nominal operation in the continuous conduction mode. Therefore, in order to implement the control, it is required to first determine the mode of nominal operation. Then, one of two separate control laws (that correspond to the two modes of operation) would be selected. Note that the detection problem involved in determining the nominal operating mode can be rather difficult. A natural question that arises is how a control scheme can be designed to easily accommodate both modes of operation. The best solution to this problem is possibly a unified con-

trol scheme that changes continuously as the nominal operation of the converter moves from one mode to the other. It is of interest to explore control methods (perhaps including the Lyapunov-based schemes of this thesis) that achieve this goal. Analysis methods from the theory of singular systems [87] may be required for this application since the state-space averaged model for a given converter changes order when the converter undergoes a transient from the continuous conduction mode to the discontinuous conduction mode, or vice-versa.

Design of Positive Real Compensators for Optimal Speed In Section 6.6, we demonstrated an ad hoc method for designing a positive real compensator for a given positive real plant that resulted in relatively fast closed-loop transient behavior. (The speed was measured in terms of the eigenvalue(s) of the closed-loop system that had least negative real part.) The problem of determining conditions under which there exists a positive real compensator for a given positive real plant that results in optimal speed still remains open. Further, the interesting problem of determining a compensator (if one exists) for optimal closed-loop speed also remains open. The procedure of Section 6.6 borrowed ideas from broadband matching theory to aid in the compensator design. It will be of interest to explore the relationship between the broadband matching problem (which attempts to maximize average "power" transfer from plant to compensator) and the problem of obtaining optimally fast transient behavior. Further questions arise in the context of nonlinear plants and nonlinear compensators. In particular, how would one design an incrementally passive compensator for an incrementally passive plant to obtain optimally fast transient behavior?

Large Signal Stability in Absence of Known Lyapunov Function In Section 6.5, it was shown that the global stability of a converter control system could be maintained in the presence of structured uncertainties in the case where the nominal duty ratio was known. However, this Lyapunov stability result did not carry over to the case where the nominal duty ratio was unknown, although

it was argued that small signal stability could be maintained for a wide range of operating conditions. It would be extremely useful to determine the region of attraction in the state-space for the given stable equilibrium point. Such a characterization (for a set of feasible parameter values) would permit conclusions on the large signal stability robustness of the control system. Fortunately, a theory for determining the region of attraction of a stable equilibrium is currently being developed in the literature [77,78,79]. Some of the results in [77,78] concern the case where every system trajectory approaches an equilibrium point as $t \rightarrow \infty$, and certain other generic conditions are in force. In this case, the stability boundary for a given stable equilibrium is composed of the stable manifolds of the equilibrium points on the stability boundary for the equilibrium point. Results in [77,78] also give a method to test if a certain equilibrium point is on the stability boundary for a given stable equilibrium point.

This type of result may prove particularly useful for systems that incorporate integral control, since for these systems, it is often possible to limit the number of possible equilibrium points to a small number (possibly one). The difficulty with this approach arises in ruling out the possible presence of limit cycles and non-periodic limit sets. Although there are many results available in the literature to characterize the possible presence or absence of limit cycles in second order systems, and to rule out other non-stationary limit sets in these systems, these results do not generally hold for higher order systems. An important and rather challenging topic for future research is to determine criteria for ruling out the possible presence of nonstationary limit sets in systems with order higher than two. The existence of an energy type function that decreases monotonically along system trajectories is one criterion for this, as discussed in [78]. For the Lyapunov-based control schemes considered in Chapter 6, which are used in the presence of structured uncertainty, it may be possible to demonstrate the existence of such a function by perturbing the original Lyapunov function. Undoubtedly, many other possibilities exist and remain to be investigated.

8.2.4 Control Design Based on Coordinate Transformations

The most severe limitation of the control scheme considered in Chapter 7 is that such a scheme can only be readily applied to a converter with a second order model. It is typically difficult or impossible to obtain a suitable transformation for a converter with a higher order model. (As noted in Chapter 3, down converters without input filters have essentially linear state-space models, and so are readily transformed to the desired form.) Other possibilities exist. In particular, it may be possible to take a time-scale separation approach where the system is partitioned into slow and fast subsystems. Then, for each of these lower order subsystems, it may be possible to apply the method using coordinate transformations.

Another possibility is to apply the so-called pseudolinearization technique [31]. This approach has been taken in [32] in the context of switching converters. The method of this approach is to determine a nonlinear state-space transformation so that for each feasible nominal operating condition, the small signal linearization has a standard invariant form. This permits the design of a coordinated feedback control that is applicable to all feasible operating points. However, this type of scheme will not necessarily result in large signal stability.

Appendix A

Network Theoretic Considerations

In this appendix, fundamental concepts from network theory, in particular passivity, reciprocity and Tellegen's theorem, are presented. These network theoretic principles were used extensively in the early work of Wolaver [26] and Duffin [25] on fundamental limitations of power conversion circuits. Passivity (and the closely related idea of dissipativeness) was used in the work of Wood [1] to obtain stability results for closed-loop switching converter systems. We apply these concepts in Chapter 4 to obtain a basic and important result on open-loop stability of switching converters, and in Chapters 5 and 6 to aid in the design of feedback control schemes.

A.1 Passivity, Incremental Passivity, Relative Passivity, and Reciprocity

Here we present essential ideas concerning passivity and reciprocity of nonlinear multiport networks, keeping in mind the important examples of purely resistive and purely reactive elements. For the purpose of developing stability results for switching converters, the concepts of incremental and relative passivity will be essential.

In order to state the following definitions in a relatively general way, we assume the input-output vector pair of an n-port to be a *hybrid pair*. That is, the

input $u(t)$ and output $y(t)$ of an n-port are n-component vectors whose elements represent port voltages or currents. The components of $y(t)$ are complementary to those of $u(t)$, and oriented such that $u(t)^* y(t)$ is the instantaneous power entering the network at its ports. In the following, the networks of interest are assumed to time-invariant unless otherwise noted.

Passivity The definition of passivity presented in Wyatt et. al. [35], Wyatt [88], and in Hasler and Neirynck [34] will be adopted here.

Definition A.1.1 (Available Energy) *Given an n-port* **N**, *let the* **available energy** $E_{A,x}$ *in state x be the maximum energy that can be extracted from* **N** *when its initial state is x, with the convention that $E_{A,x} = +\infty$ if the available energy is unbounded. That is,*

$$E_{A,x} = \sup_T \int_0^T -u(t)^* y(t)\, dt \tag{A.1}$$

Definition A.1.2 (Passivity) **N** *is* **passive** *if $E_{A,x}$ is finite for each initial state x.*

Note that this definition of passivity is directly tied to a state-space realization for the n-port in question. This will not prove objectionable for the purposes of this study since we aim to draw conclusions for switching converters for which state models are readily obtained. In the context of a switching converter, the concept of passivity will be of use in viewing a controlled converter as an interconnection of various n-ports.

With the given definition of passivity, one must search over all initial states to verify that a particular n-port is passive. However, in the case where a *completely controllable* state-space realization for the n-port is given, [35] shows that the n-port is passive if the available energy $E_A(x)$ is finite for some initial state x. We adopt the definition of complete controllability from [35], which states roughly that a state-space realization is completely controllable if any state x can be reached in finite time from any initial state x_0 via a trajectory along which only

finite energy is consumed or extracted. The claim of [35] follows essentially from the definition of complete controllability. It is rather easy to demonstrate that the network elements to be considered in this thesis have completely controllable state-space realizations. See the examples below, in particular the generalized capacitive/inductive network which has a controllable LTI input-state model.

The definition above is consistent with, but more general than some earlier definitions of passivity conceived for linear (and possibly time-varying) circuits, e.g. [36].

Alternate Definition A.1.2 (Passivity: Linear Networks) *An n-port network, assumed to be storing no energy at time t_0, is said to be* **passive** *if*

$$E(T) = \int_{t_0}^{T} v(t)^* i(t)\, dt \geq 0 \tag{A.2}$$

for all t_0, T, and all port voltage vectors $v(t)$ and current vectors $i(t)$ satisfying constraints imposed by the network.

Note that this definition of passivity is less general than the first one given, since it is based on a zero energy state. However, it is not inconsistent with the first definition in the case where a well defined zero energy state exists.

Incremental Passivity For the development of stability results for switching converters in Chapters 4, 5, and 6, the notion of incremental passivity and related concepts will be essential. The definition given here follows the system theoretic framework of Desoer and Vidyasagar [37].

Definition A.1.3 (Energy in the Increment) *Given an n-port* **N** *with initial state x, let $(u_1(t), y_1(t))$ and $(u_2(t), y_2(t))$ be any two admissible input-output trajectories on $[0, T]$ with T finite. The* **energy in the increment** *between the two trajectories is defined by*

$$W_x(T) = \int_0^T (u_1 - u_2)^* (y_1 - y_2)\, dt. \tag{A.3}$$

Definition A.1.4 (Incremental Passivity) *An n-port* **N** *with initial state* x *is* **incrementally passive at state** x *if* $W_x(T)$*, the energy in the increment defined in (A.3), is nonnegative for every pair of admissible trajectories on* $[0,T]$ *with* T *finite. If the network is incrementally passive at all states* x *in the state space, it is said to be* **incrementally passive**. *The n-port is* **strictly incrementally passive at state** x *if* $W_x(T) > 0$ *whenever the two trajectories are distinct. The network is* **strictly incrementally passive** *if it is strictly incrementally passive at every state in the state-space.*

Note that this definition is closely tied to the definition of passivity. A passive network can supply only finite energy while an incrementally passive network can absorb only nonnegative *energy in the increment* between two trajectories (W_x in (A.3)).

Relative Passivity Incremental passivity will prove to be too strong a condition in the case of certain nonlinear n-ports. In fact, many nonlinear networks that are not incrementally passive exhibit a closely related property that we shall term *relative passivity*. Another closely related notion, *local passivity* for a capacitor (or inductor) has been introduced in [34,81]. However, our definition of relative passivity is potentially applicable to any type of network (as demonstrated in this thesis). To define a relatively passive network, we examine the energy in the increment with respect to a constant nominal operating point.

Definition A.1.5 (Relative Passivity) *Given an n-port* **N** *with equilibrium state* x_n *and nominal output* y_n *corresponding to the constant input* u_n*, consider the admissible trajectory* $(u(t), y(t))$ *on* $[0,T]$ *that is obtained with initial state* $x(0) = x_n$*. The n-port is* **relatively passive at** x_n *if*

$$W_{x_n}(T) = \int_0^T [u(t) - u_n]^*[y(t) - y_n]\, dt \geq 0 \qquad \text{(A.4)}$$

for any finite T*. The n-port is* **relatively passive** *if (A.4) holds for any nominal operating point.* **N** *is* **strictly relatively passive at** x_n *if the inequality in (A.4) is strict whenever* $x(T) \neq x_n$*.* **N** *is* **strictly relatively passive** *if it*

is strictly relatively passive for ..y constant nominal state. The network is **strictly relatively passive at x_n to infinity** *if it is strictly relatively passive at x_n and $W_{x_n}(T)$ grows unboundedly as $\|x(T) - x_n\|$ tends to infinity. The n-port is* **strictly relatively passive to infinity** *if it is strictly relatively passive and $W_{x_n}(T)$ grows unboundedly as $\|x(T) - x_n\|$ tends to infinity for any nominal operating point.*

Strict relative passivity to infinity will play a role in concluding global stability for open-loop operation of switching converters in Chapter 4, and for certain control schemes for these converters in Chapter 6. In particular, for a constant nominal trajectory, this definition guarantees that $W_{x_n}(T)$ in (A.4) is bounded below by $\|x(T) - x_n\|$. Hence, in the case of lossless elements (defined below) for which $W_{x_n}(T)$ is a function of only x_n and $x(T)$, $W_{x_n}(T)$ can be useful as a Lyapunov function.

See the discussion below for examples of resistive and reactive elements that are relatively passive, and for a result concerning preservation of relative passivity in an interconnection of such elements.

Note that it is possible to make an alternate definition of relative passivity, based on a time-varying nominal trajectory. This is not needed in our development, and so will not be formally included; however, for purposes of completeness, an alternate definition is given here. For this purpose, consider the nominal input, state, and output trajectory $\{u_n(t), x_n(t), y_n(t)\}$ on the interval $[0, T]$ that is consistent with the network.

Alternate Definition A.1.5 (Rel. Passivity: Time-Varying Trajectories) *Given an n-port* **N** *and an admissible nominal trajectory $\{u_n(t), x_n(t), y_n(t)\}$ on $[0, T]$, consider the admissible trajectory $\{u(t), x(t), y(t)\}$ on $[0, T]$ that is obtained with initial state $x(0) = x_n(0)$. The n-port is* **relatively passive at** *$\{u_n(t), x_n(t), y_n(t)\}$ if*

$$W_{x_n}(T) = \int_0^T [u(t) - u_n(t)]^*[y(t) - y_n(t)]\, dt \geq 0 \qquad \text{(A.5)}$$

for any finite T. The n-port **N** *is* **relatively passive** *if (A.5) holds for any nominal trajectory.* **N** *is* **strictly relatively passive at** $\{u_n(t), x_n(t), y_n(t)\}$ *if the inequality in (A.5) is strict whenever $x(T) \neq x_n(T)$.* **N** *is* **strictly relatively passive** *if it is strictly relatively passive for any admissible nominal trajectory.*

The distinction between relative passivity with respect to a time-varying nominal trajectory and incremental passivity can be subtle; see the example below that illustrates this distinction.

Losslessness A network property exhibited by reactive networks that is of some interest in this work is *losslessness.* We shall use the definition given in [38], and refer the reader to [38] and [28,29] for additional discussion and clarification.

Definition A.1.6 (Losslessness) *A state-space representation S for an n-port network is* **lossless** *if for every pair of states x_1 and x_2, the total energy consumed at the ports along a trajectory transferring the state from x_1 to x_2 is path independent. An n-port network* **N** *is* **lossless** *if it has a completely observable lossless state-space representation.*

The observability condition is necessary to distinguish among equivalent state-space representations that may or may not be completely observable. As an example, for a simple two-terminal resistor with resistance R, it is possible to assign a state-space representation of the form

$$\begin{aligned} x' &= i^2 R \\ v &= Ri. \end{aligned} \tag{A.6}$$

This state-space model is lossless in accord with the definition above, but is evidently not observable. The definition of observability from [38] requires that for a given state-space realization, any two initial states $x_1(0)$ and $x_2(0)$ that generate identical input-output behavior must be equal, i.e. $x_1(0) = x_2(0)$.

A passive network that is also lossless possesses an internal energy function that is unique to within an additive constant. This function coincides (up to an additive constant) with the *available energy*. This fact is of use in the computation of storage functions for circuits that are constructed from purely reactive elements (which are lossless) and purely resistive elements. In particular, we may simply add up the storage functions for the reactive elements to obtain a storage function for the circuit.

Reciprocity Another network property that will be of use in this thesis is *reciprocity*. Reciprocity can be both a local and a global property for a nonlinear network, as will be reflected in the following definitions and in the examples below. The definitions here are taken from Chua [81]. (Also see Wyatt [88].)

Definition A.1.7 (Reciprocity: LTI Network) *An LTI network* **N** *is* **reciprocal** *if for any two Laplace transformable input-output signal pairs, i.e.* $\{u_1(t), y_2(t)\}$ *and* $\{u_2(t), y_2(t)\}$,

$$U_1(s)^* Y_2(s) = U_2(s)^* Y_1(s) \tag{A.7}$$

where the capitalized variables are the Laplace transforms of the respective lower case variables.

The following definition for nonlinear networks is based on the existence of a small signal linearization for any given operating point, and so we assume that such a linearization is well defined.

Definition A.1.8 (Reciprocity: Nonlinear Network) *A nonlinear network* **N** *is* **reciprocal at the constant nominal operating point** (u_n, y_n) *if the small signal linearization of* **N** *is reciprocal at* (u_n, y_n). **N** *is* **reciprocal** *if it is reciprocal at all of its nominal operating points.*

In the case of nonlinear resistive and nonlinear reactive multiports, reciprocity results in some interesting global properties of the respective representations for these elements. See the discussion below, where examples are considered.

A.2 Examples

Resistive n-Ports Since the adopted definition of passivity from [35] is based on a state-space realization, we shall assign to a purely resistive element the trivial realization where the state has zero dimension. The class of resistive n-ports of interest here can be modeled by $y = g(u)$ where (u,y) is a hybrid pair. Then, a resistive n-port is passive if and only if

$$u^* g(u) \geq 0 \tag{A.8}$$

for any admissible u. If the inequality in (A.8) is strict for nonzero u, then the resistive n-port is strictly passive.

The notion of an incrementally passive resistive network is crucial for the results in Chapters 4, 5, and 6. The resistive n-port characterized by $y = g(u)$ is incrementally passive if and only if

$$(u_1 - u_2)^*(g(u_1) - g(u_2)) \geq 0 \tag{A.9}$$

for any two admissible vectors u_1 and u_2. The n-port is strictly incrementally passive if the inequality in (A.9) is strict when u_1 and u_2 are distinct. In the case where $g(u)$ is differentiable, incremental passivity and strict incremental passivity are equivalent to the Jacobian matrix $[dg/du]$ being globally positive semi-definite and globally positive definite (except possibly at isolated points), respectively. This is easily seen by considering a line integral that is equivalent to the left-hand side of (A.9).

$$\begin{aligned}
&(u_1 - u_2)^*(g(u_1) - g(u_2)) \\
&= \int_0^1 \frac{d}{dt}\{(u_1 - u_2)^*[g(u_1) - g(u_1 + t(u_2 - u_1))]\}\, dt \\
&= \int_0^1 (u_1 - u_2)^* \left[\frac{dg}{du}\right]_t (u_1 - u_2)\, dt
\end{aligned} \tag{A.10}$$

The last integral in (A.10) is nonnegative if $[dg/du]$ is positive semi-definite, and is always positive if $[dg/du]$ is positive definite (except possibly at isolated points) and u_1 and u_2 are distinct. In the case of resistive networks there is no distinction between incremental passivity and relative passivity.

Note that an ideal DC source can be classified as a nonlinear n-port resistive network. An ideal DC source is incrementally passive, although not passive.

A nonlinear resistive element with differentiable hybrid representation $y = g(u)$ is reciprocal at the point (u_n, y_n) if the Jacobian matrix $[dg/du]_{u_n}$ satisfies

$$[dg/du]_{u_n} \Sigma = \Sigma [dg/du]^*_{u_n} \tag{A.11}$$

where Σ is a signature matrix, i.e. a diagonal matrix with all diagonal elements $+1$ or -1. The elements that are $+1$ correspond to the current-controlled ports of the resistive element, while those that are -1 correspond to the voltage-controlled ports (or vice-versa). In the case where the hybrid representation is an impedance or admittance representation, (A.11) reduces to the familiar symmetry constraint for reciprocal networks. The formula (A.11) will be of some importance in Chapter 4, where synthesis of nonlinear averaged networks is considered.

An intrinsic property of a resistive network that is globally reciprocal is the existence of a scalar 'potential' function, termed the *content*, *co-content*, or *hybrid-content* in [81], depending upon the particular representation used. For purposes of illustration, assume that the nonlinear, reciprocal, resistive network of interest has a current-controlled representation, i.e. $v = R(i)$. Then two consequences of the reciprocity of the network are: (i) the Jacobian matrix $[dR/di]$ is symmetric everywhere, and (ii) the line integral

$$\mathcal{G}(i, i_0) = \oint_{i_0}^{i} v(\sigma)^* d\sigma \tag{A.12}$$

is well defined. (The latter is a result of Stoke's theorem in vector calculus.) The quantity $\mathcal{G}(i)$ defined in (A.12) is termed the *content*, and can serve as a global representation for this resistive network. In particular, it is possible to recover the impedance representation $v = R(i)$ from the content function by taking the gradient of this function, i.e.

$$v = \nabla \mathcal{G}(i). \tag{A.13}$$

In [81], the *co-content* and *hybrid-content* functions are similarly defined.

Generalized Capacitive/Inductive n-Ports We shall deal with the class of generalized capacitive/inductive n-ports whose elements can be characterized by a state model of the form

$$\begin{aligned} x' &= u \\ y &= g(x) \end{aligned} \tag{A.14}$$

where u and y are respectively the vectors of port currents and port voltages, or vice-versa. (That is, the element is either a multiport capacitor or a multiport inductor.) Such a reactive n-port is passive if and only if there exists a scalar potential function $f(x)$, bounded below, such that $g(x) = \nabla f(x)$. See [35] and references contained therein for a proof of this fact. Figure A.1a) shows an example of a voltage-charge characteristic for a passive nonlinear capacitor. The state-space model (A.14) is lossless in the case where $g(x) = \nabla f(x)$ since the integral

$$\begin{aligned} \int_0^T yu\,dt &= \int_0^T \nabla f(x)\,x'\,dt \\ &= \int_0^T \frac{d}{dt} f(x)\,dt \\ &= f(x(T)) - f(x(0)) \end{aligned} \tag{A.15}$$

is path independent.

It is also true that a generalized capacitive/inductive element of the form (A.14) (with $g(\bullet)$ differentiable) is reciprocal if and only if $g(x) = \nabla f(x)$ for some scalar function $f(x)$. This is a result of the fact that $g(x) = \nabla f(x)$ for some $f(x)$ if and only if the Jacobian matrix $[dg/dx]$ is everywhere symmetric. The impedance or admittance matrix representation for the small signal linearization of (A.14) is symmetric if and only if $[dg/dx]$ is symmetric, and hence the generalized reactive element (A.14) is reciprocal if and only if $g(x) = \nabla f(x)$. Note that any non-reciprocal reactive element (satisfying the above smoothness condition) cannot be passive as a result of the argument here. (This is also demonstrated in [81].)

It is shown in [34] that the only element of the class of incrementally passive capacitive/inductive n-ports is the linear n-port characterized by

$$\begin{aligned} x' &= u \\ y &= Gx \end{aligned} \tag{A.16}$$

where the matrix G is symmetric, positive semi-definite. In computing $W_x(T)$, the energy in the increment between two trajectories beginning at state x, we find

$$\begin{aligned} W_x(T) &= \int_0^T (u_1 - u_2)^*(Gx_1 - Gx_2)\,dt \\ &= \int_0^T \frac{d}{dt}\left\{\frac{1}{2}(x_1 - x_2)^* G(x_1 - x_2)\right\} dt \\ &= \frac{1}{2}(x_1(T) - x_2(T))^* G(x_1(T) - x_2(T)) \end{aligned} \tag{A.17}$$

Note that in obtaining the final equality, we used the fact that $x_1(0) = x_2(0) = x$. It follows that W_x is nonnegative for any two admissible trajectories beginning at x, provided G is positive semi-definite. Since the state x is arbitrary in this calculation, it follows that W_x is nonnegative for any x, and hence the n-port is incrementally passive.

Because the class of incrementally passive reactive elements is so limited, and because we would like to include nonlinear reactive elements (e.g. saturating inductors) in our discussion of switching converter stability in Chapter 4, it is essential to consider the class of relatively passive reactive elements. For these elements, we consider the energy in the increment with respect to the nominal trajectory where the input in (A.14) is zero and the state is constant. Given a capacitive/inductive n-port **N** with initial state x_n, consider the admissible trajectory $(u(t), y(t))$ on $[0, T]$. **N** is relatively passive at x_n if

$$\begin{aligned} W_{x_n}(T) &= \int_0^T u(t)^*\{y(t) - y_{x_n}\}\,dt \\ &= \int_0^T x'(t)^*\{y(x(t)) - y_{x_n}\}\,dt \\ &= \oint_{x_n}^{x(T)} (dv)^* y(v) - \int_0^T x'(t)^* y_{x_n}\,dt \end{aligned}$$

$$= \oint_{x_n}^{x(T)} (dv)^*\{y(v) - y_{x_n}\} \geq 0 \qquad \text{(A.18)}$$

for any finite T. Note that the third line in (A.18) follows from the fact that reactive networks are lossless, and hence the consumed (or extracted) energy in a transient depends only on the endpoints of the state trajectory. Observing the fourth line in (A.18), we see that the *energy in the increment* with respect to a constant nominal trajectory also depends only on the endpoints of the state trajectory $x(t)$.

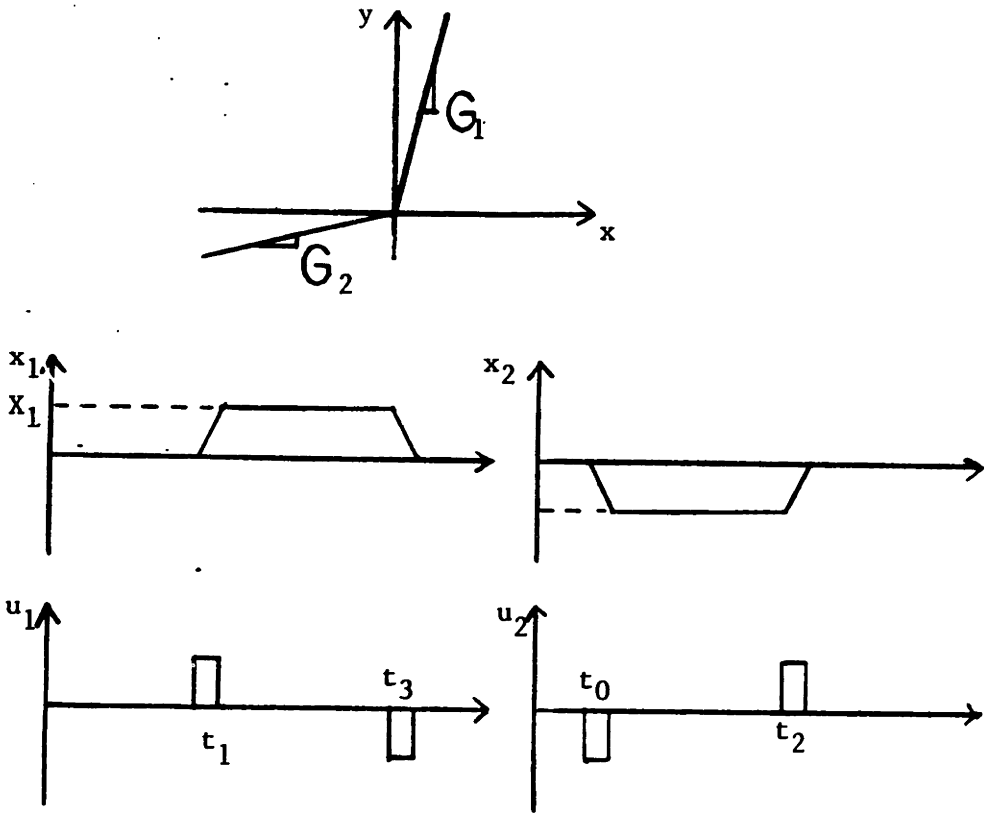

Figure A.1: (a) Relatively Passive Nonlinear Capacitor Characteristic and (b) Input/State Trajectories that Violate Incremental Passivity

To see where consideration of relatively passive reactive networks can be important, consider the one-port capacitor described by $x' = u$ and $y = g(x)$ as illustrated in Figure A.1a). In computing the energy in the increment between the two trajectories depicted in Figure A.1b), we find $W = (G_1 - G_2)X_1X_2$. This is clearly not always nonnegative, although this capacitor is strictly relatively passive. Charge-voltage characteristics for one-port capacitors that are

respectively (i) strictly relatively passive at a given x_n and (ii) strictly relatively passive at a given x_n to infinity are shown in Figures A.2a) and b). Note that any reactive element that is strictly relatively passive at all of its equilibrium states is inherently strictly relatively passive to infinity.

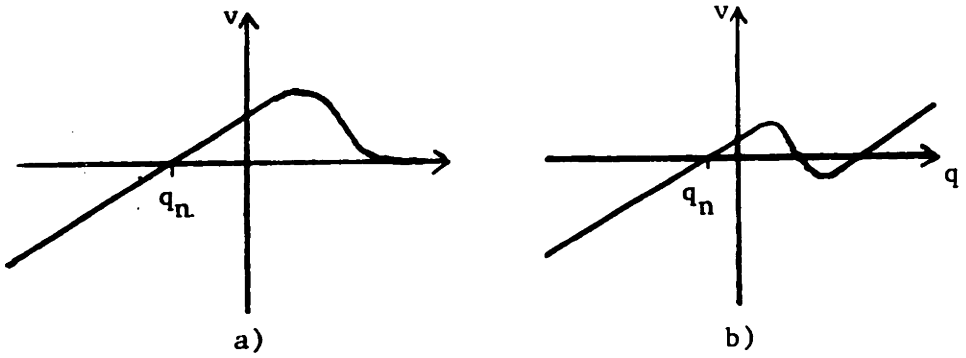

Figure A.2: Charge-Voltage Characteristics: a) Strictly Relatively Passive at x_n, and b) Strictly Relatively Passive at x_n to infinity.

More generally, a reactive n-port is relatively passive if and only if

$$(x_1 - x_2)^*(g(x_1) - g(x_2)) \geq 0 \tag{A.19}$$

for any states x_1 and x_2. In the case where $g(x)$ is differentiable, this is equivalent to the Jacobian of $g(x)$ being symmetric, positive semi-definite for all states x. Note that the case where this Jacobian is not positive definite in a neighborhood of some x_0 is degenerate, in the sense that the state realization of the n-port is locally unobservable in the neighborhood of x_0. We shall be mainly interested in the case where the Jacobian of $g(x)$ is symmetric, positive definite.

Distinction between Incremental Passivity and Relative Passivity with Respect to a Time-Varying Trajectory As noted after the alternate definition of relative passivity that encompassed time-varying nominal trajectories, the distinction between relative passivity with respect to a given time-varying

nominal trajectory and incremental passivity can be rather subtle. We illustrate this difference with an example here. Consider the system modeled by

$$\begin{aligned} x' &= Ax + (Bx + b)u \\ y &= (Bx + b)^* Qx. \end{aligned} \tag{A.20}$$

Assume that in this model $Q = Q^* > 0$, $QA + A^*Q = 0$, and $QB + B^*Q = 0$. The latter two assumptions are not necessary, but are made for convenience. This type of model is introduced in Chapter 6 to model certain input-output behavior of a switching converter. It turns out that the model (A.20) is not incrementally passive, as can be seen by considering the energy in the increment between two general time-varying trajectories, i.e.

$$\begin{aligned} W_0(T) &= \int_0^T (u_1 - u_2)(y_1 - y_2)\, dt \\ &= \int_0^T (u_1 - u_2)\{(Bx_2 + b)^* Q(x_1 - x_2) + (x_1 - x_2)^* B^* Q x_1\}\, dt \\ &= \int_0^T [\frac{d}{dt}\frac{1}{2}(x_1 - x_2)^* Q(x_1 - x_2) + (x_1 - x_2)^* B^* Q x_1]\, dt \\ &= \frac{1}{2}[x_1(T) - x_2(T)]^* Q[x_1(T) - x_2(T)] + \int_0^T (x_1 - x_2)^* B^* Q x_1\, dt \end{aligned} \tag{A.21}$$

The last term in the last line of (A.21) can be positive, negative, or zero depending on the particular trajectories x_1 and x_2, precluding the incremental passivity of the model (A.20). (This model is relatively passive at the nominal operating point $x = 0$, as is demonstrated in Chapter 6.) What is interesting is that the closely related model

$$\begin{aligned} x' &= Ax + (Bx + b)u \\ y &= (Bx_n(t) + b)^* Qx, \end{aligned} \tag{A.22}$$

where $x_n(t)$ denotes a nominal state trajectory of (A.22) (or of (A.20)) corresponding to the nominal input trajectory $u_n(t)$, is relatively passive with respect to the nominal trajectory $\{u_n(t), x_n(t), y_n(t)\}$. (This model could have been used in Chapter 5 (Section 5.5) to facilitate the presentation on handling time-varying source and/or load waveforms.) The nominal trajectory $\{u_n(t), x_n(t), y_n(t)\}$ is

a nominal trajectory for the model (A.20), as well. However, (A.20) is neither relatively passive with respect to this trajectory nor incrementally passive as previously shown.

To see that the model (A.22) is strictly relatively passive with respect to the nominal trajectory $\{u_n(t), x_n(t), y_n(t)\}$, consider the computation of $W_{x_n}(T)$, the energy in the increment for a general trajectory satisfying $x(0) = x_n(0)$:

$$\begin{aligned} W_{x_n}(T) &= \int_0^T (u - u_n)(y - y_n)\, dt \\ &= \int_0^T (u - u_n)[(Bx_n + b)^* Q(x - x_n)]\, dt \\ &= \int_0^T \frac{d}{dt}\frac{1}{2}(x - x_n)^* Q(x - x_n)\, dt \\ &= \frac{1}{2}[x(T) - x_n(T)]^* Q[x(T) - x_n(T)] \end{aligned} \tag{A.23}$$

It is therefore clear that the model (A.22) is strictly relatively passive with respect to the given nominal trajectory. However, this model is not incrementally passive, as can be seen by examining the energy in the increment between two trajectories, one of which is the zero trajectory (which is an admissible trajectory for this system). We obtain

$$\begin{aligned} W_x(T) &= \int_0^T uy\, dt \\ &= \int_0^T [u(b^* Qx) + u(x_n^* B^* Qx)]\, dt \\ &= \int_0^T [\frac{d}{dt}\frac{1}{2}x^* Qx + u(x_n^* B^* Qx)]\, dt \\ &= \frac{1}{2}x(T)^* Qx(T) + \int_0^T u(x_n^* B^* Qx)\, dt \end{aligned} \tag{A.24}$$

which evidently can be positive, negative, or zero depending upon the particular trajectory (and the nominal trajectory x_n). The conclusion is that (A.22) is not incrementally passive.

A.3 Tellegen's Theorem

Tellegen's theorem is a consequence solely of Kirchhoff's laws for the currents and voltages in a given network, and is independent of the component characteristics.

To state this theorem, we consider a network with b branches, any set of branch voltages $\{v_j; j = 1,2,\ldots,b\}$ satisfying KVL, and any set of branch currents $\{\bar{i}_j; j = 1,2,\ldots,b\}$ satisfying KCL. The overbar is used with the branch currents to emphasize that the set of branch voltages and currents $\{v_j, \bar{i}_j; j = 1,2,\ldots,b\}$ need not necessarily constitute a solution to the network. Tellegen's theorem, in its weakest form, states that the vector of branch voltages $\mathbf{v}$ is orthogonal to the vector of branch currents $\bar{\mathbf{i}}$, i.e.

$$\mathbf{v}^*\bar{\mathbf{i}} = \sum_{j=1}^{b} v_j \bar{i}_j = 0 \tag{A.25}$$

See [27] for an exposition on this remarkably general theorem and various applications.

One immediate result of Tellegen's theorem that is of use in this work is that the increments in the vectors of network voltages and currents are orthogonal. That is, given two distinct solutions $(\mathbf{v_1}, \mathbf{i_1})$ and $(\mathbf{v_2}, \mathbf{i_2})$ of a network, we have

$$(\mathbf{v_1} - \mathbf{v_2})^*(\mathbf{i_1} - \mathbf{i_2}) = 0 \tag{A.26}$$

This follows by expanding the expression in (A.26) into four terms, and noting that each is individually zero as a result of Tellegen's theorem.

A.4 Interconnected Networks

In this subsection, we aim to investigate the properties of interconnnected networks. In particular, we shall show that if all members of a set of n-ports possess one of the properties of passivity, incremental passivity, relative passivity, losslessness, or reciprocity, then under appropriate conditions, a network interconnection of the members of the set also possesses the property of interest. A network interconnection will be termed *admissible* if all relevant variables (i.e. port variables) are well defined for all time.

Interconnections of Passive n-Ports The argument to be presented here follows the one given in [35,38], and will serve as the prototype for similar

arguments involving certain other network properties of interest. Let $\mathbf{N}$ be an admissible interconnection of the set of passive networks $\{\mathbf{N_1}, \mathbf{N_2}, \ldots, \mathbf{N_k}\}$, and let $\mathbf{E}^j_{A,x_j}$ be the available energy for $\mathbf{N_j}$. Then, if the state for the interconnected network is given by $x = (x_1, \ldots, x_k)$, the available energy for the interconnection satisfies

$$\mathbf{E}_{A,x} \leq \mathbf{E}^1_{A,x_1} + \cdots + \mathbf{E}^k_{A,x_k}. \tag{A.27}$$

The statement follows from the fact that $\mathbf{E}^j_{A,x_j}$ is an upper bound on the energy that can be extracted from $\mathbf{N_j}$, and that by Tellegen's theorem the instantaneous power leaving the ports of $\mathbf{N}$ is the sum of the instantaneous powers leaving the ports of the $\mathbf{N_j}$. Hence, the network interconnection $\mathbf{N}$ is passive.

Interconnections of Incrementally Passive, Relatively Passive, and Lossless n-Ports The fact that admissible interconnections of incrementally or relatively passive n-ports are also, respectively, incrementally or relatively passive can easily be demonstrated via the prototype argument given in the previous paragraph. In these cases, we would apply Tellegen's theorem to conclude that the sum of the instantaneous *incremental powers* leaving the ports of the interconnected n-ports $\mathbf{N_j}$ is equal to the incremental power leaving the ports of the interconnected network $\mathbf{N}$. Some care is required in defining an admissible interconnection of relatively passive n-ports, since an arbitrary interconnection may not possess an equilibrium state.

The case of an interconnection of lossless n-ports has even more subtle complications since the definition of losslessness was based on a completely observable state-space realization. It is possible that an interconnection of observable lossless state-space models is not observable. However, in the case where an interconnection of lossless n-ports possesses an observable state-space realization, the interconnection is lossless. See [38] for more on this topic.

Interconnections of Reciprocal n-ports It is straightforward to demonstrate that an admissible interconnection of reciprocal networks is also reciprocal. Suppose that the interconnection of interest has a set of accessible ports

whose variables are contained in the port vectors $\mathbf{i_p}$ and $\mathbf{v_p}$. Denote the vectors of the (possibly inaccessible) port variables of the networks participating in the interconnection by $\mathbf{i_a}$ and $\mathbf{v_a}$. Application of Tellegen's theorem to the Laplace transformed port variables of a small signal linearization of this interconnected network yields

$$I_{p1}(s)^* V_{p2}(s) = -I_{a1}(s)^* V_{a2}(s) \quad \text{(A.28)}$$

$$I_{p2}(s)^* V_{p1}(s) = -I_{a2}(s)^* V_{a1}(s) \quad \text{(A.29)}$$

where the subscripts 1 and 2 indicate distinct network solutions. A consequence of the reciprocity of each of the networks participating in the interconnection is that the right-hand sides of (A.28) and (A.29) are equal. Therefore, so are the left-hand sides, and hence the interconnected network is reciprocal.

Feedback Connections Viewed as Network Interconnections

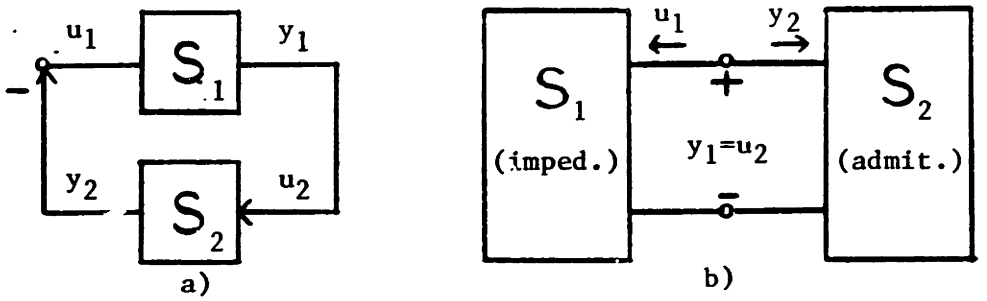

Figure A.3: a) Feedback Connection of Two Dynamical Systems and b) Equivalent Network Interconnection

Consider the feedback connection of the two multi-input, multi-output dynamical systems $\mathcal{S}_1$ and $\mathcal{S}_2$ via the constraints $u_2 = y_1$ and $u_1 = -y_2$ as shown in Figure A.3a). In the case where these two dynamical models realize, respectively, the input/output relations for two n-port networks, this feedback connection is equivalent to the network interconnection shown in Figure A.3b). Such a point of view can be of use in obtaining stability results for feedback system connections when it is known that each of the systems participating in the feedback

connection possesses a property such as passivity, incremental passivity, or relative passivity. See [28,29] and [37] for more on this subject. This point of view will be of use in Chapter 6 when we consider stabilizing feedback schemes for switching converters. Relative passivity is the property that will be most useful for our purposes in that chapter. The definition and use of this property is in itself a contribution of this thesis.

Appendix B

Averaged Circuit Synthesis for Multiply Switched Converters using Constraint Relations

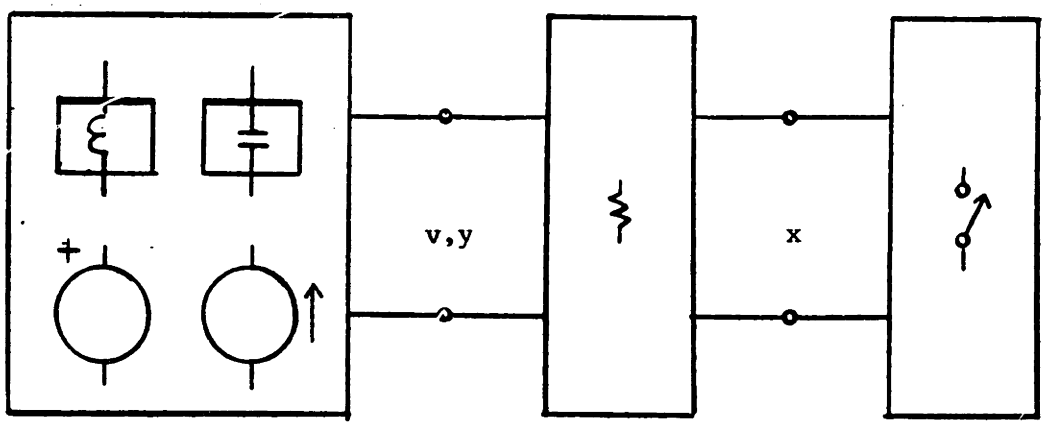

Figure B.1: Partitioned, Multiply Switched Converter

Here, we shall take a relatively formal approach to the synthesis problem that requires only the following two assumptions:

1. The state-space model for the switching converter is well defined in each switch configuration.

2. For each switch configuration and for any admissible state and source values, each branch voltage and current in the converter circuit has a unique solution.

In this development, we permit switched circuits with any finite number of switch configurations. In addition to the switches, the circuits considered here are assumed to contain sources, linear resistive elements, and nonlinear reactive elements. For each of the multiports in Figure B.1, we shall assign a constraint relation (see [47]). This is a very general way to characterize both linear and nonlinear multiports, as discussed in Chapter 4. For the constant linear resistive multiport, the constraint relation takes the form

$$C_y y + C_x x + C_v v = 0 \tag{B.1}$$

where the p-component vector v contains the controlling state and source variables, that is the inductor currents, capacitor voltages, current source currents, and voltage source voltages. The vector y contains the complementary state and source variables, and the $2r$-component vector x consists of the switch port variables. In the case where all resistive multiports are regular [81] (also see Chapter 4), the constraint relation for an n-port contains n independent constraints for the $2n$ port variables. Such a constraint relation can be represented by an $n \times 2n$ matrix, e.g.

$$\left[\begin{array}{ccc} C_y & C_x & C_v \end{array} \right] \tag{B.2}$$

for the present case. Note that it is possible to perform elementary row operations on constraint matrices without altering the imposed constraint relations. We may therefore freely reduce the constraint matrix (B.2) to upper triangular form with elementary row operations. Henceforth, we shall assume that this procedure was performed at the outset, and not change notation. The constraint relation for the switch multiport similarly has the form

$$C_u x = 0 \tag{B.3}$$

where the dependence upon the switch configuration is indicated with the subscript u.

As discussed in Chapter 4 (Subsection 4.2.1), for the purpose of averaged circuit synthesis, we need to focus only on the switch subnetwork of the converter

circuit (see Figure B.1). We take the approach of Subsection 4.2.1 to characterize an averaged resistive network that replaces the switch network. Such a characterization can be obtained by averaging the values of the switch port vector that occur in each switch configuration. The weights used in the averaging are determined by the respective duty ratios. To proceed, we require an explicit solution for $x|_u$, the switch port vector in configuration u, as obtained below.

Combining the two sets of constraints (B.1) and (B.3), we can write

$$\begin{bmatrix} C_y & C_x \\ 0 & C_u \end{bmatrix} \begin{bmatrix} y \\ x \end{bmatrix} = - \begin{bmatrix} C_v \\ 0 \end{bmatrix} v. \tag{B.4}$$

Note that because of the row-reduced form of the constraint matrix for the resistive multiport, the $(p+r) \times p$ submatrix C_y has at least r zero rows at the bottom. Keeping this in mind, we can further partition our constraint relation as

$$\begin{bmatrix} C_{y1} & C_{x1} \\ 0 & C_{x2} \\ 0 & C_u \end{bmatrix} \begin{bmatrix} y \\ x \end{bmatrix} = - \begin{bmatrix} C_{v1} \\ C_{v2} \\ 0 \end{bmatrix} v \tag{B.5}$$

where C_{y1} is $p \times p$, C_{x1} is $p \times 2r$, and C_{x2} is $r \times 2r$. Note that $C_{x2}x = 0$ represents the set of constraints imposed by the resistive multiport on the switch port variables x when all controlling source and state variables are set to zero, i.e. $v = 0$. Because of our assumption that the circuit has a unique solution for each admissible state and source value (i.e. each value of v), the system of linear equations (B.5) has a unique solution for each v. Hence, we can recover $x|_u$. For notational purposes, define the $2r \times 2r$ matrix

$$D_u = \begin{bmatrix} C_{x2} \\ C_u \end{bmatrix}.$$

Using this notation, we can solve (B.5) to obtain

$$\begin{bmatrix} y \\ x \end{bmatrix} = - \begin{bmatrix} C_{y1}^{-1} & -C_{y1}^{-1} C_{x1} D_u^{-1} \\ 0 & D_u^{-1} \end{bmatrix} \begin{bmatrix} C_{v1} \\ -- \\ C_{v2} \\ 0 \end{bmatrix} v, \tag{B.6}$$

and hence $x|_u$ takes the form

$$x|_u = -D_u^{-1} \begin{bmatrix} C_{v2} \\ 0 \end{bmatrix} v. \tag{B.7}$$

We are now in a position to solve the problem since we have obtained the form of the switch port vector $x|_u$ in terms of the constraint matrices for the resistive and switch multiports. As computed in Subsection 4.2.1 for the two configuration case, the one-cycle averaged switch port vector $\bar{x}$ is a convex combination of the $x|_u$, i.e.

$$\bar{x} = (1 - d_1 - \ldots - d_m)x|_{u=0} + d_1 x|_{u=1} + \ldots d_m x|_{u=m}. \qquad \text{(B.8)}$$

(See Chapter 2 (Section 2.1) for the particular correspondence between the switch configurations and the values of the input u.) The relation (B.8) leads to an explicit characterization of the subspace of $\mathcal{R}^{2m}$ that contains the averaged switch port vector:

$$\bar{x} = [(1 - d_1 - \ldots - d_m)D_0^{-1} + d_1 D_1^{-1} + \ldots + d_m D_m^{-1}] \begin{bmatrix} I \\ 0 \end{bmatrix} w \qquad \text{(B.9)}$$

where $w = -C_{v2}v$ is a vector in $\mathcal{R}^m$. Although w may not actually assume any arbitrary value in $\mathcal{R}^m$, the subspace defined by (B.9) where w is arbitrary must contain the vector of averaged switch port variables. As demonstrated in Subsection 4.2.1, such a characterization is adequate for the averaged resistive network required to replace the switch network in the averaged circuit. (Here, 'adequate' means that the resulting averaged circuit is a realization of the state-space averaged model, and that the circuit branch variables are equal to the one-cycle averaged waveforms of the underlying switched circuit.)

It is possible to obtain an implicit characterization (i.e. contraint relation of the form $C_d\bar{x} = 0$) for a non-switched resistive network that is equivalent to the characterization (B.9). For such a characterization, it is sufficient that the associated matrix

$$D_d = \begin{bmatrix} C_{x2} \\ C_d \end{bmatrix} \qquad \text{(B.10)}$$

satisfies the relation

$$D_d^{-1} = (1 - d_1 - \ldots - d_m)D_0^{-1} + d_1 D_1^{-1} + \ldots + d_m D_m^{-1}. \qquad \text{(B.11)}$$

If (B.11) can be solved for D_d, then C_d can be obtained from the last r rows of D_d. Note that it is possible to recover the explicit characterization (B.9) from

the implicit one involving D_d^{-1} as follows:

$$\overline{x} = D_d^{-1} \begin{bmatrix} I \\ 0 \end{bmatrix} w. \tag{B.12}$$

By hypothesis, each of the inverses D_u^{-1} is well defined since we have assumed that the switching converter circuit has a unique solution for any admissible state and source values in each switch configuration. Over the set of admissible duty ratios, it is true that D_d is well defined on an open and dense subset since the points at which D_d is not well defined correspond to points at which the determinant of the matrix on the right-hand side of (B.11) is zero. This determinant is a polynomial of finite order in the duty ratios, and is nonzero at each of the extreme values of the set of admissible duty ratios. It follows that D_d (and C_d) is well defined for almost every admissible duty ratio vector.

Upon determining the constraint matrix for the resistive network that replaces the switch multiport, one can synthesize a resistive network realizing this constraint matrix. One approach for this is to deduce a hybrid representation from the constraint matrix, and then apply the synthesis methods of [36] to obtain a network realization. The following example demonstrates how to recover the result of Section 4.2.1 where a particular hybrid representation is assumed to be well defined.

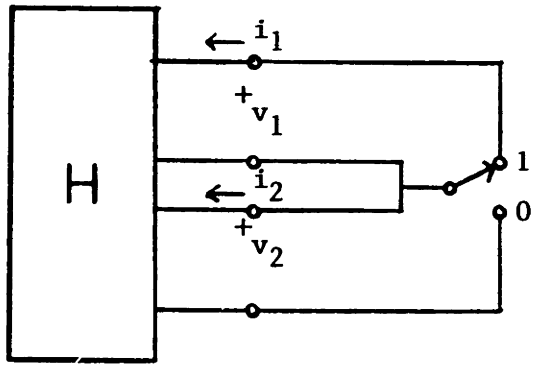

Figure B.2: Port Variable Definitions

Example: Hybrid Formulation Result Consider the interconnection of the switch two-port and the resistive two-port obtained by setting to zero all

voltage source voltages, all current source currents, all capacitor voltages, and all inductor currents as shown in Figure B.2. This circuit contains all the information necessary to determine an averaged circuit synthesis. Suppose the resistive network in Figure B.2 has a well defined hybrid representation H with the controlling port variables taken as v_1 and i_2. The constraint matrix C_{x2} for this network can be expressed as

$$C_{x2} = [\ I \quad -H\ ] \tag{B.13}$$

where the vector of port variables is taken as $x = [i_1\, v_2\, v_1\, i_2]^*$. The constraint matrices for the switch network take the form

$$C_0 = [\ I \quad 0\ ], \tag{B.14}$$

$$C_1 = [\ 0 \quad I\ ]. \tag{B.15}$$

Using the notation defined above, the associated matrices D_u are given by

$$D_0 = \begin{bmatrix} I & -H \\ I & 0 \end{bmatrix}, \tag{B.16}$$

$$D_1 = \begin{bmatrix} I & -H \\ 0 & I \end{bmatrix}. \tag{B.17}$$

The matrix D_d which contains the constraint matrix C_d must satisfy the relation

$$D_d^{-1} = (1-d)D_0^{-1} + dD_1^{-1} \tag{B.18}$$

$$= \begin{bmatrix} I & 0 \\ 0 & H^{-1} \end{bmatrix} \left\{ \begin{bmatrix} 0 & I \\ -I & I \end{bmatrix} + d \begin{bmatrix} I & (H-I) \\ I & (H-I) \end{bmatrix} \right\}. \tag{B.19}$$

Note that H^{-1} exists since we have implicitly assumed that D_0 and D_1 have full rank. Computing the inverse, we find

$$D_d = \begin{bmatrix} I & 0 \\ 0 & [I + d(H-I)]^{-1} \end{bmatrix} \begin{bmatrix} I & -H \\ (1-d)I & dH \end{bmatrix}. \tag{B.20}$$

By examining the last row of the matrix on the far right in (B.20), the constraint matrix $C_d = [\ (1-d)I \quad dH\ ]$ can be extracted. By noting that the polarities of the non-controlling switch port variables are opposite from those of the resistive port variables, we obtain the hybrid representation

$$H_s(d) = \frac{d}{1-d} H \tag{B.21}$$

for $d \neq 1$. This is the same result as that obtained with the hybrid matrix formulation. •

Bibliography

[1] J. R. Wo[illegible] "Power Conversion in Electrical Networks," PhD Thesis, EECS Dept., MIT, 1973.

[2] G. C. Verghese, M. E. Elbuluk, and J. G. Kassakian, "A General Approach to Sampled-Data Modeling for Power Electronic Circuits," *IEEE Trans. Power Electronics*, pp. 76-89, April 1986.

[3] K.D.T. Ngo, "Topology and Analysis in PWM Inversion, Rectification, and Cycloconversion," PhD Thesis, EE Dept., Caltech, 1984.

[4] V.I. Utkin, *Sliding Mode Control and its Applications to Variable Structure Systems*, Mir, Moscow, 1978.

[5] V. Itkis, *Control Systems of Variable Structure*, Wiley, 1976.

[6] J.J. Slotine and S.S. Sastry, "Tracking Control of Nonlinear Systems using Sliding Surfaces, with Application to Robot Manipulators," *Int. J. Control*, 1983, vol. 38, no.2, pp.465-492.

[7] F. Harashima, H. Hashimoto, and S. Kondo, "MOSFET Converter-Fed Position Servo System with Sliding Mode Control," IEEE Power Electronics Specialists Conf. (PESC) Record, 1983, pp.73-79.

[8] R. Venkataramanan, A. Sabonovic, S. Cuk, "Sliding Mode Control of DC-to-DC Converters," Proc. 1985 Int. Conf. Indust. Elec. Contr. Instr. (IECON'85), pp. 251-258.

[9] H. Sira-Ramirez, "Sliding Motions in Bilinear Switched Networks," *IEEE Trans. Circ. and Syst.*, vol. CAS-34, no. 8, August 1987, pp. 919-933.

[10] C. W. Deisch, "Simple Switching Control Method Changes Power Converter into a Current Source," IEEE PESC Record, 1978, pp. 300-306.

[11] A. Capel, G. Ferrante, D. O'Sullivan, and A. Weinberg, "Application of the Injected Current Model for the Dynamic Analysis of Switching Regulators with the New Concept of LC^3 Modulator," IEEE PESC Record, 1978, pp. 135-147.

[12] A. Sabonovic, N. Sabonovic, and O. Music, "Sliding Mode Control of DC-AC Converters," IEEE PESC Record, 1986, pp. 560-566.

[13] T. Kailath, *Linear Systems*, Prentice-Hall, 1980.

[14] W. Burns and T. Wilson, "Analytic Derivation and Evaluation of a State-Trajectory Control Law for DC-DC Converters," IEEE PESC Record, 1977, pp.70-85.

[15] S. Huffman, W. Burns, T. Wilson, and H. Owens, "Fast-Response Free-Running DC-DC Converter Employing a State-Trajectory Control Law," IEEE PESC Record, 1977, pp.180-189.

[16] R. W. Erickson, S. Cuk, and R. D. Middlebrook, "Large-Signal Modelling and Analysis of Switching Regulators," IEEE PESC Record, 1982, pp. 240-250.

[17] R. W. Brockett and J. R. Wood, "Electrical Networks Containing Controlled Switches," Addendum to IEEE Symposium on Circuit Theory, April 1974.

[18] R. W. Brockett, "Feedback Invariants for Nonlinear Systems," IFAC Congress, Helsinki (1978).

[19] R. Su, "On the Linear Equivalents of Nonlinear Systems," *Systems and Control Letters*, vol.2, no.1, July 1982, pp.48-52.

[20] L.R. Hunt, R. Su, and G. Meyer, "Global Transformations of Nonlinear Systems," *IEEE Trans. Aut. Contr.*, vol. AC-28, Jan. 1983, pp.24-31.

[21] G. Salut, J.C. Marpinard, and M. Valentin, "Large Signal Feedback Control for Power Switching Conversion," IEEE PESC Record, 1985, pp. 741-750.

[22] R.W. Brockett and J.R. Wood, "Understanding Power Converter Chaotic Behavior Mechanisms in Protective and Abnormal Modes," Proceedings of Powercon 11, paper E-4. Power Concepts, Inc. 1984.

[23] R.D. Middlebrook and S. Cuk, "A General Unified Approach to Modelling Switching Power Converter Stages," IEEE PESC Record, 1976, pp. 18-34.

[24] J. G. Kassakian, "Simulating Power Electronic Systems - a New Approach," *Proc. IEEE*, 67, 10, pp. 1428-1439, October 1979.

[25] R.J. Duffin, "Impossible Behavior of Nonlinear Networks," 1953 *Proc. Symp. on Nonlinear Circuit Analysis*, Polytechnic Inst. of Brooklyn, N.Y., pp.124-138.

[26] D.H. Wolaver, "Fundamental Study of DC to DC Conversion Systems," PhD Thesis, EECS Dept., MIT, 1969.

[27] P. Penfield, Jr., R. Spence, and S. Duinker, *Tellegen's Theorem and Electrical Networks*, MIT Press, 1970.

[28] J.C. Willems, "Dissipative Dynamical Systems. Part I: General Theory," *Arch. Rational Mech. Anal.*, vol. 45, no. 5, pp.321-351, 1972.

[29] J.C. Willems, "Dissipative Dynamical Systems. Part II: Linear Systems with Quadratic Supply Rates," *Arch. Rational Mech. Anal.*, vol. 45, no. 5, pp. 352-393, 1972.

[30] A. Isidori, *Nonlinear Control Systems: An Introduction*, Springer-Verlag Lecture Notes in Control and Information Sciences, no. 72, 1985.

[31] C. Reboulet and C. Champetier, "A New Method for Linearizing Nonlinear Systems: The Pseudolinearization," *Int. J. Cont.*, vol. 40, no. 4, pp. 631-638, 1984.

[32] H. Sira-Ramirez, "Switched Control of Bilinear Circuits via Pseudolinearization," preprint.

[33] Oruganti, Yang, and Lee, "Implementation of Optimal Trajectory Control of Series Resonant Converter," IEEE PESC Record, 1987, pp. 451-459.

[34] M. Hasler and J. Neirynck, *Nonlinear Circuits*, Artech House, 1986.

[35] J.L. Wyatt, Jr., L.O. Chua, J.W. Gannett, I.C. Goknar, and D.N. Green, "Energy Concepts in the State-Space Theory of Nonlinear n-Ports: Part I-Passivity," *IEEE Trans. Circ. and Syst.*, vol. CAS-28, no. 1, Jan. 1981.

[36] B.D.O. Anderson and S. Vongpanitlerd, *Network Analysis and Synthesis: A Modern Systems Theory Approach*, Prentice-Hall, 1973.

[37] C.A. Desoer and M. Vidyasagar, *Feedback Systems: Input-Output Properties*, Academic Press, 1975.

[38] J.L. Wyatt, Jr., L.O. Chua, J.W. Gannett, I.C. Goknar, and D.N. Green, "Energy Concepts in the State-Space Theory of Nonlinear n-Ports: Part II-Losslessness," *IEEE Trans. Circ. and Syst.*, vol. CAS-29, no. 7, July 1982.

[39] G. Figalli, M. La Cava, and L. Tomasi, "An Optimal Feedback Control for a Bilinear Model of Induction Motor Drives," *Int. J. Control*, vol. 39, no. 5, pp. 1007-1016, 1984.

[40] L. LaWhite and M. Schlecht, "Active Filters for High Frequency Power Circuits under Strict Ripple Limitations," IEEE PESC Record, 1986.

[41] L. LaWhite and M. Schlecht, "Design of Active Ripple Filters for Power Circuits Operating in the 1-10 MHz Range," IEEE PESC Record, 1987, pp. 195-203.

[42] F.W. Warner, *Foundations of Differentiable Manifolds and Lie Groups*, Springer-Verlag, 1983.

[43] S.R. Sanders, G.C. Verghese, and D. Cameron, "Nonlinear Control Laws for Switching Power Converters," Proc. IEEE Conf. Dec. and Con. 1986, pp. 46-53.

[44] S. Cuk and R.D. Middlebrook, *Modeling, Analysis, and Design of Switching Converters*, NASA Report CR-135174.

[45] R. Tymerski, V. Vorperian, F.C. Lee, and W. Baumann,"Nonlinear Modeling of the PWM Switch," IEEE PESC Record, 1988.

[46] G.W. Wester and R.D. Middlebrook, "Low Frequency Characterization of Switched DC-DC Converters," IEEE PESC Record, 1972.

[47] L.O. Chua and P.M. Lin, *Computer Aided Analysis of Electronic Circuits: Algorithms and Computational Techniques*, Prentice-Hall, 1975.

[48] J.G. Kassakian, M.F. Schlecht, and G.C. Verghese, *Principles of Power Electronics*, Addison-Wesley, 1989.

[49] I. Derese and E. Noldus,"Optimization of Bilinear Control Systems," *Int. J. of Systems Science*, vol. 13, no. 3, pp. 237-246, 1982.

[50] R. Genesio and A. Tesi,"The Output Stabilization of SISO Bilinear Systems," *IEEE Trans. Aut. Control*, vol. 33, no. 10, pp.p950-952, Oct.,1988.

[51] M.F. Schlecht, "Time-Varying Feedback Gains for Power Circuits with Active Waveshaping," IEEE PESC Record, 1981, pp.52-59.

[52] R.P. O'Shea, "A Combined Frequency-Time Domain Stability Criterion for Autonomous Continuous Systems,"*IEEE Trans. Aut. Control*, vol. AC-11, no. 3, pp. 477-484, July, 1966.

[53] P. Kapasouris, M. Athans, and G. Stein,"Design of Feedback Control Systems for Stable Plants with Saturating Actuators," Proc. IEEE Conf. on Decision and Control, 1988.

[54] J.E. Colgate, "The Control of Dynamically Interacting Systems," PhD Thesis, M.E. Dept., MIT, 1988.

[55] Y.T. Chan and E.S. Kuh, "A General Matching Theory and Its Application to Tunnel Diode Amplifiers," *IEEE Trans. on Circuit Theory*, vol. CT-13, no.1, pp.6-18, March 1966.

[56] H.W. Bode, *Network Analysis and Feedback Amplifier Design*, Van Nostrand, 1947.

[57] R.M. Fano, "Theoretical Limitations on the Broadband Matching of Arbitrary Impedances,"*J. Franklin Inst.*, vol. 249, pp. 57-83, Jan. 1960.

[58] R.M. Fano, "Theoretical Limitations on the Broadband Matching of Arbitrary Impedances,"*J. Franklin Inst.*, vol. 249, pp.139-155, Feb. 1960.

[59] D.C. Youla, "A New Theory of Broad-band Matching," *IEEE Trans. on Circuit Theory*, vol. CT-11, pp. 30-50, March 1964.

[60] R.A. Rohrer, "Optimal Matching: A New Approach to the Matching Problem for Real Linear Time-Invariant One-Port Networks," *IEEE Trans. on Circuit Theory*, vol. 15, no. 2, pp.118-124, June 1968.

[61] H.J. Carlin, "A New Approach to Gain-Bandwidth Problems," *IEEE Trans. on Circ. and Syst.*, vol. CAS-24, no.4, pp.170-175, April 1977.

[62] C.A. Desoer and R.W. L. ., "Global Parametrization of Feedback Systems with Nonlinear Plants," *Systems and Control Letters*, vol. 1, no. 4, pp. 249-251, Jan. 1982.

[63] B.A. Francis, *A Course in H_∞ Optimal Control*, Springer-Verlag, 1987.

[64] B.D.O. Anderson, R.R. Bitmead, C.R. Johnson, Jr., P.V. Kokotovic, R.L. Kosut, I.M.Y. Mareels, L. Praly, and B.D. Riedle, *Stability of Adaptive Systems: Passivity and Averaging Analysis*, MIT Press, 1986.

[65] H. Sira-Ramirez and M. Ilic, "Exact Linearization in Switched Mode DC to DC Power Converters," to appear in *Int. J. of Control.*

[66] G.C. Verghese, B. Fernandez, and J.K. Hedrick, "Stable Robust Tracking by Sliding Mode Control," *Systems and Control Letters*, 10, 1988, pp. 27-34.

[67] D. Gouttenegre and B. Velaerts, "Modeling and Analysis of DC-DC Converters Control by Power Equalization," IEEE PESC Record, 1988, pp. 960-967.

[68] S. Cuk and R.D. Middlebrook, "A General Unified Approach to Modeling Switching Converters in Discontinuous Conduction Mode," IEEE PESC Record, 1977, pp.36-57.

[69] D.H. Wolaver, "Requirements on Switching Devices in DC-DC Converters," IEEE PESC Record, 1973, pp. 111-117.

[70] H.J. Sira-Ramirez and M. Ilic, "A Geometric Approach to the Feedback Control of Switch Mode DC-to-DC Power Supplies," *IEEE Trans. on Circuits and Systems*, vol. 35, no. 10, pp. 1291-1298, Oct. 1988.

[71] Y.P. Tsividis, "Analytical and Experimental Evaluation of a Switched-Capacitor Filter and Remarks on the Resistor/Switched Capacitor Correspondence," *IEEE Trans. on Circuits and Systems*, vol. CAS-26, no. 2, pp.140-144, Feb. 1979.

[72] J.A. Nossek and H. Weinrichter, "Equivalent Circuits for Switched-Capacitor Networks Including Recharging Devices," *IEEE Trans. on Circuits and Systems*, vol. CAS-27, no. 26, pp. 539-544, June 1980.

[73] A. Knob and R. Dessoulavy, "Analysis of Switched-Capacitor Networks in the Frequency Domain Using Continuous-Time Two-Port Equivalents," *IEEE Trans. on Circuits and Systems*, vol. CAS-28, no. 10, pp.947-953, Oct. 1981.

[74] M. Athans and P.L. Falb, *Optimal Control*, New York: McGraw-Hill, 1966.

[75] E. Guillemin, *Synthesis of Passive Networks*, New York: John Wiley & Sons, 1957.

[76] J. Palis and W. de Melo, *Geometric Theory of Dynamical Systems: An Introduction*, New York: Springer-Verlag, 1981.

[77] H.D. Chiang, M.W. Hirsch, and F.F. Wu, "Stability Regions of Nonlinear Autonomous Dynamical Systems," *IEEE Trans. on Aut. Contr.*, vol. 33, no. 1, pp.16-27, Jan. 1988.

[78] J. Zaborsky, G. Huang, B. Zheng, and T.C. Leung, "On the Phase Portrait of a Class of Large Nonlinear Dynamic Systems Such as the Power System," *IEEE Trans. on Aut. Contr.*, vol. 33, no. 1, pp.4-15, Jan. 1988.

[79] H.D. Chiang, F.F. Wu, and P.P. Varaiya, "Foundations of Direct Methods for Power System Transient Stability Analysis," *IEEE Trans. on Circ. and Syst.*, vol. CAS-34, no. 2, pp.160-173, Feb. 1987.

[80] R.A. DeCarlo, S.H. Zak, and G.P. Matthews,"Variable Structure Control of Nonlinear Multivariable Systems: A Tutorial," *Proc. of IEEE*, vol. 76, no. 3, pp. 212-232, March 1988.

[81] L.O. Chua, *Lecture Notes for Network Theory*, EECS 223, University of California, Berkeley, 1980.

[82] J.K. Zuidweg, "Every Passive Time-Invariant Linear n-Port Has At Least One 'H Matrix'," *IEEE Trans. on Circuit Theory*, vol. CT-12, pp. 131-132, March 1965.

[83] B.D.O. Anderson, R.W. Newcomb, and J.K. Zuidweg, "On the Existence of H Matrices," *IEEE Trans. on Circuit Theory*, vol. CT-13, no.1, March 1966, pp.109-110.

[84] L.C. Fu, M. Bodson, and S.S. Sastry, "New Stability Theorems for Averaging and Their Application to the Convergence Analysis of Adaptive Identification and Control Schemes," *Proc. 24th IEEE Conf. Dec. and Control*, Ft. Lauderdale, FL, pp. 473-477.

[85] J.J. Slotine, "Putting Physics in Control - The Example of Robotics," *IEEE Control Systems Magazine*, vol. 8, no. 6, Dec. 1988, pp. 12-18.

[86] Y. Yamamoto and S. Hara, "Relationships Between Internal and External Stability for Infinite-Dimensional Systems with Applications to a Servo Problem," *IEEE Trans. Aut. Control*, vol. 33, no. 11, Nov. 1988, pp. 1044-1052.

[87] G.C. Verghese, "A Generalized State-Space for Singular Systems," *IEEE Trans. Aut. Contr.*, vol. AC-26, no. 4, Aug. 1981, pp. 811-831.

[88] J.L. Wyatt, Jr., "Lectures on Nonlinear Circuit Theory," VLSI Memo 84-158, revised August 1984. All VLSI Memos are available from the Microsystems Research Center, Room 39-321, MIT, Cambridge, MA 02139, or from the author. (Second Edtion will appear Spring 1989.)

[89] K.A. Loparo, J.T. Aslanis, and O. Hajek, "Analysis of Switched Linear Systems in the Plane, Part 1: Local Behavior of Trajectories and Local Cycle Geometry," *J. Opt. Theory and Appl.*, vol. 52, no. 3, pp.365-394, March 1987.

[90] K.A. Loparo, J.T. Aslanis, and O. Hajek, "Analysis of Switched Linear Systems in the Plane, Part 2: Global Behavior of Trajectories, Controllability and Attainability," *J. Opt. Theory and Appl.*, vol. 52, no. 3, pp. 395-427, March 1987.

[91] B.E. Paden and S.S. Sastry, "A Calculus for Computing Filippov's Differential Inclusion with Application to the Variable Structure Control of Robot Manipulators," *IEEE Trans. Circ. and Syst.*, vol. CAS-34, no. 1, pp. 73-82, January 1987.

[92] I. Horowitz, M. Sidi, and R. Erickson, "Quantative Feedback Synthesis for Non-Linear Switched-Mode Uncertain Regulators," *Int. J. Electronics*, vol. 57, no. 4, pp. 461-476, 1984.